Production Of Activated Carbon And Its Catalytic Application For Oxidation Of Hydrogen Sulphide

A thesis
submitted to the college of graduate studies and research
in partial fulfillment of the requirements for the degree of
Doctor of Philosophy
in the Department of Chemical Engineering
University of Saskatchewan
Saskatoon, Saskatchewan

by

Ramin Azargohar

Spring 2009

Copyright

Abstract

Hydrogen sulphide is an environmentally hazardous gas which is present in many gas streams associated with oil and gas industry. Oxidation of H_2S to sulphur in air produces no bulky or waste material and requires no further purification. Activated carbon is known as a catalyst for this reaction.

In this research, a coal-based precursor (luscar char) and a biomass-based precursor (biochar) were used for production of activated carbons by two common methods of activation: physical and chemical activation in which steam and potassium hydroxide (KOH), respectively, were used. Experiments were designed by the statistical central composite design method. Two models were developed for the BET surface area and reaction yield of each activation process. These models showed the effects of operating conditions, such as activation temperature, mass ratio of activating agent to precursor, activation time, and nitrogen flowrate on the BET surface area and reaction yield for each activation method for each precursor. The optimum operating conditions were calculated using these models to produce activated carbons with relatively large BET surface area (> 500 m^2/g) and high reaction yield (> 50 wt %). The BET surface area and reaction yield for activated carbons produced at optimum operating conditions showed maximum 7 and 7.4 % difference, respectively, comparing to the values predicted by models.

The activated carbons produced at optimum operating conditions were used as the base catalysts for the direct oxidation of 1 mol % hydrogen sulphide in nitrogen to sulphur at the temperature range of 160-205 ^oC and pressure of 700 kPa. Originally activated carbons showed a good potential for oxidation of hydrogen sulphide by their selectivity for sulphur product and low amount of sulphur dioxide production. To

improve the performance of steam-activated carbons, the catalysts were modified by acid-treatment followed by thermal desorption. This method increased the break-through times for coal-based and biomass-based catalysts to 115 and 141 minutes, respectively. The average amounts of sulphur dioxide produced during the reaction time were 0.14 and 0.03 % (as % of hydrogen sulphide fed to the reactor) for modified activated carbons prepared from biochar and luscar char, respectively. The effects of porous structure, surface chemistry, and ash content on the performances of these activated carbon catalysts were investigated for the direct oxidation reaction of hydrogen sulphide.

The acid-treatment followed by thermal desorption of activated carbons developed the porosity which produced more surface area for active sites and in addition, provided more space for sulphur product storage resulting in higher life time for catalyst. Boehm titration and temperature program desorption showed that the modification method increased basic character of carbon surface after thermal desorption in comparison to acid-treated sample. In addition, the effects of impregnating agents (potassium iodide and manganese nitrate) and two solvents for impregnation process were studied on the performance of the activated carbon catalysts for the direct oxidation of H_2S to sulphur.

Sulphur L-edge X-ray near edge structure (XANES) showed that the elemental sulphur was the dominant sulphur species in the product.

The kinetic study for oxidation reaction of H_2S over LusAC-O-D(650) was performed for temperature range of 160-190 ^oC, oxygen to hydrogen sulphide molar ratio of 1-3, and H_2S concentration of 6000-10000 ppm at 200 kPa. The values of activation energy were 26.6 and 29.3 $kJ.gmol^{-1}$ for Eley-Rideal and Langmuir-Hinshelwood mechanisms, respectively.

Acknowledgements

I wish to express my deep appreciation to my supervisor Professor A. K. Dalai for his guidance, encouragement and perseverance throughout the course of my graduate studies and research. I also would like to thank the other members of the advisory committee, professors M. Nemati, T. Pugsley, H. Wang, and L. Wilson, for their helpful discussions and suggestions.

Thanks are also due to the following people for their assistance and cooperation provided during my PhD program:

K. Bader, R. Blondin, C. Botchwey, D. Cekic, J. Horosko, Dr. H. K. Mishra, professor H. (Catherine) Niu, and T. Wallentiny all from the Chemical Engineering Department, all members of Catalysis and Chemical Reaction Engineering Laboratories of Chemical Engineering Department, J. H. Kwon, and M. Zahedi from the Department of Chemistry, and Drs Y. Hu and L. Zuin from the Canadian Light Source.

I am grateful, always, of the continuous love and support of my mother, Zahra, and my sister, Rozita.

Table of Contents

List of Tables

List of Figures

Glossary of Symbols

A Coded factor for activation temperature defined by Equations 4-3, 4-7, and 4-13; Parameter in Eq. 6-52

A_1 Parameter defined by Eq. 6-28

A_M The area occupied by the adsorbate molecule, $Å^2$

a H_2S mole percentage in the feed gas, (%)

B Coded factor for mass ratio of steam to char defined by Equations 4-4, 4-8, and 4-14; Parameter defined by Eq. 6-52

B_1 Weight of crucible, g

C Constant in BET equation; Parameter defined by Eq. 6-52

C Mass of char, g

C_1 Weight of crucible plus original sample, g

C_{AS} Surface concentration of reactant A, moles/cm^3

C_i Concentration of species i, gmol/cm^3; The surface concentration of sites occupied by species i, gmol/g_{cat}

C_t Total concentration of active sites, gmol/g_{cat}

C_v The concentration of vacant sites, gmol/g_{cat}

C_{WP} Weisz-Prater factor defined by Eq. 6-14

D The pore diameter defined by Eq. 2-8, μm

D Coded factor for activation time defined by Equations 4-5 and 4-9, and coded factor for nitrogen flow arte by Eq.4-15; Parameter defined by Eq. 6-52

D_1 Weight of crucible plus ashed sample, g; Parameter defined by Eq. 6-28

D_{AB} Diffusivity of A in B, m^2/s

D_e Effective diffusivity, m^2/s

d_P Average diameter of particle , m

d_t Inner diameter of the reactor, m

E Parameter defined by Eq. 6-52

E_1 Parameter defined by Eq. 6-28

F Nitrogen flow rate, ml/min

K_i Equilibrium adsorption constant for species i (kPa^{-1})

$K^{'}$ Unit conversion coefficient defined by Eq. 2-7

k Number of parameters

k The Boltzmann constant, $1.381*10^{-23}$ $m^2.kg.s^{-2}.K^{-1}$

k_C The average mass transfer coefficient defined by Eq. F8, m/s

k_s Forward rate constant, $g_{cat}/gmol/min$

$k_s^{'}$ Reverse rate constant, $g_{cat}/gmol/min$

M_i Molecular weight of species i, g/gmol

m Reaction order with respect to oxygen

m_s The mass of the solid used for BET analysis

N Number of experiments defined by Eq. 3-1

N Number of experiments performed for kinetic study

N_A Avogadro's number, $6.022 * 10^{23}$

n Reaction order with respect to hydrogen sulphide

n_C Number of central runs

p	Gas pressure, kPa (for Eq. F2), atm (for Eq. H1), mmHg (for Eq. 2-6)
p^o	Gas saturation pressure, mmHg (for Eq. 2-6)
Q	Gas Flow rate, cm^3/min
q_l	Heat of adsorption for first layer, kJ/gmol
q_L	Heat of liquefaction of the adsorptive, kJ/gmol
R	Universal gas constant, 0.008314 kJ/gmol/K
R	Mass ratio of potassium hydroxide to char
r_o	Reaction rate without deactivation of catalyst by sulphur deposition, gmol/min/g_{cat}
r_A'	Reaction rate per unit mass of catalyst, gmol/g/min
Re	Reynolds number ($u\rho d_p/\mu$)
r_m	Pore radius, m
S	Mass of steam, g
S_r	Cross sectional area of the reactor, m^2
S_{BET}	The BET surface area, m^2/g
Sc	Schmidt number ($\mu/\rho D$)
Sh	Sherwood number ($k_c d_p/D$)
T_a	Absolute Temperature, K
T	Temperature, ^oC
U	Fluid velocity, m/s
V_a	The quantity of gas adsorbed on the surface at pressure P (in BET equation), cm^3
V_M	Molar volume, 22,414 cm^3/mol

V_m	The quantity of gas adsorbed when the entire surface is covered with a monomolecular layer, cm^3
Y_1	The BET surface area, m^2/g
Y_2	The reaction yield for activation process, wt %
W	Catalyst mass, g
W_S	Total amount of sulphur produced per unit mass of carbon till time t, g_S/g_c
W_S^{∞}	Amount of sulphur produced when all sites are covered on the carbon, g_S/g_c
Z	Gas compressibility factor; Parameter defined by Equations 6-22 and 6-46

Greek Alphabets

α	The distance of axial point from the center point in central composite design method
α	Line gradient defined by Equation B2
β	Line ordinate at the origin point
γ	Surface tension defined by Equation 2-8, dyne/cm
γ	Constriction factor
δ	The mass transfer boundary layer thickness, m
ε	The force constant in the Lennard-Jones potential function [Satterfield, 1970], $m^2.kg/s^2$
ξ_i	Average conversion of species i in the reaction, %
θ	The angel between mercury and surface
μ	Dynamic viscosity of fluid, Pa.s
ρ	Fluid density, kg/m^3
ρ_c	Catalyst density, kg/m^3
σ_{12}	The force constant in the Lennard-Jones potential function [Satterfield, 1970], Å
τ	Tortuosity factor defined by Equation G6
ϕ_p	Pellet porosity, cm^3/cm^3
Ω_D	Collision integral [a function of kT/ε_{12} in Satterfield, 1970]

1.0 Introduction

Hydrogen sulphide (H_2S) is a colorless gas which is a by-product of many industrial processes such as oil refining [Gary and Hendwerk, 2001], gas processing [Crammore and Stanton, 2000], and wastewater treatment facilities. It can be found in many gas streams which are used as energy sources or chemical feedstocks. It is an extremely toxic gas. Industrially, even low amounts of this compound can affect the process efficiency and equipment life in industry [Craige and Anderson, 1995]. Oxidation of hydrogen sulphide and its incineration produce sulphur dioxide (SO_2) which can be converted to sulphuric acid (H_2SO_4) in the atmosphere in the presence of moisture and is one of the main reasons for acid rain [Allen and Shonnard, 2002; Miller, 2005]. Acid rain causes acidification of lakes and streams that kills aquatic animals and in addition, accelerates the soil erosion and decay of building materials and paints.

Absorption is a common method used for the removal of hydrogen sulphide from gas streams. Amine solutions or potassium solutions are used for absorption process followed by stripping operation to regenerate solvent and recycle of it [Mokhatab, 2006]. Hydrogen sulphide separated by the absorption is converted to elemental sulphur in sulphur recovery unit using two different methods called “Liquid redox” and “Claus process”. The former is based on liquid phase oxidation [Dalrymple and Trofe, 1994; Kohl and Nielsen, 1997] and the latter uses partial oxidation with air [Gary and Hendwerk, 2001; Thomas, 1970]. Claus process [Gary and Hendwerk, 2001] is used for removal of hydrogen sulphide with high concentration [Mikhalovsky and Zaitsev, 1997] from gas streams produced in different purification steps of gas and oil refinery processes. Although the single stage Claus units can only recover 70 % of sulphur, but

modified Claus sulphur recovery units are capable of achieving over 97% recovery of sulphur. This system is not useful for low concentration of hydrogen sulphide. Then, it must be followed by a tail gas treatment unit, such as SCOT tail gas clean-up unit [Rojey, 1997; Mokhatab, 2006; Crammer and Stanton, 2000], to provide recovery efficiency more than 99%. The tail gas treatment unit increases the cost of sulphur recovery unit by two times [Gary and Hendwerk, 2001]. In addition, there are some other methods for removal of low-concentration hydrogen sulphide, such as Liquid-phase absorption [Hardison, 1985] or Dry sorption processes. The main drawbacks for these methods are the production of byproducts and solutions which need further purification, low quality of sulphur product, and relatively high cost of operation [Busca and Pistarino, 2003; Mikhalovsky and Zaitsev, 1997]. In addition, microbiological oxidation has been used for feed with low H_2S concentration by oxidizing hydrogen sulphide to elemental sulfur or to sulfate by using dissolved oxygen, metal oxides (e.g. iron oxyhyroxides and manganese oxides) or nitrate as oxidant [Sublette, 1987; Lizama and Sankey, 1993].

Carbon is known as an effective catalyst for direct oxidation of hydrogen sulphide [Cariaso and Walker, 1975] and can remove this pollutant to the range of ppb at reaction temperatures less than 200 ^{o}C [Gamson and Elkins, 1953]. Activated carbon can be one of the best options for oxidation of hydrogen sulphide to sulphur because of cheap and abundant precursors, highly developed porosity, and flexible surface chemistry. Generally, performance of activated carbon for adsorptive or catalytic applications depends on three parameters; porous structure, surface chemistry, and ash content. Porous structure of activated carbon includes miropores, mesopores, and macropores. Heteroatoms such as oxygen and nitrogen form the surface chemistry. These heteroatoms

can produce surface functionalities by different treatments. Ash content mostly includes inorganic oxides.

The products of direct oxidation of hydrogen sulphide using activated carbon catalyst are elemental sulphur and water. The sulphur is trapped into pores of activated carbon and causes a gradual deactivation of catalyst. One of the main challenges for this process is the formation of sulphur dioxide (SO_2) as an undesired by-product which has to be maintained as low as possible. Operating conditions such as low pressure and high temperatures result in higher rate of SO_2 production. The sulphur deposited inside the pores can be simply removed by thermal regeneration in an inert atmosphere [Dalai et al, 1993]. This process produces no chemicals and thus requires no further purification.

In this research, a comprehensive study on the production of activated carbons (as reference catalysts) using physical and chemical activation, was performed. Coal and biomass are two common precursors used for the production of activated carbon around the world [El-Hendawy, 2001; Lua and Yang, 2004; Lozano-Castello et al, 2001]. In this study, Luscar char which its source was lignite coal, was used as one of the precursors. There are several mines of this coal in Saskatchewan, such as Poplar River, Boundary Dam, and Bienfait mines.

The source of the second precursor was biomass which can be obtained from forest residue or agricultural wastes. Canada and Saskatchewan have abundant waste streams of biomass. Canada has approximately 10 % of the world's forest cover [Natural Resources Canada, 2008] and wood residues production was more than $21*10^6$ bone-dry tones in Canada in 2004 [Natural Resources Canada, 2005]. The amount of agricultural wastes produced from straw and chaff was approximately $26*10^6$ tonnes in Saskatchewan in

2004 [Saskatchewan Government, 2004]. The production of activated carbons from biomass not only is a solution for waste disposal problems but also converts it to value-added products which can be used for environmental applications. These two types of precursors were used in this study to investigate their potentials for the production of activated carbon catalyst for direct oxidation of hydrogen sulphide to sulphur in gas streams.

Steam was used for physical activation while KOH was used for chemical activation process. The effects of activation operating conditions on the BET surface area and reaction yield were studied. Two statistical models for each activation process for producing activated carbons with relatively large BET surface area and high reaction yield were developed and validated with new experimental data. These catalysts were used for direct oxidation of H_2S to elemental sulphur. The performances of these catalysts were improved for hydrogen sulphide oxidation using one modification method including acid-treatment/thermal desorption. The effects of this modification on porous structure and surface groups, were also investigated. The study showed that modified activated carbons are efficient catalysts for H_2S oxidation reaction. Modeling the activation processes and study the effects of surface chemistry, porosity structure, and ash content on the performance of activated carbons for the catalytic oxidation of hydrogen sulphide to sulphur were the main goals in this study.

1.1. Research objectives

The overall objective of this research included the development of activated carbon catalysts, from biomass as well as from Saskatchewan coal, which are able to oxidize low

concentrations (< 1 mol %) of hydrogen sulphide in gas phase to elemental sulphur, using direct oxidation process, with high activity and selectivity. This objective was achieved in various phases of the research which are described as follows:

Phase I. A coal-based (Luscar char) and a biomass-based (Biochar) precursors were used as the raw material for production of activated carbons. Two common methods of physical activation and chemical activation were used for production of activated carbons in this study. Physically activated carbons were produced from both precursors using steam as oxidizing agent. Chemically activated carbon was produced from biochar using potassium hydroxide (KOH). The BET surface area and reaction yield related statistical models were developed for activation process of each precursor. The operating conditions investigated for physical activation were activation temperature, mass ratio of steam to precursor and activation time whereas those studied for chemical activation were activation temperature, mass ratio of KOH to biochar, and nitrogen (N_2) flow rate. A statistical method called central composite design was used to plan the experiment. These models showed the effect of operating conditions, including three parameters for each activation process, on the BET surface area and reaction yield of activated carbons. Statistical tests showed these models can navigate the data in the operating range. To produce activated carbons with relatively large surface area and high reaction yield, the optimum operating conditions were calculated for each activation process using the above mentioned models. Activated carbons were produced at the optimum operating conditions and their BET surface area and reaction yield were in good agreement with the values obtained by models.

Phase II. Performance of activated carbons produced at optimum operating conditions was evaluated for direct oxidation of hydrogen sulphide to sulphur. Performance of each catalyst was evaluated with three parameters including break-through time, mass of sulphur captured per mass of catalyst, and average production of sulphur dioxide. A modification method such as acid-treatment followed by thermal desorption was used and its effects on the catalytic performance of these catalysts in direct oxidation of hydrogen sulphide, basic and acidic character of carbon surface, and porous structure of catalysts were investigated. The effects of reaction temperature, reaction pressure, impregnating agents, and impregnating solvents on the modified activated carbon produced from Luscar char were investigated.

Phase III. The type of sulphur species produced in direct oxidation reaction using activated carbon catalysts was investigated. X-ray absorption near edge structure (XANES) analysis showed that the elemental sulphur at the range of operating conditions used for this reaction was the main product for both precursors. The effect of thermal regeneration time on one of the modified catalysts was studied.

Phase IV. Kinetic study was performed for modified physically activated carbon produced from luscar char for temperature range of 160-190 ^{o}C, oxygen to H_2S molar ratio in the range of 1-3, and H_2S concentration range of 6000-10000 ppm . Eley-Rideal and Langmuir-Hinshelwood mechanisms were used for this study.

First chapter of this thesis includes introduction and describes research objectives. Chapter Two explains activated carbons production methods, physical and chemical structure of activated carbons, and their applications as well as existing methods for removal of hydrogen sulphide from gas streams. Third chapter is about experimental and

characterization methods used in this study. Chapter Four discusses results of chemical activation of biochar and physical activation of luscarchar and biochar. Fifth chapter is about results of direct oxidation of hydrogen sulphide sulphide over activated carbon catalyst including performance of modified and unmodified catalyst, the effects of impregnating agents and solvents, and type of sulphur products for this reaction. Chapter six describes the kinetic study of the oxidation reaction of hydrogen sulphide using Langmuir-Hinshelwood and Eley-Rideal mechanisms. These chapters are followed by Conclusions and Recommendations, References, and Appendixes.

2.0 Literature review

2.1. Introduction

This chapter provides a review of the precursors, production methods, and industrial applications for activated carbons. In addition, it discribes the porous structure of activated carbons as well as their surface chemistry including surface functional groups on the carbon materials. The last part of this chapter discusses about toxicity of hydrogen sulphide, the sources of this pollutant in industry, and common removal methods.

2.2. Activated carbon

2.2.1. Structure of carbonaceous materials

Carbon has the electron configuration of $1s^2\ 2s^2\ 2p^2$ and its possible valence states are 2, 3, or 4. Carbon is capable of forming sp^3-hybrid, sp^2-hybrid, and sp-hybrid [Byrne and Marsh, 1995]. In sp^3-hybrid, which is the basis of diamonds and aliphatic compounds, orbitals point towards the apexes of a tetrahedron at an angle of $109^0\ 28^{/}$ to one another. sp^2 orbitals, which are the basis of graphitic and aromatic structures, are directed in a plane at 120^0 to each other and the fourth electron in a p-orbital is free to form π-bond with neighboring atoms. In sp-hybrid which is the basis of alkynes, carbon has two orbitals of this type, which lie in a straight line and two electrons with unpaired spins in p orbitals available for π-bonds [Morgan, 2005]. Although the most known forms of carbon are cubic (tetragonal) diamond and hexagonal graphite [McEnaney, 1999] and recently discovered fullerenes [Morgan, 2005; Rouquerol et al, 1999], most of carbon

materials in nature have less ordered structures. Six-member carbon rings are unit cell of graphite structure. Each carbon atom within a plane, called graphene layer, is bonded to three adjacent carbons and there are weak Van der Waals forces between parallel neighboring planes [Rodriguez-Reinoso, 1997]. Within each graphene layer, the bonding is trigonal sp^2-hybrid σ-bonds with delocalized π-bonds within the layer [Marsh and Rodriguez-Reinoso, 2006]. These layers are not exactly above and below each other [Morgan, 2005]. They are displaced and form hexagonal and rhombohedral graphite structures. The latter is thermodynamically less stable. The Fig. 2.1 shows the structure of hexagonal graphite.

Perfect graphite in nature is rare. According to the crystallographic ordering, members of carbon family can be categorized into graphitic and non-graphitic carbons [Byrne and Marsh, 1995]. Graphitic carbons exhibit X-ray diffraction (XRD) lines of 3-dimensional graphite [Marsh and Rodriguez-Reinoso, 2006].

Non-graphitic carbon is classified as graphitizable (cokes) and non-graphitizable carbons (chars) [Rodriguez-Reinoso, 1997]. Graphitizable carbons can be converted into graphitic carbons by the heat treatment under atmospheric pressure [Marsh, 1991]. Non-graphitizable carbons do not pass through a fluid phase during pyrolysis (carbonization) [Byrne and Marsh, 1995]. These materials are the main precursors for activated carbon. Activated carbons are porous materials with highly developed internal surface area and porosity. The structure of these carbons is formed by imperfect sections of graphene layers which are bonded together to build a 3-dimensional structure, as shown in Fig. 2.2.

This structure includes many defects and spaces between different layers which are the source of activated carbon porosity. This structure not only provides different porous

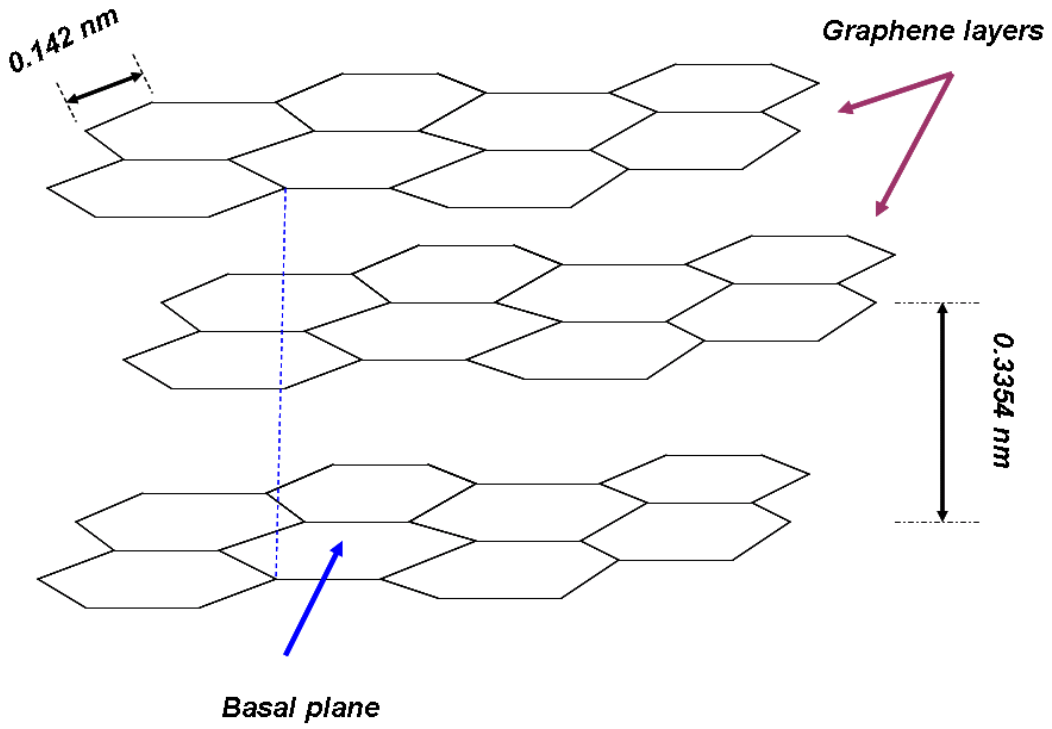

Fig. 2.1: The structure of hexagonal graphite [Redrawn from Marsh and Rodriguez-Reinoso, 2006]

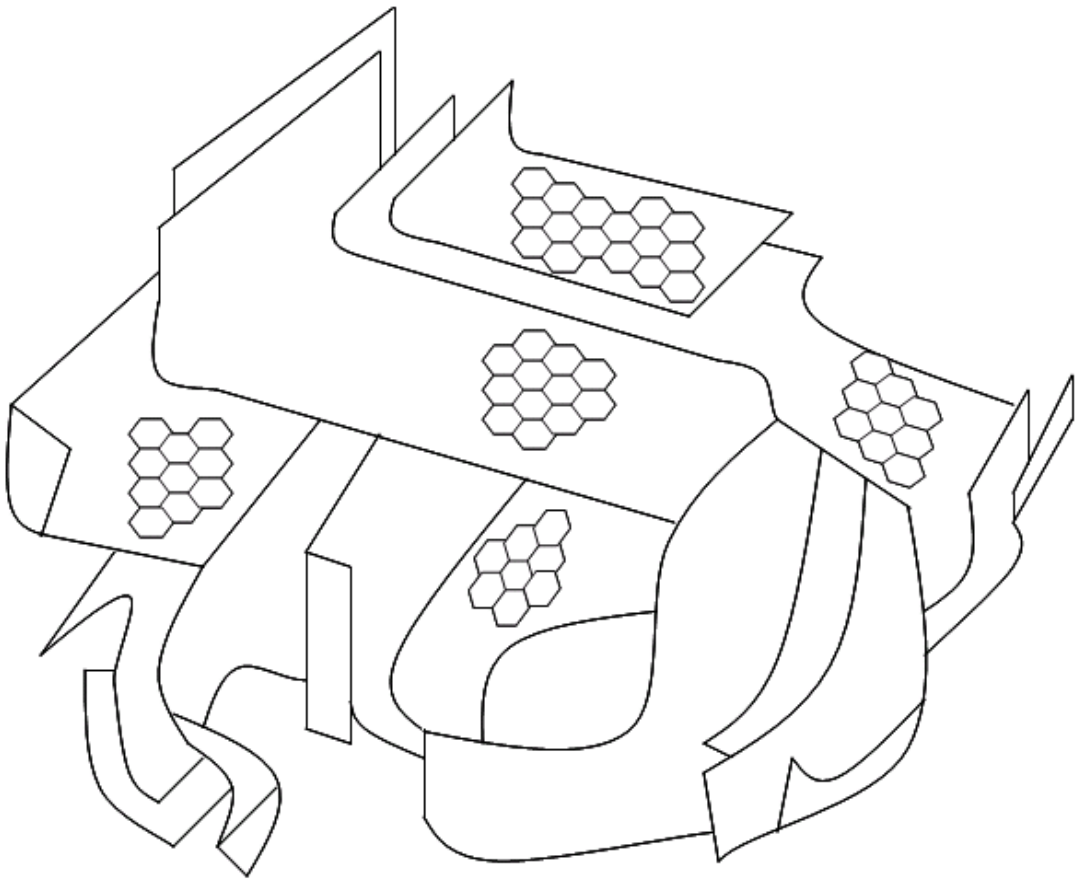

Fig. 2.2: Schematic representation of the structure of activated carbon [Redrawn from Stoeckli, 1990]

structures but also has a significant effect on the bulk density, mechanical strength, and other physical properties of activated carbon [Rodriguez-Reinoso and Molina-Sabio, 1998]. The porous structure of activated carbon is formed by three types of pores as shown in Fig. 2.3. In this Figure, pores are categorized as follows:

Micropores: width less than 20 Å, Mesopores: width between 20-500 Å, and Macropores: width larger than 500 Å [Sing et al, 1985].

Human being started using carbon materials as purifying agent before 1550 B.C. [Rodriguez-Reinoso, 1997]. In World War I, activated carbons were used in gas masks as adsorbents [McEnaney, 1999], as catalysts [Dalai et al, 1993; Rodriguez-Reinoso, 1998], and catalyst support [Byrne and Marsh, 1995*;* Rodriguez-Reinoso, 1998*;* Radovic and Rodriguez-Reinoso, 1997] as well as in many adsorption processes for removal of impurities from liquids and gases.

2.2.2 Synthesis

Physical and chemical activation methods are commonly used for production of activated carbon [Rodriguez-Reinoso, 1997; Kyotani, 2000] from different precursors.

2.2.2.1. Precursors

Activated carbons can be produced from most of carbon-containing organic materials [Rodriguez-Reinoso, 2002; Rodriguez-Reinoso and Molina-Sabio, 1998], but commercial processes to make activated carbon use precursors, which are either of degraded and coalified plant matter (e.g. peat, lignite and all ranks of coal) or of the botanical origin

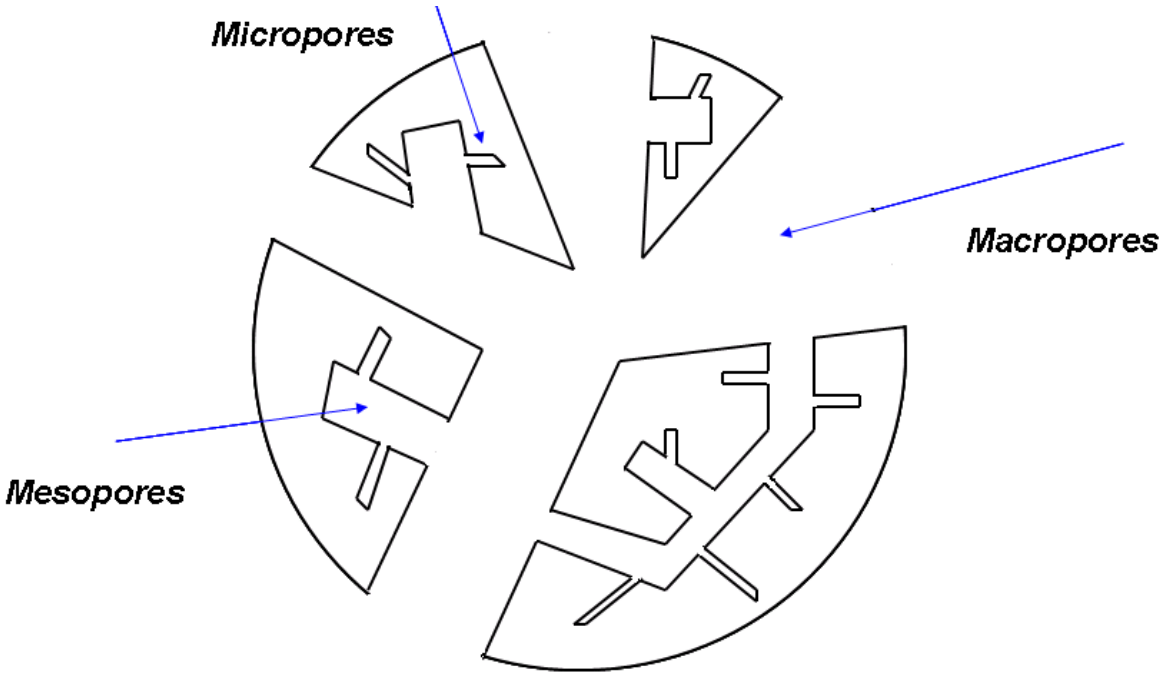

Fig. 2.3: Schematic representation of activated carbon porous structure [Redrawn from Rodriguez-Reinoso, 1997]

(e.g. wood, coconut shells and nut shells) [El-Hendawy, 2001; Lua and Yang, 2004; Lozano-Castello et al, 2001].

These materials have high carbon content and are inexpensive [Rodriguez-Reinoso, 1997]. Coal is commonly used for producing high yields of activated carbon [Munoz-Guillene et al, 1992; Linares-Solano et al, 2002]. Materials from botanical origin or in other word, lignocellulosic materials have low inorganic and relatively high volatile content. The first characteristic results in producing activated carbon with low ash and the second helps to control the production process [Rodriguez-Reinoso, 2002].

2.2.2.2. Physical activation

In physical activation, char is produced, at the first step, by carbonization (pyrolysis) of precursor. This step removes non-carbon species [Rodriguez-Reinoso, 1997] and produces char with a high percentage of carbon. Because of blockage of the pores by tars [Rodriguez-Reinoso and Molina-Sabio, 1998], the internal surface area of char is too low and it does not have a developed porous structure. Second step of physical activation is high temperature gasification (activation) using oxidizing agents such as steam or carbon dioxide (CO_2), which produces activated carbon with high porosity [Rodriguez-Reinoso, 1997; Rodriguez-Reinoso, 2002; Rodriguez-Reinoso and Molina-Sabio, 1998]. Porosity development is due to the penetration of oxidizing agent into the internal structure of char and removal of carbon atoms by reaction which results in opening and widening of inaccessible pores [Rodriguez-Reinoso, 2002; Rodriguez-Reinoso and Molina-Sabio, 1998].

Both reactions between steam-carbon (heterogeneous water-gas reaction) and CO_2-carbon are endothermic [Muhlen and Van Heek, 1995] as follows:

$C + H_2O = H_2 + CO$ $\Delta H = + 118$ kJ/mol (2-1)

$C + CO_2 = 2CO$ $\Delta H = + 162$ kJ/mol (2-2)

This endothermic characteristic of reactions facilitates the control of reaction, but there is a need for external heat source, such as a furnace, to maintain the reaction temperature [Marsh and Rodriguez-Reinoso, 2006]. For steam activation, two further reactions are also possible; At high temperatures used for this type of activation, the water-gas shift reaction can be catalyzed on the surface of carbon as follows [Marsh and Rodriguez-Reinoso, 2006]:

$CO + H_2O = CO_2 + H_2$ $\Delta H = - 41$ kJ/mol (2-3)

The other possible reaction in steam activation is methanation as follows:

$CO + 3H_2 = CH_4 + H_2O$ $\Delta H = - 206$ kJ/mol (2-4)

Both reactions are exothermic, but the heterogeneous water-gas reaction is dominant and the overall process is endothermic [Muhlen and Van Heek, 1995].

Oxygen is not used as oxidizing agent because of the exothermic reaction between carbon and oxygen, which makes difficult to control the process temperature and prevents the development of high porosity due to external burning of carbon particles [Rodriguez-Reinoso, 1997; Rodriguez-Reinoso, 2002].

Compounds of alkali and alkaline-earth metals, iron, manganese, aluminum, etc. are used as catalysts for physical activation [Rodriguez-Reinoso, 2002; Leboda et al, 1996; Higashiyama, 1985; Shen et al, 2003; Laine and Calafat, 1991]. These catalysts help to develop different porosity, for instance iron nitrate (less than 0.5 wt% Fe) develops meso-

and macroporosity. Alkali compounds, such as hydroxides or carbonates of potassium and sodium develop micropores, whereas transition metals and alkaline-earth compounds promote the formation of mesoporosity [Rodriguez-Reinoso, 1990].

Different types of furnaces, such as rotary kiln, multiple heart, vertical shaft, and fludized-bed, can be used for the production of activated carbons. Rotary kilns are most commonly used because of their ability to produce a large range of particle sizes [Rodriguez-Reinoso, 1997].

Carbon monoxide (CO) and hydrogen (H_2) are known as strong inhibitors for steam activation. In industry, a small flow of air is injected at adequate points to burn these inhibitors to provide a part of heat required for the activation [Rodriguez-Reinoso, 1997]. Activation using steam first opens the blocked pores in char and develops the micropores and follows by only widening the developed micropores which results in larger development of meso- and macropores and less development of micropores [Rodriguez-Reinoso and Molina-Sabio, 1998]. But CO_2 activation basically develops micropores [Rodriguez-Reinoso, 1997].

Physical activation process can be combined with pyrolysis and conducted in one stage. This method was used in some continuous reactors [Derbyshire et al, 1995]. Although 2-step process is more common and has many advantages, but one-step process is used for precursors with high carbon content.

2.2.2.3. Chemical activation

Chemical activation of the precursor with a chemical (dehydrating) agent is another important industrial process for producing activated carbons. It is shown that some

operating conditions such as temperature and heating rate affect the micropores distribution size to some extent [Gonzales et al, 1997]. The chemical activation is considered as a suitable method for producing highly microporous activated carbons. The most common activating agents are potassium hydroxide, phosphoric acid and zinc chloride. In comparison with the physical activation, the chemical activation mechanism is not well understood [Lozane-Castello et al, 2001], but it seems that the chemical agent dehydrates the sample, inhibits the tar formation and volatile compounds evolution, and therefore enhances the yield of the carbonization process [Rodriguez-Reinoso, 1997, Williams and Reed, 2004]. After impregnating the precursor by chemical agent and heat treatment of the mixture, the impregnating agent is eliminated by washing with acid/base and water. The washing step makes the pore structure available, by removing the impregnating agent and its salts. In some cases, the precursor is in the form of fiber, cloth, or felt and the final activated carbon is in the same form. The recovery of chemical agent is the most determinant step for the economy of this process [Rodriguez-Reinoso, 2002].

Fig. 2.4 shows the general flow sheet for chemical activation [Rodriguez-Reinoso, 2002]. Zinc chloride ($ZnCl_2$) was used as the first chemical agent for chemical activation, but because of environmental concerns associated with zinc compounds it was displaced by other chemical agents. The activated carbon produced by $ZnCl_2$ activation are dominantly microporous, but with a significant mesopores which increases by an increase in the impregnation ratio ($ZnCl_2$/precursor) [McEnanney, 2002].

The use of phosphoric acid is increased in industry for either non-carbonized or carbonized raw materials, especially because of the improvement in the process of acid

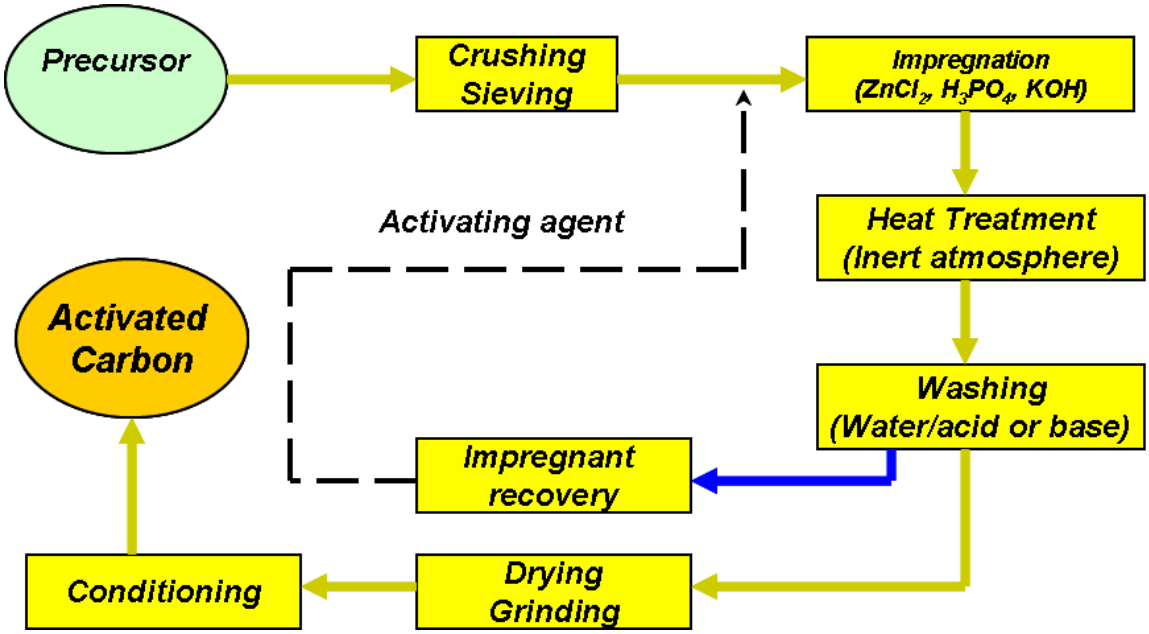

Fig. 2.4: The general flow sheet for chemical activation

recovery in recent years. This method produces activated carbons with finer pores in comparison with $ZnCl_2$ [Rodriguez-Reinoso, 1997; Teng et al, 1998].

Activated carbon with highly developed microstructure, even with BET surface area more than 3000 m^2/g, can be produced by KOH chemical activation [McEnanney, 2002; Otowa et al, 1997; Robau-Sanchez et al, 2005]. Generally, the surface area is a function of the KOH to precursor weight ratio. However, the high cost for the chemical agent recovery and low bulk density are the main problems for commercializing this process [Rodriguez-Reinoso, 2002]. The development of porosity in KOH chemical activation is somehow different from that for $ZnCl_2$ and H_3PO_4. It can be a result of the reduction of KOH to potassium by a reaction such as given below:

$$4KOH + C = 4K + CO_2 + 2H_2O \qquad (2\text{-}5)$$

Then, this free metal (K) penetrates between the graphene layers of the carbon which expands the structural graphene layers. Finally, with increasing temperature, the free metal is removed rapidly from the graphene layers thus creating the microporosity [Marsh and Rodriguez-Reinoso, 2006].

2.2.3. Applications

Activated carbons have a wide range of adsorptive and catalytic applications for gas-phase and liquid-phase as follows;

2.2.3.1. Gas-phase applications

Activated carbons are widely used for gas-phase applications because of their developed porosity which provides high adsorptive capacity per unit volume and their

flexible surface chemistry which makes them suitable for different applications. In addition, a large capacity for gas adsorption in the presence of moisture and high desorption capacity at low pressures and high temperatures are other positive aspects of using activated carbons for gas-phase application [Rodriguez-Reinoso, 1997].

Solvent recovery: Activated carbon can be used for recovery of solvents such as acetone, pentane, methylene chloride, and methyl ethyl ketone. The recovery is performed using an adsorption-desorption cyclic process. This method is used in many industries such as dry cleaning, the manufacture of paints, adhesives, and polymers [Derbyshire et al, 1995].

Gas storage: Methane has a greater ratio of H/C than other fuels and therefore, possesses higher amount of energy per unit mass, but methane density is lower compared to that of other hydrocarbons and hence, it is not preferable to store it [Cook et al, 1999]. The strong adsorption potential of micropores can significantly increase this density. The use of activated carbon can provide the same delivery (per unit volume of storage) at relatively low pressure of 3.5 MPa in comparison with the storage of liquid methane at much higher pressure of 20 MPa. This method reduces the cost and potential risks of high pressure systems [Rodriguez-Reinoso, 2006].

Catalyst support and Catalyst uses: Activated carbon can be used as catalyst support because of a) its resistance to acidic and basic compounds, b) its well developed porosity, c) the importance of carbon surface inertness in the activity and selectivity of catalysts, d) its stability at high temperatures (even above 1000 K) in the absence of air, e) easy recovery of precious metals (as active site) by burning away the carbon support, and f) lower cost of carbon supports in comparison with conventional support such as alumina

and silica [Rodriguez-Reinoso, 2006]. There are many commercial catalysts using activated carbon as support, especially for palladium, platinum, iron, etc [Rodriguez-Reinoso, 1997]. The internal surface area of carbon support was found as one of the effective parameters on the activity of catalyst [Rodriguez-Reinoso, 1990]. Several industrial reactions use activated carbon as catalyst. Table 2.1 shows a brief overview of these reactions [Trim, 1981]. There is a good correlation between surface area of activated carbon and the catalyst activity in case of carbon supports, but generally this correlation is not observed for carbon catalysts [Rodriguez-Reinoso, 2006] and parameters such as surface chemical characteristics must be considered too.

2.2.3.2. Liquid-phase applications

Consumption of activated carbons for liquid-phase is more than that for gas-phase because of more large-volume applications for the former use [Baker et al, 1992]. Activated carbons used for liquid-phase applications are mostly meso- or macroporous. The larger pore size of these activated carbons is suitable for the adsorption of large size dissolved molecules and facilitates the diffusion of liquid phase into porous structure of activated carbon [Hutchins, 1980; Rodriguez-Reinoso, 1997; Rodriguez-Reinoso, 2002].

Water treatment: The presence of natural organic materials in potable water affects its taste and odor. Synthetic organic materials produced mostly by chlorination of water are another source of water contamination. Activated carbons because of their adsorptive properties and selectivity are widely used for this application. Small organic molecules have dimensions of 6-8 Å and can be adsorbed in micropores. Color bodies and humic acids are in the size range of 15-30 Å which can be mostly adsorbed in mesopores.

Table 2.1: Some reactions catalyzed by activated carbon [Trim, 1981]

General type	Examples
Reactions involving hydrogen	$RX+H_2 \rightarrow RH + HX$ (X= Cl, Br) $HCOOH \rightarrow CO_2+H_2$ $CH_3CHOHCH_3 \rightarrow CH_3COCH_3+H_2$
Reactions involving oxygen	$SO_2+(1/2)\ O_2 \rightarrow SO_3$ $NO+(1/2)O_2 \rightarrow NO_2$ $H_2S+(1/2)O_2 \rightarrow S+H_2O$
Reactions involving halogen	$CO+Cl_2 \rightarrow COCl_2$ $C_2H_4+5Cl_2 \rightarrow C_2Cl_6+4HCl$ $SO_2+Cl_2 \rightarrow SO_2Cl_2$

Bacteria have diameters of 5,000-20,000 Å which are suitable for adsorption in macropores [Derbyshire et al, 1995].

For adsorption of polar compounds such as phenol, surface chemistry plays an important role in comparison with porous structure [Mahajan et al, 1980]. Both granular and powdered activated carbons are used for water treatment. For low dosage of contaminants, normally activated carbon can last for around one year and therefore powdered activated carbon, which is cheaper, is used, whereas for higher dosages, granular activated carbon is used which can be regenerated easier [Rodriguez-Reinoso, 1997].

Decolorizing in sugar industry: Activated carbon is used to remove the color from sugar which is originated from the raw material and/or the refining process. The last step in the decolorization of sugar is performed by activated carbon to remove compounds such as dyes, caramels, iron oxides which results in a white product as well as facilitates the crystallization and separation of sugar crystals [Rodriguez-Reinoso, 1997].

Gold recovery: After the treatment of finely ground ore with sodium cyanide and oxygen, gold in cyanide form is extracted in a solution with other metals. It can be adsorbed by activated carbon and then be recovered by elution using metal salts or organic solvents [Derbyshire et al, 1995; Rodriguez-Reinoso, 2002].

2.2.4. Porous structure

2.2.4.1. BET surface area and assessment of microporosity

The Brunauer-Emmett-Teller (BET) analysis method [Brunauer et al, 1938] is the most common method used to characterize internal surface area for more than 70 years.

They extended the Langmuir mechanism to multilayer adsorption. The Langmuir model is more applicable for some forms of chemisorption [Rouquerol et al, 1999]. The BET model is used for describing physical adsorption and is based on the following assumptions [Uzio, 2001]:

a) Each site is similar in nature and can accept one adsorbed molecule, and surface is homogeneous.

b) The adsorbate molecule is small enough to completely cover the surface.

c) No interaction between the adsorbed molecules

d) For second and higher layers, the adsorption energy is equal to that of the condensation and is constant for all layers.

The BET equation can be shown as follows:

$$\frac{p}{V_a(p^o - p)} = \frac{1}{V_m C} + \frac{C-1}{V_m C}\left(\frac{p}{p^o}\right) \qquad (2\text{-}6)$$

where, V_m = monolayer capacity, p^o= gas saturation pressure, p= gas pressure, C= constant which is related exponentially to the heat of the first-layer adsorption [exp $(q_1 - q_L)/(R*T_a)$], and V_a= amount of gas adsorbed on the surface at pressure p. According to this equation, a plot of $p/[V_a(p^o-p)]$ vs. p/p^o should yield a straight line with intercept of $1/V_mC$ and slope of $(C-1)/V_mC$. Therefore, the values of V_m and C can be calculated using this line. Practically, the linearity of this plot is always restricted to a part of the isotherm [Gregg and Sing, 1982]. For many materials, the range of linearity is for relative pressure of 0.05-0.3, but for activated carbons it is limited to relative pressures less than 0.1 [Sing, 1995].

The pore filling by adsorbate includes a two-step process for defined range of relative pressure; monolayer formation followed by a condensation process. Micropores can be

divided into two groups: a) Ultramicropores (pore diameter less than 7 Å) and b) Supermicropores (pore diameter in the range of 7-20 Å). This mechanism can be used for adsorption on supermicropores at high relative pressures [Greg and Sing, 1982]. But, in narrow micopores (ultramicropores), the pore fills in a single step over a narrow range of relative pressure. The narrowest pores commence filling at very low relative pressure, e.g. 10^{-8}, which is associated with enhanced adsorbent-adsorbate interactions [Rouquerol et al, 1999]. The micropores are filled by adsorptive before the formation of monolayer coverage on the surface. Some assumptions for derivation of the BET equation are in doubt as follows: 1) all sites are identical, 2) all layers after the first one have liquid-like properties, and 3) interactions between adsorbate molecules can be neglected [Rouquerol et al, 1999; Web and Orr, 1997].

In spite of these facts, the BET equation is still the most commonly used isotherm equation for microporous materials and can be used for comparing the surface area of activated carbons.

In the last 50 years many researchers tried to develop new methods for study the porous structure of micropores and their pore size distribution. Dubinin's theory of pore filling in micropores was used in the development of some equations such as Dubinin-Radushkevich (DR) and Dubinin-Astakhov (DA) [Dubinin and Astahakov, 1971] to calculate pore size distribution in micropores. There are some other methods for calculation of pore size distribution based on t-curve methods such as MP method [Mikhail et al, 1968] and Horvath-Kawazoe (HK) method [Horvath and Kawazoe, 1983].

Horvath and Kawazoe (HK) method is a semi-empirical, analytical method to calculate pore size distribution using nitrogen adsorption isotherm for microporous

materials. The basis of this method is a statistical analysis for a fluid with slit pores which is applicable to active carbons [Lowell and Shields, 2004]. An extension of the HK method was developed by Saito and Foley [1995] for cylindrical pore geometry. Everett and Powl [1976] calculated the potential energy profiles for nobel gas atoms adsorbed in a slit between two graphitized carbon layer planes. Horvath and Kawazoe related this energy to free energy change of adsorption, resulting in a relation between filling pressure and the effective pore width.

The basic idea of HK method is that the relative pressure required for the filling of micropores with a given size and shape is a function of adsorbent-adsorbate interaction energy [Rouquerol, 1999]. This method is not applicable for mesopore size analysis [Lowell et al, 2004]. The accuracy of this method is under discussion because of; a) the assumption that the fluid confined in the pore is similar to bulk fluid, b) the density of fluid is assumed not to be a function of its distance to the pore wall, and c) discontinuous mechanism assumed for pore filling [Lowell et al, 2004].

The limitations of macroscopic-thermodynamic approaches, e.g. the DR method, and semi-emperical methods such as Horvath-Kawazoe (HK) method for explaining the micropore filling resulted in using molecular-based theories based on the molecular modeling of adsorption phenomena. Density functional theory (DFT) is one of these methods. This method can be used for measuring the pore size distribution in micropores and mesopores.

Density functional theory: In traditional adsorption theories, an isotherm equation containing some parameters were used to describe adsorption isotherms and the methods were empirical [Rouquerol et al, 1999] or were based on macroscopic quantities [Lowell

et al, 2004], but using the molecular-based statistical thermodynamic theory, adsorption isotherms can be explained by microscopic properties such as the fluid-fluid and fluid-solid interaction energy parameters, the pore size, the pore geometry, and the temperature. This method can be used to study the pore size distribution for a wide range of pores (micropores and mesopores). Density functional theory (DFT) is based on the statistical thermodynamics and mechanics [Olivier, 1995; Balbuena and Gubbins, 1992] and can describe inhomogeneous systems. In this model, pores are presented by slit-shape and smooth graphite walls. At defined temperature and pressure, fluid (adsorptive) is confined in an open pore with known pore size and shape. The bulk fluid is a homogeneous system with constant density. Its chemical potential is specified by the pressure. Because of adsorption forces of the pore walls, the confined fluid is inhomogeneous and is not of constant density. This density distribution is a function of distance from the walls [Rouquerol et al, 1999]. At equilibrium, system has minimum free energy known as the grand potential energy (GPE). DFT introduces GPE as a function of the single-particle density distribution. The density profile can be calculated by minimizing the GPE. The calculation method requires iterative numerical methods for the solution of a system of complex integral equations [Webb and Orr, 1997].

2.2.4.2. Assessment of mesoporosity

Gas adsorption method: The pore space of a mesoporous solid is filled with condensed adsorbate at pressures below the saturated vapour pressure of the adsorbate. Kelvin equation (Eq. 2.7) was developed by combining the above concept with a correlating function that relates pore size with critical condensation pressure. This

equation helps to characterize the mesopore size distribution of the adsorbent. This equation can be shown as follows:

$$\ln\left(\frac{p}{p_o}\right) = \frac{2\gamma V_l \cos(\theta)}{RT_a r_m} \qquad (2\text{-}7)$$

where, γ and V_l are the surface tension and molar volume, respectively, of the adsorbate, R is the gas constant and T_a the absolute temperature. In this equation, p_o is the equilibrium pressure of the liquid on a flat surface, but p is the equilibrium vapor pressure of the liquid in the pore with a curved surface (critical condensation pressure) [Lowell et al, 2004]. The r_m is pore radius. θ is the angle between mercury and surface.

Eq. 2-7 is used for calculation of pore size distribution. This procedure involves filling/emptying of condensed adsorptive in the pores in a stepwise manner as the relative pressure is likewise increased/decreased [Sing, 1995]. The mathematics of the technique is equally applicable whether following the adsorption branch of the isotherm downward from high to low pressure or following the desorption branch. The relative pressure of 99.5 % (p/p^o=0.995) is the condition where all pores are to be considered filled. The calculation method follows generally that described by Barrett, Joyner, and Halenda [Barrett et al, 1951], hence called the BJH method. One of disadvantages of this method is underestimating the pore sizes and that its reliability may not extend below a pore size of 75 Å [Seaton et al, 1989; Lastoskie et al, 1993a; Lowell et al, 2004].

Mercury porosimetry: Mercury porosimetry is applied to a wide range of pore sizes, which includes both mesopores and macropores. Mercury does not wet the surface of carbon and its contact angle with a carbon surface is greater than 90^o. Mercury porosimeter data are usually presented as a cumulative open-pore volume distribution, i.e. cumulative amount of mercury intruded versus open pore entrance diameter which is

obtained from pressure measured by the Washburn equation (Eq. 2-8). The mercury porosimetry can also be used to obtain the cumulative open-pore surface area of macropores.

$$D = \frac{-4\gamma \cos\theta}{p} \tag{2-8}$$

The commercial mercury porosimeters can attain maximum pressures of 60,000 psia (414 MPa). They include two sections: low-pressure and high-pressure. The low-pressure section primarily is for evacuating and preparing the sample. The largest pore that can be measured conveniently with each instrument is 360 μm in diameter, and the smallest pore diameter measurable is 0.006 μm (60 Å) in the lower maximum pressure units and 0.003 μm (30 Å) in the higher maximum pressure units.

There are some limitations for mercury porosimetry as follows [Rodriguez-Reinoso, 1997]: 1- There are practical problems of selecting suitable values of γ and θ to use in the Washburn equation. 2- The Washburn equation assumes cylindrical pores, but the type of the pores can be different for various samples. 3- The mercury intrusion at high pressure can damage the porous materials. Existing open-pore walls may be prized apart and pore walls may be breached, allowing access to previously closed porosity. Conversely, compaction may occur leading to closure of previously opened pores. 4- Perhaps the most serious limitation of the Washburn equation is that the model of non-intersecting, cylindrical capillaries neglects pore network effects. In most porous solids, pores of different sizes are interconnected and the manner of their connection can play an important role in analysis by mercury porosimetry. The partial overlap in pore-size ranges between mercury porosimetry (3.5 nm-200 μm) and pore-size distributions determined by gas adsorption (2-50 nm) enables the two methods to be compared.

2.2.4.3. Assessment of macroporosity

Although the main internal surface area is formed by micro- and mesopores, macropores have a significant effect on mechanical and thermal properties. The thermal conductivity decreases with an increase in porosity of materials such as in case of activated carbon and number of macropores has a greater effect on this property in comparison with that for other types of pores. An increase in porosity decreases the mechanical properties because of the reduction in cross sectional area required for distribution of stresses [McEnany and Mays, 1995].

To characterize the macropores, both open and close pores have to be considered. Mercury porosimetry, as mentioned in last section, can be used for characterization of macropores.

Fluid flow method: This method is used for characterization of open macropores. In this method, experimental measurements of a known external fluid condition are used for estimation of geometry of macropores using an assumed model pore structure. The structure of macropores in activated carbons is so complex that it can not be defined precisely. Therefore, a model for that is assumed and the parameters of fluid flow are defined according to that model [Hewitt and Morgen, 1964; Hewitt, 1965; Grove, 1967]. This approach helps to relate flow, fluid conditions and pore structure. Normally, pores are divided into two groups of transport and blind. The fluid flows during steady-state condition through the first group, but blind pores cause pressure and concentration gradients and flow in unsteady-state. The most common fluid flow models are developed by measurements for a) isothermal, steady-state permeation of a pure gas and b)

isothermal, isobaric, steady-state diffusion of components of a binary gas mixture [McEnany and Mays, 1995].

Quantitative microscopy of carbon macropores: Modern computer-based image analysis methods for quantitative microscopy have been also used to characterize the macroposity for different carbons [Rodriguez-Reinoso, 1997]. This method needs no assumption about pore model. To view the macropores, an optical microscope or scanning electron microscope (SEM) can be used which have the resolution equal to 1 μm and 0.05 μm, respectively. This method can provide qualitative information regarding the pore size, pore shape, the orientation of pores [McEnany and Mays, 1995].

2.2.5. Surface chemistry

The adsorptive and catalytic properties of activated carbon are determined not only by its porous structure but also by its surface chemistry. Due to hydrophobic character of activated carbon, it is supposed to be only a good adsorbent for non-polar compounds, but because of defects in microcrystalline structure, the presence of ash compounds and heteroatoms, activated carbon can be used for adsorption of polar molecules [Rodriguez-Reinoso, 1997]. These heteroatoms have a greater effect than inorganic ash compounds on the catalytic and adsorptive properties of activated carbon. The source of heteroatoms can be precursor, activation agent/method, and post-treatments [Bansal et al, 1988]. Oxygen, hydrogen, nitrogen, phosphorus, sulphur, and halogens are the main heteroatoms in the activated carbon structure. Hydrogen is bonded to edge atoms of graphene layers but others are connected to edges and also in-ring within graphene layers [Rodriguez-Reinoso, 2006]. These atoms form acidic, basic or neutral functional groups, somehow

similar to those in organic chemistry [Puri, 1970; Boehm, 1994; Boehm, 1966; Fanning and Vannice, 1993]. These heteroatoms, by changing the acidic/basic character of carbon, can contribute to changes in the catalytical properties of the matrix [Leon et al, 1994 ; Stohr et al, 1991; Lahaye et al, 1999].

2.2.5.1. Oxygen surface groups

Oxygen surface groups have most significant functionalities on the activated carbon surface because of their abundant quantities in comparison with other surface groups and also they have large effects on the catalytic and adsorptive properties of activated carbon. The chemical structures of some of oxygen surface groups are shown in Fig. 2.5 [Rodriguez-Reinoso and Molina-Sabio, 1998].

Carboxylic, lactone and hydroxyl groups of phenolic character, which are present on activated carbon surface, are considered as weakly acidic groups of Brönsted-type acid base reactions [Boehm, 1994; Donnet, 1968; Leon et al, 1994; Puri, 1970]. Rest of groups such as pyrone, chromene, and quinone are more basic in nature [Boehm, 1994; Garten and Weiss, 1957; Menendez et al, 1999; Montes-Moran et al, 2004]. Basic properties of chromene-like structure which can be neutralized by hydrochloric acid were studied in the 1950s [Garten and weiss, 1957]. The contribution of pyrone-like structure in graphene layer or in some reactions involving with proton addition was shown by researchers [Voll and Boehm, 1971; Boehm, 1994]. In ammonia treatment, nitrogen can replace the ether-type oxygen and increases the basic characteristic of the surface [Boehm, 1994]. Researchers have also suggested the presence of quinone group (See Fig. 2.6) on carbon

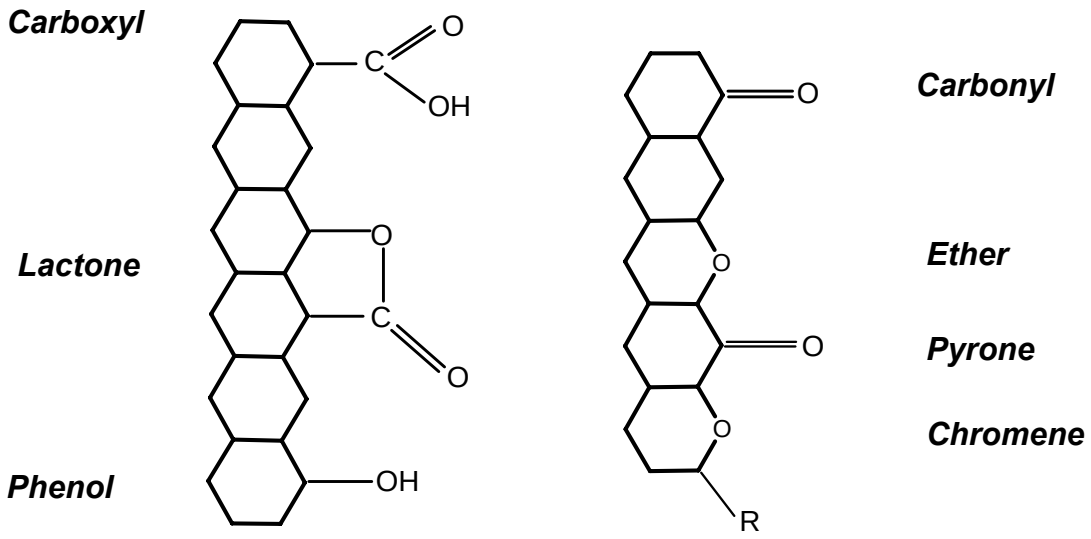

Fig. 2.5: Examples of oxygen functional groups on carbon surface [Redrawn from Rodriguez-Reinoso and Molina-Sabio, 1998]

which can bind protons from aqueous solutions [Leon et al, 1994; Contescu et al, 1998; Epstein et al, 1971; Menendez et al, 1999].

The origin of surface basicity is still under discussion. Besides those oxygen surface groups which act as basic sites, one reason for a basic behavior of carbon surface can be the π basicity of the exposed graphene layers [Boehm and Voll, 1970; Leon et al, 1992; Montes-Moran et al, 1998]. Although this basicity is relatively weak [Boehm, 2002], it is sufficiently basic to bind protons from aqueous solutions [Rivin, 1963; Leon et al, 1992] and are able to work as Lewis base centers [Fabish and Schleifer, 1984; Menendez et al, 1996; Menendez et al, 1996a].

Oxygen can be adsorbed on the carbon surface by physisorption at low temperatures and by chemisorption at high temperatures. In the later case, oxygen atoms are produced by dissociation of oxygen molecule and form oxygen surface groups after reaction by carbon atoms. All types of carbon are metastable against oxygen-containing gases and oxidizing agents [Rodriguez-Reinoso, 2006]. Generally, carbon-oxygen complexes can be formed by reaction of carbon with oxidizing agents such as ozone and nitric oxide, or with oxidizing solutions such as nitric acid and hydrogen peroxide [Rodriguez-Reinoso and Molina-Sabio, 1998]. These processes bind oxygen to carbon skeleton and form structures with different chemical and thermal stability. The oxygen surface functionalities are stable below 200 ^{o}C, but at higher temperatures they decompose to water, carbon monoxide and carbon dioxide. CO_2 evolution is related to carboxylic groups, some anhydride and lactone groups and less acidic groups containing –OH functions [Otake and Jenkins, 1993; Malino-Sabio et al, 1991; Rodriguez-Reinoso and Molina-Sabio, 1998; Rodriguez-Reinoso, 2002]. CO evolution is attributed to some

oxygen surface groups such as quinone, carbonyl, and ether oxygen [Rodriguez-Reinoso and Molina-Sabio, 1998; Marsh and Rodriguez-Reinoso, 2006]. It is believed that the peak of CO evolution, especially above 475 ^{o}C, relates to desorption of more basic and inert (stable) oxygen groups [Rodriguez-Reinoso, 2002].

Fig. 2.6 shows some surface groups on activated carbon and their decomposition temperature ranges by temperature programmed desorption (TPD) [Figueiredo et al, 1999]. Studies performed in last two decades showed that surface chemistry of activated carbon can be changed by oxidizing agents or oxidizing solutions. These oxidizing agents produce some oxygen functionalities on the surface of activated carbon [Rodriguez-Reinoso, 1997; Pradhan and Sandle, 1999]. This process was used for improvement of adsorption for hydrogen sulphide at 550 ^{o}C [Cal et al, 2000] and organic compounds [Ania et al, 2002] on activated carbons. As it was discussed in this section, heat treatment of activated carbon under an inert atmosphere (thermal desorption) can be used separately or following acid-treatment for selective decomposition of surface groups [Tremblay et al, 1978] and tailoring surface chemistry of activated carbon for special applications [Rodriguez-Reinoso and Molina-Sabio, 1998]. This method was used for improvement of sulphur dioxide adsorption by activated carbon at temperature range of 80-120 ^{o}C [Lizzio and DeBarr, 1996] and for H_2S oxidation by Brazhnyk et al [2007].

2.2.5.2. Nitrogen surface groups

Nitrogen incorporation affects the adsorptive and catalytic properties of activated carbon [Stohr et al., 1991; Adib et al, 2000; Bagreev et al, 2002; Pels et al, 1995; Mochida et al, 2000; Elsayed and Bandosz, 2002] .

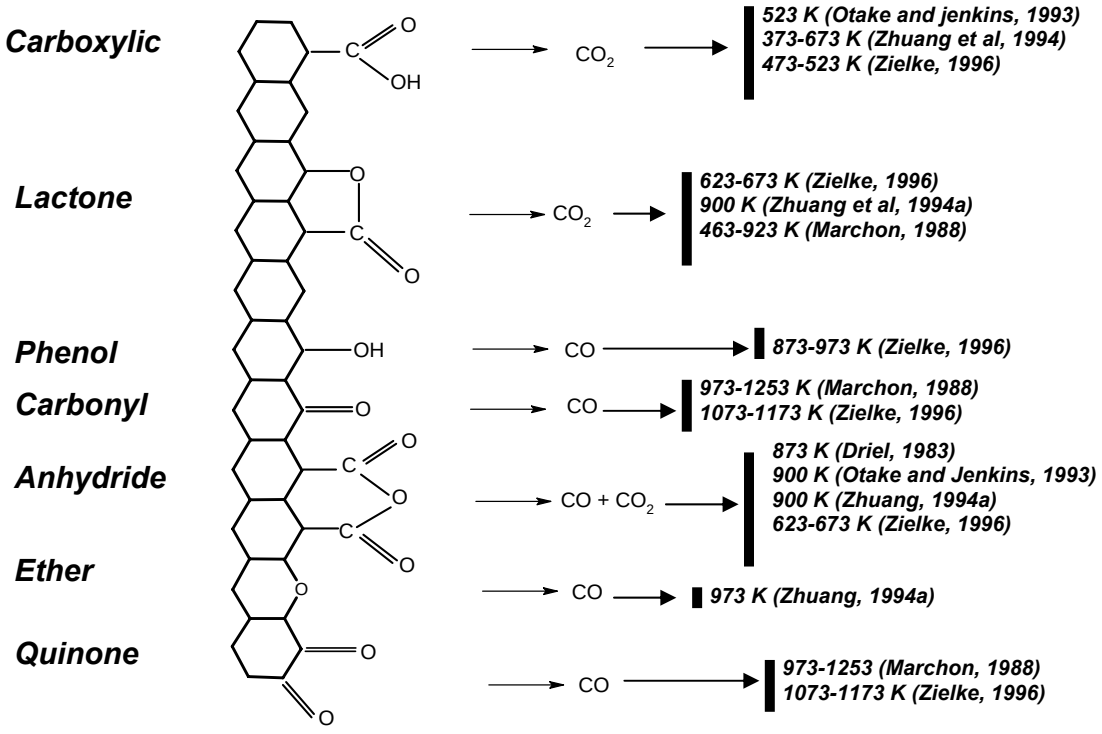

Fig. 2.6. Oxygen surface groups on carbon and their decomposition temperatures by TPD [Redrawn from Figueiredo et al, 1999]

It can be due to the basic character of functional groups formed by incorporation of nitrogen within carbon matrix [Lahaya et al, 1999; pels et al, 1995]. One of the most effective commercial activated carbons for removal of hydrogen sulphide called Centaur® is produced by low-temperature nitrogen –modification using urea [Hayden, 1995; Mativiya and Hayden, 1994]. It was found that by increasing the temperature of the nitrogen modification processes, nitrogen tends to appear more within the carbon matrix [Marsh and Rodriguez-Reinoso, 2006; Bagreev et al, 2002] and produces more stable basic functionalities. The chemical structure of some possible nitrogen surface functionalities can be seen in Fig. 2.7.

Some researchers have used modification of nitrogen functionalities on the carbon surface for different applications. An activated carbon was modified by urea and melamine at 650-850 ^{o}C for hydrogen sulphide adsorption at room temperature [Bagreev et al, 2004]. Ammonia at 500-800 ^{o}C was used for modification of activated carbon to adsorb perchlorate at room temperature [Chen et al, 2005]. Other research groups showed that quaternary and pyridinic type nitrogen enhance sulphur dioxide adsorption [Bagreev et al, 2002].

2.2.5.3. Other surface groups

The aqueous HF treatment fixes no fluorine on the carbon surface, while HCl treatment produces some chemisorbed chlorine on the activated carbon surface. It can be due to weak acidity of HF in aqueous solutions (pK_a = 2.95 at 298 K) and strong acidity of HCl aqueous solutions (pK_a = -7 at 298 K). [Moreno-castilla et al, 1998; Puri B. R., 1970; Greenwood and earnshaw, 1986].

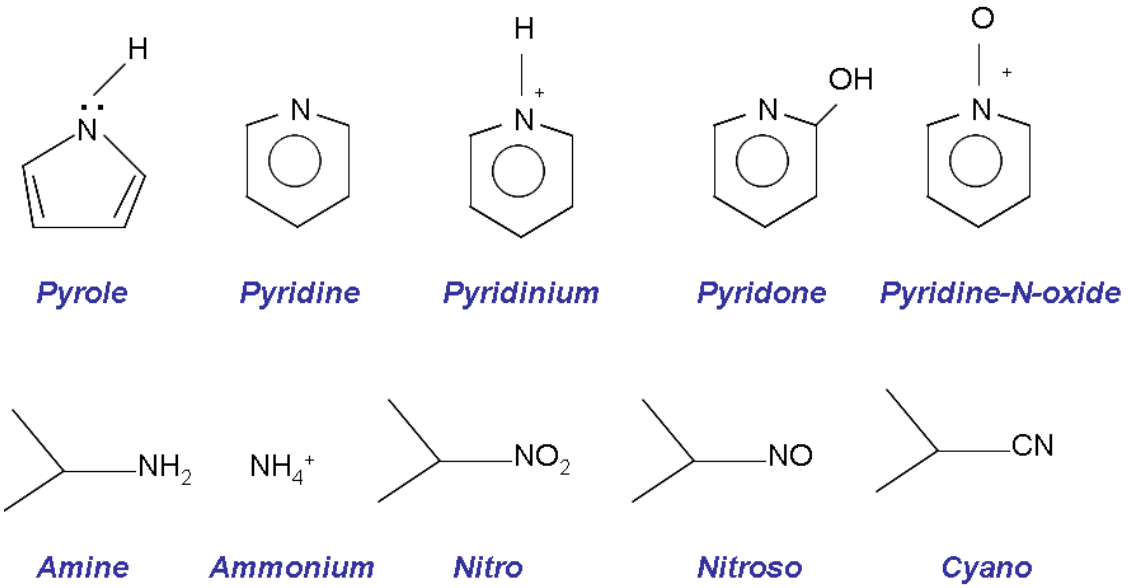

Fig. 2.7: Examples of nitrogen functional groups on carbon surface [Redrawn from Rodriguez-Reinoso, 2006]

Chlorine is bonded covalently to carbon and is distributed on the external and internal surfaces of carbon. This process increases the Lewis acidity of the activated carbon, but has negative effect on the Brönsted acidity of oxygen functionalities which can be explained by resonance effect introduced into aromatic rings of graphene layers [Perez-Cadenas et al, 2003]. Chemisorption of bromine on the carbon surface is also possible, but the bond qualities are lower [Boehm, 1994].

High-temperature hydrogen treatment removes oxygen and leaves a stable basic surface without active sites capable of oxygen adsorption at room temperature. Therefore, it helps to prevent the aging phenomenon for activated carbon [Menendez et al, 1996; Dastgheib and Karanfil, 2004]. In aging effect, activated carbon is gradually oxidized in the presence of oxygen [Corapcioglu and Huang, 1987; Adams et al, 1988]. Higher temperature and more severe conditions of H_2 treatment is more effective for preventing carbon aging process because of a) removal of more acidic oxygen functional groups, b) stabilization of free carbon sites against oxidation by forming stable C-H bonds, and c) decreasing concentration of active sites by gasification of the most reactive unsaturated carbon atoms [Menendez et al, 1996] .

2.3. Hydrogen sulphide

Hydrogen sulphide (H_2S) is a colourless and flammable gas with the odor of rotten eggs. It is heavier than air with a specific gravity equal to 1.19 . It can be produced naturally [Swaddle, 1997] or by human industrial activities, especially associated with oil and gas industry. Hydrogen sulphide (H_2S) present in gas streams is considered as an environmentally hazardous material which can cause corrosion of equipment [Craige and

Anderson, 1995] and catalyst poisoning. In addition, this gas is a serious threat for personal safety [Wang, 2003]. Hydrogen sulphide can remain in atmosphere for 15 hours and can be converted to sulphur dioxide (SO_2) and sulphuric acid (H_2SO_4) depending on process conditions. It is soluble in water and shows weak acidity function [ATSDR, 2006]. Hydrogen sulphide is one of the significant causes of casualties in the gas industry [Crammore and Stanton, 2000].

2.3.1. Toxicology

Hydrogen sulphide can be smelled in the range of low concentration of 0.0005-0.3 ppm. Exposure to low concentration of hydrogen sulphide causes irritation of eyes, throat, and/or nose [ATSDR, 2006]. At concentrations higher than 100 ppm, people can not smell it [Busca and Pistarino, 2003]. Any exposures to concentrations more than 500 ppm results in a loss of consciousness and can be fatal [ATSDR, 2006]. Exposure to high concentrations of hydrogen sulphide results in anoxia and damages directly to the cells of the central vascular systems [Wieckowska, 1995].

OSHA (the Occupational Safety and Health Administration) has established an acceptable ceiling concentration of 20 ppm for hydrogen sulfide in the workplace, with a maximum level of 50 ppm allowed for 10 minutes maximum duration if no other measurable exposure occurs. NIOSH (the National Institute for Occupational Safety and Health) has set a maximum Recommended Exposure Limit (REL) ceiling value of 10 ppm for 10 minutes maximum duration [ATSDR, 2006].

2.3.2. Sources

Hydrogen sulphide is one of the components in the bad breath of the mouth produced by natural bacteria. It can also be found in natural gases such as volcanic gases and hot springs [Swaddle, 1997].

Hydrogen sulphide is produced in many industrial activities such as oil refinery [Gary and Hendwerk, 2001], natural gas treatment [Crammore and Stanton, 2000] and production of synthetic gases by coal gasification [Cal et al, 2000]. Some hydrogen sulphide in refinery gases is produced by the conversion of sulphur compounds in some processes such as hydrotreating, cracking, and coking [Gary and Handwerk, 2001]. Natural gas is composed of a mixture of methane and ethane (light hydrocarbons), with smaller amounts of heavier hydrocarbons, as well other types of gases such as carbon dioxide, hydrogen sulphide, nitrogen and helium [Crammore and Stanton, 2000]. Natural gas being prepared for sale is required to contain no more than 5 ppm hydrogen sulphide [Mokhatab et al, 2006]. In addition, during the gas combustion process, hydrogen sulphide is converted to sulphur dioxide (SO_2) [Chandra, 2006], which is an air pollutant and causes acid rain [Allen and Shonnard, 2002; Miller, 2005]. The sulphur content in synthetic fuels obtained from coal can be in the range of 100-10,000 ppm depending on the type of the coal and the process [Kohl and Nielsen, 1997]. The concentration of hydrogen sulphide in the hydrogen produced from these synthetic fuels must be reduced further to make the fuel suitable for use in processes such as proton exchange membrane fuel cell, ammonia production, and hydroprocessing [Wu et al, 2005; Bashkova et al, 2007].

2.3.3. Hydrogen sulphide removal methods

2.3.3.1 Existing processes for removal of hydrogen sulphide

There are many physicochemical and chemobiological processes used for removal of hydrogen sulphide from gas streams. In most common methods for removal of hydrogen sulphide, the first step is an absorption stage which includes absorption into a solvent, stripping and then recycling the absorbent. Amine solutions and potassium solutions are used for absorption process [Mokhatab, 2006]. The amine solutions include MEA (monoethanolamine), DEA (diethanolamine), MDEA (methyldiethanolamine), and DGA (diglycolamine) [Gary and Handwerk, 2001; Busca and Pistarino, 2003]. Tripotassium phosphate (K_3PO_4) is a potassium solution which is used for absorption [Mokhatab, 2006]. The acid gas stream obtained from these treatment processes can include even more than 50 mol % of hydrogen sulphide [Gary and Handwerk, 2001]. After adsorption and regeneration of solvent, the acid gas stream is sent to sulphur recovery unit. In this unit, hydrogen sulphide is converted to elemental sulphur. There are two common methods for sulphur recovery; Claus process and Liquid redox.

Claus process: It is commonly used, especially in conjunction with an amine plant [Gary and Hendwerk, 2001; Thomas, 1970]. Hydrogen sulphide is converted to elemental sulphur in a Claus plant using partial oxidation with air in a series of reactors [Crammer and Stanton, 2000]. This process includes two steps:

Burner: $H_2S + (3/2)\ O_2 \longrightarrow SO_2 + H_2O$ (2-9)

Reactor: $2H_2S + SO_2 \longrightarrow 3\ S + 2H_2O$ (2-10)

First, the gas stream is burned with one-third of H_2S and its the stoichiometric amount of O_2 in air required for oxidation and then the hot gases containing SO_2 are passed through a series of fixed bed reactor including alumina catalyst at 200-300 ^oC to react with rest 2/3 of H_2S [Gary and Hendwerk, 2001]. This process is efficient only at H_2S concentration more than 5 mol % [Mikhalovsky and Zaitsev, 1997]. The conversion can reach up to 97% using three catalytic steps.

SCOT process: In large plants, to achieve higher conversions and remove traces of sulphur compounds, SCOT tail gas clean-up unit is used for tail gases of Claus unit. Claus unit tail-gas contains small amounts of hydrogen sulphide and sulphur dioxide which can be removed in a SCOT tail-gas clean-up unit. This unit uses chemical reaction at 250-300 ^oC through a fixed catalyst bed over a cobalt/molybdenum and converts various sulphur compounds to hydrogen sulphide by reaction with hydrogen [Rojey, 1997]. This hydrogen sulphide is selectively absorbed by an aqueous amine solvent and then is recovered and recycled to Claus unit. The efficiency of this method is more than 99 %, but the addition of a SCOT unit increases the cost of the sulphur recovery by two times [Gary and Handwerk, 2001]. To remove small amounts of H_2S (< 20 ppm), a bed of zinc oxide can be used [Crammore and Stanton, 2000]. However, zinc oxide needs to be replaced on a continuum basis adding to the overall cost of sulphur recovery process.

Liquid Redox process: "Liquid redox" is based on liquid phase oxidation using aqueous solution of iron or vanadium [Crammore and Stanton, 2000; Heguy and Nagl, 2003]. Generally, this method includes sorption of H_2S in a solution, oxidation of hydrogen sulphide/reduction of metal ion, and removal of participated sulphur/regeneration of metal ion in the solvent. The overall flow schemes of liquid phase

oxidation processes differ very little. These differences lie in the absorbing and oxidizing solutions. The main disadvantages of these methods are by-product sulphur salts, poor quality sulphur, and environmental problems for disposal of liquid acid solutions [Busca and Pistarino, 2003; Yang, 1996].

Direct gas phase oxidation process: This method is developed in last two decades. This method limits the oxidation reaction to produce sulphur and water using a highly selective catalyst. The direct oxidation reaction is highly exothermic therefore this method is limited to dilute H_2S gas streams. Superclaus from Comprime BV and MODOP from Mobil Oil Co. are some current field proven of DO processes [Kensell and Leppin, 1995]. The former uses iron metal on alpha-alumina substrate as catalyst and the second uses titanium dioxide based Claus catalyst. This area has not been fully developed and has the potential to reduce sulphur recovery and improve quality of sulphur.

Biological methods: Several groups of bacteria can use hydrogen sulphide as fuel, oxidizing it to elemental sulfur or to sulfate by using dissolved oxygen, metal oxides (e.g. Fe oxyhyroxides and Mn oxides) or nitrate as oxidant. Microbiological oxidation can be performed for less concentrations and/or lower pressure streams with the action of Thiobacillus thiooxidans such as the Shell-THIOPAQ process [Sublette, 1987]. In this process, low-concentration hydrogen sulphide is absorbed by a buffered alkaline solution on the first step. To remove hydrocarbons absorbed by caustic solution at high pressure (> 55 psig) on the first step, a low –pressure flash drum is needed between two steps [Beasley and Abry, 2003]. Then, using a bioreactor including aerobic Thiobacillus bacteria the absorbed hydrogen sulphide is converted to sulphur. This bacterium can oxidize sulphide or sulphur (at low pH) as its sole source of metabolic energy [Lizama

and Sankey, 1993]. The sulphur produced in the bioreactor is gravimetrically separated and directed to a dryer and sulphur melter. To prevent further oxidation of sulphur to sulphate a small caustic make-up has to be injected in the bioreactor, but normally less than 3.5% of the sulphide is converted to sulphate [Beasley and Abry, 2003]. This method is reliable for low production rates and produces low quality sulphur [Busca and Pistarino, 2003].

2.3.3.2. Catalytic oxidation of H_2S to sulphur using activated carbon

Activated carbon is known to be a catalyst for the oxidation of hydrogen sulphide to sulphur based on the following exothermic reaction:

$$H_2S + \left(\frac{1}{2}\right)O_2 \rightarrow \left(\frac{1}{n}\right)S_n + H_2O \qquad \Delta H = -206 \text{ kJ/mol} \qquad (2\text{-}11)$$

Where n denotes the allotrope of the sulphur molecule produced. n can be 2, 4, or 8 [Chowdhury and Tollefson, 1990]. The sulphur product remains in the pores of activated carbon. Scanning electron micrographs showed that elemental sulphur is formed first in the pores [Mikhalovsky and Zaitsev, 1997]. This sulphur covers the entire internal surface as a condensed phase and as the reaction proceeds, the active sites are gradually covered and are not available for the reactants. This deposition results in a slow deactivation of the catalyst [Dalai and Tollefson, 1998]. The most stable forms of elemental sulphur are rhombic and monoclinic. The latter is stable at temperatures above 96 ^{o}C while rhombic sulphur is stable at room temperature.

Studies on the oxidation of hydrogen sulphide using activated carbon were conducted at two different conditions; a) oxidation at room temperature in the presence of moist air [Meeyoo and Trimm, 1997; Bandosz et al, 2000; Adib et al, 1999; Primavera et al, 1998]

and b) oxidation at high temperature (100-250 ^{o}C) and dry conditions [Ghosh and Tollefson, 1986; Dalai et al, 1993; Dalai and Tollefson, 1998; Gardner et al, 2002; Wu et al, 2005;]. According to the literature, water has an important role in low-temperature oxidation and its presence enhances the performance of activated carbon and depending on the operating conditions, hydrogen sulphide can be oxidized to sulphur or sulphur dioxide.

For high temperature oxidation, it is reported that the reaction activity is maximized in the temperature range of 150-200 ^{o}C [Ghosh and Tollefson, 1986; Sreeramamourthy and Menon, 1974]. The formation of sulphur dioxide (SO_2) is a challenge in this process and its formation is significant especially above 300 ^{o}C. It is an undesirable byproduct of this process. SO_2 can react in the air with moisture and oxygen in the presence of sunlight to form mild solutions of sulphuric acid (H_2SO_4), which is one of the main reasons of acid rain [Allen and Shonnard, 2002; Miller, 2005]. The activity and selectivity of activated carbon for hydrogen sulphide oxidation is high and light hydrocarbons do not react adversely in the presence of activated carbons [Yang et al, 1998; Gardner et al, 2002].

To improve the performance of activated carbon for catalytic oxidation of H_2S to sulphur, impregnation with caustic materials such as NaOH [Chiang et al, 2000] and K_2CO_3 [Przepiorski et al, 1999] are used at low-temperature reactions. Although this method is effective for the removal of acid gases such as H_2S, these caustic-impregnated materials have low ignition temperatures [Bandosz et al, 2000] and are considered corrosive.

In this research, two different carbon precursors such as Saskatchewan lignite coal and biomass were used for the production of activated carbon. Activated carbons were

produced using two common activation methods; physical and chemical activation. The performances of these activated carbons and the modified activated carbons produced from them were evaluated for the H_2S oxidation reaction. Acid-treatment followed by thermal desorption was used as the modification method. The possible effects of porous structure, surface features, and ash content on the catalytic performance of activated carbons were studied.

3.0 Experimental

This chapter outlines the experimental procedures used in this work for physical activation, chemical activation, activated carbon catalysts modification, hydrogen sulphide oxidation reaction, and kinetic study. The chapter also describes the experimental set-ups used for activation and hydrogen sulphide oxidation reaction. In addition, it provides basic information about precursors used for activation processes as well as the details of characterization methods and equipment used for precursors, activated carbon catalysts, and products.

3.1. Precursors

Two types of precursors were used for the activation processes in this research: luscar char and biochar.

3.1.1. Luscar char: This precursor was supplied by Prairie Mines & Royalty Ltd. Their mine operations are being performed in Saskatchewan and Alberta in Canada as well as in some other countries. The source of this precursor was lignite coal which is the lowest rank of the coal [Highman and Van der Burgt, 2003]. The as-received precursor was sieved, and particles between -8 and +20 mesh (0.85 – 2.38 mm) were collected for steam activation.

3.1.2. Biochar: This precursor was produced from whitewood (Spruce) using fast pyrolysis process by Dynamotive Energy Systems Corporation. The operating conditions for this process were 500 ^{o}C, atmospheric pressure (in nitrogen gas), and residence time less than one second. The typical biochar yield from this process is 12 wt %

[Dynamotive, 2007]. The as-received char was sieved, and particles between -30 and +100 mesh (150 - 600 μm) were collected for activation processes.

3.2. Reactor set-ups

The schematic diagram of experimental set-up for physical activation process is shown in Fig. 3.1. A fixed bed, inconel tubular reactor (25.4 mm OD, 22 mm ID, length of 870 mm) was used for physical (steam) activation. A 3210-series furnace, made by Applied Test System Inc., mounted vertically on a steel frame was used to supply heat to the reactor. It could be operated to a maximum temperature of 1200 ^{O}C. For steam activation, char was placed on an inconel web welded to the wall of the reactor. Bed temperature was recorded by placing a K-type thermocouple in the middle of the char bed. Nitrogen flow (as the carrier gas) into the reactor was controlled by a mass flow controller (Brooks Instrument, 5850S/B). Temperatures of the furnace and boiler were controlled by two temperature controllers (Eurotherm 2416 and Schemaden SR22, respectively). Steam was generated in a boiler consisting of a 6.35 mm stainless steel tube embedded in a cylindrical insulated aluminum block. Water was injected to the boiler by using a metering pump (A-60-S, Eldex Laboratories Inc.). An ice bath was used to condense unreacted steam. The outlet gases were sent to the vent. The furnace temperature controller and mass flow controller were calibrated before performing all experiments. The reactor set-up as in the case of physical activation method was also used for chemical activation. The only change was the elimination of water line to the boiler.

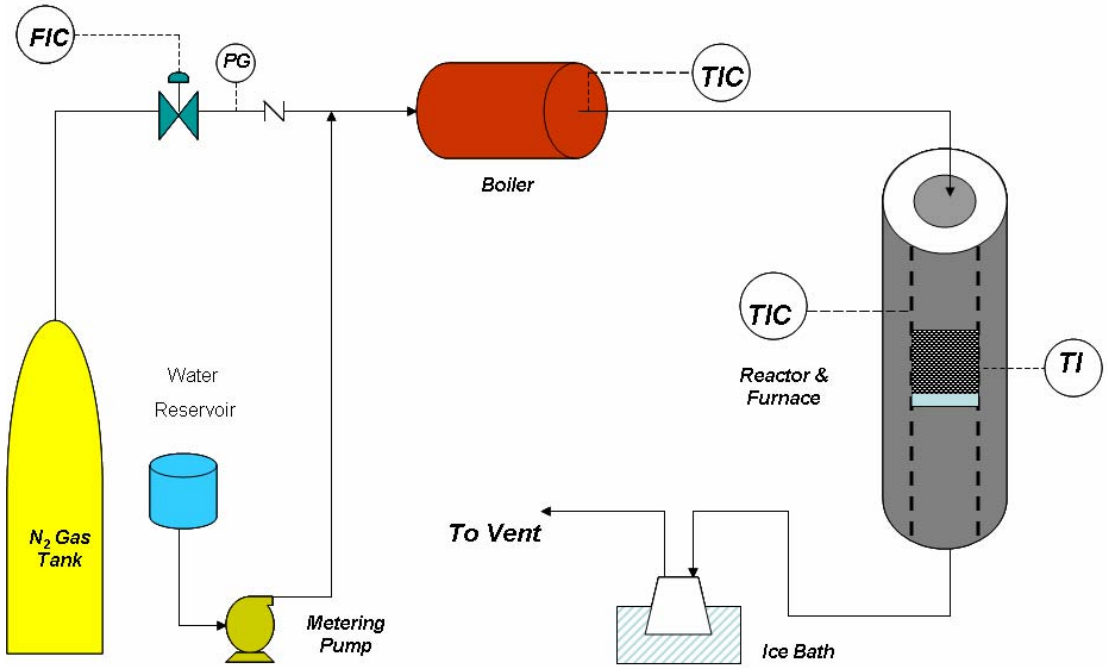

Fig. 3.1: The schematic diagram of the experimental set-up for physical activation

Fig. 3.2 shows the schematic view of reactor set-up used for hydrogen sulphide oxidation reaction. This reaction was carried out in a fixed-bed stainless steel reactor (12.7 mm ID and 300 mm length). A screen was fitted 20 mm from the end of the tube to support the activated carbon catalyst. The reactor was fitted into an aluminum block with a 55 mm diameter and was externally heated by a ceramic beaded electrical resistance coil placed in grooves on the outside of the aluminum block to provide a uniform temperature throughout the reactor. The aluminum block with heating coil was then wrapped with a layer of insulation to prevent the heat loss. The temperature of the reactor was controlled by an Eurotherm 2132 controller. The temperature calibration for different types of catalysts was performed using a K-type thermocouple in the center of the bed. The calibration curves are given in Appendix A. In addition, the thermocouple was moved along the bed while the reactor was heated with flowing nitrogen in order to determine the bed temperature profile. The maximum difference in bed temperature was in the range of 1 ^{o}C in comparison to the temperature of where the thermocouple was normally positioned (middle of the bed). Pressure inside the reactor was controlled by a 26-1727-24-043 back pressure regulator (BPR) made by Tescom Corporation. This back pressure regulator was protected from particulate matter by a SS-4TF-7 filter supplied by Swagelok.

Sour gas (1 mol % of H_2S in nitrogen as balance gas) and air (supplied by Praxair) flow-rates were controlled by two mass flow controllers (Brooks Instrument, 5850S and 5850TR) connected to read-out and control electronics type 0152 and 0152E supplied by Brooks Instruments. These mass flow controllers were calibrated by passing the gases through a bubble flow meter.

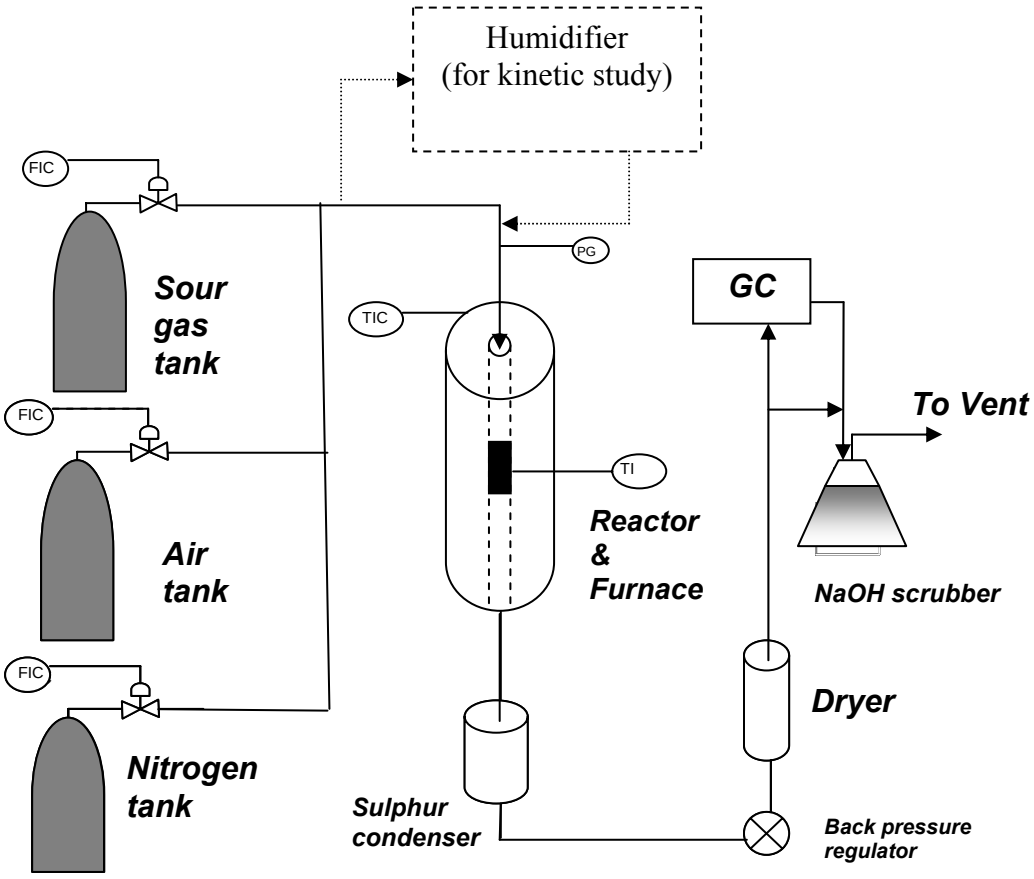

Fig. 3.2: The schematic diagram of the experimental set-up for hydrogen sulphide oxidation

Calibration curves for mass flow controllers are given in Appendix A. Nitrogen (supplied by Praxair) was used for pressurizing the system. The system pressure was measured by a Matheson pressure gauge (0-2800 kPa) placed before the reactor. The pressure gauge was verified by comparing with the regulated pressure read from nitrogen tank. The error associated in the pressure measurement from the gauge was less ±10 kPa.

The sulphur condenser was constructed from a 29 mm ID and 145 mm long stainless steel pipe. Flanges were welded on both ends and metal supports were welded 23 mm from the bottom of the pipe. The sulphur condenser was filled with glass wool to collect the condensed sulphur. The sulphur condenser was connected to the reactor via a 10-cm long connecting tube wrapped with heating tape. The line was externally heated to maintain temperature above 140 ^{o}C to prevent condensation of sulphur. Type 3PN1010 variac variable transformer supplied by Staco Energy Products Co. was used with Thermolyne flexible electric heating tape to heat the connecting tubing.

The dryer contained 8-mesh-size Dri-rite desiccant (provided by W. A. Hammond Drierite Co.) to remove the product water. The line between sulphur condenser and dryer, containing the filter and back pressure regulator, was heated to temperature above 110 ^{o}C using type 3PN1010 variac variable transformer with Thermolyne flexible electric heating tape to prevent condensation of water in the line. The connecting tubing temperatures (between the reactor and sulphur condenser, and sulphur condenser and dryer) were checked by a Cole Palmer model 8530 temperature indicator with a K-type thermocouple. The temperature was measured by placing the tip of the thermocouple on the outside wall of the stainless steel tubing.

The product gas was sent to GC for analysis, then was passed through sodium hydroxide (NaOH) scrubber to remove the unreacted hydrogen sulphide and was finally vented. A by-pass line was used for feed gas sampling for its analysis. A Varian CP-3800 gas chromatograph equipped with a pulse flame photometric detector (PFPD) was used on-line to detect the concentrations of hydrogen sulphide (H_2S) and sulphur dioxide (SO_2). Samples were automatically taken by GC every three minutes. The calibrations were performed using the reactor set-up by on-line injection of hydrogen sulphide and sulphur dioxide. The calibration curves are given in Appendix A.

3.3. Sample preparation procedures

Physical (steam) activation: The as-received lucar char was sieved, and particles between -8 and +20 mesh (0.85 – 2.38 mm) were collected for activation. The particle size range for biochar was -30 and +100 mesh (150 – 600 μm).

Chemical (KOH) activation: The as-received biochar was sieved, and particles between -30 and +100 mesh (150 - 600 μm) were collected for activation. Specified amount of potassium hydroxide was impregnated in biochar. The char was mixed with 100 ml of water having desired concentration of KOH. This mixture was kept for 2 hours at the room temperature to ensure the access of KOH to the interior of the biochar, and then was dried at 120 ^{0}C in an oven for overnight.

Acid (HNO_3)-treatment of activated carbon: Typically, 10 g of activated carbon was added to 64 ml of 70 wt % HNO_3 solution. This mixture was refluxed at 90 ^{o}C for 2.5 h using a reflux column to recover the acid evaporated during the operation. A magnet

stirrer was used for mixing during reflux. The sample was washed with water to remove remaining acid on it. The product was dried overnight.

Thermal desorption of activated carbon: 6.0 g of sample was heated under nitrogen flow to desorption temperature with a heating rate of 5 ^{o}C/min and held for one hour at that temperature. Then, the sample was cooled down to ambient temperature.

Impregnation of activated carbon: One gram of catalyst was completely wetted with aqueous solution containing appropriate amount of impregnating agent. The wet catalyst was placed into an oven and heated to 275 ^{o}C and held for three hours at that temperature. In the case of using Dimethyl Sulfoxide (DMSO) as impregnating solvent, the sample, after impregnation by solution, was washed by acetone to remove DMSO and then it was placed in the oven for heating as discussed above.

3.4. Design of experiment

The activation process was carried out following a standard Response Surface Method (RSM) design called Central Composite Design (CCD). This method can optimize the effective parameters with a minimum number of experiments, as well as to analyze the interaction effect between those parameters. Generally, the CCD consists of a 2^k factorial runs with 2k axial or star runs and n_c center runs (6 replicates) [Montgomery, 1997], where k is the number of parameters. For physical and chemical activation, the effects of three parameters were studied as follows:

Activation temperature (T), mass ratio of steam to char (S/C) and activation time (t) were the three parameters investigated for physical activation of luscar char and biochar. Activation temperature (T), mass ratio of KOH to biochar (R), and nitrogen flow rate (F)

were the three parameters investigated for chemical activation of biochar. The responses were BET surface area (Y_1) and reaction yield (Y_2). Six replications were performed at the centre point. Therefore, the total number of experiments (N) required is as follows;

$$N = 2^k + 2k + n_c = 2^3 + 2*3 + 6 = 20 \quad (3\text{-}1)$$

According to the range of each variable, the independent variables are coded to the (-1, 1) interval. The low and high levels are coded -1 and +1, respectively. Fig. 3.3 shows the layout provided by CCD for experiments needed to study a 3-parameter process. In this Figure, the factorial portion is represented by the points forming a box and the star (axial) points are located at the end of the arrows that come from the center point. The axial points are located at (± α, 0, 0), (0, ±α, 0), (0, 0, ±α) where α is the distance of the axial point from center and makes the design rotatable. Center runs include 6 replications which are performed by setting all factors at their midpoints to estimate the residual error. They can be considered as a barometer to evaluate the variability in the system [Lazic, 2004] and to estimate the residual error. Each parameter is varied over 5 levels: ±α (axial points), ±1 (factorial points) and the center points. α, the distance of the axial points from center, is equal to $(2^k)^{0.25}$ [Montgomery, 1997]. This kind of design provides equally good predictions at points equally distant from the center, a very desirable property for RSM. The value of α depends on the number of points in the factorial portion of the design; in fact, $\alpha = (2^k)^{0.25}$ [Montgomery, 1997]. Design-Expert software version 6 was used to design these sets of experiment.

3.5. Physical (steam) activation

Procedure for physical (steam) activation of luscar char is as follows:

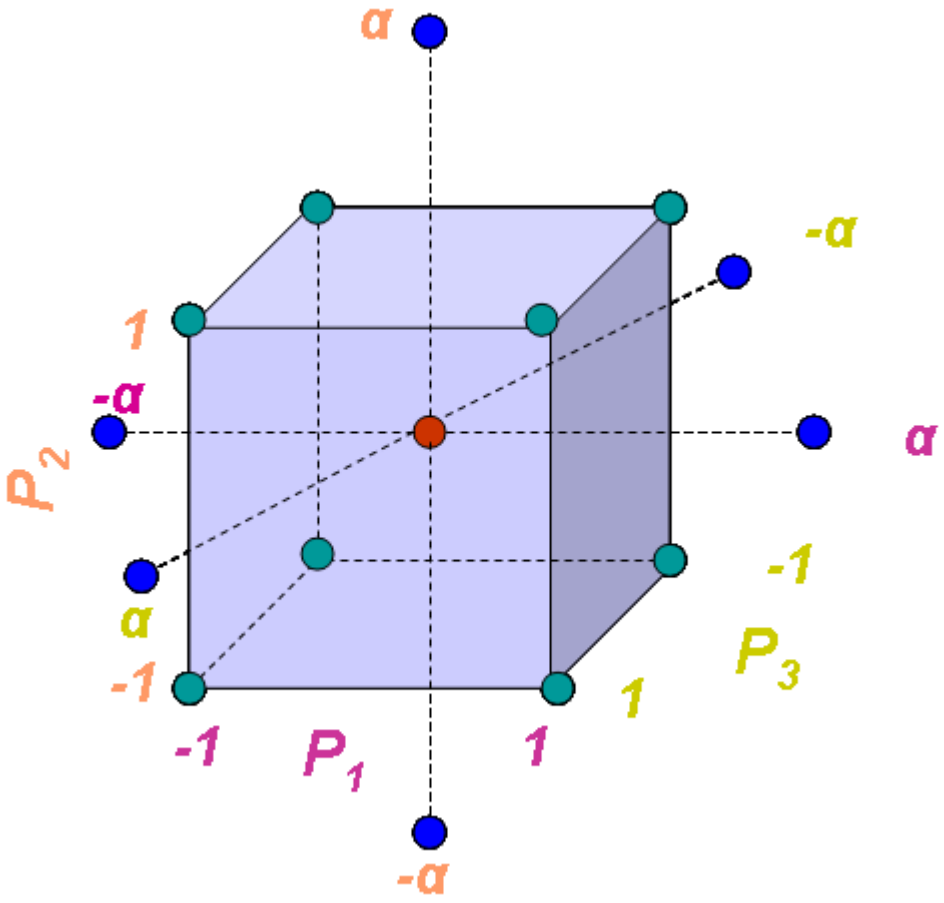

Fig. 3.3: Layout provided by CCD for experiments needed to study a 3-parameter process

i. 15.0 g of luscar char with the particle size range of 0.85-2.38 mm was placed in the reactor.

ii. The nitrogen stream was turned on and it was adjusted to 138 ml/min.

iii. The temperature increased to the activation temperature with the heating rate of 3 ^{o}C/min.

iv. The temperature controller of boiler was turned on and set at 250 ^{o}C.

v. After reaching the activation temperature, the injection of steam was started with desired flow rate and injection time.

vi. After finishing the injection, the temperature controller of boiler was turned off and the sample was cooled down under a slow ramp to reach the ambient temperature.

The same procedure was used for physical activation of biochar excepting using 20.0 g biochar with the particle size range of 150-600 μm.

3.6. Chemical (potassium hydroxide) activation

Procedure for chemical activation of biochar is as follows:

i. 20.0 g of sample prepared according to the procedure mentioned in section 3.3. for chemical (KOH) activation, was placed in the reactor.

ii. Nitrogen stream was turned on and it was adjusted to the desired flow rate.

iii. The temperature o fthe bed was increased to 300 ^{o}C with the heating rate of 3 ^{o}C/min and held at this temperature for one hour to prevent carbon loss by the direct reaction with steam [Otowa et al, 1997].

iv. The temperature was increased to the desired activation temperature with the same heating rate and held for 2 hours at that temperature.

v. Then, the sample was cooled down under a slow cooling rate to reach the ambient temperature.

vi. The product was thoroughly washed with distilled water, followed by 0.1 M HCl, and finally by distilled water to remove the soluble salts [Rodriguez-Reinoso, 2002], and the potassium compounds due to acid washing [Lozane-Castello et al, 2001]. The chlorine ions were eliminated with the distillated water [Lillo-Ródenas, 2001].

vii. When the pH of the filtrate was between 6 and 7, the sample was dried at 110 ^{O}C for 12 hours.

3.7. Hydrogen sulphide oxidation

3.7.1. Procedure for testing activated carbon catalysts

i. 1.000 g (dry base) of the activated carbon sample was weighed. Then, it was mixed with sand to ensure a constant 12 ml bed volume. Ottawa sand (20-8 mesh) was used for coal-based catalysts and other type of sand (100-45 mesh) provided by Acro Organics was used for biomass-based catalysts.

ii. The catalyst and sand mixture was placed inside the reactor on a small piece of glass wool on the screen at the bottom of the bed. The bed was not packed.

iii. An appropriate amount of glass wool to fill the sulphur condenser was weighed and loaded into the condenser.

iv. 15 ml of fresh Dri-rite desiccant was placed in the dryer.

v. The condenser, dryer, and the reactor were installed in the experimental system.

vi. A small stream of nitrogen was used to pressure the system to the experimental pressure using the back pressure regulator.

vii. The temperature controller was turned on and set on the desired temperature using calibration curve for the catalyst.

viii. The variac transformers were turned on to heat the connecting lines between reactor- sulphur condenser and sulphur condenser-dryer to 140 and 110 ^{o}C, respectively.

ix. The gas chromatograph was turned on to take the samples from outlet gases every 3 minutes.

x. The sour gas was turned on and adjusted to its operating flow-rate. The nitrogen was turned off after the sour gas was turned on.

xi. The air stream was turned on and adjusted to its required flow-rate.

xii. The process was stopped when H_2S conversion dropped to 80 %. System pressure was decreased to atmospheric pressure, the sour gas and air turned off, and a small stream of nitrogen flowed through the system until the reactor temperature was below 30 ^{o}C. A fan aided the cooling process. Gas chromatograph was turned off.

3.7.2. Procedure for regeneration of activated carbon catalysts

The activated carbon catalyst was tested in the same manner as described in section 3.7.1. Then, it was regenerated under the nitrogen flow-rate of 300 ml/min and operating temperature of 275 ^{o}C. Regeneration experiments were carried out for two different regeneration times of 8 and 24 hours to observe the effect of regeneration time. After each regeneration process, the catalyst was tested again for H_2S oxidation reaction.

3.8. Kinetic study

3.8.1. Procedure for determination of reaction kinetics

Kinetic study of H_2S oxidation reaction over activated carbon was performed using reactor set-up described in section 3.2. The catalyst (LusAC-O-D(650)) with particle size range of 150-208 μm was diluted by mixing with sand provided by Acro Organics to ensure bed length of 5 cm. Catalyst weight used for each run was 70 mg. The effects of O_2 and SO_2 were examined by changing their flow rates. Three different levels of oxygen flowrate (1, 2, and 3 * stoic.) were used for this study. A 0.5 mol % SO_2 (nitrogen as balance) cylinder was used to study the effect of SO_2. Three levels of SO_2 flowrate (40, 60, and 80 ml/min) were used in this study. The effect of H_2S concentration was examined by changing the concentration of H_2S in the feed (6000, 8000, and 10000 ppm). To study the effect of water concentration, a humidifier was connected to the reactor setup before the reactor and the feed stream was saturated with different amounts of water by varying the humidifier temperature which was controlled using a thermal heating tape connected to a variable transformer. The amount of water used for saturation of feed stream was determined by the weight loss of the humidifier. The humidifier was a

steel pressure vessel, 20 cm long with 7 cm diameter, with an inlet tube immersed into the vessel 4.3 cm from the bottom. The outlet was located at the top of the vessel. The humidifier must be saturated with hydrogen sulphide before starting the reaction. This is accomplished by flowing the sour gas through the humidifier and periodically analyzing the exit stream, until the exit stream composition matched the sour gas composition. The experimental design of this study is given in Tables 3.1-3.4. The run was performed as described in section 3.7.1.

3.9. Characterization methods

3.9.1. Ash content

Ash contents of samples were determined according to ASTM D 2866-94 (Approved 1999). This method includes the following procedure:

i. The sample was put into a crucible and was dried to constant weight at 150 ± 5 ^{o}C (generally 3 h is sufficient), then, the crucible was placed in a muffle furnace having air circulation at 650 ± 25 ^{o}C. Ashing requires from 3-16 h depending on the size and type of activated carbon. Ashing can be considered complete when constant weight is achieved.

ii. The crucible was placed in a desiccator to allow cooling to room temperature. After cooling, sample was weighed to the nearest 0.1 mg.

iii. Total ash % = $[(D_1-B_1)/(C_1-B_1)]*100$ where,

B_1 = Weight of crucible (g)

C_1 = Weight of crucible plus original sample (g)

D_1 = Weight of crucible plus ashed sample (g)

Table 3.1: Experimental design for the kinetic study (Oxygen-effect)

(Pressure = 200 kPa, H_2S flowrate = 500 ml/min, H_2S concentration = 10000 ppm, $F_{H_2O} = 0$, and $F_{SO_2} = 0$)

Run	T(^{0}C)	F_{O2} (* stoic.)
1.1	160	1
1.2	160	2
1.3	160	3
1.4	175	1
1.5	175	2
1.6	175	3
1.7	190	1
1.8	190	2
1.9	190	3

Table 3.2: Experimental design for the kinetic study (Hydrogen sulphide-effect)

(Pressure = 200kPa, H_2S flowrate = 500 ml/min, Oxygen flowrate: 1* stoic., $F_{H_2O} = 0$, and $F_{SO_2} = 0$)

Run	Temp. (^{o} C)	H_2S Concentration (ppm)
2.1	160	6000
2.2	160	6000
2.3	160	6000
2.4	175	8000
2.5	175	8000
2.6	175	8000
2.7	190	10000
2.8	190	10000
2.9	190	10000

Table 3.3: Experimental design for the kinetic study (Water-effect)

(Pressure = 200 kPa, H_2S flowrate = 500 ml/min, H_2S concentration = 10000 ppm, Oxygen flowrate: 1* stoic., F_{SO_2} =0)

Run	Temp. (^{o} C)	F_{H_2O} (vol % of feed)
3.1	160	0.6
3.2	160	1.0
3.3	160	1.8
3.4	175	0.6
3.5	175	1.0
3.6	175	1.8
3.7	190	0.6
3.8	190	1.0
3.9	190	1.8

Table 3.4: Experimental design for the kinetic study (Sulphur dioxide-effect)

(Pressure = 200 kPa, H_2S flowrate = 500 ml/min, H_2S concentration = 10000 ppm, Oxygen flowrate: 1* stoic., F_{H_2O}=0)

Run	Temp. (^{o} C)	F_{SO_2} (ml/min)
4.1	160	40
4.2	160	60
4.3	160	80
4.4	175	40
4.5	175	60
4.6	175	80
4.7	190	40
4.8	190	60
4.9	190	80

3.9.2. BET surface area and pore structure analysis using nitrogen adsorption isotherms

BET (Brunauer, Emmett, and Teller) surface area and pore structure of precursors and activated carbons were determined by an automated gas adsorption analyzer, ASAP 2020 (Micromeritics, Instruments Inc., GA USA). After degassing of samples at 300 ^{o}C to a vacuum of 550 μmHg, nitrogen adsorption-desorption isotherms at -196 ^{o}C were measured by this equipment. The BET surface area was calculated by using the BET equation (See Appendix B). For each analysis ~ 0.2 g of sample was used. The accuracy of measurements performed by this equipment was ± 5 % . The micropore size distribution was determined using two methods; density functional theory, and Horvath-Kawazoe (HK) method. The mesopore size distribution was measured by density functional theory.

3.9.3. Boehm titration analysis

The concentrations of oxygenated surface groups were determined according to the Boehm titration method [Boehm, 2002; Boehm, 1994] . About 0.2 g of activated carbon was placed in 25 ml of each of the following 0.02 N solutions: sodium hydroxide, sodium bicarbonate, and hydrochloric acid. The vials were shaken for 24 h and after filtration, 5 ml of each filtrate was titrated with HCl or NaOH, depending on the original titrant used. The numbers of acidic sites of various types were calculated under the assumption that NaOH neutralizes carboxylic, phenolic, and lactonic groups; and $NaHCO_3$ neutralizes only carboxylic groups. The number of surface basic sites was calculated from the

amount of hydrochloric acid which reacted with the carbon sample. The error analysis of this method is shown in Appendix C.

3.9.4. Elemental analysis

a) CHNS elemental analysis: Carbon, hydrogen, nitrogen, and sulphur percentages were measured by Elementar Vario EL III. Through quantitative high temperature decomposition, solid substances are changed into gaseous combinations. 0.1 g sample was burned at 1000 ^{o}C and the released gases were separated into their components and the composition, through efficient detectors, was determined with a precision and accuracy of up to 0.1%.

b) ICP-MS: The analysis of the impurities composition, namely, Al, Ca, Cu, Fe, Li, Mg, Mn, , P, Ti, V, and Zn in the activated carbon catalysts was performed using an inductively coupled plasma-mass spectrometer (ICP-MS, Model Sciex Elan 5000 manufactured by Perkin Elmer) in the Department of Geological Sciences, University of Saskatchewan. Doubly distilled acids were used during sample processing. A standard method of HF-HNO_3 acid digestion in a teflon screw-capped vessel (Savillex^{R}) was employed to decompose ~100 mg sample powder. The dissolved sample was diluted gravimetrically ~1000 times with 0.2 N HNO_3 to give <0.1% total dissolved salt (TDS).

The Perkin Elmer Sciex 500 was operated at a power setting of 1000W, argon plasma gas flow at 15 l/min, auxiliary gas flow and nebulizer gas flow at 0.8 l/min; B, P, E1, and S2 ion lens settings were 45, 45, 25, and 45 digipots respectively. Platinum tipped sampler and skimmer with orifices of 1.1 mm and 0.89 mm, respectively, were employed with a sample delivery rate of 1.0 ml/min. Peak hopping mode was used for

measurement, with 3 counts/per mass. Total counting time was 10 s per mass, and dwell time was 50 s per mass. Sample equilibration time was 150 s, and inter-sample washing time was 180 s. Isotopes measured were as follows:

^{7}Li , ^{26}Mg, ^{27}Al, ^{29}Si , ^{31}P, ^{44}Ca, ^{47}Ti, ^{51}V, ^{55}Mn, ^{54}Fe , ^{60}Ni , ^{65}Cu , ^{66}Zn , ^{90}Zr , ^{95}Mo , ^{182}W.

Precision and accuracy were determined by duplication of selected samples and international rock standards, such as BCR-2. The error analysis of this method is shown in Appendix C.

3.9.5. Fourier transform infrared spectroscopy

The IR spectra of catalysts were obtained using diffuse reflectance infrared Fourier transform spectroscopy (DRIFTS). Undiluted activated carbons, in the powdered form (after grinding), were scanned and recorded using a spectroscope (Spectrum GX, Perkin-Elmer) by 256 scans at a resolution of 4 cm^{-1} and in the wave number range of 4000 - 400 cm^{-1}. Before each measurement, the instrument was run with empty sample holder to establish the background, which was then automatically subtracted from the sample spectrum.

3.9.6. Gas chromatography

The concentrations of hydrogen sulphide and sulphur dioxide in the exhaust gases from the reactor were monitored using gas chromatography (GC). The GC apparatus (Model CP-3800, Varian Inc.) had a pulse flame photometric detector (PFPD). The

column type was DB1. Column length, inside diameter, and film thickness were 25 meters, 0.15 mm, and 1.2 μm, respectively.

3.9.7. Particle size distribution analysis

Particle size distribution of precursors and activated carbons was determined using set of sieves with different mesh numbers. For biochar and activated carbons prepared from this precursor, sieves with mesh numbers of 150, 250, 354, and 600 μm were used. The weight percentages of particles in the following ranges of particle size were measured: <150, 150-250, 250-354, and 354-600 μm. For luscar char and activated carbon prepared from this precursor, sieves with mesh numbers of 850, 1180, 1700, 1999, and 2380 μm were used. The weight percentages of particles in the following ranges of particle size were measured; <850, 850-1180, 1180-1700, 1700-1999, and 1999-2380 μm.

3.9.8. pH measurement (for solid samples)

pH of samples was determined according to ASTM D 3838-80 (Approved 1999). This method includes the following procedure using a boiler-reflux condenser apparatus:

i. A sample of 10.00 g was weighed on a dry basis. This sample was added into a 250 ml Erlenmeyer boiler flask.
ii. 100.0 ml of boiling water was added to the carbon in the flask.
iii. The water in flask was brought to a boil on a hot plate using thermometer reading (to ~ 110 ^{o}C) and was boiled gently for 900 s.
iv. The flask was removed from the hot plate and its contents were filtered immediately through a filter paper premoisturized with the distilled water.

v. 50.0 ml filtrate was poured in a flask with carefulness to prevent carbon-fines from overrunning into the flask.

vi. The filtrate was cooled to 50 ^{o}C.

vii. pH measurement was the last step.

3.9.9. Scanning electron microscopy (SEM)

SEM analysis of samples was performed by using a Phillips SEM-505 scanning electron microscope. The SEM instrument was operated at 300 kV/SE and 50° inclination. Before analysis, all samples were ground and coated in a sputter coating unit (Edwards Vacuum Components Ltd., Sussex, England) to reduce charging and improve the secondary electron signals for imaging. The micrographs were recorded using photographic techniques.

3.9.10. Temperature programmed desorption (TPD)

This method was used to study the evolution of carbon monoxide (CO) and carbon dioxide (CO_2) from oxygen surface groups of samples. This study was performed using CHEMBET3000 instrument (Quantachrome Corporation). 0.7 g of sample for biochar and activated carbons produced from that and 0.4 g of samples for activated carbons prepared from luscar char were placed in an U-shaped quartz tube and heated in 18 ml/min nitrogen from room temperature to 900 ^{o}C at a heating rate of 10 ^{o}C/min. The amounts of CO and CO_2 were determined by a HP 5890 gas chromatograph (Hewlett Packard) with the thermal conductivity detector (TCD) having Carbosive S II column (length of 3 m and ID of 3.18 mm). It was programmed using following conditions:

initial temperature 40 ^{o}C, initial temperature hold time of one min, heating rate 12 ^{o}C/min, final temperature 200 ^{o}C, final temperature hold time of one min, and detector temperature of 250 ^{o}C.

3.9.11. X-ray absorption near edge structure (XANES) analysis

To specify the oxidation state of sulphur in products of reaction, X-ray absorption near edge structure (XANES) spectra at sulphur L-edge were recorded using plane grating monochromator (PGM) beamline (5.5 – 250 eV) on the 2.9 GeV synchrotron light source at the Canadian light source (CLS) in Saskatoon (Canada). Total electron yield (TEY) was used as detection method [Stohr, 1992]. Spectra were normalized for I_o (the X-ray fluctuations of the synchrotron ring). The samples were ground to form finely ground powders and then pressed lightly on a stainless steel holder using a carbon conducting tape.

3.9.12. X-ray diffraction (XRD)

XRD analysis was performed using Rigaku diffractometer (Rigaku, Tokyo, Japan) using Cu K_α (λ = 1.5406 Å) radiation filtered by a graphic monochromator at a setting of 40 kV and 130 mA. The powdered catalyst samples were smeared on glass slide with methanol and dried at room temperature. The X-ray diffraction analysis was carried out at room temperature for the scanning angle (2θ) range of 3 to 85 ° at scanning speed of 5 °/min.

4.0 Physical and chemical activation of precursors

This chapter describes the results obtained in first phase of the present experimental study. It deals with the physical (steam) activation of biochar and luscar char. It includes the models developed for the BET surface area and reaction yield of activated carbons produced by steam activation and the calculation of optimum operating conditions for production of activated carbons with relatively large BET surface area and high yield using the above mentioned models. Also, the chapter describes the chemical (KOH) activation of biochar. In this section, the BET surface area model for activated carbons produced by this method and the reaction yield model are presented. Optimum operating conditions were calculated using these models.

Analysis of precursors: The ultimate (moisture free) and the bulk ash analyses of both precursors are given in Tables 4.1 and 4.2, respectively. The pH and BET surface area of biochar were, respectively, 7.4 and 10 m^2/g. The BET surface area of luscar char was 46 m^2/g and its pH was 9.2. These measurements indicate low surface area of precursors. This low surface area is due to the rudimentary porous structure of precursors.

Based on the ultimate analysis, the main difference between precursors is the ash content. As it can be seen the percentage of ash content and its composition depend on the type of precursor. The ash content of coal-based precursor is close to four times of that in the biochar. Large amount of ash content is a limiting factor in the activation process and the development of the porosity, but some components in ash content, such as iron, calcium, and alkaline compounds, have shown catalytic effect for physical activation process [Rodriguez-Reinoso, 1997].

Table 4.1: Ultimate analysis of biochar and luscar char

Element (Wt %)	C	H	N	S	O	Ash
Biochar	83.09	3.76	0.11	0.01	9.60	3.44
Luscar char	78.23	2.07	0.85	0.66	5.14	13.06

Table 4.2: Bulk ash analysis of biochar and luscar char

Compound (wt %)	SiO_2	Al_2O_3	TiO_2	Fe_2O_3	CaO	MgO	Na_2O	K_2O	P_2O_5	SO_3	Undetermined
Biochar	53.48	7.73	0.10	2.52	17.98	4.20	2.07	6.93	0.94	1.06	2.99
Luscar char	25.36	16.73	0.56	8.00	19.80	4.34	9.64	0.46	0.63	11.90	2.58

4.1. Physical (steam) activation of biochar

The effects of three parameters were investigated for this process as follows; activation temperature (in the range of 600-900 ^{o}C), mass ratio of steam to biochar (in the range of 0.4-2.0), and activation time (in the range of 0.90-4.00 h).

4.1.1. The effects of activation process parameters on the BET surface area and reaction yield

Figures 4.1 and 4.2 are the 3-D plots of BET surface area and reaction yield models and show the effects of activation temperature and mass ratio on the BET surface area and yield of activated carbons prepared at a constant activation time of 2.46 h. As it can be inferred from these figures, increasing the activation temperature increases BET surface area and decreases the yield which is expected for an overall endothermic process such as steam activation [Muhlen and Van Heek, 1995]. In addition, increasing the mass ratio, i.e., using more oxidizing agent, has similar effects. The effect of activation time was not as strong as two other parameters. However, at constant T and S/C, an increase in this parameter results in higher BET surface area which can be due to lower injection rate of steam and less mass transfer resistance.

The typical isotherm plot of physically activated carbon prepared at T = 750 ^{o}C, S/C = 1.2 and t = 2.46 h is shown in Fig. 4.3. This isotherm plot can be categorized into type IV of isotherms [Sing, 1995].

Physically activated carbons produced in this study have average pore diameter in the range of 13 – 26 Å, maximum BET surface area more than 950 m^2/g, and maximum pore volume more than 0.83 cc/g.

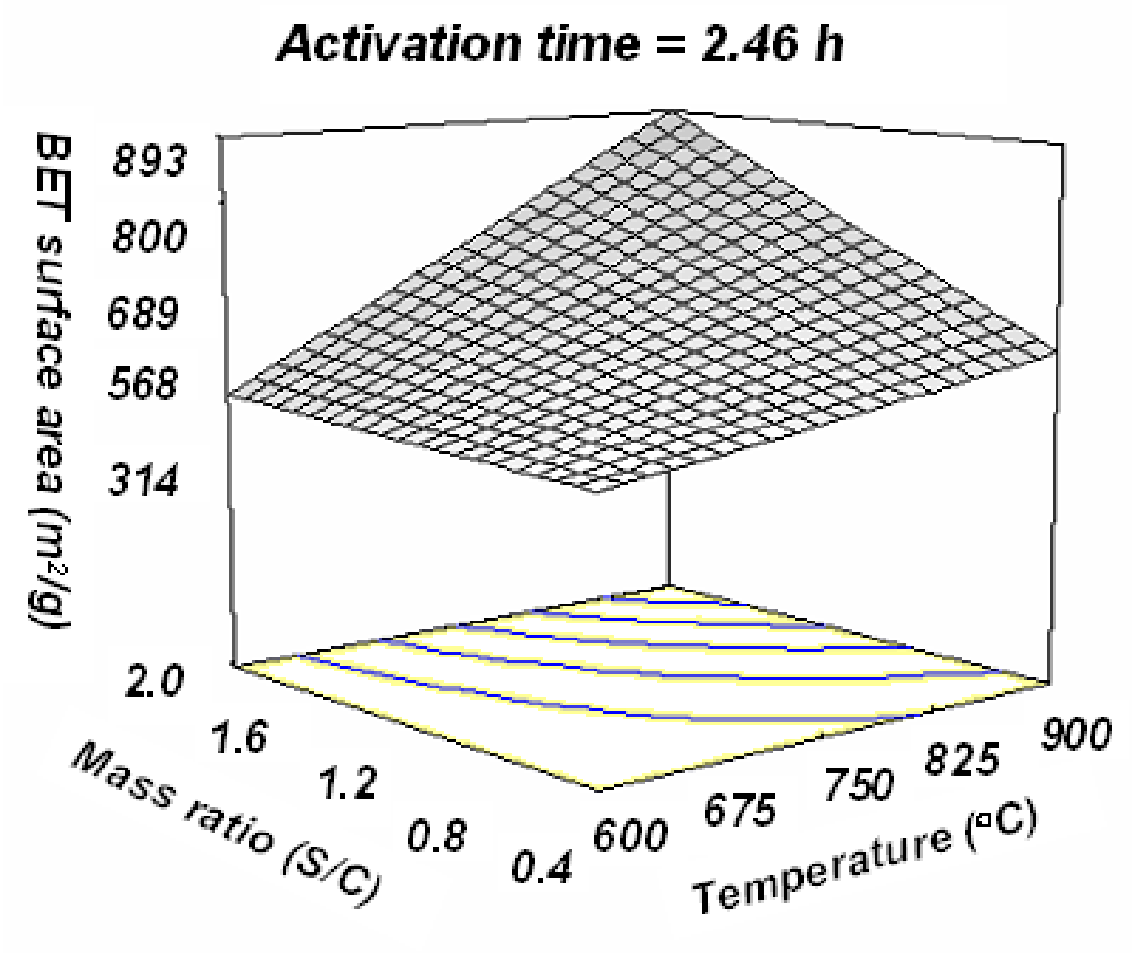

Fig. 4.1: 3-D plot of BET surface area model of physically activated carbon produced from biochar (at t = 2.46 h)

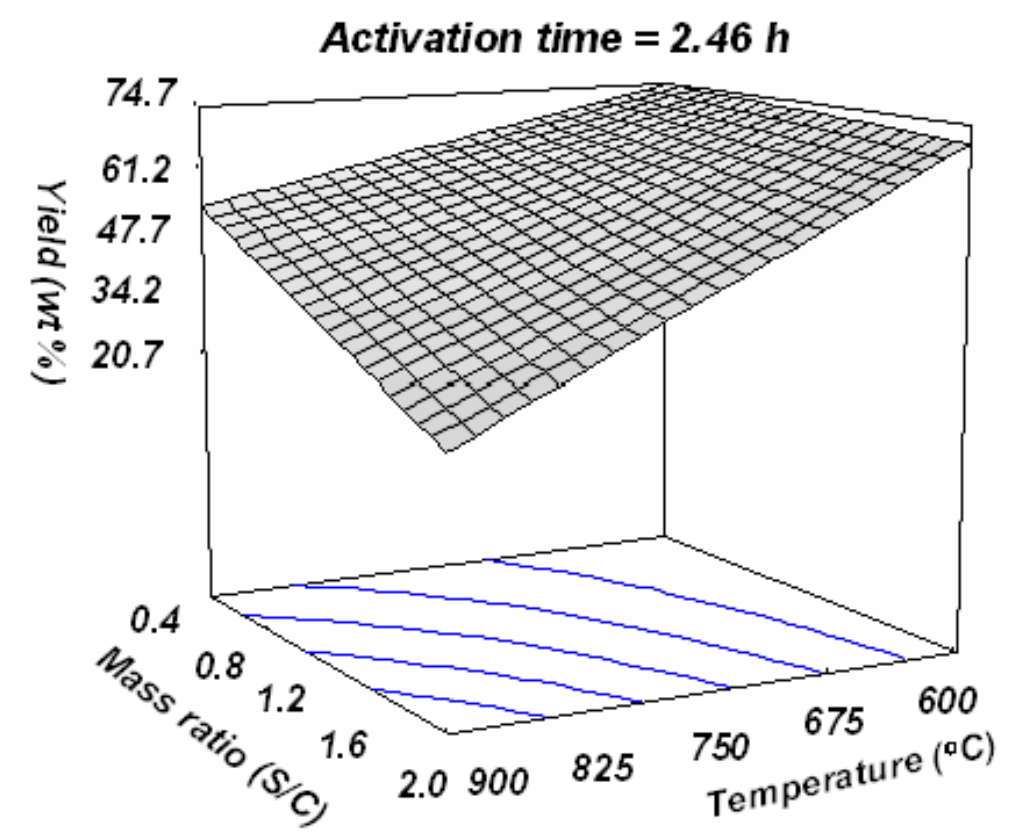

Fig. 4.2: 3-D plot of reaction yield model of physically activated carbon produced from bichar (at t = 2.46 h)

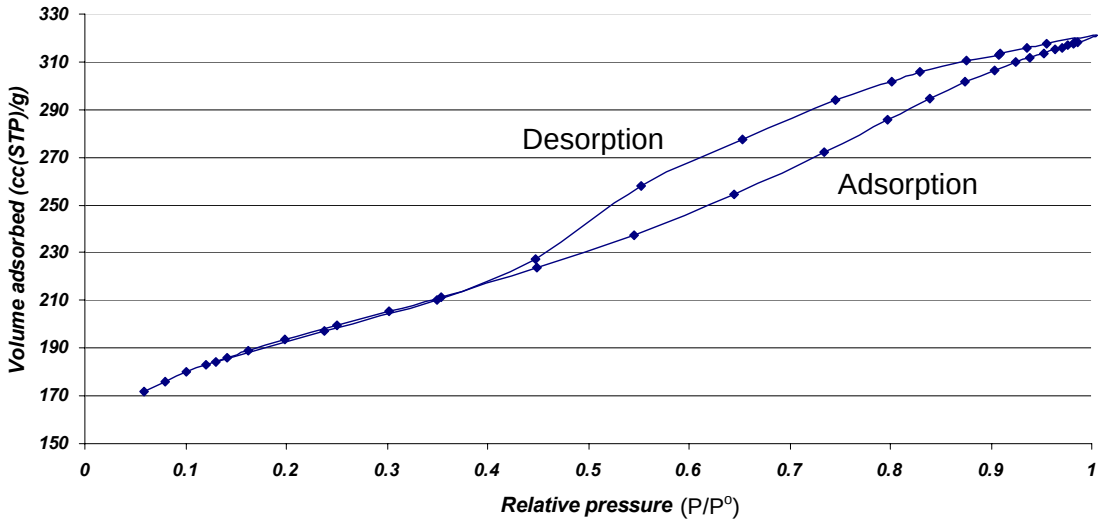

Fig. 4.3: Typical isotherm plot of physically activated carbon produced from biochar (T=750 ^{o}C, S/C=1.2, and t = 2.46 h)

4.1.2. Statistical analysis

The model (response surface) for the BET surface area (Y_1 in m^2/g) was obtained (see Eq. 4-1) after performing 20 experiments, power transformation, and discarding the insignificant effects.

$$(Y_1 - 25)^{2.5} = -3.600*10^6 + 5226.098*T - 2.040*10^7*(S/C) + 7.871*10^5*t + 35146.501*T*(S/C) \quad (4-1)$$

The model for the yield (Y_2 in wt %) is given by Eq. (4-2).

$$Y_2 = 94.85 - 0.01*T + 33.65*(S/C) + 0.31*t + 1.49*t^2 - 0.06*T*(S/C) - 0.01*T*t \quad (4-2)$$

where, T is activation temperature (in the range of 600-900 ^oC), S/C is mass ratio of steam to char (in the range of 0.4-2.0), and t is activation time (in the range of 0.90-4.00 h).

From statistical point of view, three tests are required to evaluate the model;

a) Test of significance of factors and interactions,

b) R-squared test, and

c) The lack-of-fit test.

Test of significance means leaving out insignificant factors or terms of a model, which in turn produces a simpler mathematical model and easier interpretation [Lazic, 2004]. Table 4.3 shows the result of the test of significance of factors and interactions for the Y_1 and Y_2 before and after discarding insignificant terms. When p-value (probability value) of one term is more than 0.05, it indicates that this term is insignificant at the 95% confidence level and therefore that term must be discarded. A, B and D, in Tables 4.3 and 4.4, are coded factors of activation temperature, mass ratio and activation time, respectively. Coding factor is a linear transformation process which converts actual range

Table 4.3: Results of test of significance of factors and interactions for the models Y_1 and Y_2 of physically activated carbons produced from biochar

	p-value of factors of Y_1		***p-value of factors of Y_2***	
Factor or interaction	***All factors Included***	***Insignificant factors excluded***	***All factors Included***	***Insignificant factors excluded***
A	***<0.0001***	***<0.0001***	***<0.0001***	***<0.0001***
B	***<0.0001***	***<0.0001***	***<0.0001***	***<0.0001***
D	***0.0878***	***0.048***	***0.0004***	***<0.0006***
A^2	***0.0142***	***-***	***0.1175***	***-***
B^2	***0.2212***	***-***	***0.4285***	***-***
D^2	***0.3222***	***-***	***0.0395***	***0.0103***
AB	***0.0009***	***<0.0001***	***<0.0001***	***<0.0001***
AD	***0.9740***	***-***	***0.0053***	***0.0099***
BD	***0.1391***	***-***	***0.0959***	***-***
Model	***<0.0001***	***<0.0001***	***<0.0001***	***<0.0001***

of variable to the range of (-1, +1), where, -1 and +1 are coded factors for lower and upper actual ranges, respectively. A, B, and D are calculated based on the following equations:

$$A = -1 + (T - 600)/150 \quad (4-3)$$

$$B = -1 + ((S/C) - 0.4)/0.8 \quad (4-4)$$

$$D = -1 + (t - 0.91)/1.55 \quad (4-5)$$

R-square is the relative predictive power of a model and is in the range of 0 to 1. If it is much closer to one, the model can better predict real data.

Table 4.4 shows the R-square values for the Y_1 and Y_2 before and after discarding insignificant terms. For each of the models (Y_1 and Y_2), the predicted R^2 is in reasonable agreement with the adjusted R^2 because they are within 0.20 of each other. It is better to use adjusted R^2 instead of R^2, because R^2 increases by adding the number of variables, but the adjusted R^2 does not always increase as variables are added to the model [Montgomery, 1997].

The test of lack-of-fit is used to determine whether discrepancies between measured and expected values can be attributed to random or systematic error. The lack-of-fit test compares the residual error to pure error from replicated design points. If p-value for lack-of-fit is less than 0.05, there is statistically significant lack-of-fit at the 95% confidence level. P-values for two models (Y_1 and Y_2) were 0.1278 and 0.1037, respectively after excluding insignificant factors for these models. Results of statistical tests showed that the models can navigate experimental data at the mentioned ranges of operating conditions.

Table 4.4: R-squared statistics for models Y_1 and Y_2 of physically activated carbons produced from biochar

	R^2		Adjusted R^2		Predicted R^2	
Model	All factors included	Insignificant factors excluded	All factors included	Insignificant factors excluded	All factors included	Insignificant factors excluded
Y_1	0.9689	0.9480	0.9409	0.9342	0.8142	0.8822
Y_2	0.9878	0.9780	0.9768	0.9679	0.9281	0.9233

4.1.3. Optimum operating conditions

Fig. 4.4 exhibits the effect of burn-off degree (percentage of feed mass loss due to activation) on the BET surface area and the total pore volume of seven activated carbons prepared at constant steam to feed mass ratio (S/C = 1.2) and activation time (t = 2.46 h).

It shows that by increasing the burn-off degree, BET surface area and total pore volume per gram of activated carbon (product) increase. In industry, it is more conventional to express these porosity characteristics per unit mass of the raw material (biochar) instead of product [Rodriguez-Reinoso, 2002; Daud and Ali, 2004], as it is plotted in Fig. 4.5. According to Fig. 4.4, porosity can increase by increasing the burn-off degree, or activation level, but from Fig. 4.5 it can be inferred that the porosity exhibits a maximum at 40-50 wt % of burn-off degree. Similar phenomenon was observed by other researchers [Daud and Ali, 2004; Rodriguez-Reinoso, 1995; Rodriguez-Reinoso and Molina-Sabio, 1992; Rodriguez-Reinoso, 1990].

It can be due to widening of the porosity or the external burning of the carbon particles at high degree of burn-off [Rodriguez-Reinoso, 1997; Rodriguez-Reinoso, 2002]. Therefore, if the prime objective is to obtain activated carbon with high surface area from a specific amount of char, the level of burn-off should be in the range of 40-50 wt % . In addition, the activation time should be as low as possible to increase the overall yield of a batch process.

The following constraints were used to calculate the optimum operating conditions:

1- BET surface area ≥ 600 m^2/(g of activated carbon)

2- $50 \leq$ Yield (wt %) ≤ 60

3- $0.90 \leq$ activation time (h) ≤ 1.50

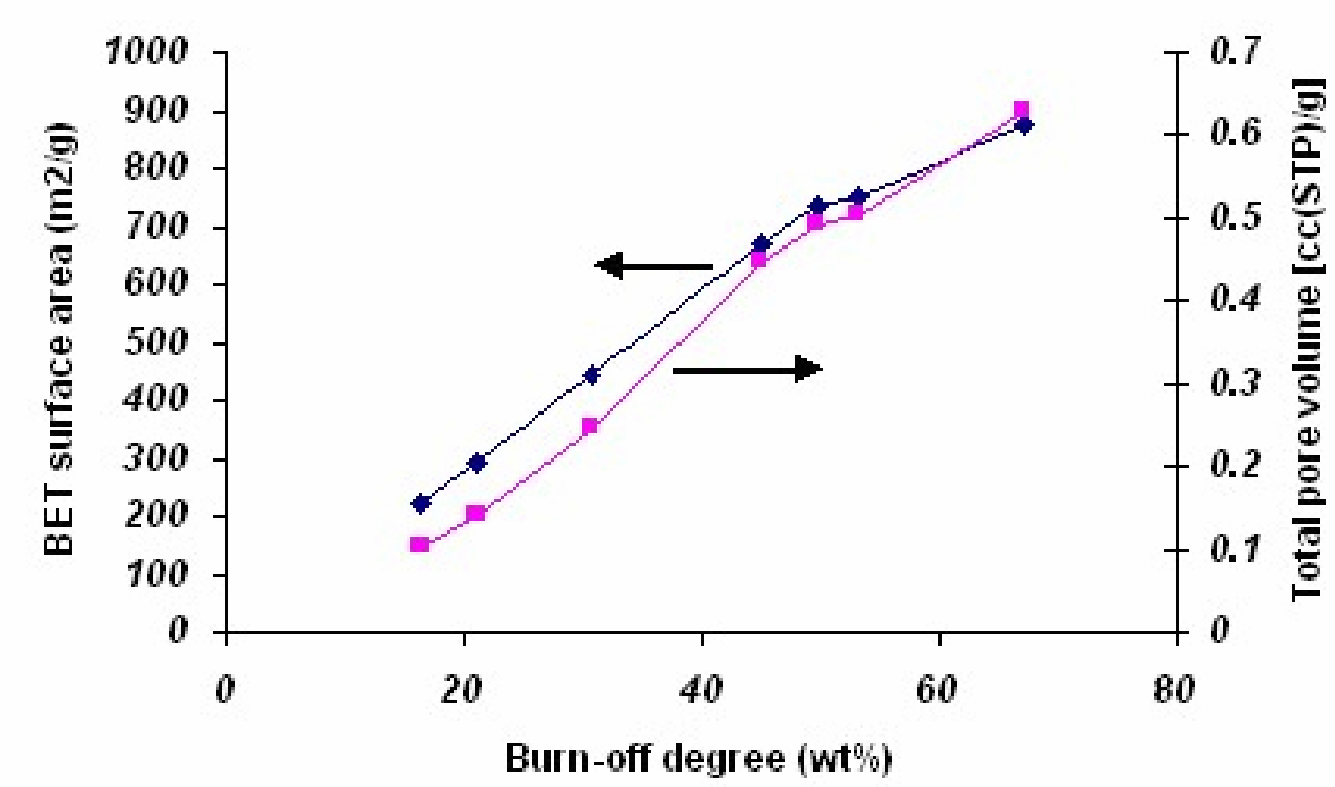

Fig. 4.4: The effect of burn-off degree on the BET surface area and the total pore volume of physically activated carbon prepared from biochar at S/C = 1.2 and t = 2.46 h

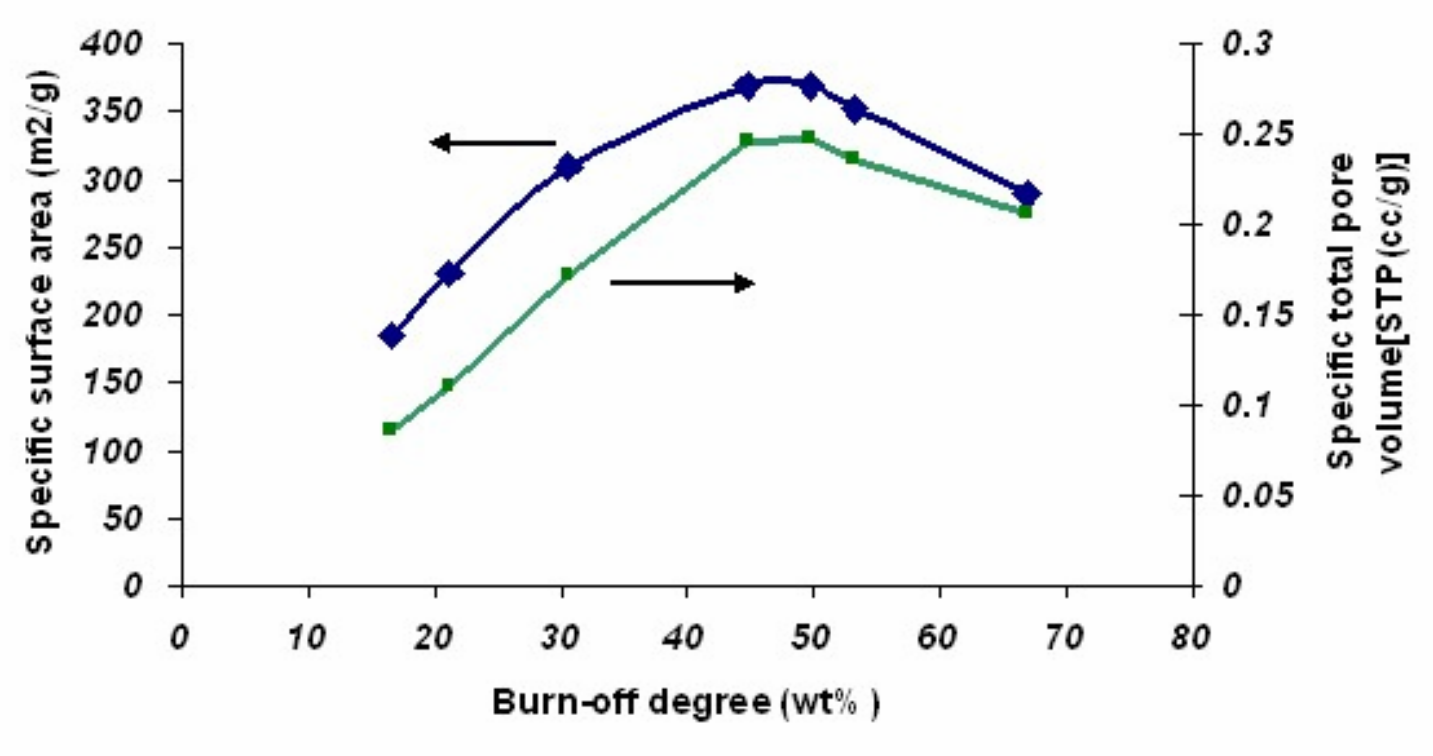

Fig. 4.5: The effect of burn-off degree on the specific BET surface area and the total pore volume of physically activated carbon prepared from biochar at S/C = 1.2 and t = 2.46 h

The optimum operating conditions were calculated based on the constraints, by Design expert soft ware, are as follows: T = 792 ^{o}C, S/C = 1.06, t = 1.39 h.

At these operating conditions, the experiment was performed and the results are presented in Table 4.5. As it can be seen, the difference of BET surface area and product yield for experiment and model are less than 4 % and 0.6 %, respectively.

The micropore and mesopore size distributions for this activated carbon are presented in Figures 4.6 and 4.7. The former is calculated using micropore analysis (HK method) and the latter is provided by density functional (DFT) theory.

Second method for the optimization: The optimum operating conditions were calculated using one objective function instead of two functions. This function was defined as "BET surface area * Product yield". The optimum operating conditions based on the constraints similar to the ones mentioned for the first method of optimization, were calculated using Solver and the solution was as follows;

T = 900 ^{o}C, S/C = 0.94, and t = 0.90 h.

The predicted surface area and the product yield for this optimum conditions calculated using the models developed for this process were 674 m^2/g and 60 wt %, respectively. The differences between these values and values obtained by the first optimization method (See Table 4.5) were not significant (4.6 % for the BET surface area and 5.2 % for the product yield). The optimum operating conditions for the second method showed higher activation temperature, but the activation time required for it was lower than that for the first method. Assuming that the simulation results can be reproduced experimentally, one can use either of these two optimization methods to produce high quality activated carbons.

Table 4.5: The predicted and observed values of optimum BET surface area and reaction yield of physically activated carbon prepared at T = 792 ^{o}C, S/C = 1.06, and t = 1.39 h

	Values predicted by models	Observed values
BET surface area (m^2/g)	643	664
Reaction yield (wt %)	56.9	56.6

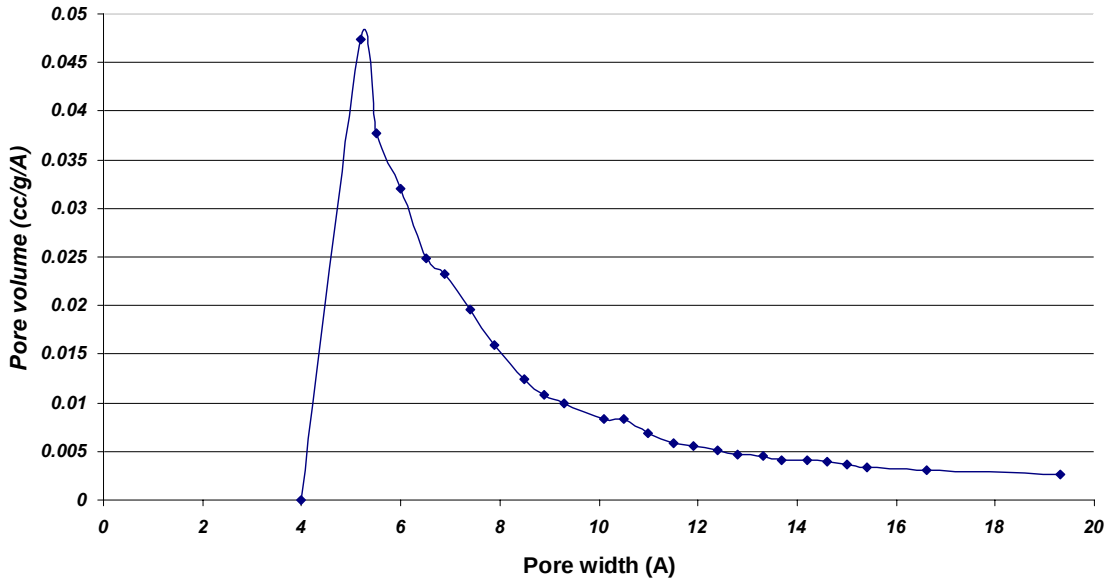

Fig. 4.6: Micropore size distribution for BioAC (measured using HK method)

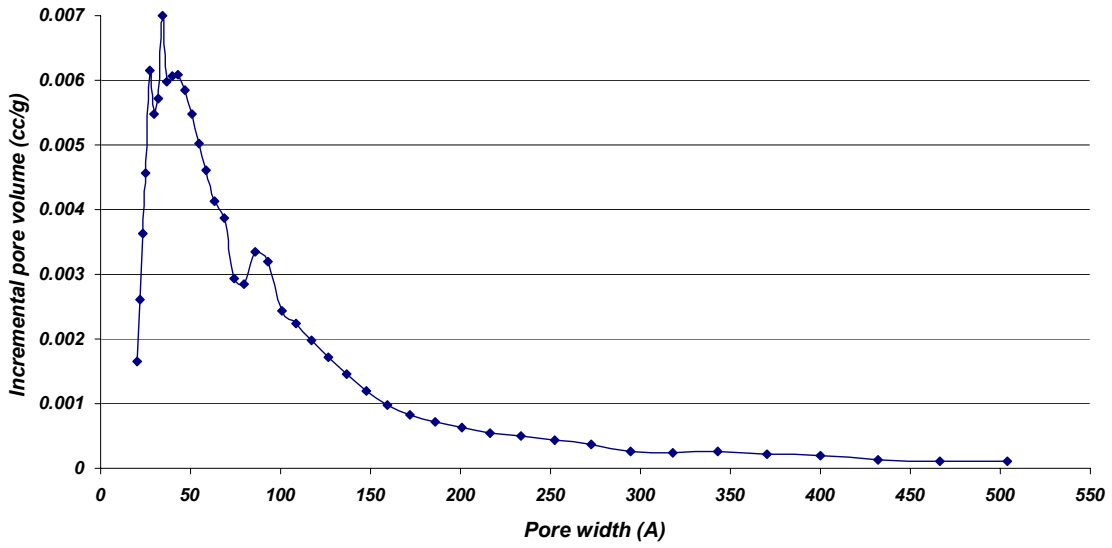

Fig. 4.7: Mesopore size distribution for BioAC (measured using DFT)

4.2. Physical (steam) activation of luschar char

The effects of three parameters were investigated for this process as follows; activation temperature (in the range of 650-850 ^{o}C), mass ratio of steam to luscar char (in the range of 0.7-2.0), and activation time (in the range of 1.10-4.00 h).

4.2.1. Effects of operating conditions on BET surface area and reaction yield

Fig. 4.8 is 3-D plot of BET surface area model for a constant activation time of 2.55 h. This Figure shows the influence of activation temperature and mass ratio on the BET surface area. Activation process is an overall endothermic process [Muhlen and Van Heek, 1995], therefore, it is expected that the rate of reaction increases by an increase in temperature. But in Fig. 4.8, when temperature goes beyond a certain limit, the surface area decreases. The same phenomenon was previously reported on steam activation of another kind of char [Tennant and Mazyck, 2003]. It can be due to the following reasons:

a- If activation is pursued beyond a certain level, the walls of the pores become so thin that they collapse and cause a reduction in the available surface area [Dalai et al, 1996; Arenas and Chejne, 2004].

b- The ash content increases in direct proportion to the degree of activation, e.g. by increasing the temperature [Rodriguez-Reinoso, 1997]. The ash offers a resistance to the diffusion of activating agent [Arenas and Chejne, 2004]. These dispersed inorganic elements that act as catalyst at lower temperatures [Rodriguez-Reinoso, 1997] may sinter and block pores and reduce surface area. In addition, ash does not contribute significantly to surface area and its presence can reduce surface area [Dalai et al, 1996]. The same phenomenon was observed related to another kind of coal [Walker and Almagro, 1995].

Fig. 4.9 is 3-D plot of reaction yield model for activation time of 2.55 h. As expected, by

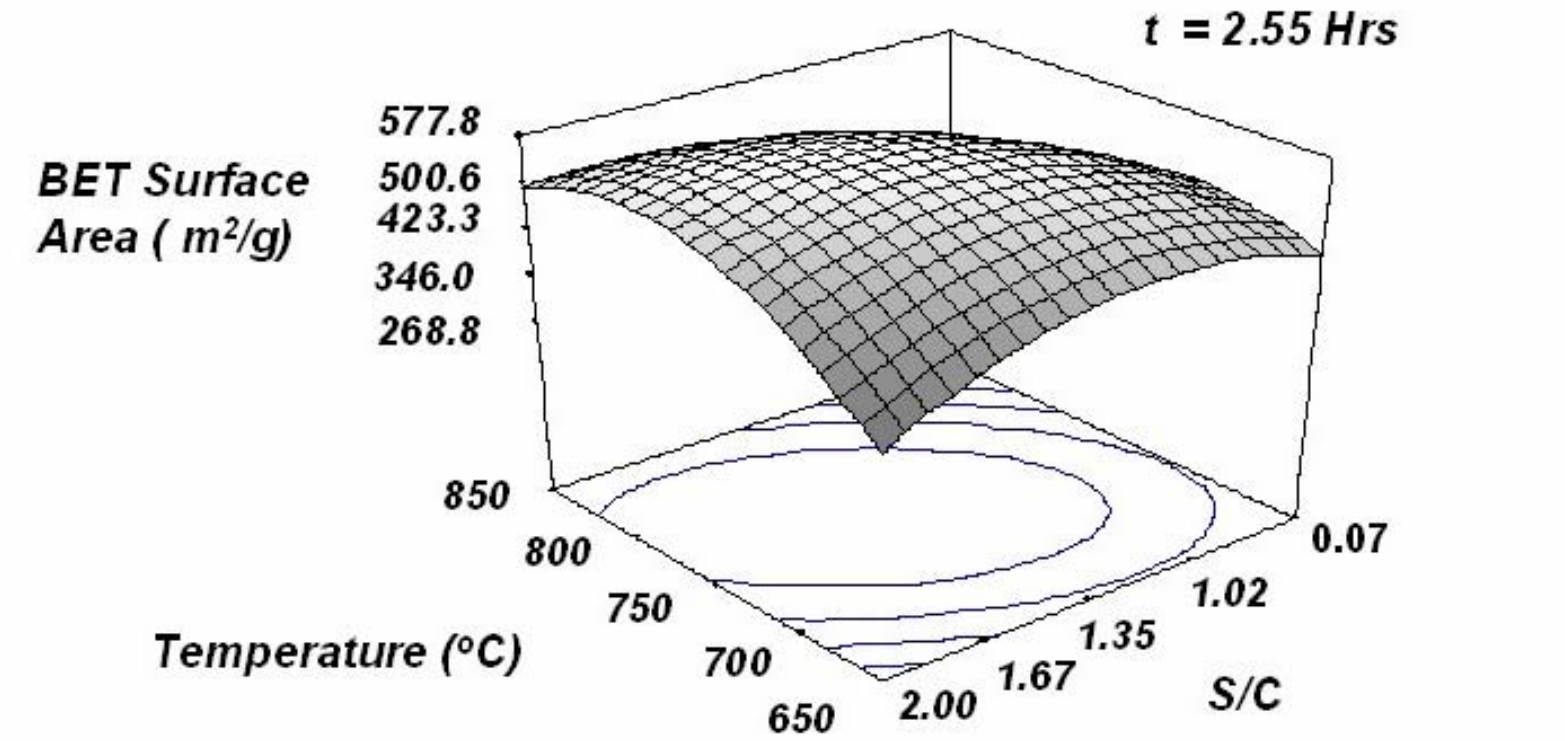

Fig. 4.8: 3-D plot of BET surface area of activated carbons produced from luscar char (for t = 2.55 h)

increasing the amount of activation agent (steam) or temperature, the yield decreases. The effects of mass ratio on the BET surface area are shown in Fig 4.10. This Figure shows the adsorption isotherm plots for luscar char and three activated carbons prepared using different mass ratios. The nitrogen volume adsorbed, or in other words BET surface area, increases by increasing S/C to 1.35, but at a mass ratio of 2.44 there is a decrease in BET surface area. It shows again that beyond a certain level of activation the surface area decreases. The same trend was previously observed from steam activation of another kind of char [Tennant and Mazyck, 2003].

4.2.2. Statistical analysis

The model (response surface) for the BET surface area (Y_1 in m^2/g) obtained, after performing 20 experiments, the power transformation (applying a mathematical power function to all the response data) and discarding the insignificant effects, is as follows:

$$(Y_1)^3 = 1.906*10^8 - 1.922*10^7 * A - 4.602*10^7 * A^2 - 6.237*10^7 * B^2 - 2.630*10^7 * D^2 - 4.358*10^7 * A * B \quad (4\text{-}6)$$

A, B and D are coded factors of activation temperature, mass ratio and activation time, respectively, according to the following equations:

$$A = -1 + (T - 650)/100 \quad (4\text{-}7)$$

$$B = -1 + ((\frac{S}{C}) - 0.7)/0.65 \quad (4\text{-}8)$$

$$D = -1 + (t - 1.10)/1.45 \quad (4\text{-}9)$$

Statistical analyses showed that the model is not hierarchical and then, coded factors must be used instead of actual factors. Hierarchical model includes all parental terms.

The related model for the reaction yield (Y_2 in wt %) is as follows:

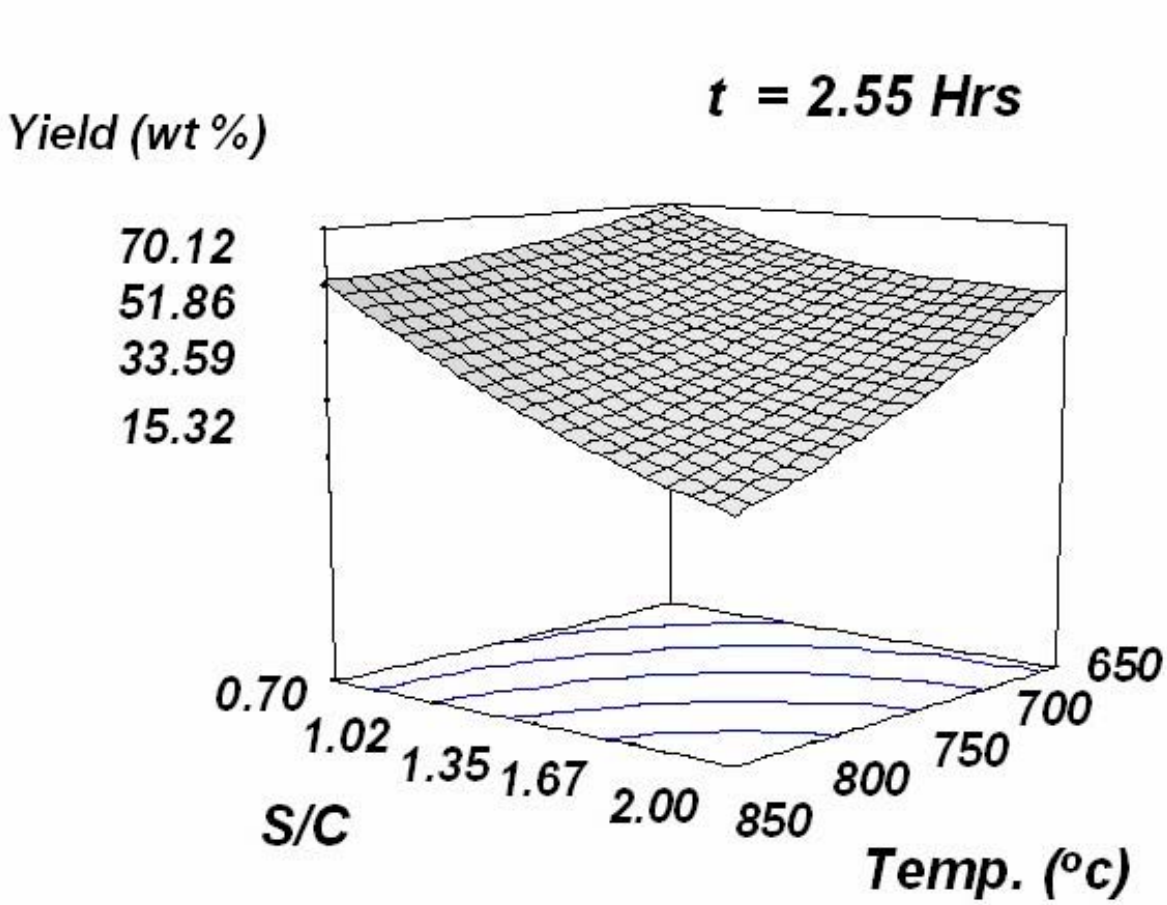

Fig. 4.9: 3-D plot of reaction yield of activated carbons produced from luscar char (for t = 2.55 h)

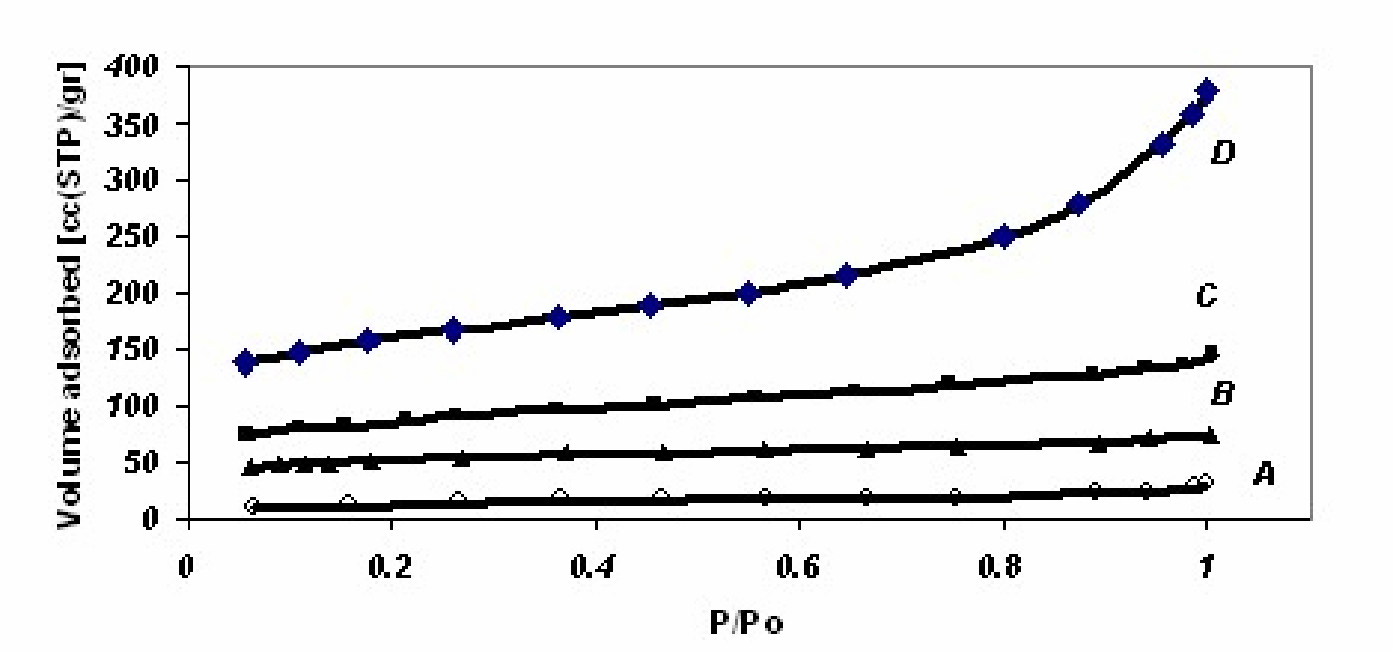

Fig. 4.10: Influence of S/C on the isotherm plots of activated carbons for
A – Luscar char; B – (T = 750 ^{O}C, S/C = 0.26, t = 2.55 h) ;
C- (T = 750 ^{O}C, S/C = 2.44, t = 2.55 h); D- (T = 750 ^{O}C, S/C = 1.35, t = 2.55 h)

$$Y_2 = 32.84 - 17.02 * A - 19.52 * B + 3.35 * A^2 + 6.21 * B^2 - 8.82 * A * B - 5.12 * B * D \quad (4\text{-}10)$$

where, T is activation temperature (in the range of 650-850 ^oC), S/C is mass ratio of steam to char (in the range of 0.7-2.0), and t is activation time (in the range of 1.10-4.00 h). Statistical tests were used to evaluate the models. Table 4.6 shows the result of the test of significance of factors and interactions for the Y_1 and Y_2 before and after discarding insignificant terms. When p-value (probability value) of one term is more than 0.05, indicating that this is insignificant at the 95% confidence level and therefore that term must be discarded. For each of the models (Y_1 and Y_2), the predicted R^2 is in reasonable agreement with the adjusted R^2 because they are within 0.20 of each other (Table 4.7). For lack-of-fit test, P-values for two models (Y_1 and Y_2), after excluding insignificant factors, were 0.0512 and 0.0595, respectively, which shows there is statistically insignificant lack-of-fit at 95% of confidence level.

4.2.3. Optimum operating conditions

The industrial-scale production of activated carbon is dominated by the compromise between porosity development and yield of the process [Rodriguez-Reinoso, 1997]. Therefore, for production of activated carbon with high surface area and large yield in a batch process, the optimum operating conditions were defined according to the following constraints:

1) BET surface area $\geq$ 500 m^2/g; 2) yield $\geq$ 50 wt %; and 3) t : minimum

Activation time should be minimized because in a batch process, small reaction time increases overall yield of the process. The optimum operating conditions based on these constraints, were calculated using Design-Expert. The solution is as follows:

Table 4.6: Results of test of significance of factors and interactions for the models Y_1 and Y_2

	p-value of factors of Y_1		p-value of factors of Y_2	
Factor or interaction	All factors Included	Insignificant factors excluded	All factors Included	Insignificant factors excluded
A	0.0230	0.0205	<0.0001	<0.0001
B	0.1288	-	<0.0001	<0.0001
D	0.7574	-	0.5191	-
A^2	<0.0001	<0.0001	0.0396	0.0303
B^2	<0.0001	<0.0001	0.0015	0.0006
D^2	0.0037	0.0025	0.5544	-
AB	0.0009	0.0005	0.0011	0.0004
AD	0.3499	-	0.0255	0.0165
BD	0.351	-	0.3454	-
Model	<0.0001	<0.0001	<0.0001	<0.0001

Table 4.7: R-squared statistics for models Y_1 and Y_2 of physically activated carbons produced from luscar char

	R^2		Adjusted R^2		Predicted R^2	
Model	All factors included	Insignificant factors excluded	All factors included	Insignificant factors excluded	All factors included	Insignificant factors excluded
Y_1	0.9383	0.9090	0.8828	0.8765	0.5768	0.7840
Y_2	0.9723	0.9673	0.9474	0.9523	0.8150	0.8772

T = 707 ^{O}C, S/C = 0.93, and t = 1.10 h.

The experiment was performed at these operating conditions and BET surface area and yield of the product were measured. BET surface area and yield of this product were, respectively, 502 m^2/g and 54.1 wt % which showed less than 1 and 7% difference in comparison with the predicted values by the models (Table 4.8).

The micropore and mesopore size distributions for this activated carbon are presented in Figures 4.11 and 4.12. The former is calculated using micropore analysis (HK method) and the latter is provided by density functional theory method.

The results of particle size analysis are shown in Appendix D. It shows that activated carbon produced by steam activation of luscar char at optimum operating conditions is finer than the precursor (See Fig. D.1).

Second method for the optimization: The optimum operating conditions were calculated using one objective function instead of two functions. This function was defined as "BET surface area * Product yield". The optimum operating conditions based on the constraints similar to the ones mentioned for the first method of optimization, were calculated using Solver and the solution was as follows;

T = 650 ^{o}C, S/C = 1.35, and t = 1.10 h.

The predicted surface area and the product yield for this optimum conditions calculated using the models developed for this process were 516 m^2/g and 53 wt %, respectively. The differences between these values and values obtained by the first optimization method (See Table 4.5) were not significant (2.7 % for the BET surface area and 6 % for the product yield). The optimum operating conditions for the second method showed higher activation temperature, but the activation time required for it was lower than that

Table 4.8: The predicted and experimental values of BET surface area and reaction yield for physically activated carbons produced from Luscar char

	Values predicted by models	Observed values
BET surface area (m^2/g)	502	502
Reaction yield (wt %)	50.2	54.1

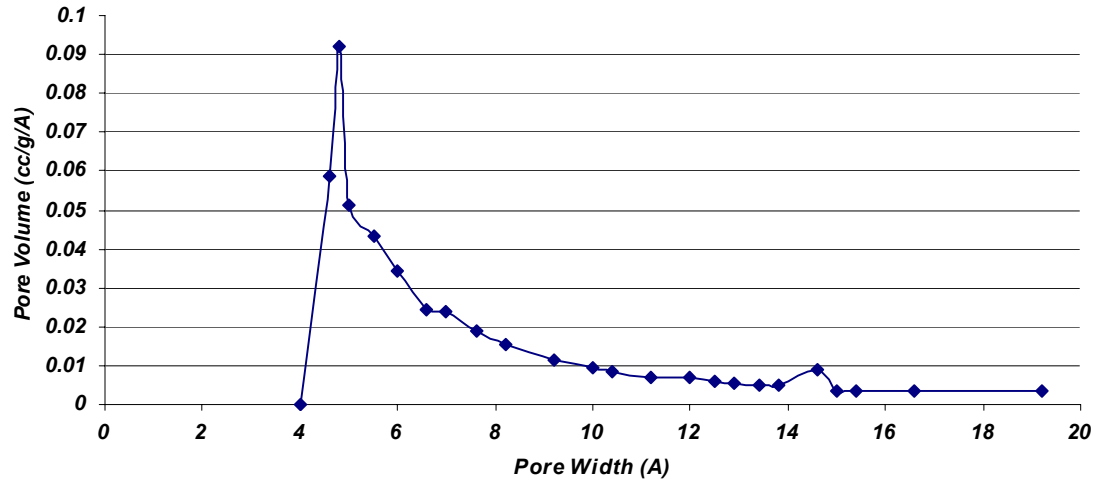

Fig. 4.11: Micropore size distribution for LusAC (measured using HK method)

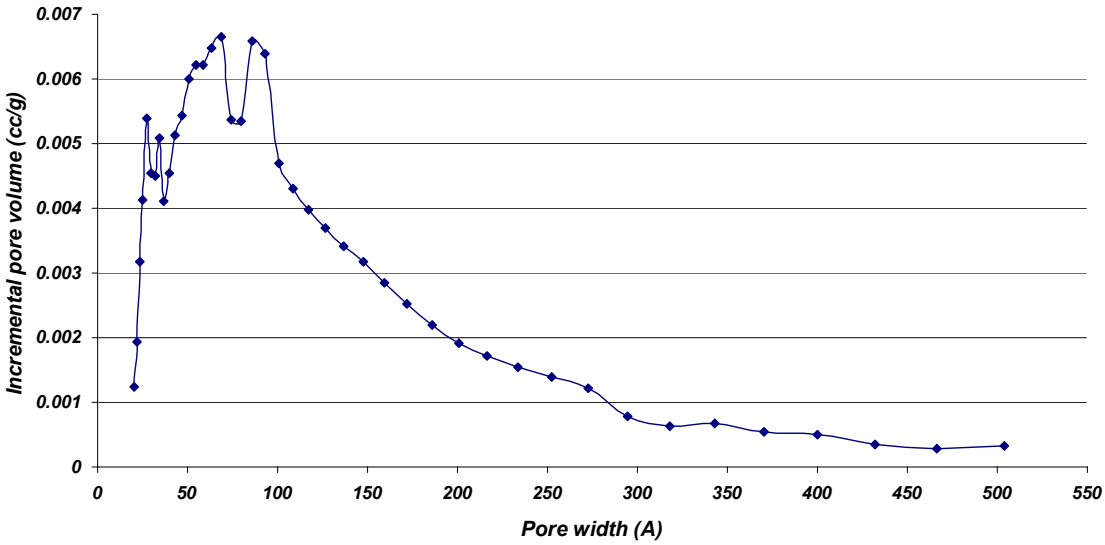

Fig. 4.12: Mesopore size distribution for LusAC (measured using DFT)

for the first method. Assuming that the simulation results can be reproduced experimentally, one can use either of these two optimization methods to produce high quality activated carbons.

4.3. Chemical (potassium hydroxide) activation of biochar

The effects of three parameters wer investigated for this process as follows; activation temperature (in the range of 550-800 ^{o}C), mass ratio of KOH to biochar (in the range of 0.25-3.00), and nitrogen flow rate (in the range of 80-250 ml/min).

4.3.1. The effects of activation process parameters on the BET surface area and reaction yield

Figures 4.13 and 4.14 are the three-dimensional plots of BET surface area and reaction yield models and show the effects of temperature and mass ratio on the BET surface area of activated carbon (prepared at constant nitrogen flow rate of 165 cc/min) and the effects of temperature and nitrogen flow-rate on yield of product before acid washing (prepared at a constant mass ratio of 1.63).

As it can be inferred from Fig. 4.13, increasing the temperature increases BET surface area. Increase in the temperature enhances reactions between carbon and potassium compounds resulting in the porosity development and especially above 700 ^{o}C, formation of metallic potassium and its intercalation to the carbon matrix has a great influence on the increasing the porosity [Rodriguez-Reinoso, 2002; Otowa et al, 1993]. Because of the complexity of the mechanism of chemical activation by KOH, many sets of reactions have been proposed for it [Otowa et al, 1993; Lillo-Rodenas et al, 2003].

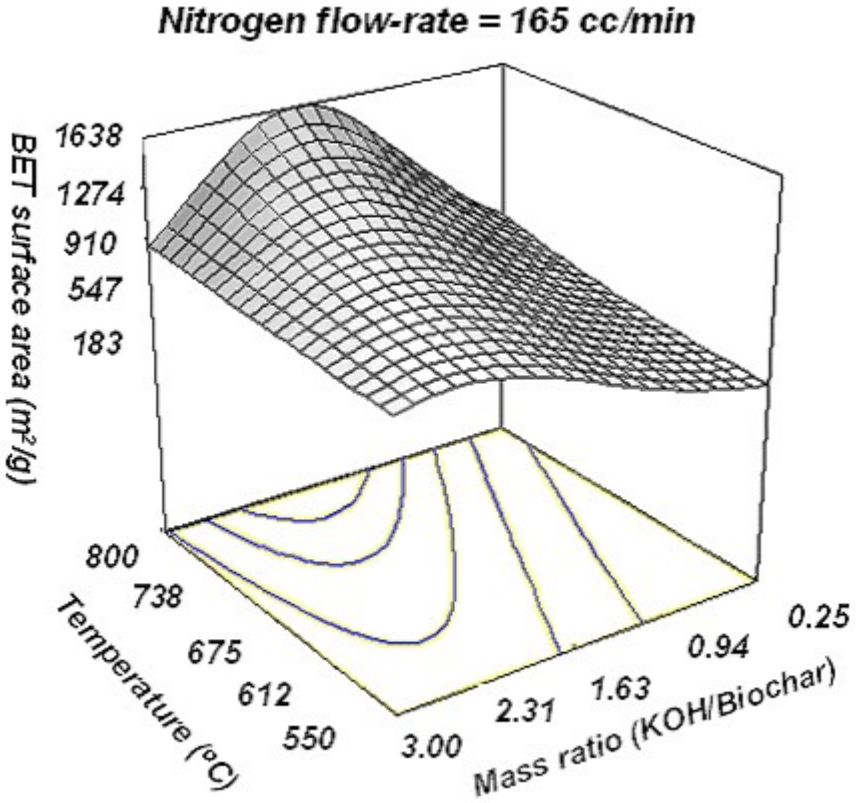

Fig. 4.13: Three-dimensional plot of BET surface area model of chemically activated carbon (N_2 flow-rate = 165 cc/min)

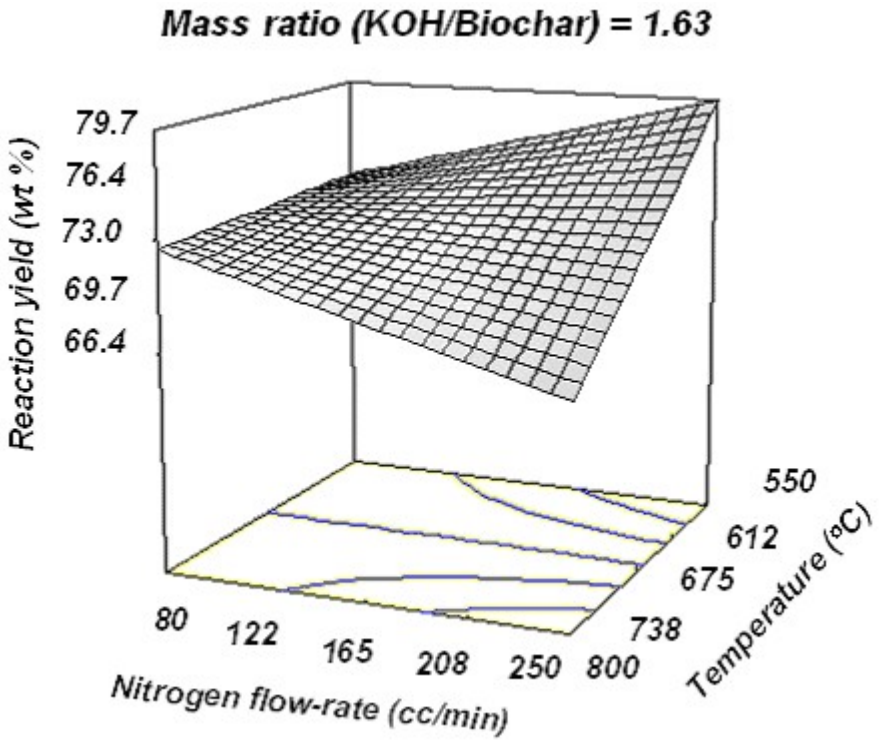

Fig. 4.14: Three-dimensional plot of reaction yield model of chemically activated carbon (KOH/biochar = 1.63)

Even recently, reactions between nitrogen, potassium compounds and carbon have been detected in this process [Robau-Sanchez, 2005]. However, Gibbs free energies of most reactions of these mechanisms show they are more favored at higher temperatures

[Otowa et al, 1993; Lillo-Rodenas et al, 2003, Robau-Sanchez, 2005]. BET surface area increases with increase in the mass ratio up to a maximum, e.g., mass ratio of 1.93 at 800 ^{o}C, and then decreases. This phenomenon has been reported by some researchers for other precursors [Lozane-Castello et al, 2001 ; Teng et al, 1999]. It can be attributed to predominantly pore widening at higher mass ratios [Rodriguez-Reinoso, 2002] and gasification on the external surface of the carbon which destroy the porous structure. It can be also inferred from Fig. 4.13 that the maximum value of BET surface area at higher temperatures happens at lower mass ratios. It is because of the severe effects of pore widening and removal of external carbon atoms in carbon gasification at higher temperatures [Teng et al, 1999]. Experimental data showed that activated carbons prepared at constant activation temperature and mass ratio (675 ^{o}C and 1.63, respectively), but at different nitrogen flow rates (71.5, 165, and 258 cc/min), have BET surface areas equal to 582, 927, and 1210 m^2/g, respectively. Therefore, the sample prepared at higher nitrogen flow rate had larger BET surface area. This can be due to faster removal of reaction products from the reactor at higher flow rates, which favors the activation reactions [Lozane-Castello et al, 2001].

Fig. 4.14 shows that increase in activation temperature decreases the reaction yield. It is related to the favorable effect of the temperature on BET surface area which causes formation of porosity by removal of some products in effluent gases from the reactor. At higher nitrogen flow-rate, the reaction yield is reduced at higher temperatures. It is due to

the similar effect of temperature on the BET surface area. However, at low temperatures such as 550 ^{o}C, an increase in the flow-rate of nitrogen has increased the reaction yield. In addition, it was observed that increase in mass ratio fortifies this effect. According to the literature, there are many possible products for chemical activation process by reactions between KOH, carbon and nitrogen. Some of these products evaporate and leave the carbon material at higher temperatures [Robau-Sanchez et al, 2005]. Probably, formation of these products increases by higher flow rates of nitrogen and it results in an increase in reaction yield at lower temperatures. Some of these products are removed at higher temperatures thus lowering the yield. But more study on the mechanism is needed for better clarification. The effect of mass ratio on the reaction yield is shown in Table 4.9.

This Table shows that increase in the mass ratio for three activated carbons prepared at the same temperature and nitrogen flow rate, at 675 ^{o}C and 165 cc/min, respectively, decreases the reaction yield. This is due to increase in carbon gasification rate by CO_2, evolved from decomposition of K_2CO_3 (formed during carbonization), or by potassium compounds [Teng et al, 1999].

The typical isotherm plot of chemically activated carbon prepared at T=675 ^{o}C, R=1.63, and F=165 cc/min is shown in Fig. 4.15. This isotherm plot can be categorized into type I of isotherms [Sing, 1995] due to the development of microporous material.

Chemically activated carbons produced in this study had an average pore diameter, BET surface area and total pore volume, respectively, in the range of 13 - 15 Å, 178-1578 m^2/g, and 0.09-0.75 cc/g.

Table 4.9: The effect of the mass ratio of KOH / biochar on the reaction yield of chemically activated carbons prepared at T = 675 ^{o}C and F = 165 cc/min

Mass ratio of KOH/biochar	*Reaction yield (wt%)*
0.11	**78.1**
1.63	**74.0**
3.40	**49.8**

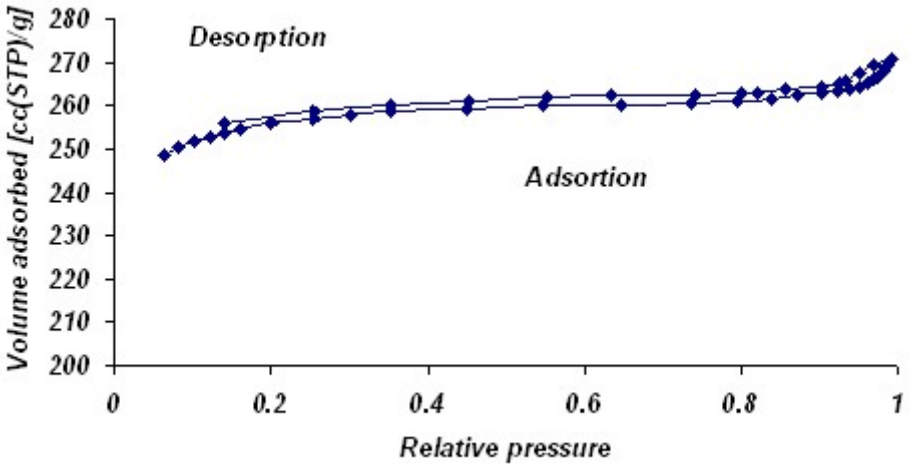

Fig. 4.15: Typical isotherm plot of chemically activated carbon produced from biochar (T = 675 ^{o}C, KOH/biochar = 1.63, and N_2 flow-rate = 165 cc/min)

4.3.2. Statistical analysis

Twenty experiments were performed to obtain a model (response surface) for the BET surface area of the product after acid washing (Y_1 in m^2/g) by the power transformation and discarding the insignificant effects. The response Y_1 in terms of process parameters is given by Eq (4-11).

$$\left(\frac{1}{\sqrt{Y_1}}\right) = 0.155 - 1.248*10^{-4}*T - 0.0586*R - 2.263*10^{-5}*F + 7.431*10^{-3}*R^2 + 3.794*10^{-5}*T*R \quad (4-11)$$

where, T is activation temperature (in the range of 550-800 ^oC), R is mass ratio of KOH to char (in the range of 0.25-3.00), and F is nitrogen flow rate (in the range of 80-250 ml/min).

Similarly, The model for the yield (Y_2 in wt %) of the product after activation reaction was also obtained as follows:

$$Y_2 = 73.05 - 3.5*A - 10.25*B - 5.21*B^2 - 3.17*A*D \quad (4-12)$$

where,

$$A = -1 + (T - 550)/125 \quad (4-13)$$

$$B = -1 + (R - 0.25)/1.375 \quad (4-14)$$

$$D = -1 + (F - 80)/85 \quad (4-15)$$

Table 4.10 shows the result of the test of significance of factors and interactions for the Y_1 and Y_2 before and after discarding insignificant terms. When p-value (probability value) of one term is more than 0.05, it indicates that this term is insignificant at the 95% confidence level and therefore that term must be discarded. Table 4.11 shows the R-square values for Y1 and Y_2 before and after discarding insignificant terms. For each of

Table 4.10: Results of test of significance of factors and interactions for the models Y_1 and Y_2 of chemically activated carbons

	p-value of factors of Y_1		***p-value of factors of Y_2***	
Factor or interaction	***All factors Included***	***Insignificant factors excluded***	***All factors Included***	***Insignificant factors excluded***
A	***<0.0001***	***<0.0001***	***0.0182***	***0.0092***
B	***<0.0001***	***<0.0001***	***<0.0001***	***<0.0001***
D	***0.0723***	***0.0359***	***0.8581***	***-***
A^2	***0.6253***	***-***	***0.3723***	***-***
B^2	***<0.0001***	***<0.0001***	***0.0206***	***0.0056***
D^2	***0.6544***	***-***	***0.2087***	***-***
AB	***0.0001***	***<0.0001***	***0.9554***	***-***
AD	***0.7339***	***-***	***0.0494***	***0.0317***
BD	***0.9276***	***-***	***0.2944***	***-***
Model	***<0.0001***	***<0.0001***	***0.0005***	***<0.0001***

Table 4.11: R-squared statistics for models Y_1 and Y_2 of chemically activated carbons

	R^2		***Adjusted R^2***		***Predicted R^2***	
Model	***All factors included***	***Insignificant factors excluded***	***All factors included***	***Insignificant factors excluded***	***All factors included***	***Insignificant factors excluded***
Y_1	***0.9747***	***0.9734***	***0.9519***	***0.9639***	***0.8663***	***0.9508***
Y_2	***0.9036***	***0.8712***	***0.8168***	***0.8369***	***0.0844***	***0.7353***

the models (Y_1 and Y_2), the predicted R^2 is in reasonable agreement with the adjusted R^2 because they are within 0.20 of each other. For lack-of-fit test, P-values for two models (Y_1 and Y_2) were 0.5001 and 0.1193, respectively.

Therefore, results of statistical tests showed that the models can navigate experimental data at the mentioned operating conditions.

4.3.3. Optimization of operating conditions

The optimum operating conditions were defined according to the following constraints:

1) BET surface area $\geq$ 700 m^2/g; 2) reaction yield $\geq$ 70.0 wt %.

The solution for the model is as follows: T = 680 ^{O}C, KOH/biochar = 1.23, N_2 flow rate = 240 cc/min.

The experiments were performed at these operating conditions and BET surface area of product and reaction yield were measured. The experimental results and the model predictions are presented in Table 4.12. As it can be seen, the difference of BET surface area is less than 7% and that of yield is less than 4%.

The product yield after acid washing was 25.6 wt%. Since mass ratio of KOH to biochar equals to 1.23, more than 50 wt% of the feed for this optimum product is impregnating agent (KOH). The price of this chemical is several times higher than that of biochar.

Therefore, the recovery of the chemical agent and its related cost have strong effects on the economy of chemical activation [Rodriguez-Reinoso, 2002] and an economical recovery method by acid washing should be developed for the production of low cost

Table 4.12: Predicted and experimental values of BET surface area and reaction yield for chemically activated carbons prepared at T = 680 ^{o}C, KOH/biochar = 1.23, and F = 240 cc/min

	Values predicted by models	Observed values
BET surface area (m^2/g)	783	836
Reaction yield (wt %)	75.3	78.0

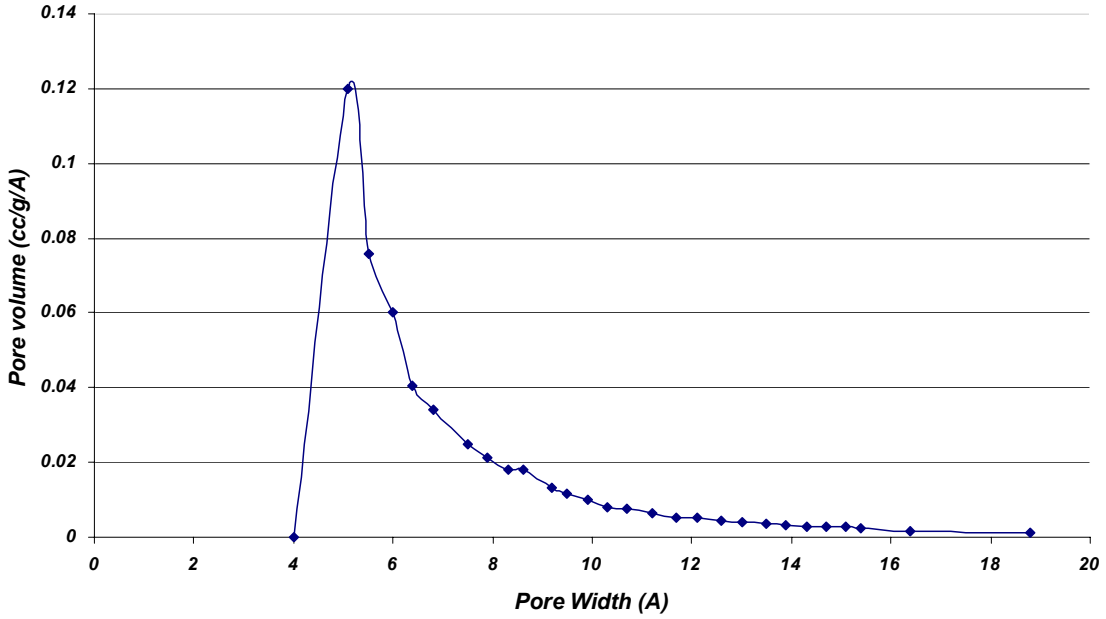

Fig. 4.16: Micropore size distribution for BioAC-Chem (measured by HK method)

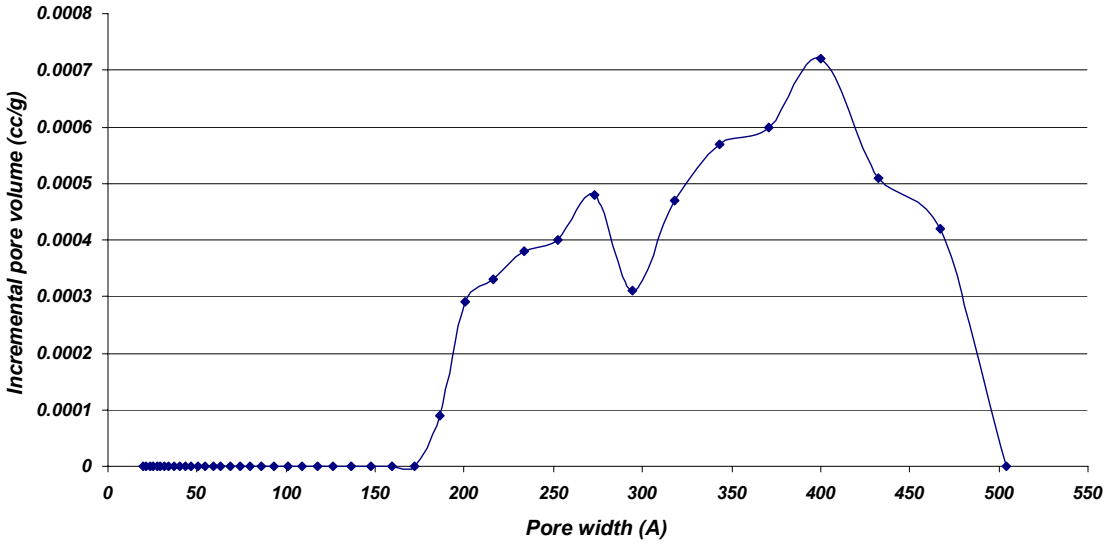

Fig. 4.17: Mesopore size distribution for BioAC-Chem (measured by DFT)

activated carbon by KOH chemical activation. The micropore and mesopore size distributions for this activated carbon are presented in Figures 4.16 and 4.17. The former is calculated using micropore analysis (HK method) and the latter is provided by density functional theory method.

The results of particle size analysis are shown in Appendix D. It shows that activated carbons produced by steam and KOH activations of biochar at optimum operating conditions are finer than the precursor (See Fig. D.2).

4.3.4. Crystalinity and surface chemistry of activated carbon

Fig. 4.18 shows the XRD-plot of activated carbon prepared at activation temperature of 675 ^{o}C, mass ratio of 1.63 and nitrogen flow rate of 165 cc/min, before acid washing. According to the observed peaks, $K_2CO_3.(1.5)H_2O$ was identified in the product of chemical activation before acid washing (peaks at 2θ = 12.8^{o}, 29.8^{o}, 32.2^{o}, 32.5^{o}, 32.7^{o} and 41.5^{o} for $K_2CO_3.(1.5H_2O)$). More study is required to specify the other possible potassium compounds in the product before acid washing. The products were then acid washed and subjected to XRD analysis.

Fig. 4.19 shows the X-ray diffraction spectra for biochar and two activated carbons prepared at the same mass ratio and nitrogen flow-rate but at different activation temperatures. It shows that by increasing activation temperature from 537.5 to 675 ^{o}C a small graphite-like structure forms in activated carbon (peaks at 2θ = 26.6 ^{o} and 44.5^{o}). This structure, known as turbostratic [Fan et al, 2004], can be two-dimensional order created by parallel orientation of carbon layer planes. This also indicates that potassium species are completely removed from the activated carbon.

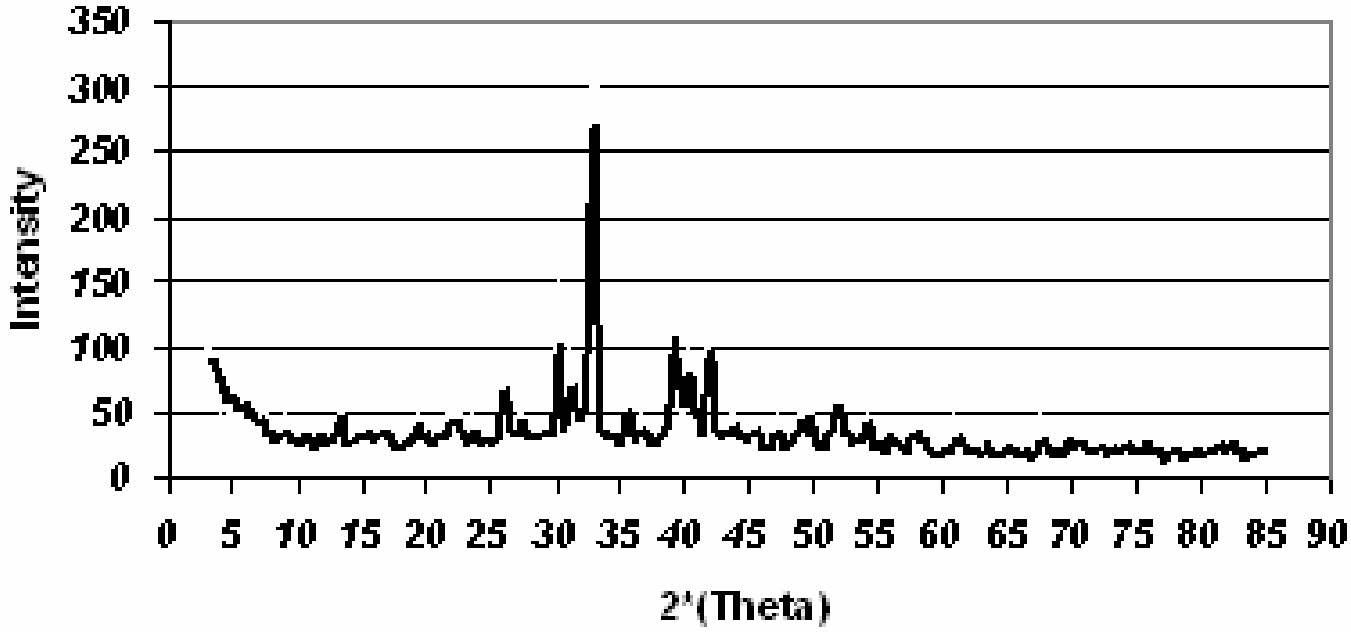

Fig. 4.18: X-ray diffraction of activated carbon prepared at T=675 ^{o}C , Mass ratio= 1.63 and F=165 cc/min (before acid washing)

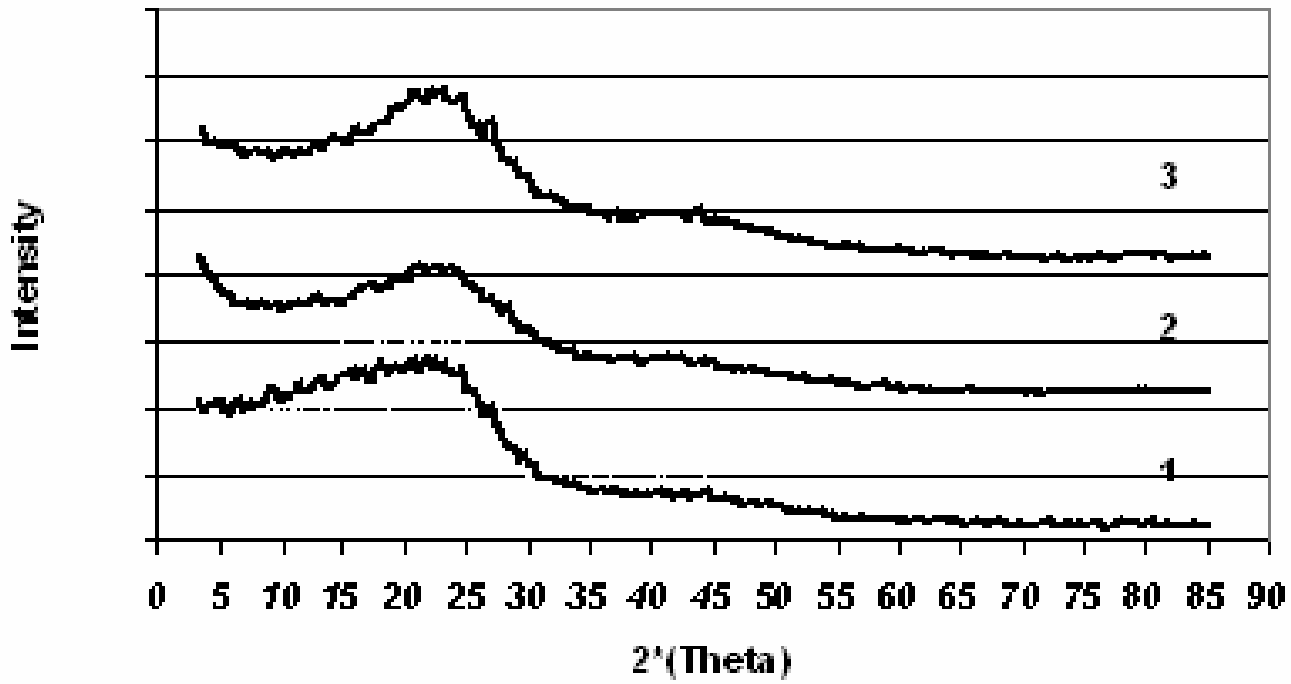

Fig. 4.19: XRD of biochar (1) and activated carbons prepared at mass ratio=1.63 and F=165 cc/min (2- T=537 ^{o}C and 3-T= 675 ^{o}C)

The scanning electron micrographs were taken for biochar, activated carbon prepared at activation temperature of 675 ^{o}C, KOH to biochar mass ratio of 1.63 and nitrogen flow rate of 165 cc/min before and after acid washing to examine their porous structures (see Figures 4.20 a, b, c). According to these micrographs, biochar does not have a porous structure, as confirmed by its low BET surface area, and for activated carbons, before acid washing pores are blocked by potassium and basic compounds, but washing with HCl/water removes them and exposes the porosity of the product.

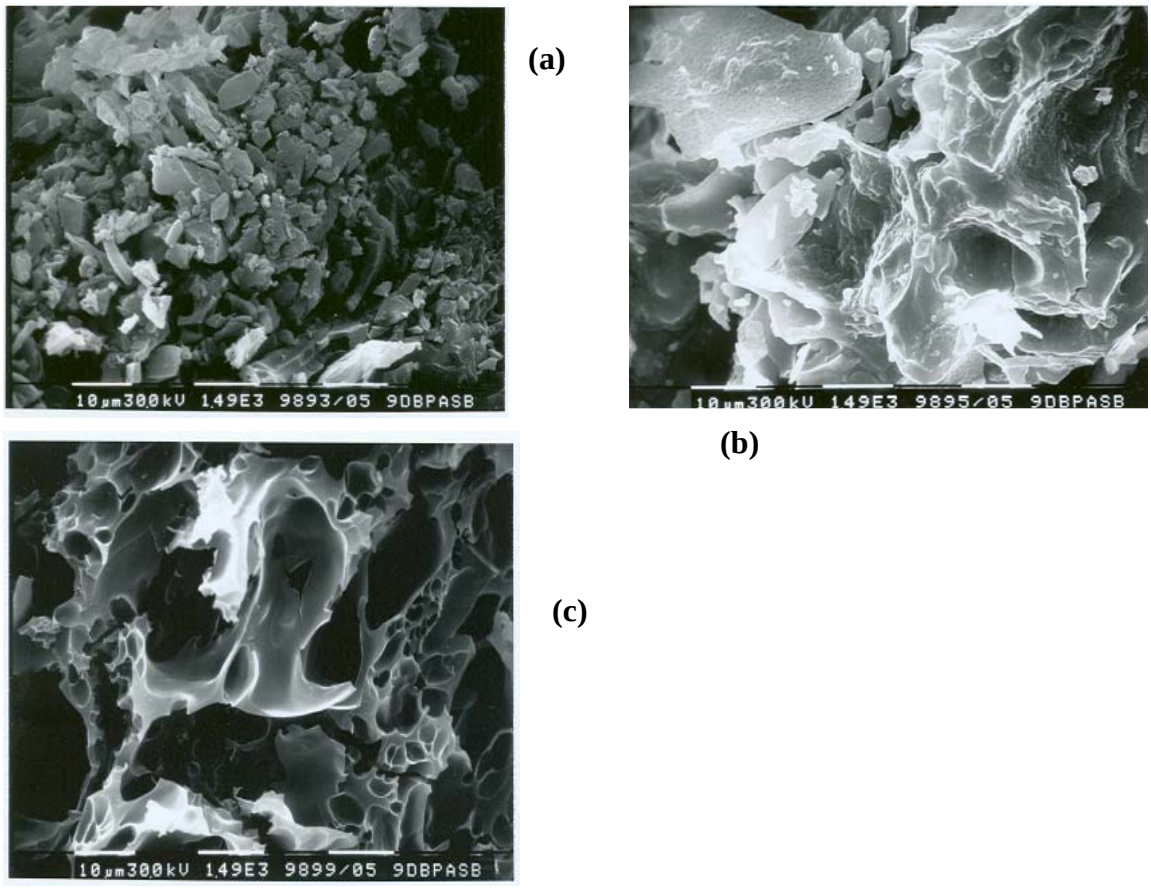

Fig. 4.20: Scanning electron micrographs of biochar (a), activated carbon before acid washing (b), and after acid washing (c) (prepared at activation temperature of 675 ^{o}C, KOH to biochar mass ratio of 1.63, and nitrogen flow rate of 165 cc/min), [Magnification: 1490X].

5.0. Hydrogen sulphide oxidation reaction using activated carbon

Hydrogen sulphide oxidation reaction using activated carbon catalyst is discussed in this chapter. The effects of one modification method on the porous structure, surface chemistry, and performance of activated carbons for catalytic oxidation of hydrogen sulphide to sulphur were discussed. The effect of impregnation process on the performance of catalyst is also described in this chapter. The other parts of this section deal with types of sulphur species in the products of reaction and regeneration of catalyst. Activated carbons were produced at optimum operating conditions using physical and chemical activations of biochar and physical activation of luscar char as discussed in previous chapter. They were used as catalysts for oxidation reaction of hydrogen sulphide. These activated carbons are referred to as LusAC (activated carbon produced from luscar char by steam activation), BioAC (activated carbon produced from biochar by steam activation), and BioAC-Chem (activated carbon produced from biochar by chemical activation) in this chapter. In addition, activated carbons prepared by acid-treatment/thermal desorption and impregnation from the originally steam-activated carbons were used as catalyst for oxidation reaction of hydrogen sulphide. These activated carbons are referred as:

BioAC-O : Activated carbon prepared by acid (HNO_3) -treatment of BioAC

BioAC-O-D(750) : Activated carbon prepared by thermal desorption of BioAC-O at 750 ^oC

LusAC-O : Activated carbon prepared by acid (HNO_3) -treatment of LusAC

LusAC-O-D(650) : Activated carbon prepared by thermal desorption of LusAC-O at 650 ^oC

LusAC-O-D(650)-K(5%): LusAC-O-D(650) impregnated with 5 wt % of KI

The preparation of these activated carbons is discussed in chapter 3.

5.1. Performance of modified catalysts

The performances of original activated carbons, modified catalysts prepared from them, impregnated catalysts, and a commercial activated carbon (Centaur supplied by Calgon Co.) were evaluated for H_2S oxidation reaction at 175 ^oC, 700 kPa, and oxygen concentration of 1.05 times of stoichiometric ratio and are documented in Table 5.1. The performances are evaluated in terms of break-through time of H_2S, $g_{Sulphur}/g_{Carbon}$, and average production of SO_2 (as % of H_2S concentration in the feed gas). When the H_2S conversion dropped below 80 % (2000 ppm of H_2S outlet concentration), the reaction was stopped and this reaction time period was called break-through time. $g_{Sulphur}/g_{Carbon}$ shows the amount of sulphur captured per unit mass of activated carbon during the reaction time. The average production of SO_2 is the ratio of SO_2 produced in the reaction time to the total amount of H_2S fed to the reactor during this time period.

The break-through times for the originally activated carbons (LusAC, BioAC, and BioAC-Chem) were more than one hour and the production of SO_2 was very low. To improve the performance, increasing the number of active sites and surface area can be useful. Generally, the performance of activated carbon for catalytic reactions is not directly correlated to the surface area [Marsh and Rodriguez-Reinoso, 2006], then the modification method must be able to affect surface chemistry and surface area, both. To improve the performance of activated carbons prepared by physical activation of both precursors, oxidation with nitric acid (HNO_3) followed by thermal desorption was used.

Figuers 5.1, 5.2, and 5.3 show the H_2S conversion and SO_2 concentration during the reaction time for BioAC-O-D(750), LusAC-O-D(650)-K(5%), and LusAC-O-D(650) catalysts, respectively. As it was mentioned, these runs were stopped when the H_2S conversion dropped less than 80 %. These Figures show that;

a) SO_2 production increased only prior to point at which complete conversion of H_2S ceases to occur. It can be due to increase in vapor pressure of sulphur to a maximum allowing production of SO_2 possibly by the following gas phase reaction or surface reaction between adsorbed suphur and oxygen on the carbon surface (reactions 6-4 and 6-5):

$$S + O_2 \rightarrow SO_2 \qquad \Delta H = -297 \text{ kJ/mol} \qquad (5\text{-}1)$$

When the conversion of H_2S is less than 100%, the residual H_2S reacts with the SO_2 according to the following reaction producing sulphur and water, thus lowering SO_2 production.

$$2H_2S + SO_2 \rightarrow 3S + 2H_2O \qquad \Delta H = -146 \text{ kJ/mol} \qquad (5\text{-}2)$$

b) Comparing Figures 5.2 and 5.3 shows the effect of impregnation (using KI) on the performance of catalyst. Performance of LusAC-O-D(650) increased by addition of 5 wt % of KI. As it can be seen, the break-through time increased after impregnation, but it produced more SO_2 in small extent.

The reproducibility of H_2S oxidation runs is shown in Appendix E for LusAC-O-D(650)-K(5%). This catalyst was impregnated using dimethyl sulfoxide (DMSO) as impregnating solvent. As it is shown in this Appendix, For $g_{Sulphur}/g_{Carbon}$ and break-

Table 5.1 : Performance of activated carbons prepared at optimum operating conditions by physical and chemical activation of precursors, the modified catalysts, and a commercial activated carbon at reaction temperature of 175 ^{o}C, pressure of 700 kPa, and oxygen concentration of 1.05 times of stoichiometric ratio

Catalyst	BET surface area (m^2/g)	Total pore Volume (cc/g)	B-T$^{\#}$ time (min)	$g_{Sulphur}/g_{Carbon}$	Avg. SO_2 production^{+}
BioAC	664	0.332	77	0.44	0.01
BioAC-O	640	0.310	65	0.39	0.33
BioAC-O-D(750)	794	0.368	141	0.90	0.14
BioAC-Chem	836	0.396	90	0.54	0.00
LusAC	502	0.303	63	0.38	0.01
LusAC-O	601	0.363	62	0.36	0.22
LusAC-O-D(650)	736	0.432	115	0.69	0.03
LusAC-O-D(650)-K(5%) (Solution: Water)	729	-	138	0.85	0.05
LusAC-O-D(650)-K(5%) (Solution: DMSO*)	718	-	155	1.00	0.31
Centaur	773	0.380	113	0.67	0.56

Break-through, + as % of H_2S in feed, * Dimethyl sulfoxide [CH_3-S(=O)-CH_3]

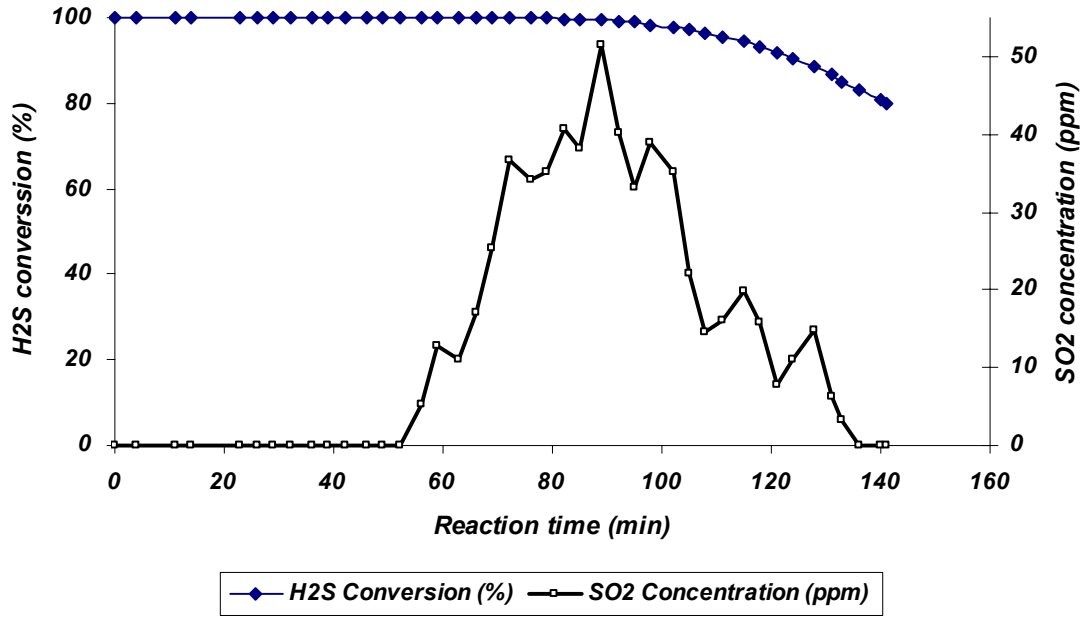

Fig. 5.1: H_2S conversion and SO_2 concentration vs. reaction time for BioAC-O-D(750) catalyst at reaction temperature and pressure of 175 ^oC and 700 kPa, respectively, and oxygen concentration of 1.05 times of stoichiometry

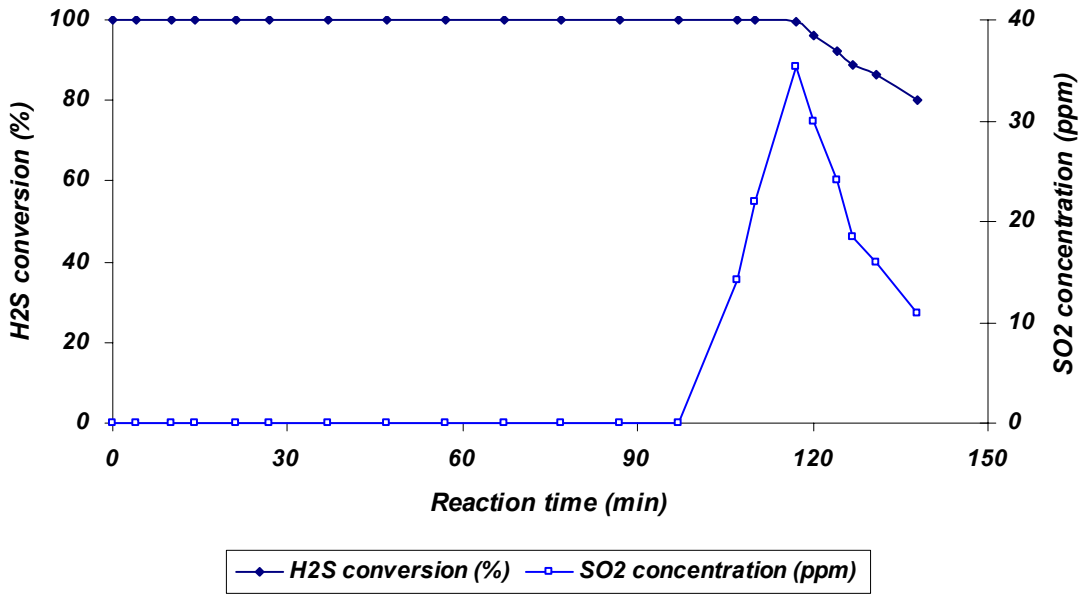

Fig. 5.2:H_2S conversion and SO_2 concentration vs. reaction time for LusAC-O-D(650)-K(5%) catalyst at reaction temperature and pressure of 175 ^oC and 700 kPa, respectively, and oxygen concentration of 1.05 times of stoichiometry

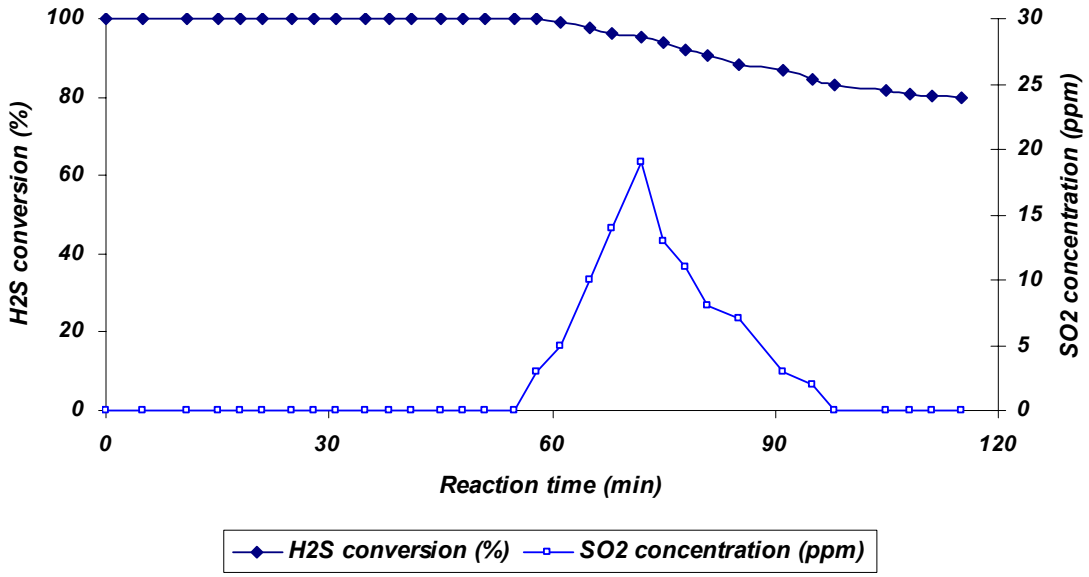

Fig. 5.3: H_2S conversion and SO_2 concentration vs. reaction time for LusAC-O-D(650) catalyst at reaction temperature and pressure of 175 ^oC and 700 kPa, respectively, and oxygen concentration of 1.05 times of stoichiometry

through time of two runs the difference in percentage was 3.72 and 3.87 %, respectively. The percentage difference of average SO_2 production was 6.84 %.

5.1.1. Effect of porous structure

One of the main reasons for extensive applications of activated carbons as adsorbent, catalyst support, and catalyst is their highly developed porous structure which can provide a good dispersion of active sites for adsorption or reaction and appropriate space for storing adsorbed species or reaction products. Micro, meso, and macropores form the porous structure of activated carbons. This structure is a function of activation method, post treatments, and precursor.

Table 5.2 shows the ultramicropore (≤ 7 Å), supermicropore (7-20 Å), micropore, mesopore, total pore volume, and the BET surface area of original steam activated carbons and activated carbons prepared by acid-treatment and thermal desorption from them. All parameters in this Table, excepting BET surface area, are measured using density functional theory (DFT) method. For activated carbons prepared by treatment on BioAC, it can be seen that acid-treatment decreased all porous characteristics excepting supermicropore volume in small extent. It can be because of the formation of some surface groups which results in blockage of some pores. This phenomenon was observed by some other researchers too [Rodriguez-reinoso and Molina-Sabio, 1998]. Thermal desorption increased all porous characteristics by removal of some surface groups and in addition, some blocked pores in original activated carbon was opened by acid-treatment/thermal desorption process. Therefore, total, mesopore, and micropore volume

increased by 11, 10 and 11 %, respectively. This method increased the BET surface area for 20 %.

For activated carbons prepared by treatment on LusAC, all porous characteristics increased after each step of treatment. An increase in porous characteristics after acid treatment can be because of the high amount of ash content in LusAC (19.2 wt %). After acid-treatment, this ash content decreased to 7.11 wt %. It is because of removal of ash content by nitric acid in acid-treatment. Thermal desorption increased this value to 9.93 wt % by removal of some functional groups. Table 5.2 shows that total, mesopore, and micropore volume increased by 43, 43 and 43 %, respectively. This method increased the BET surface area for 47 %. Although acid-treatment/thermal adsorption method was effective for porosity development of this activated carbon, but removal of ash content can not be ignored. This removal can be the main reason for higher porosity development in modified activated carbon prepared from LusAC comparing with that for modified activated carbon prepared from BioAC. Figures 5.4 and 5.5 show the incremental micropore and mesopore volumes for LusAC and modified activated carbons prepared from that. For entire range of pores, each step of modification improved the pore volume. Figures 5.6 and 5.7 show the incremental micropore and mesopore volumes for BioAC and modified activated carbons prepared from that, respectively. It can be seen that BioAC-O has lower amount of incremental pore volume for approximately entire range of micropores and mesopores comparing to BioAC. It means that acid-treatment blocked some pores by surface functional groups [Pradhan and Sandle, 1999]. But BioAC-O-D(750), excepting pores smaller than 7 Å and pores larger than 180 Å, has higher incremental pore volume comparing to BioAC.

Table 5.2: Porous characteristics of original and modified activated carbons prepared from luscar char and biochar (measured using DFT)

Catalyst	Pore volume (for pores ≤7Å), cc/g	Pore volume (for pores 7-20 Å), cc/g	Micropore volume (for pores ≤20 Å), cc/g	Mesopore volume (for pores 20-500 Å), cc/g	Total pore volume, cc/g	BET surface area, m^2/g
BioAC	0.163	0.057	0.220	0.112	0.332	664
BioAC-O	0.141	0.074	0.215	0.094	0.310	640
BioAC-O-D(750)	0.151	0.093	0.244	0.124	0.368	794
BioAC-Chem	0.207	0.121	0.328	0.006	0.396	836
LusAC	0.108	0.049	0.157	0.146	0.303	502
LusAC-O	0.110	0.072	0.182	0.180	0.363	601
LusAC-O-D(650)	0.130	0.093	0.224	0.210	0.432	736

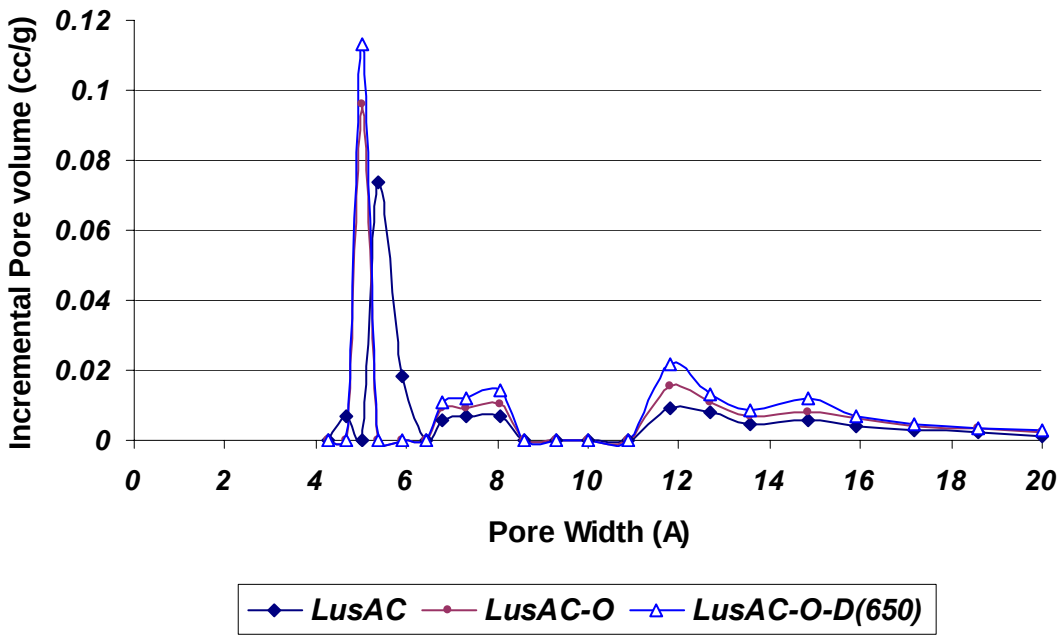

Fig. 5.4: Incremental micropore volume for LusAC and modified catalysts prepared from that (measured using DFT)

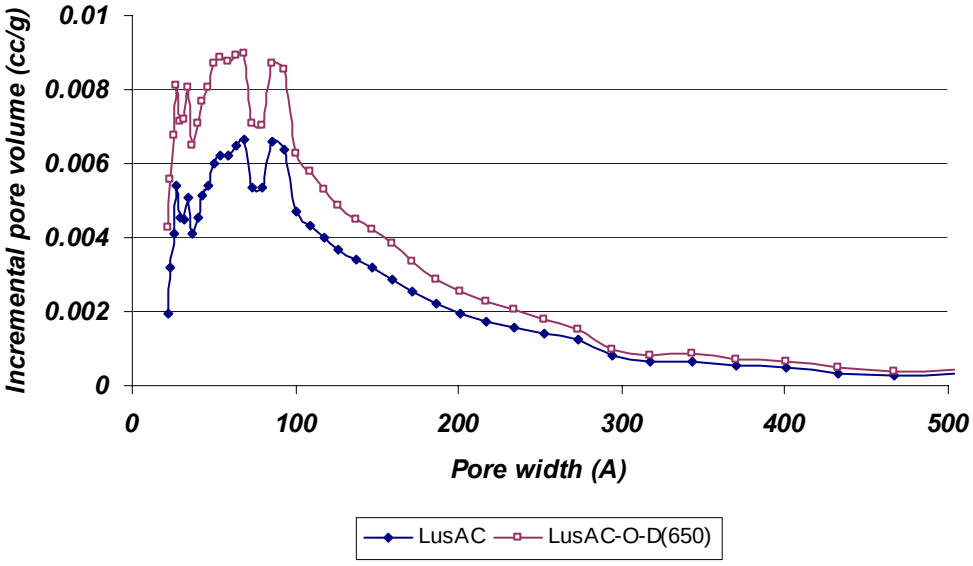

Fig. 5.5: Incremental mesopore volume for LusAC and modified catalyst prepared from that (measured using DFT)

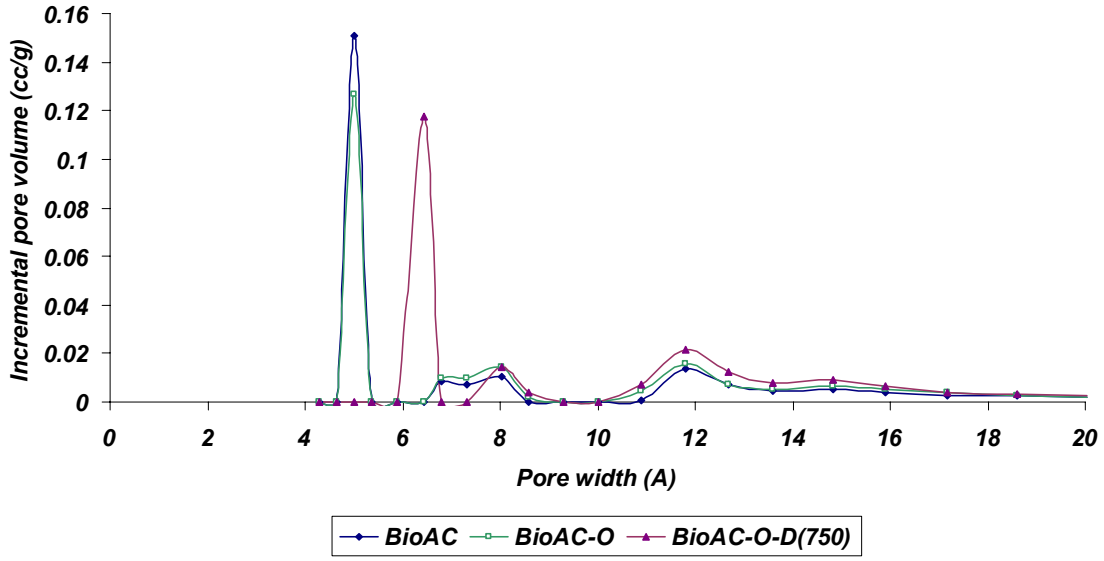

Fig. 5.6: Incremental micropore volume for BioAC and modified catalysts prepared from that (measured using DFT)

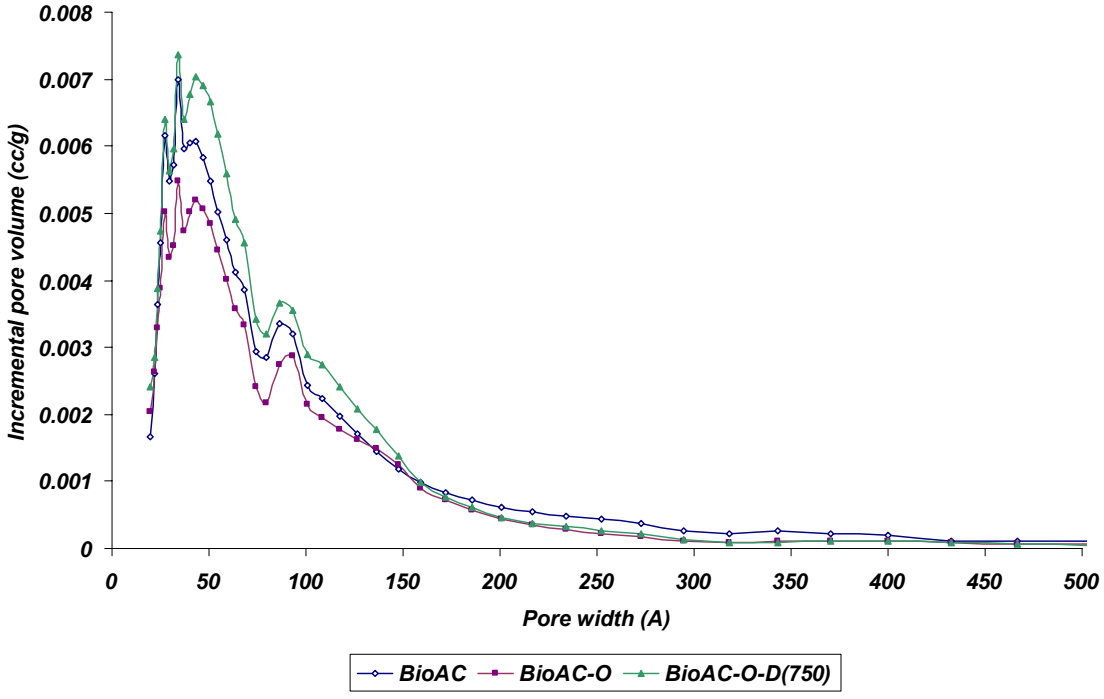

Fig. 5.7: Incremental mesoopore volume for BioAC and modified catalysts prepared from that (measured using DFT)

These results showed that for both precursors, the modification method increased micropore, mesopore, and total pore volume of originally steam-activated carbon for relatively equal percentages. Better performance of BioAC-O-D(750) and LusAC-O-D(650) can be due to higher pore volume of these modified catalysts comparing with that for original steam activated carbons (BioAC and LusAC). This enhancement in pore structure provides more storage space for sulphur product resulting in higher break-through time and more amount of $g_{Sulphur}/g_{Carbon}$.

Using this treatment, ultramicropore (<7 Å) volume of BioAC-O-D(750) decreased by 7 %, while that for LusAC-O-D(650) increased by 20 %. But supermicropore (7-20 Å) volume increased by 63 and 92 % for BioAC-O-D(750) and LusAC-O-D(650), respectively, using this treatment. Considering the important effect of micropores in enhancement of catalytic reaction on activated carbons, this large increase in supermicropore volume can be one of the reasons for better performance of modified catalyst by providing more active sites.

Although reactions are mostly supposed to take place in micropores [Steijns and Mars, 1977; Choi et al, 1991; Steijns and Mars, 1974], mesopores can serve as the channels for access to micropores [Rodriguez-Reinoso, 1997]. Then, improvement in mesopore volume is necessary for enhancement of the performance of catalyst. The modification method increased mesopore volume for BioAC-O-D(750) and LusAC-O-D(650) comparing with the original steam activated carbons.

Porous characteristics, such as surface area and pore volume, are an important factor for performance of activated carbon as catalyst, but effects of other parameters such as active sites and surface chemistry can not be ignored. For example, BET surface area of LusAC-

O was 22 % more than that for the original activated carbon (LusAC) due to the activation effect of nitric acid and lower amount of ash content [Derbyshire et al, 1995] and other porous characteristic of that were larger than those for LusAC (see Table 5.2), but there was no improvement in the performance of oxidized catalyst compared with LusAC (see Table 5.1). It can be because of the formation of some acidic groups on the carbon surface by acid-treatment which are discussed in the next section. Lower performance of BioAC-O comparing to BioAC can be due to the same reason. Another example is BioAC-Chem which has better porous characteristics comparing with BioAC-O-D(750), (see Table 5.2), but the performance of the latter is better than the former catalyst (see Table 5.1). It can be because of lower percentage of mesopores in BioAC-Chem in comparison with that in BioAC-O-D(750) or its different surface chemistry features (See Table 5.3).

5.1.2. Effect of surface chemistry

The adsorptive and catalytic properties of activated carbon are governed not only by its porous structure but also by its surface properties and chemical structure [Rodriguez-Reinoso, 1998]. Activated carbon structure includes heteroatoms such as oxygen and nitrogen, carbon active sites (energetic carbon surface sites), e.g., dangling carbon bands, and inorganic ash components [McEnaney, 2002]. Heteroatoms are a part of precursor which are formed in activation process, or are produced by post-treatments [Rodriguez-Reinoso, 1997]. The presence of these heteroatoms introduces active sites on the carbon surface [Rodriguez-Reinoso, 1998]. Adsorptive and catalytic properties of activated carbon surface can be enhanced by modification (as post treatment) and impregnation

[Bagreev and Bandosz, 2002]. This modification is based on the alternation of surface chemistry of the carbon matrix and incorporation of heteroatoms [Bagreev et al, 2004]. These heteroatoms not only change the acidic/basic character of carbon but also contribute to changes in the electrochemical and catalytical properties of the matrix [Leon et al, 1994 ; Stohr et al, 1991; Lahaye et al, 1999]. Oxygen surface groups are considered as the most significant functionalities on the activated carbon surface because of their abundant quantities in comparison with other surface groups and their effects on the catalytic and adsorptive properties of activated carbon. Carboxylic, lactone, phenol, carbonyl, ether, pyrone and chromene groups are examples of oxygen functionalities. The chemical structures of some of these groups are shown in Fig. 2.6. Carboxylic, lactone and hydroxyl groups of phenolic character groups are considered as the acidic groups. The origin of surface basicity is still not clear. Source of basic behavior of carbon surface can be the π basicity of the exposed graphene layers or some chemical groups such as chromene, quinone, and pyrone. However, one of the reasons why not enough information is available on the nature of basic groups is the lack of adequate and selective evaluation methods for basic groups [Rodrigiez-Reinoso and Molina-Sabio, 1998; Boehm, 2002].

To analyze carbon surface chemistry and surface functionalities, it is recommended to use only chemical analytical methods with probe reactions. These methods are based on titration and are more selective and accurate than other methods [Boehm and Voll, 1970; Voll and Boehm, 1971]. Direct titration methods are not suitable for this purpose because of the complicated pore structure of activated carbon and hydrophobic character of carbon. These factors make the equilibration of chemical reagent with surface groups

slow [Sclögl, 2002]. The back titration is more reliable [Boehm and Voll, 1970; Papirer and Guyon, 1978]. In this method, sample is brought into contact with a reagent and after 24 hours of shaking, the filtrate is titrated with suitable chemical reagent. The result of this method can be supported by TPD analysis. Vibrational spectroscopy may be useful for focusing on the average local structure [Sclögl, 2002]. Although molecular organic compounds are the main basis for assignment of the bands, there are disagreements in that [Boehm, 2002]. This problem is due to the contribution of each band in different groups which makes the interpretation of the spectra difficult [Figueiredo et al, 1999]. Physical-analytical methods are not recommended for characterization of surface characteristics of activated carbons [Sclögl, 2002].

Highly porous activated carbons consist of sp^2-hybridized carbon atoms (non-graphitized, turbostratic carbons). Therefore, the internal structure is formed by many graphene sheets and edges of such layers which are more reactive than the atoms in the interior of the graphene sheets. These edges are the most suitable sites for chemisorbed foreign elements, in particular oxygen [Boehm, 2002]. When molecular oxygen is introduced to an outgassed carbon surface, it can be either physically, reversibly adsorbed or it is chemisorbed on the surface depending on the temperature. At low temperatures the adsorption is completely reversible, but at high temperatures, oxygen is adsorbed chemically and the molecule dissociates into atoms that react chemically with the atoms of carbon to form oxygen surface groups [Leon and Radovic, 1994]. Activated carbons produced by thermal processes have a low amount of oxygen surface groups which are produced by sorption of oxygen from the air [Rodrigiez-Reinoso and Molina-Sabio1998; Mattson and Mark, 1971]. Oxygen surface groups are not only formed by reaction with

oxygen but they can be produced by reaction with oxidizing gases such as ozone, nitrous oxide and nitric oxide or reaction with oxidizing solutions such as nitric acid and hydrogen peroxide [Tremblay et al, 1978; Rodriguez-Reinoso, 1998].

In this study, Boehm titration and temperature programmed desorption (TPD) were used to study the acidic and basic character of carbon surface. The results obtained by Boehm titration were presented in Table 5.3.This Table shows the total acidic, total basic and carboxylic groups concentrations measured by Boehm titration method and ratio of total basic to total acidic groups for BioAC-O, BioAC-O-D(750), BioAC-Chem, LusAC-O, and LusAC-O-D(650) catalysts. It can be seen that, after acid-treatment, activated carbons possessed relatively high amount of acidic groups such as carboxylic groups. Generally, an increase in oxygen content increases the acidity of carbon material [Rodriguez-Reinoso, 1997], which can be the reason of no improvement in the performance of oxidized activated carbon (LusAC-O and BioAC-O) comparing with original activated carbons. For both types of activated carbons prepared from luscar char and biochar the amount of total acidic groups decreased by thermal desorption of oxidized sample. This process not only removed carboxylic groups produced by nitric acid treatment, but also strongly increased the ratio of total basic to total acidic groups in comparison with oxidized samples. As it was mentioned in section 2.2.5.1., one of the common methods for qualitative study of surface groups on the activated carbons is the heat treatment of sample under an inert atmosphere from room temperature to high temperatures such as 800-900 ^{o}C, called temperature programmed desorption (TPD).

Table 5.3: Boehm titration results for original steam-activated carbons and modified activated carbons

Catalyst	Total acidic groups (mmol/g)	Total basic Groups (mmol/g)	Basic/Acidic	Carboxylic groups (mmol/g)
BioAC-O	2.18	0.34	0.16	1.38
BioAC-O-D(750)	0.20	0.55	2.75	0.00
BioAC-Chem	0.50	0.29	0.58	0.22
LusAC-O	1.88	0.20	0.11	1.18
LusAC-O-D(650)	0.31	0.64	2.06	0.00

According to the literature [Figueiredo et al, 1999; Molina-Sabio et al, 1991; Marsh and Rodriguez-Reinoso, 2006], evolutions of CO_2 and CO at special range of temperatures during the heat treatment can be related to different acidic and basic groups. This method was used for oxidized samples and thermally desorbed samples to study the acidic and basic groups on them.

As can be seen in Fig. 5.8, thermal treatment of LusAC-O in an inert atmosphere produces two peaks for carbon dioxide evolution (at 300-400 ^{o}C and 600-800 ^{o}C) and two peaks for carbon monoxide evolution (at 700-800 ^{o}C and 800-900 ^{o}C). The similar result can be found in literature [Rodriguez-Reinoso, 1997]. To study the effect of thermal desorption temperature on the CO_2 and CO evolution, three samples were produced by thermal desorption of LusAC-O at three different temperatures of 550, 650, and 750 ^{o}C. Fig. 5.9 shows the concentration of CO_2 evolution from LusAC-O, LusAC-O-D(550), LusAC-O-D(650), and LusAC-O-D(750) during heat treatment from 25 to 1000 ^{o}C under flow of nitrogen gas. It can be observed in this Figure that CO_2 evolution from thermally desorbed samples is very small compared to that from the oxidized sample. This phenomenon is evident from CO_2 evolution peak at 300 ^{o}C. There is no peak for thermally desorbed samples at this temperature. Therefore, it can be inferred that the desorption helped to remove main part of carboxylic groups.

Fig. 5.10 shows the concentration of CO evolution from LusAC-O, LusAC-O-D(550), LusAC-O-D(650), and LusAC-O-D(750) during heat treatment from 25 to 1000 ^{o}C under flow of nitrogen gas. In this Figure, it can be seen that by an increase in the thermal desorption temperature, less amount of CO evolved from thermally desorbed sample which may be related to the removal of more basic groups from the carbon surface.

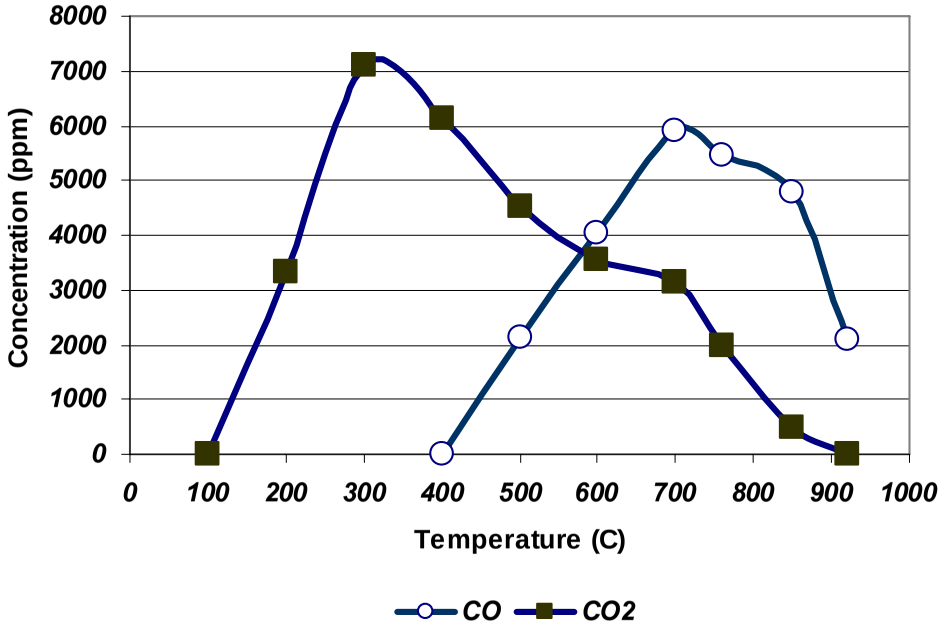

Fig. 5.8: Concentration of CO and CO_2 evolved during heat treatment of LusAC-O from 25 to 900 ^{o}C under nitrogen flow

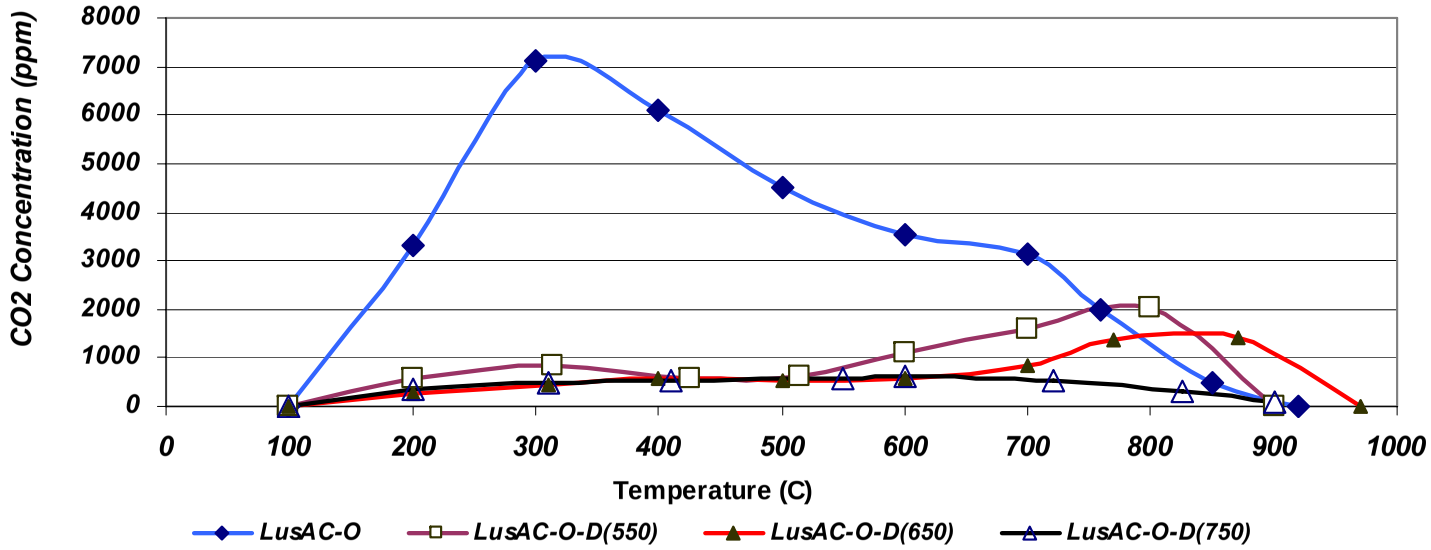

Fig. 5.9: Concentration of CO_2 evolved during heat treatment of LusAC-O, LusAC-O-D(550), LusAC-O-D(650), and LusAC-O-D(750) from 25 to 1000 ^{o}C under nitrogen flow

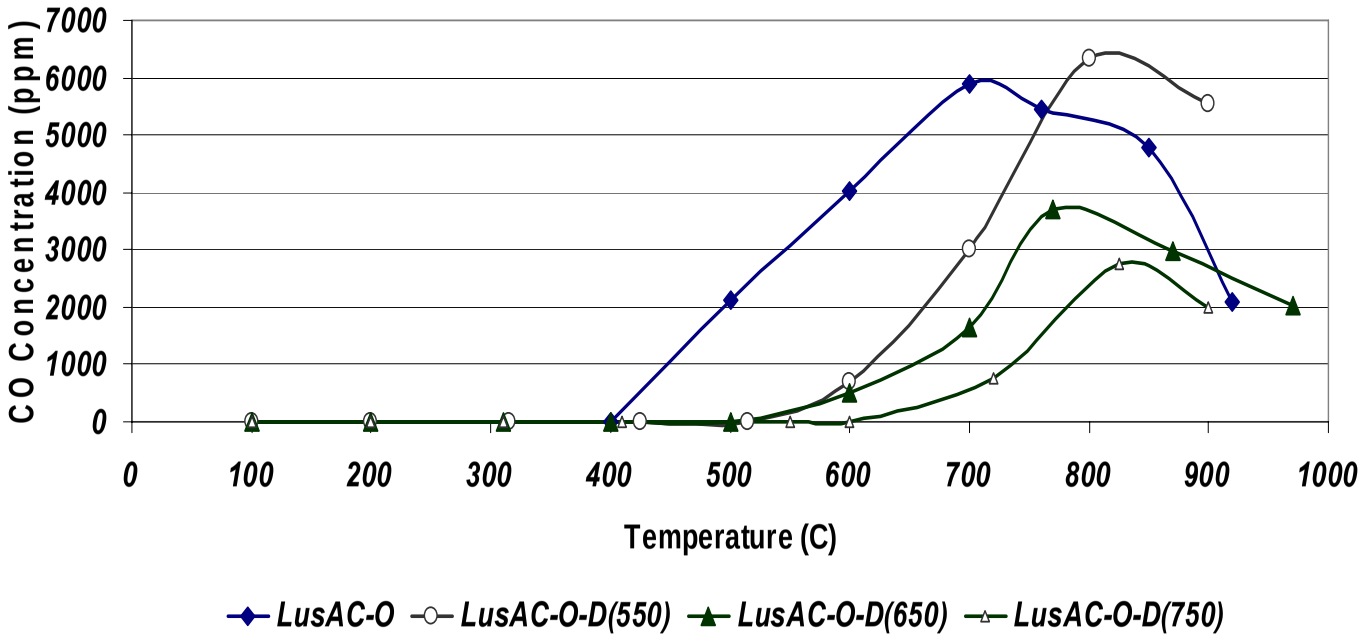

Fig. 5.10: Concentration of CO evolved during heat treatment of LusAC-O, LusAC-O-D(550), LusAC-O-D(650),and LusAC-O-D(750) from 25 to 900 ^{o}C under nitrogen flow

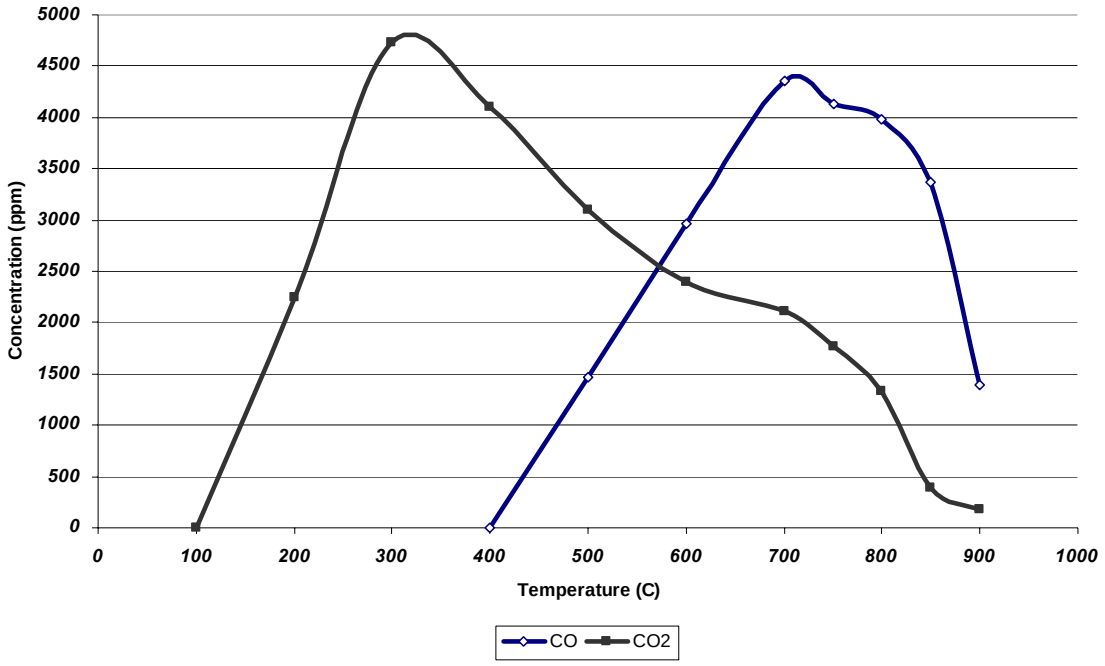

Fig. 5.11: Concentration of CO and CO_2 evolved during heat treatment of BioAC-O from 25 to 900 ^{o}C under nitrogen flow

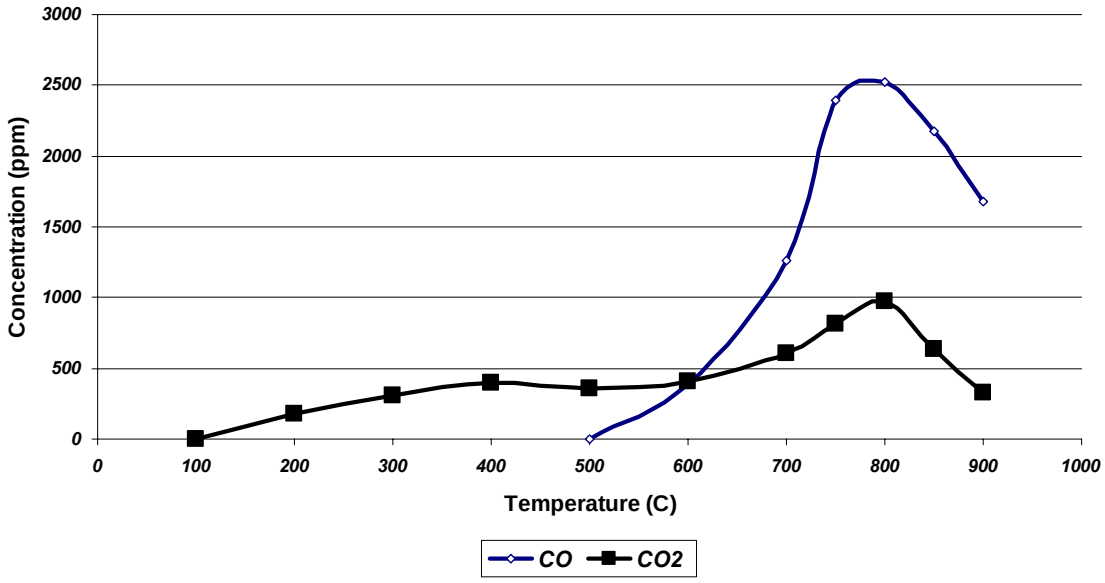

Fig. 5.12: Concentration of CO and CO_2 evolved during heat treatment of BioAC-O-D(750) from 25 to 900 ^{o}C under nitrogen flow

Figures 5.11 and 5.12 show the evolution of CO and CO_2 from BioAC-O and BioAC-O-D(750), respectively. They showed the same trend observed for LusAC-O and LusAC-O-D(650). After thermal desorption, there is no peak for CO_2 evolution at 300 ^oC and absolute values of evolution for CO and CO_2 decreased too.

Boehm titration showed that original steam-activated carbons (LusAC and BioAC) had high basic character, 2.19 and 1.03 mmol/g for LusAC and BioAC, respectively. LusAC had a high ash content (19.20 wt %) and removal of them by HCl in the mixing stage can be one reason for this high basicity observed by Boehm titration. The basic character of BioAC can be ascribed to the π electron system of the basal planes of carbon. It is known that activated carbons produced by thermal processes have a low amount of oxygen surface groups [Rodrigiez-Reinoso and Molina-Sabio1998; Mattson and Mark, 1971] and although the basicity of carbon basal planes is relatively weak, it is sufficiently basic to bind protons from aqueous solutions of acids [Rivin, 1963; Leon et al, 1992; Boehm and Voll, 1970; Montes-Moran et al, 1998].

Fig. 5.13 shows the CO_2 and CO evolved from BioAC in the temperature range of 25-900 ^oC. It can be seen that amount of gases evolved are lower than that for modified catalysts. In addition, BioAC was thermally desorbed at 750 ^oC to remove the possible surface groups from the carbon surface and then Boehm titration was used to measure acidic and basic character of this sample. It showed approximately the same basicity measured for BioAC (1.07 mmol/g). Therefore, maybe the high basicity of BioAC measured by Boehm titration can be due to be π-electron of basal planes and not basic surface groups.

Figures 5.14 and 5.15 show the FTIR spectra for the original steam activated carbon and oxidized activated carbons prepared from luscar char and biochar, respectively. The formation of some functional groups after acid-treatment can be seen in these Figures. However, based on the literature, the following assignment of the bands is possible:

Peak in the range of 1710-1760 cm^{-1} can be assigned to C=O stretch for carboxyl and lactone group [Ishizaki and Marti, 1981]. Peak in the range of 1500-1670 cm^{-1} can be assigned to C=O stretch for carboxyl group [Ishizaki and Marti, 1981]. Peak in the range of 1585-1600 cm^{-1} can be related to aromatic C=C stretching [Fanning and Vannice, 1993]. Peak at 1600 cm^{-1} can be associated with quinone [Fanning and Vannice, 1993; Studebaker, 1955]. The broad band centered around 1250 cm^{-1} can be for C-O stretching in ethers, lactones, phenols, and carboxylic anhydrides [Figueiredo et al, 1999; Boehm, 2002; Boehm, 1994]. This information shows the effect of acid treatment on the formation of some functional groups on the carbon surface which are mostly acidic.

Results of TPD for thermally desorbed, oxidized samples were in agreement with that for other researchers who have used this method [Rodriguez-Reinoso and Molina-Sabio, 1998; Lizzio and DeBarr, 1996]. Results of Boehm titration and TPD showed that acid-treatment produced some functional groups (C-O complexes), especially acidic groups, on the surface of carbon. Thermal desorption removed most of these acidic groups, such as carboxylic groups, and increased the ratio of basic to acidic groups for LusAC-O-D(650) and BioAC-O-D(750) comparing with oxidized samples.

The modification process had a positive effect on the performance of catalysts for H_2S oxidation reaction. The nature of basic character of activated carbon is still under discussion. Some oxygen functional groups such as pyrone [Voll and Boehm, 1971;

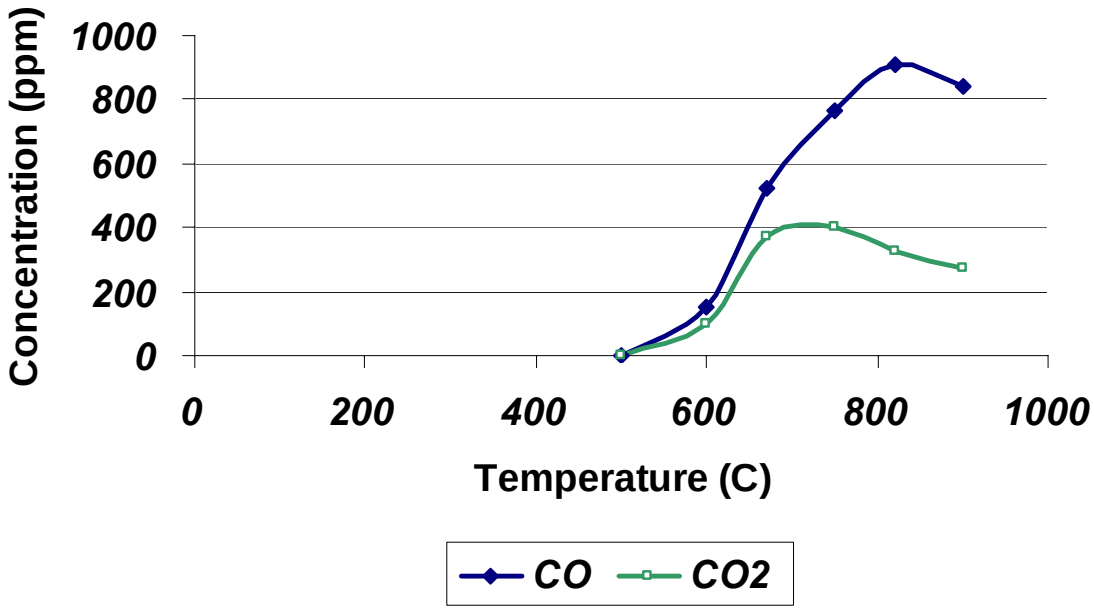

Fig. 5.13: Concentration of CO and CO_2 evolved during heat treatment of BioAC from 25 to 900 ^{o}C under nitrogen flow

Bagreev et al, 2002], chromene [Garten and Weiss, 1957], and quinone [Boehm, 1994] are considered as the origins of basicity. Some researchers supposed that modification methods such as acid-treatment/thermal desorption produce active sites by the removal of C-O complexes [Cal et al, 2000; Phillips, 1996; Mangun et al, 2001] and some others related it to the type of chemisorbed charged oxygen species [Brazhnyk et al, 2007].

But there is no selective and accurate characterization method to show the relative strength of these basic sources [Marsh and Rodriguez-Reinoso, 2006] and more study is needed to identify the nature of these active sites.

Use of one-step process including thermal desorption instead of the two-step process of acid-treatment/thermal desorption had no effect on the performance of the catalyst. For example, thermal desorption of LusAC at 650 ^{o}C increased the BET surface area by 7.6 %. The yield of thermal desorption process of LusAC at 650 ^{o}C was 96.7% and the ash content of LusAC-D(650), (19.3 wt %), was approximately similar to that of LusAC, (19.2 wt %). These facts show that LusAC has a small amount of surface functional groups and to improve its catalytic performance for the removal of H_2S, oxidation by nitric acid was necessary.

The amount of acidic groups on the surface of chemically activated carbon was more than basic groups and ~ 44 % of that was carboxylic groups (see Table 5.3). The surface chemistry modification was not performed for chemically activated carbon produced from biochar because of the low product yield of this activation process (25.6 wt % after removal of potassium compounds). Compared to the yield of physically activated carbon produced from biochar, the production cost for this catalyst would be higher compared to

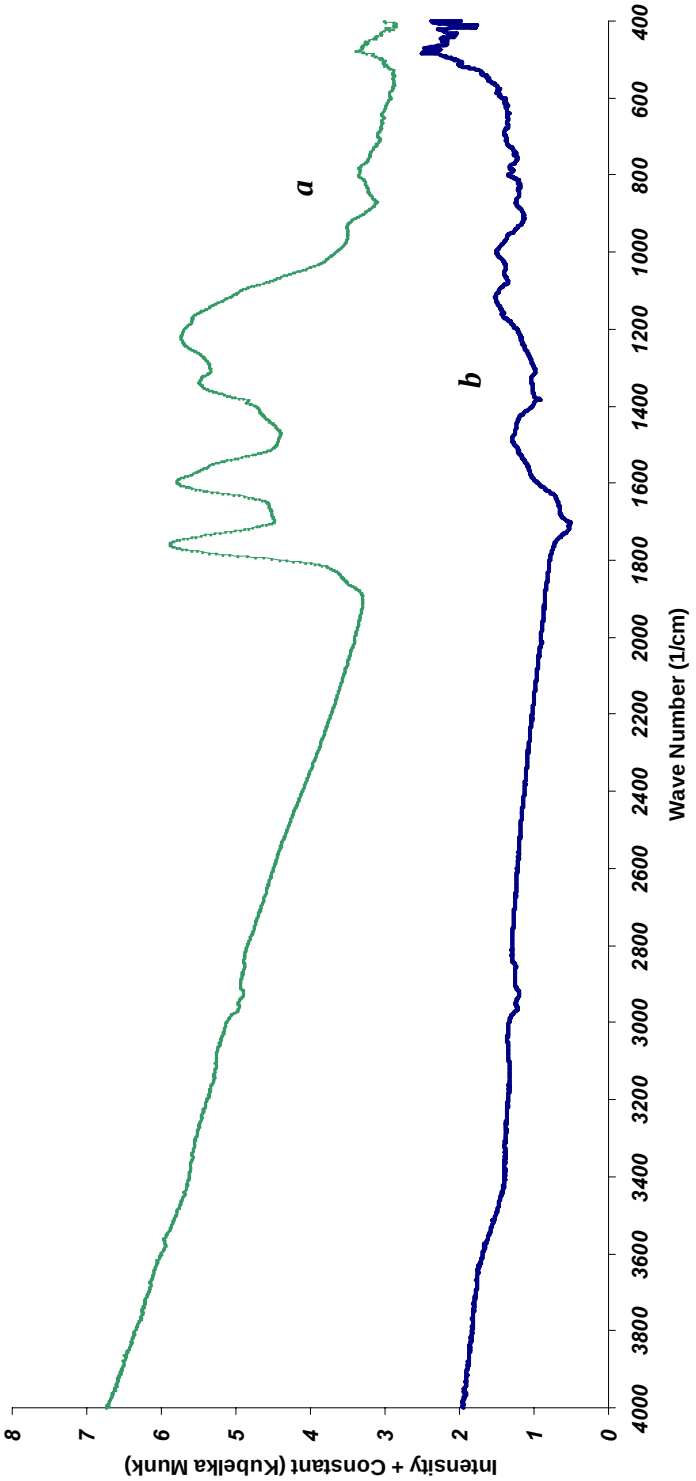

Fig 5.14: IR spectra for a- LusAC-O and b- LusAC [K-M : Kubelka – Munk]

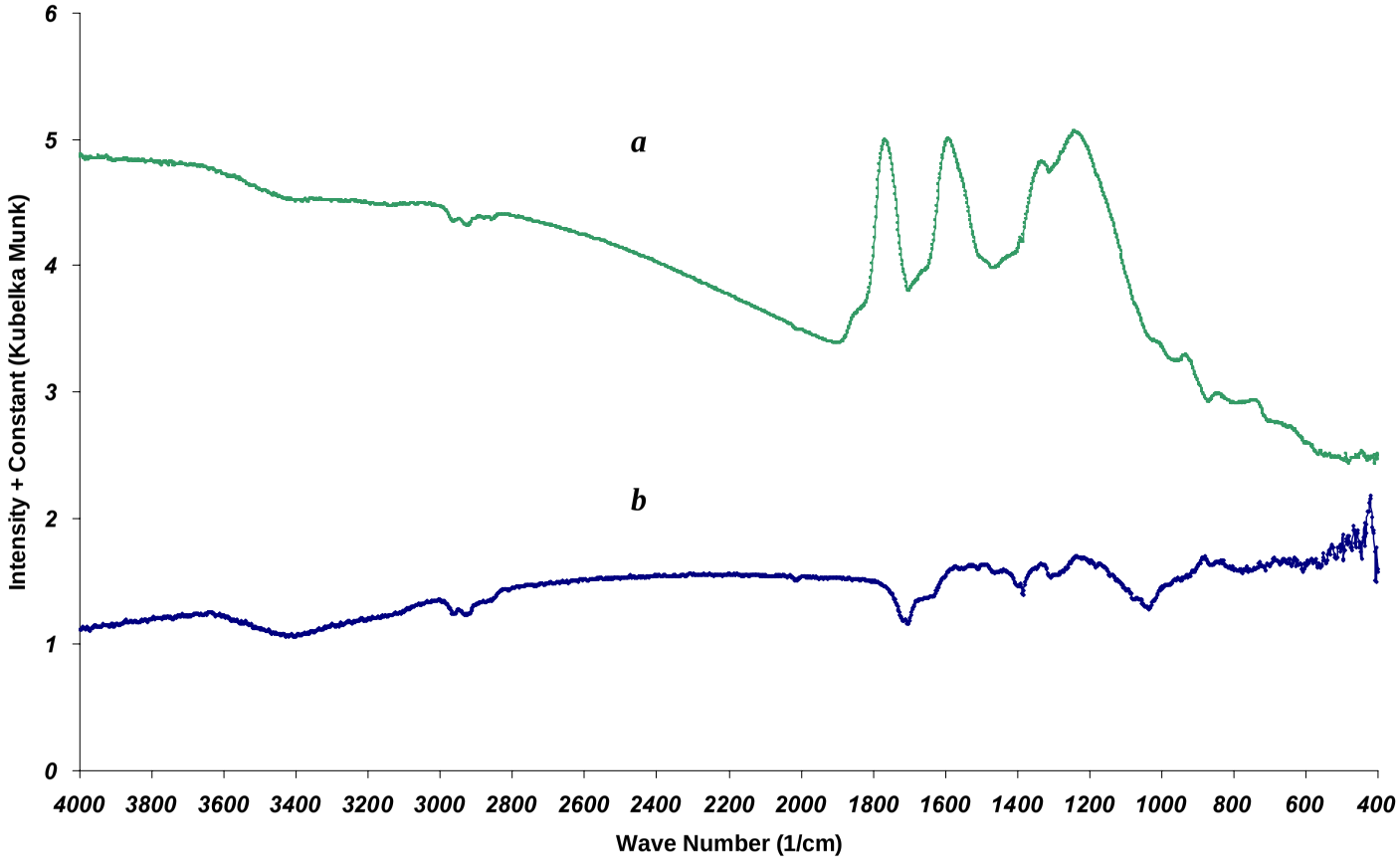

Fig 5.15: IR spectra for a- BioAC-O and b- BioAC [K-M : Kubelka – Munk]

that of physically activated carbon and there was not a significant difference in its performance for H_2S oxidation in despite of its highly microporous structure.

5.1.3. Effect of ash components

Oxides of some metals such as vanadium, titanium, iron and zinc have good activity for H_2S oxidation [Park et al, 2002; Chun et al, 1998; Li et al, 1997; Steijns and Mars, 1977]. Table 5.4 shows the concentration of these metals in original activated carbons and modified catalysts. These data show that there is no direct correlation between the concentrations and catalysts' performances. The only exception is the zinc concentration for BioAC-O-D(750), even for this case, the absolute concentration difference is not large. No correlation between the concentration of these metals and the performance of these catalysts can be because of different chemical states of those elements in these activated carbons, which are not suitable for H_2S oxidation [Wu et al, 2005].

5.2. The effects of impregnating agents and impregnating solvents

5.2.1. Effect of impregnating agent

Use of impregnating agents is a common method to increase the performance of the catalyst. Potassium iodide (KI) and Manganese nitrate [$Mn(NO_3)_2$] were used as impregnating agents in this study for impregnation of LusAC-O-D(650) catalyst. These promotors had shown their effects on the improvement of activated carbon catalysts for the H_2S oxidation reaction [Mikhalovsky and Zeitsev, 1997; Rodriguez-Reinoso, 2002]. The reaction was performed at pressure of 700 kPa and reaction temperatures of 160, 175, 190 and 205 ^oC for all samples. Three different weight percentages (2.5, 5.0, and 10 wt %) of each impregnating agent was used in this study. Water was used as

Table 5.4: Concentration of some metals in original and modified activated carbons (measured using ICP method)

Catalyst	Fe (ppm)	Cu (ppm)	V (ppm)	Zn (ppm)
LusAC	7550	12	15	27
LusAC-O	1942	5	4	9
LusAC-O-D(650)	2379	<4	3	12
BioAC	486	4	<1	6
BioAC-O	140	<4	<1	5
BioAC-O-D(750)	186	<4	<1	16

impregnating solution. The performances of these impregnated catalysts are shown in Tables 5.5 and 5.6. For thermally desorbed LusAC-O (see Table 5.5), the breakthrough time and SO_2 production increased by an increase in the oxidation temperature at a constant percentage of $Mn(NO_3)_2$. It is known that higher temperature, especially beyond 200 ^oC, decreases the selectivity of catalyst and increases the SO_2 production. The similar trends with small exceptions can be seen for KI in Table 5.6. $g_{sulphur}/g_{carbon}$ for thermally desorbed, oxidized samples impregnated with KI, showed no special trend but all were in the range of 0.637 to 0.875 (see Table 5.6). $g_{sulphur}/g_{carbon}$ for samples impregnated by $Mn(NO_3)_2$ are generally less than those for KI excepting the impregnated samples used for the highest reaction temperature (205 ^oC). Comparison of breakthrough times of catalysts LusAC, LusAC-O-D(650) and LusAC-O-D(650)-K(5%) shows that the use of impregnating agent for thermally desorbed, oxidized sample increased its breakthrough time by 20% and 119% in comparison to LusAC-O-D(650) and LusAC, respectively (in Tables 5.1 and 5.6). Based on the performances obtained for these two impregnating agents, it can be said that at higher temperatures, manganese nitrate increased break-through time more than that for KI, but it produced more SO_2. KI had better performance at lower temperatures and lower SO_2 production at higher temperatures.

5.2.2. Effect of impregnating solvent

Since carbon is essentially nonhydrophilic in nature, it has a very low affinity for solvents of polar character such as water [Rodriguez-Reinoso, 1997]. The polarity of solvents can be measured by dielectric constant. For impregnation of impregnating agents such as potassium iodide and manganese nitrate, polar solvents are needed, but use of

polar solvents with lower dielectric constant helps to increase the affinity of carbon for solvent. Polar solvents are divided into polar protic solvents (such as water and methanol) and polar aprotic solvents (such as acetone and dimethyl sulfoxide). A polar protic solvent contains an O-H or N-H bond. A polar aprotic solvent contains no O-H or N-H bond. Dielectric constant of water (H-O-H) is 80, but that for dimethyl sulfoxide [CH_3-S(=O)-CH_3] is 47. This constant for acetone is 21, but it is not able to dissolve potassium iodide and manganese nitrate. However, the lower polarity of an aprotic solvent in comparison to that for a protic solvent provides better penetration of that in the porous structure of activated carbon. Two samples of LusAC-O-D(650) were impregnated by 5 wt% of KI using water and dimethyl sulfoxide as impregnating solvents, respectively.

These two impregnated catalysts were used for oxidation of hydrogen sulphide at 175 ^oC and 700 kPa. As it can be seen in the Table 5.1, impregnation with dimethyl sulfoxide provided catalyst with higher break-through time (12.3 %) and it increased $g_{sulphur}/g_{carbon}$ by 17.6 % in comparison to the impregnation with water.

Use of dimethyl sulfoxide increased the average SO_2 production to 0.31 % of H_2S concentration in the feed. It can be because of incomplete removal of dimethyl sulfoxide during washing and drying stages. The better performance of catalyst impregnated by dimethyl sulfoxide showed that an aprotic solvent or in other word a solvent with lower dielectric constant can help the better penetration of impregnating agent throughout carbon particles which provides a more uniform distribution for this agent [Rodriguez-Reinoso, 1998].

Table 5.5: Performance of LusAC-O-D(650) catalyst impregnated by manganese nitrate [$Mn(NO_3)_2$] for H_2S oxidation reaction at reaction pressure of 700 kPa

$Mn(NO_3)_2$ (wt %)	Reaction temperature(^oC)	Break –Through time (min)	$g_{sulphur}/g_{carbon}$	Avg. SO_2 production (as % of H_2S in feed)
2.5	160	88	0.538	0.01
2.5	175	110	0.639	0.18
2.5	190	126	0.755	0.12
2.5	205	136	0.831	1.56
5.0	160	98	0.570	0.01
5.0	175	125	0.725	0.58
5.0	190	143	0.860	0.64
5.0	205	157	0.954	0.88
10.0	160	102	0.582	0.01
10.0	175	128	0.721	0.18
10.0	190	144	0.875	0.67
10.0	205	167	1.022	1.09

Table 5.6: Performance of LusAC-O-D(650) catalyst impregnated by potassium iodide [KI] for H_2S oxidation reaction at reaction pressure of 700 kPa

KI (wt %)	Reaction temperature(^oC)	Break –Through time (min)	$g_{sulphur}/g_{carbon}$	Avg. SO_2 production (as % of H_2S in feed)
2.5	160	106	0.637	0.01
2.5	175	137	0.851	0.16
2.5	190	128	0.772	0.08
2.5	205	125	0.750	0.43
5.0	160	137	0.832	0.04
5.0	175	138	0.853	0.05
5.0	190	143	0.875	0.05
5.0	205	137	0.831	0.61
10.0	160	126	0.787	0.01
10.0	175	135	0.816	0.01
10.0	190	135	0.825	0.01
10.0	205	135	0.824	0.72

5.3. The effect of pressure on the performance of catalyst in the oxidation reaction

LusAC-O-D(650)-K(2.5%) was used for oxidation reaction at 175 ^{o}C at three different pressures of 100, 300 and 700 kPa. The performance of catalyst at each pressure is shown in Table 5.7. It shows that by an increase in pressure, break-through time and $g_{sulphur}/g_{carbon}$ increased and average SO_2 production decreased.

An increase in pressure can decrease the partial pressure of sulphur and therefore, the rate of gas-phase reaction between sulphur and oxygen and hence the production of SO_2 decrease.This observation is in agreement with the results of other researchers [Dalai and Tollefson, 1998; Chowdhury and Tollefson, 1990].

5.4. Products of H_2S oxidation reaction

The catalyst was collected after each experiment and was used for Sulphur L-edge X-ray absorption near edge structure (XANES) spectroscopy to characterize sulphur species in the reaction products. Common oxidation states of sulphur include -2, 0, +2, +4 and +6. Blank carbon tape was examined for sulphur impurities. No trace of sulphur species was found. In order to identify the sulphur species, sulphur L-edge spectra of elemental sulphur, $Na_2S_2O_3$ and Na_2SO_4 were recorded and in Fig. 5.16, the spectra of these reference materials are compared with those of LusAC-O-D(650)-K(5%)-175C (spent catalyst used for reaction at 175 ^{o}C and 700 kPa).

Differences between spectra of elemental sulphur and other reference materials can be related to the chemical structures (crown-shaped for elemental sulphur and tetrahedral for thiosulphate and sulphate), but difference between spectra of thiosulphate ($S_2O_3^{2-}$) and sulphate (SO_4^{2-}) is due to the replacement of one oxygen by sulphur for thiosulphate in

Table 5.7: Effect of pressure on the performance of LusAC-O-D(650)-K(2.5%) For H_2S oxidation reaction at reaction temperature of 175 ^oC

Pressure (kPa)	B-T time (min)	$g_{Sulphur}/g_{carbon}$	Avg. SO_2 production (as % of H_2S in feed)
100	44	0.232	0.32
300	87	0.536	0.30
700	137	0.851	0.16

comparison to sulphate [Kasrai et al, 1996]. Fig. 5.16 shows that the spectrum of the spent catalyst has exactly the same features of the elemental sulphur spectrum. Main peaks at 163 and 164.5 eV and two small shoulders for elemental sulphur at 169 and 170.5 eV, in this Figure, are in agreement with peaks of the spent catalyst.

The spectra for spent AC-O-D(650)-K(5%) catalysts used at different reaction temperatures (Fig. 5.17) showed similar characteristics. Therefore, it can be concluded that the elemental sulphur was the dominant sulphur species in products for different reaction temperatures. The spectra of AC-175C, AC-D(650)-175C, AC-O-175C, AC-O-D(650)-175C and AC-O-D(650)-K(5%)-175C are shown in Fig. 5.18. The same trend can be observed for all spent catalysts.

Fig. 5.19 shows the spectra for two spent catalysts, BioAC and BioAC-O-D(750), prepared from biochar and used for reaction at 175 ^{o}C and 700 kPa. These biomass-based activated carbons showed the same trend observed for coal-based catalysts.

5.5. Catalyst regeneration

Table 5.8 shows the performances of LusAC-O-D(650)-K(5%) as a fresh catalyst and after 8-h and 24-h regenerations and reuse in the oxidation reaction. It can be seen that after 3 cycles of use and regeneration, the break-through time of the catalyst after 8-h regenerations decreased by approximately 38%, but after 24-h regenerations, the reduction was ~ 32%. For both regeneration times, $g_{sulphur}/g_{carbon}$ decreased by 42 % and 36 % for 8-h and 24-h regeneration respectively. Average SO_2 production was 4 times larger for 8-h regenerated samples in comparison to 24-h regenerated samples. The increase in average SO_2 production suggests that sulphur is not fully removed from the

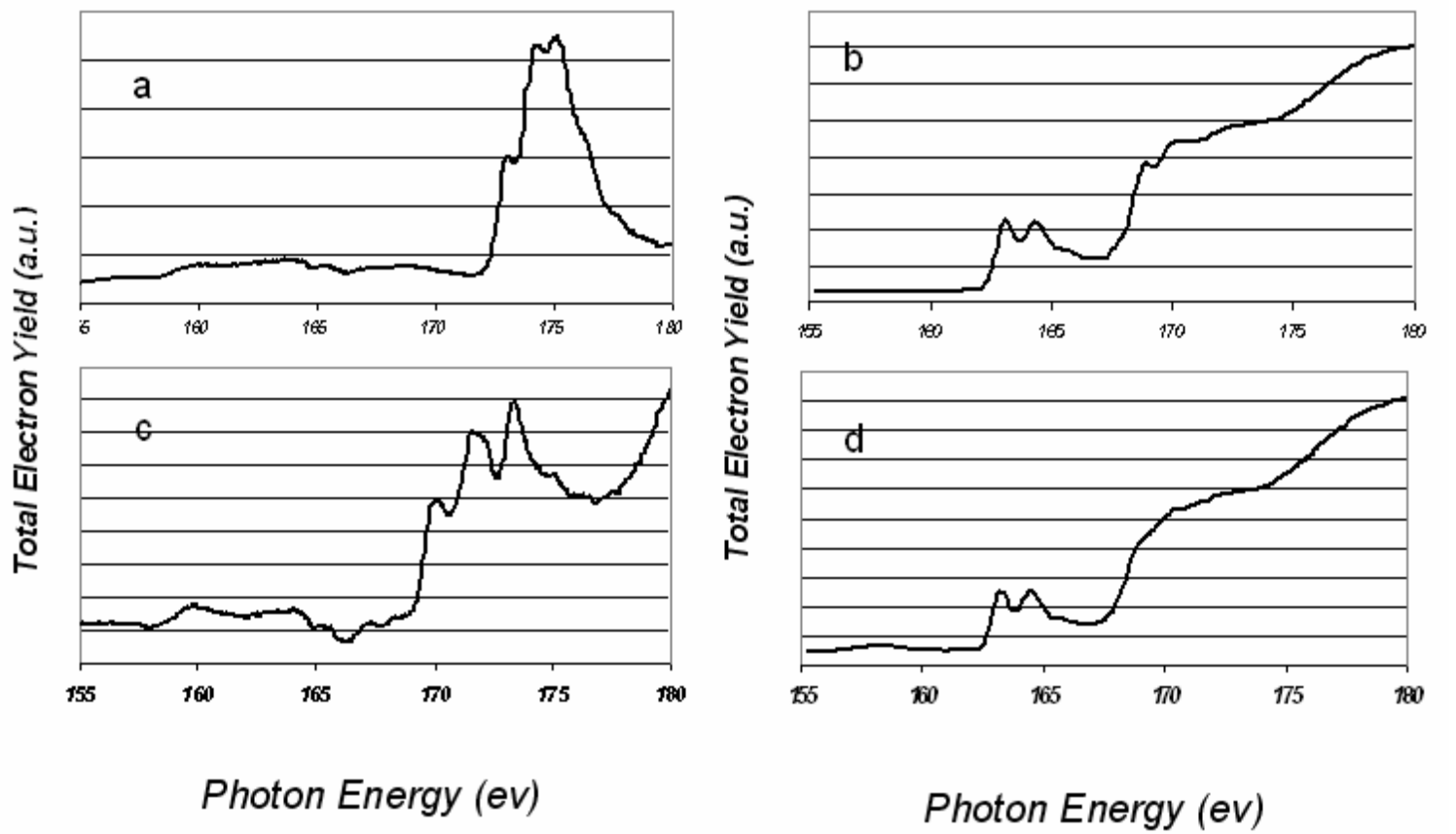

Fig. 5.16: Sulphur L-edge XANES spectra for reference materials [a: Na_2SO_4, b: Sulphur, c: $Na_2S_2O_3$] and one spent catalyst [d: LusAC-O-D(650)-K(5%)]

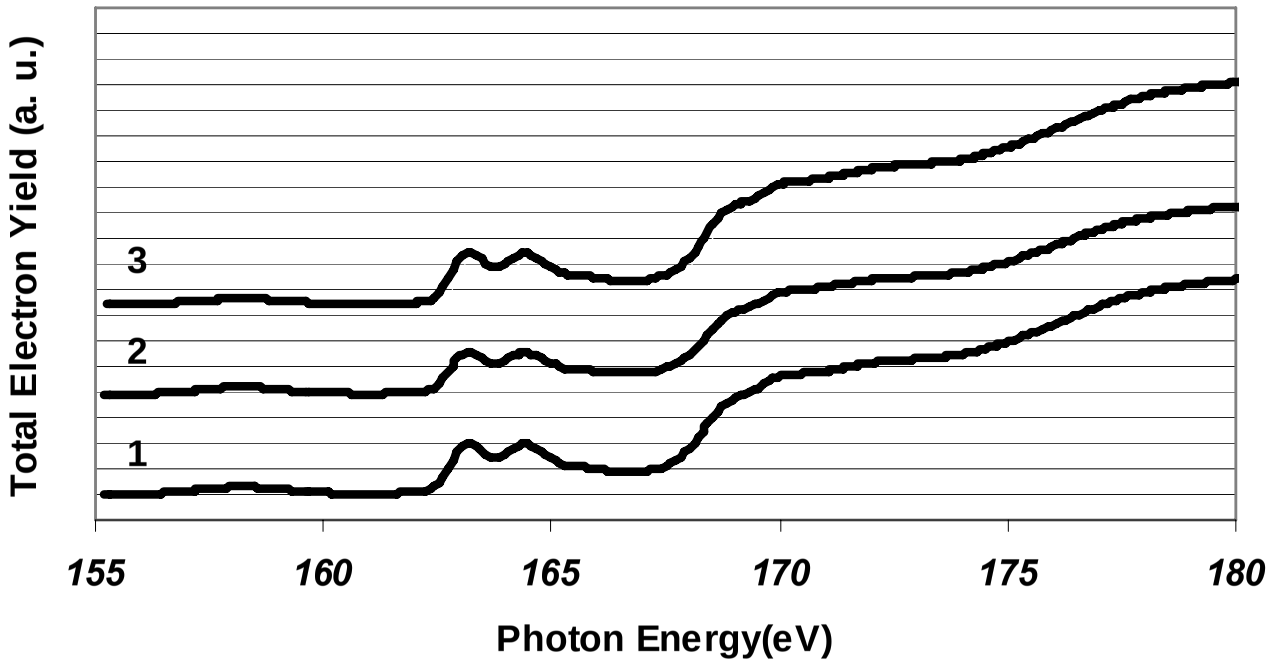

Fig. 5.17: Sulphur L-edge XANES spectra for spent LusAC-O-D(650)-K(5%) at different reaction temperatures [1: 160 ^{o}C, 2: 175 ^{o}C and 3: 190 ^{o}C]

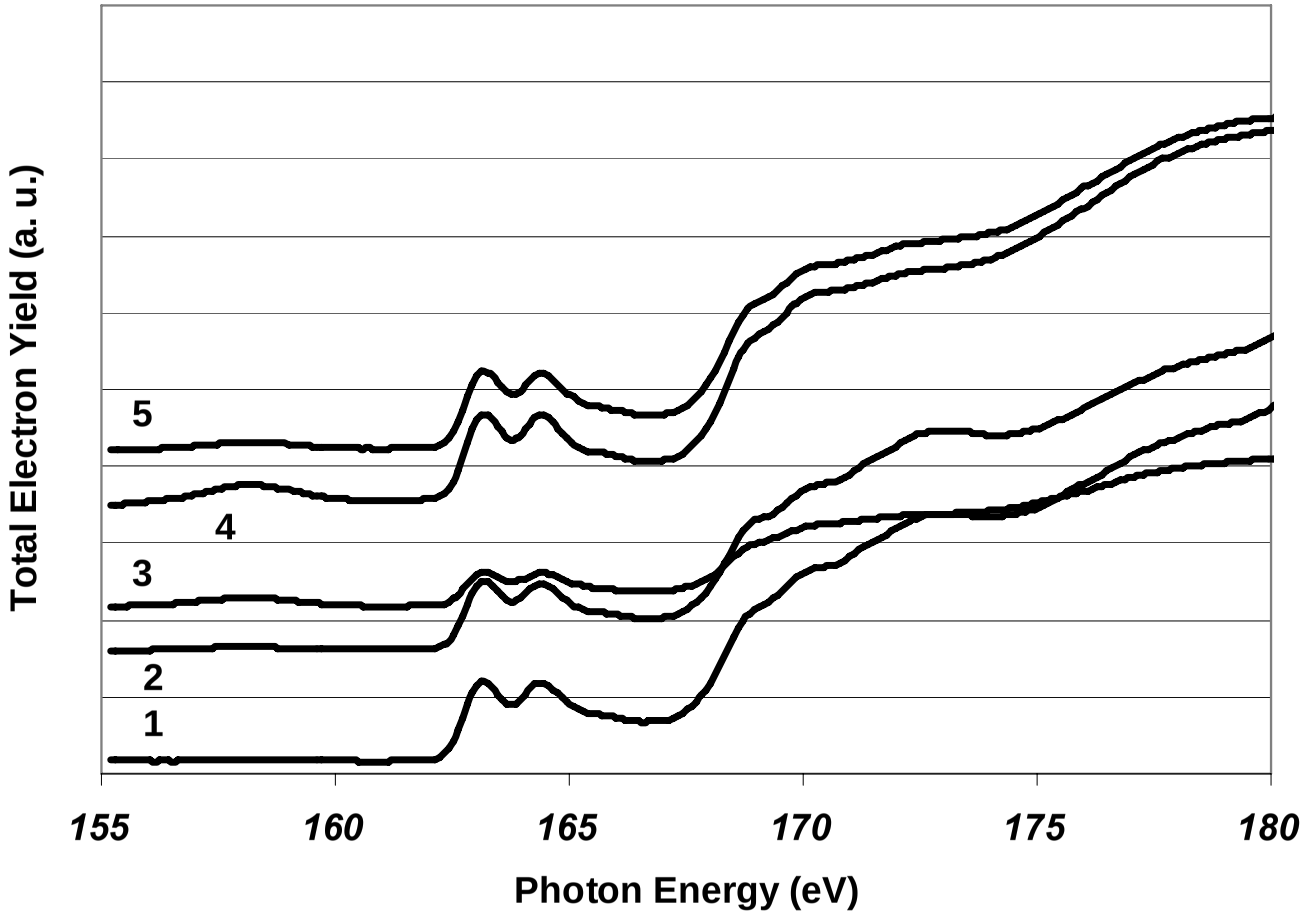

Fig. 5.18: Sulphur L-edge XANES spectra for different types of spent catalysts [1: LusAC, 2: LusAC-D(650), 3: LusAC-O, 4: LusAC-O-D(650) and 5: LusAC- O-D(650)-K(5%)] at reaction temperature of 175 ^{o}C

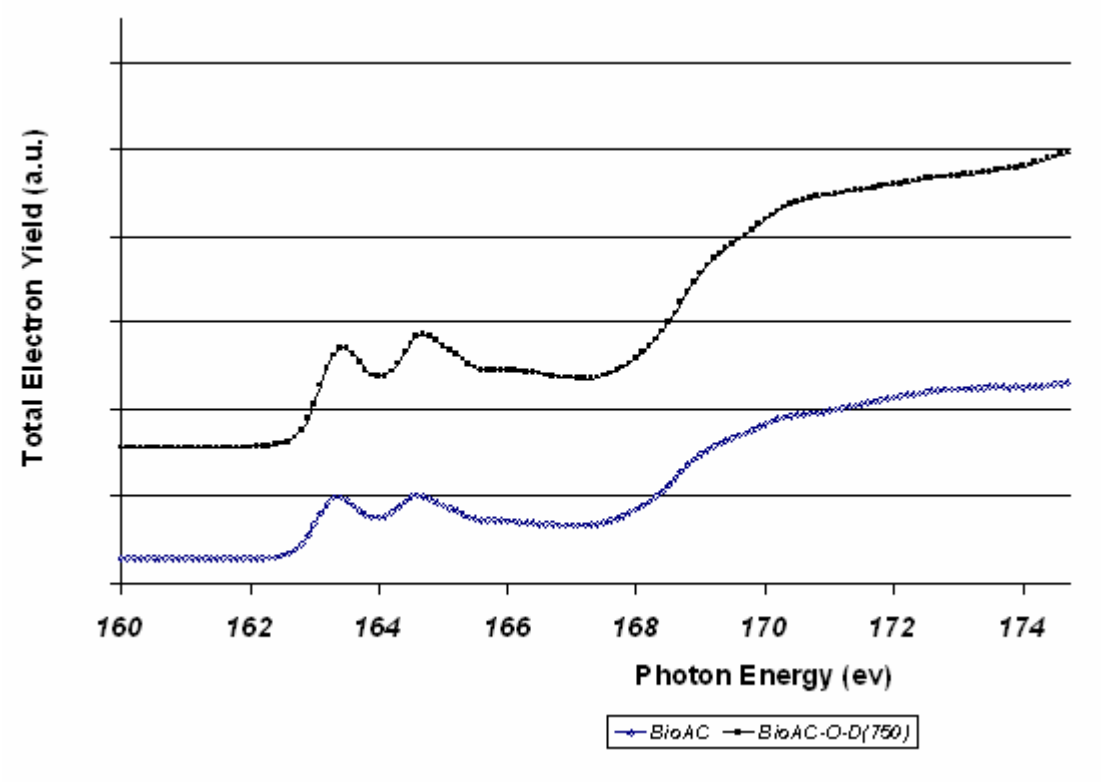

Fig.5.19: Sulphur L-edge XANES spectra for two spent catalysts [BioAC-O-D(750) and BioAC]

pores of the activated carbon and because of the same reason break-through time of regenerated sample is less than that of the fresh catalyst.

The large difference in the average SO_2 production and higher break-through time show that 24-h regeneration can provide a better removal of sulphur from activated carbons. The performance of the regenerated catalyst showed that this activated carbon can be used at least for three cycles.

Table 5.8: performance of LusAC-O-D(650)-K(5%) as a fresh catalyst and regenerated catalyst at reaction temeperature of 175 ^{o}C

	B-T time (min)	$g_{Sulphur}/g_{carbon}$	Avg. SO_2 production (as % of H_2S in feed)
Fresh catalyst	138	0.85	0.05
Spent catalyst after 1st regeneration (8-h)	85	0.53	0.41
Spent catalyst after 2nd regeneration (8-h)	87	0.53	1.56
Spent catalyst after 3rd regeneration (8-h)	85	0.50	1.88
Spent catalyst after 1st regeneration (24-h)	97	0.56	0.30
Spent catalyst after 2nd regeneration (24-h)	96	0.56	0.42
Spent catalyst after 3rd regeneration (24-h)	94	0.54	0.44

6.0. Kinetic study of oxidation reaction of H_2S to sulphur

This chapter discusses kinetics for oxidation of hydrogen sulphide over modified activated carbon produced from steam activation of luscar char. Langmuir-Hinshelwood mechanism was used for reaction between oxygen and H_2S adsorbed on the carbon surface. Eley-Rideal approach was used for reaction between a gas- phase H_2S molecule and oxygen molecule adsorbed on the carbon surface. The effects of reactants and products on the reaction rate were investigated in this study. Reaction temperature range, H_2S concentration range and oxygen concentration range used in this study were 160-190 ^oC, 6000-10000 ppm, and 1-3 times of stoichiometric ratio, respectively.

Generally, hydrogen sulphide oxidation has been studied at two different conditions; one approach is based on the oxidation at room temperature in the presence of moist air. At this operating condition, the oxidation of H_2S may proceed in the liquid phase (water). For example, below 50 ^0C a complete exhaustion of H_2S needs a relative humidity of at least 60% [Steijns and Mars, 1974].The second process introduces oxidation at temperature range of 100-250 ^0C and dry conditions. The kinetics of hydrogen sulphide oxidation is quite complex and such as other oxidations probably occurs by a free radical mechanism [Gamson and Elkins, 1953]. Hydrogen sulphide is a highly stable gas and does not react with oxygen to any noticeable extent by itself at the above mentioned range of temperatures [Puri et al, 1971]. An important role can be attributed to free radicals on the carbon surface [Steijns and Mars, 1974]. Steijns and co-workers suggested sulphur radicals as species playing an important role in the chemisorption of oxygen on the carbon [Steijns and Mars 1974]. Some impurities present in the structure of activated carbon can also play a role as catalyst for the oxidation [Cariaso and Walker, 1975;

Steijns and Mars 1974]. Catalytic activity can be altered by introduction of heteroatoms in the surface layer of activated carbon or by impregnation with various catalytically active substances [Mikhalovsky and Zaitsev, 1997].

Sreeramamurthy and Menon [1975] postulated that the chemisorption of both hydrogen sulphide and oxygen on the catalyst surface were the first steps of the reaction. The chemisorption of oxygen was considered dissociative. The reaction between these two adsorbed molecules was considered to be the rate controlling step. According to Cariaso and Walker work [1975], oxygen is dissociatively chemisorbed and the reaction is between this adsorbed oxygen and an H_2S molecule from the gas phase colliding with it. Steijns et al. [1974, 1976] proposed a different mechanism for the oxidation reaction. The oxidation reduction mechanism proposed by them is based on the autocatalytic effect of the sulphur product. Sreeramamurthy and Menon [1975], Iwasawa and Ogasawarw [1977] as well as Coskun and Tollefson [1980] found no evidence from their work to support the catalytic property of sulphur for this particular oxidation reaction. Ghosh and Tollefson [1986] supposed that the sorption of O_2 is dissociative while that of H_2S is molecular. The reaction occurs between an oxygen radical and one H_2S molecule, sorbed adjacent to one another. This surface reaction is the rate controlling step.

6.1. Kinetic study of hydrogen sulphide oxidation over activated carbon

The term of intrinsic kinetics refers to the reaction rate in the absence of concentration or temperature gradients. Depending on the operating conditions, these gradients can exist during reaction. In the experimental work, the objective is to eliminate them so that mass and heat resistances are not controlling steps.

Diffusion resistances in a heterogeneous catalytic reaction can be categorized into two groups; a) external resistance: diffusion of the reactants or products between the bulk fluid and the external surface of the catalyst, and b) internal resistance: diffusion of the reactants from the external surface (pore mouth) to the interior of the particle and diffusion of products from the interior of the particles to the external surface [Fogler, 1999].

To study the adsorption of hydrogen sulphide on the carbon surface, an Eley-Rideal mechanism and a Langmuir-Hinshelwood approach were used. In Eley-Rideal mechanism, oxygen is adsorbed on the surface and the reaction takes place between the adsorbed oxygen and a gas-phase hydrogen sulphide molecule as it was proposed by Cariaso and Walker (1975). In Langmuir-Hinshelwood approach, both oxygen and hydrogen sulphide are adsorbed on the carbon surface and then the reaction takes place using a dual-site mechanism as supposed by Ghosh and Tollefson (1986).

a) Eley-Rideal mechanism: Reaction mechanism is as follows:

Sorption: $O_2 + 2X \leftrightarrow O\text{-}X + O\text{-}X$ (6-1)

Reaction: $O\text{-}X + H_2S \leftrightarrow X\text{-}S + H_2O$ (6-2)

Desorption of sulphur: $S\text{-}X \leftrightarrow S\downarrow + X$ (6-3)

Production of sulphur dioxide: $S\text{-}X + 2\,(O\text{-}X) \leftrightarrow SO_2\text{-}X + 2X$ (6-4)

Desorption of sulphur dioxide: $SO_2\text{-}X \leftrightarrow SO_2 \uparrow + X$ (6-5)

b) Langmuir-Hinshelwood surface reaction model: Reaction mechanism is as follows (Ghosh and Tollefson , 1986; Dalai and Tollefson, 1998);

Sorption: $O_2 + 2X \leftrightarrow O\text{-}X + O\text{-}X$ (6-6)

$$H_2S + X \leftrightarrow H_2S\text{-}X \quad (6\text{-}7)$$

Surface reaction: $H_2S\text{-}X + O\text{-}X \leftrightarrow H_2O\text{-}X + S\text{-}X$ (6-8)

Desorption of water: $H_2O\text{-}X \leftrightarrow H_2O \uparrow + X$ (6-9)

Desorption of sulphur: $S\text{-}X \leftrightarrow S\downarrow + X$ (6-10)

SO_2 as a by-product can be produced as follows:

Production of sulphur dioxide: $S\text{-}X + 2\,(O\text{-}X) \leftrightarrow SO_2\text{-}X + 2X$ (6-11)

Desorption of sulphur dioxide: $SO_2\text{-}X \leftrightarrow SO_2 \uparrow + X$ (6-12)

Where X represents an active site on the carbon surface, ↑ represents desorption, and ↓ represents deposition.

6.1.1. Elimination of external mass transfer resistance

In a heterogeneous reaction sequence, mass transfer of reactants first takes place from the bulk fluid to the external surface of catalyst. The mass transfer boundary layer thickness (δ) is defined as the distance from a solid object to where the concentration of the diffusing species reaches 99% of the bulk concentration. The change in the concentration of reactant from bulk concentration to surface concentration takes place in this very narrow fluid layer next to the surface of the particle. Nearly all external mass transfer resistance is found in this layer. At low velocities the mass transfer boundary layer thickness is large and diffusion limits the reaction. As the velocity past the particle is increased, the boundary layer thickness decreases and the mass transfer across the boundary layer no longer limits the rate of reaction. One also can note that for a given velocity, reaction-limiting conditions can be achieved by using very small particles. Therefore, to obtain reaction rate data in the laboratory, one must operate at sufficiently

high velocities or sufficiently small particle sizes to ensure that the reaction is not external mass transfer-limited [Fogler, 1999].

In this study to investigate the effect of external mass transfer, the performances of catalysts with different particle size ranges were evaluated for the direct oxidation of hydrogen sulphide (1 mol %) at sour gas inlet flow rate of 500 ml/min and three reaction temperatures of 160, 175 and 190 ^{o}C. For all these experiments, the oxygen concentration was maintained at stoichiometric ratio and reaction pressure was 200 kPa. Samples of five particle size ranges of LusAC-O-D(650) were prepared: 1000-2380 μm, 710-850 μm, 410-500 μm, 208-300 μm and 150-208 μm. Fig. 6.1 shows the H_2S conversions of this catalyst for different particle sizes at three different reaction temperatures. 0.07 g of catalyst was used for each experiment. In this Figure, by decreasing the particle size of activated carbon to less than 410-500 μm, there is no significant change in H_2S conversion.

It means that as the catalyst particle size decreased, for all three temperatures, the mass transfer across the boundary layer no longer limited the rate of reaction. Then use of activated carbon in the particle size range of 150-208 μm ensured that the film resistance to external mass transfer was negligible for the kinetic parameter estimation experiments.

To show the effect of particle size on the boundary layer thickness and mass transfer coefficient, the Frössling correlation [Frössling, 1938] was used. This mass transfer correlation for flow around a spherical particle can be shown as follows:

$$Sh = 2 + 0.6(\mathrm{Re})^{\frac{1}{2}}(Sc)^{\frac{1}{3}} \qquad (6.13)$$

where, $Sh = \dfrac{k_c d_p}{D_{AB}}$, $\mathrm{Re} = \dfrac{u\rho d_p}{\mu}$, and $Sc = \dfrac{\mu}{\rho D_{AB}}$

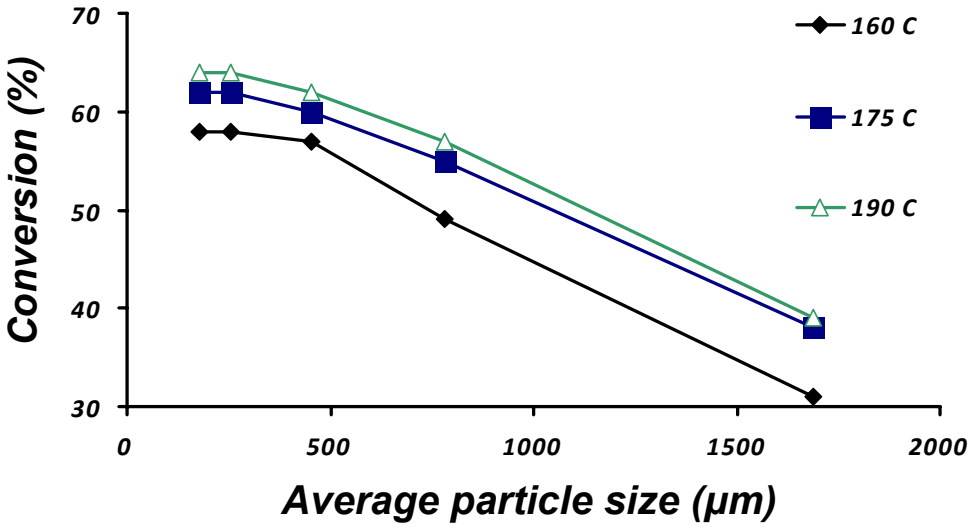

Fig. 6.1: Hydrogen sulphide conversion vs. average particle size for the oxidation reaction

In the above equations: k_c= the average mass transfer coefficient from the bulk flow to activated carbon surface (m/s), d_p= average diameter of particle (m), D_{AB}= the diffusivity of A in B (m^2/s), u= free stream velocity of fluid (m/s), ρ= gas density (kg/m^3), and μ= gas dynamic viscosity (Pa.s).

Table 6.1 shows that by decreasing the average particle size of activated carbons particles (d_p) from 0.169 cm to 0.0179 cm, the mass transfer coefficient of hydrogen sulphide from the bulk flow to the surface of activated carbon particle(k_c) increased for more than 5 times and the boundary layer thickness (δ) decreased to 18.2 % of the initial value . The sample calculation is presented in the Appendix (F).

6.1.2. Elimination of internal mass transfer resistance

In the next step of a heterogeneous reaction sequence, the reactants diffuse from the external surface into and through the pores within the catalyst. Reaction takes place only on the catalytic surface of the pores. The internal mass transfer resistance is related to diffusion of either reactants or products between the external surface and the interior of catalyst. In this study, Weisz-Prater criterion (C_{WP}) is used for estimation of internal mass transfer resistance. This criterion can be shown by the following equation [Fogler, 1999]:

$$C_{WP} = \frac{-r'_{A(Obs)} * \rho_C * R^2}{D_e * C_{AS}} \qquad (6.14)$$

where,

r_A' : reaction rate per unit mass of catalyst, ρ_c : catalyst density, R : particle radius, C_{AS} : surface concentration of reactant A, D_e : effective diffusivity.

If $C_{WP} \ll 1$, there is no internal diffusion limitation and if $C_{WP} \gg 1$, internal diffusion limits the reaction severely [Fogler, 1999]. The C_{WP} calculation is presented in Appendix (G).

Table 6.1: Effect of particle size on the mass transfer boundry layer thickness and mass transfer coefficient in this layer

Particle size range (μm)	d_P (cm)	Sh	k_C (m/s)	δ (m)*10^4
2380 - 1000	0.1690	5.13	0.00655	3.3*
850 - 710	0.0780	4.12	0.01442	1.9
500 - 410	0.0455	3.62	0.0172	1.3
300 - 208	0.0254	3.21	0.02731	0.8
208 - 150	0.0179	3.02	0.03640	0.6

* The sample calculation in Appendix (F)

The value of this parameter was 0.119 which is less than one and therefore, internal diffusion limitation can be neglected.

6.1.3. Eley-Rideal surface reaction model

Assuming the reaction 6-2 to be rate controlling for the oxidation of hydrogen sulphide and having sorption and desorption stages at equilibrium, the surface concentration can be written as follows;

From Eq. (6-1): $C_O = K_{O_2}^{0.5}.P_{O_2}^{0.5}.C_v$ (6-15)

From Eq. (6-3): $C_S = K_S.P_S.C_v$ (6-16)

From Eq. (6-5): $C_{SO_2} = K_{SO_2}.P_{SO_2}.C_v$ (6-17)

Site balance is as follows;

$$C_t = C_v + C_O + C_S + C_{SO_2} \quad (6\text{-}18)$$

where;

C_i = The surface concentration of sites occupied by species i

C_v= The concentration of vacant sites

C_t= The total concentration of active sites

The reaction rate can be expressed using Eq. (6-2):

$$r_{H_2S} = k_S.P_{H_2S}.C_O - k'_S.P_{H_2O}.C_S \quad (6\text{-}19)$$

Substitution of (6-15), (6-16), and (6-17) in Eq. (6-19), one has;

$$r_{H_2S} = k_S.P_{H_2S}.K_O^{0.5}.P_{O_2}^{0.5}.C_v - k'_S.P_{H_2O}.K_S.P_S.C_v \quad (6\text{-}20)$$

$$r_{H_2S} = k_S.K_O^{0.5}.C_v\,(P_{H_2S}.P_{O_2}^{0.5} - \frac{k'_S.K_S}{k_S.K_O^{0.5}}.P_{H_2O}.P_S) \quad (6\text{-}21)$$

Using Equations (6-15), (6-16), (6-17), and (6-18), one has;

$$z = \frac{C_t - C_S}{C_v} = 1 + K_O^{0.5}.P_{O_2}^{0.5} + K_{SO_2}.P_{SO_2} \quad (6\text{-}22)$$

Therefore, Eq. (6-21) can be written as follows;

$$r_{H_2S} = \frac{k_S.K_O^{0.5}.C_t}{z}\left(P_{H_2S}.P_O^{0.5} - \frac{1}{K}.P_{H_2O}.P_S\right).\left(1 - \frac{C_S}{C_t}\right) \quad (6\text{-}23)$$

where, $K = \frac{k_S.K_O^{0.5}}{k_S'.K_S}$ (6-24)

$\left(1 - \frac{C_S}{C_t}\right)$ can be considered as a deactivation term and the ratio of C_S/C_t can be replaced by $\frac{W_S}{W_S^{\infty}}$ where:

W_S=The total amount of sulphur which is produced per unit mass of carbon after t minutes

W_S^{∞} = The amount of sulphur produced when all sites are covered

Eq. (6-23) can be written as:

$$32 * r_{H_2S} = \frac{dW_S}{dt} = 32 * r_0.\left(1 - \frac{W_S}{W_S^{\infty}}\right) \quad (6\text{-}25)$$

where,

$$r_0 = \frac{k_S.K_O^{0.5}.C_t}{z}\left(P_{H_2S}.P_O^{0.5} - \frac{1}{K}.P_{H_2O}.P_S\right) \quad (6\text{-}26)$$

r_0 in the above equation is the rate without deactivation or in other word initial rate.

Eq. (6-25) can be written as follows;

$$\frac{dW_S}{dt} = 32 * r_0 - 32 * \left(\frac{r_0}{W_S^{\infty}}\right)W_S \quad (6\text{-}27)$$

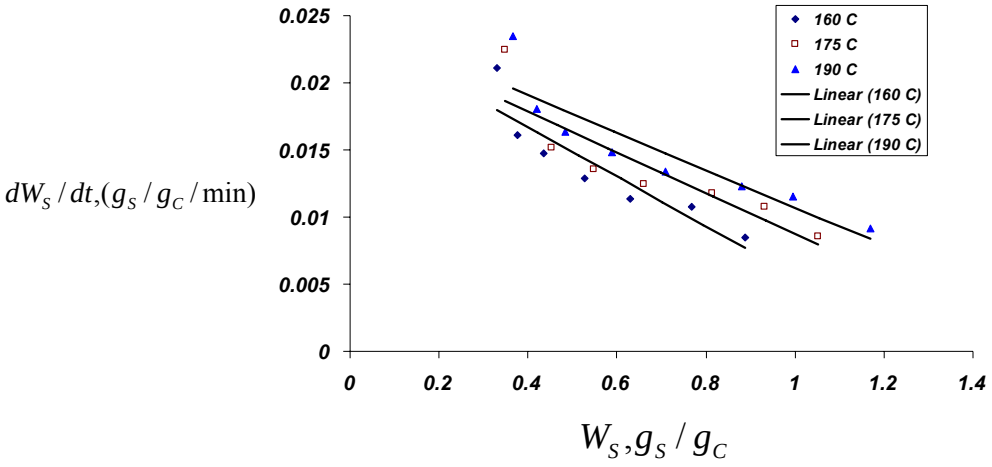

Fig. 6.2: Relationship between the rate of sulphur deposition on carbon and the amount of the sulphur

Fig. 6.2 shows the plot of W_S versus dW_S/dt. Using the slope and intercept of the trend line, W_S^{∞} can be estimated for different temperatures such as 160, 175, 190 ^oC.

Ghosh and Tollefson (1986) found that the equilibrium constant (K) varied from 8.56 $*10^{23}$ (at 125 ^oC) to $3.79*10^{19}$ (at 200 ^oC). Also, the value of P_S is initially very small because practically all sulphur produced is deposited in the pores. Then, the term of $\frac{P_{H_2O}.P_S}{K}$ in Eq. (6-23) can be neglected and this Equation reduces to:

$$\left(\frac{P_{H_2S}.P_{O_2}^{0.5}}{r_{H_2S}}\right).\left(1-\frac{W_S}{W_S^{\infty}}\right)=A_1+D_1.P_{SO_2}+E_1.P_{O_2}^{0.5} \tag{6-28}$$

where,

$$A_1=\frac{1}{K_O^{0.5}.(k_S.C_t)} \tag{6-29}$$

$$E_1=\frac{1}{k_S.C_t} \tag{6-30}$$

$$D_1=\frac{K_{SO_2}}{K_O^{0.5}.(k_S.C_t)} \tag{6-31}$$

To determine E_1, a series of runs were conducted in which the partial pressures of H_2S and SO_2 were kept approximately constant while the partial pressure of oxygen and temperature were varied at three different levels for each of them (See Table 3.1). $\left(\frac{P_{H_2S}P_{O_2}^{0.5}}{r_{H_2S}}\right)\left(1-\frac{W_S}{W_S^{\infty}}\right)$ was plotted against $(P_{O2})^{0.5}$ for three different temperatures (See Fig. 6.3). The slope was E_1 for each temperature. The values of E_1 are presented in Table 6.2. To determine D_1 and A_1 , a series of runs were conducted in which the partial pressures of H_2S and O_2 were kept approximately constant while the partial pressure of

SO_2 and temperature were varied at three different levels for each of them (See Table 3.4). $\left(\frac{P_{H_2S}P_{O_2}^{0.5}}{r_{H_2S}}\right)\left(1-\frac{W_S}{W_S^{\infty}}\right)-E_1P_{O_2}^{0.5}$ was plotted against P_{SO2} for three different temperatures (See Fig. 6.4). The slope was D_1 and intercepts was A_1 for each temperature. The values of D_1 and A_1 are presented in Table 6.2. Data for kinetic study are given in Appendix (H). Using the calculated values of A_1, D_1, and E_1, and Equations (6-29), (6-30), and (6-31), the following equations were obtained for K_{O2}, K_{SO2}, and k_SC_t were calculated.

$$\ln(K_{SO_2}) = -16.047 + \frac{57.70}{RT} \qquad (6-32)$$

$$\ln\left(K_{O_2}\right) = -32.785 + \frac{131.07}{RT} \qquad (6-33)$$

$$\ln(K_S C_t) = -0.6465 - \frac{26.57}{RT} \qquad (6-34)$$

The above equations are plotted in Fig. 6.5.

Therefore, the activation energy for H_2S oxidation was 26.6 kJ/gmol and heat of adsorption for O_2 and SO_2 , are -131.1 and -57.7 kJ/gmol, respectively. This value shows that adsorption of O_2 on active sites is chemical in nature.

The reaction rate can be written as follows;

$$r_{H_2S} = \frac{K_{O_2}^{0.5}.k_s.C_t.P_{H_2S}.P_{O_2}^{0.5}}{1+K_{O\ 2}^{0.5}P_{O_2}^{0.5}+K_{SO_2}P_{SO_2}}\left(1-\frac{W_S}{W_S^{\infty}}\right) \qquad (6\text{-}35)$$

Fig. 6.6 shows that R^2 for experimental and calculated reaction rates is equal to 95%. R^2 for runs of oxygen-effect and SO_2-effect is 93% and 77%, respectively. Values for W^{∞} at three different temperatures (160, 175, and 190 ^{o}C) are given in Table 6.2.

Table 6.2: Values of constants in Eq. (6- 28) as a function of temperature

Temp. (^oC)	A_1	E_1	D_1	W_S^∞ (g_s/g_C)
160	248.23	851.36	249.43	1.311
175	426.70	634.35	229.82	1.579
190	498.28	528.48	177.69	1.770

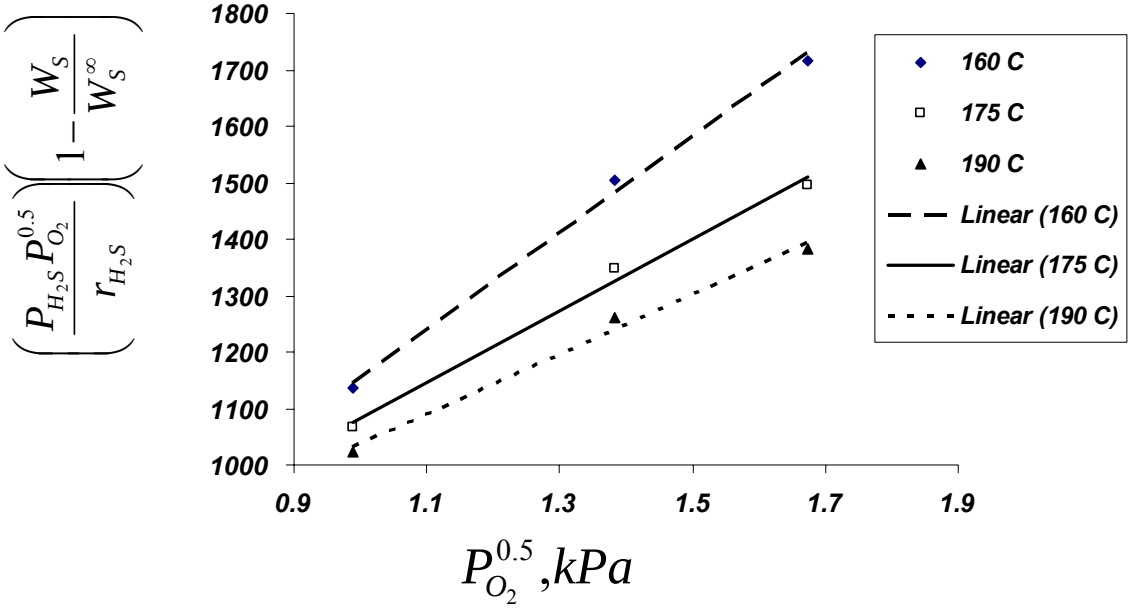

Fig. 6.3: Determination of variable E_1 in Eq. (6-28)

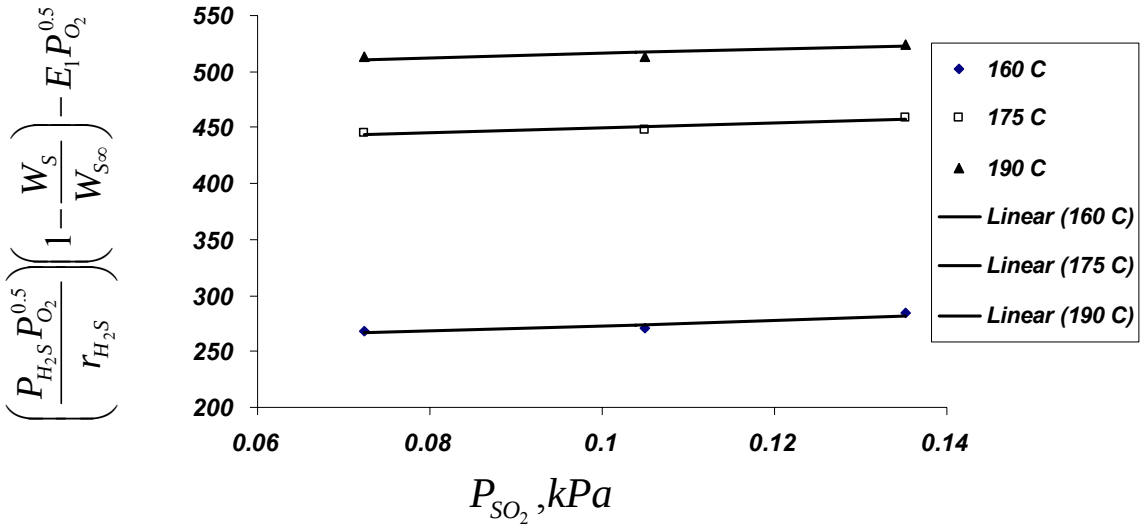

Fig. 6.4: Determination of variables D_1 and A_1 in Eq. (6-28)

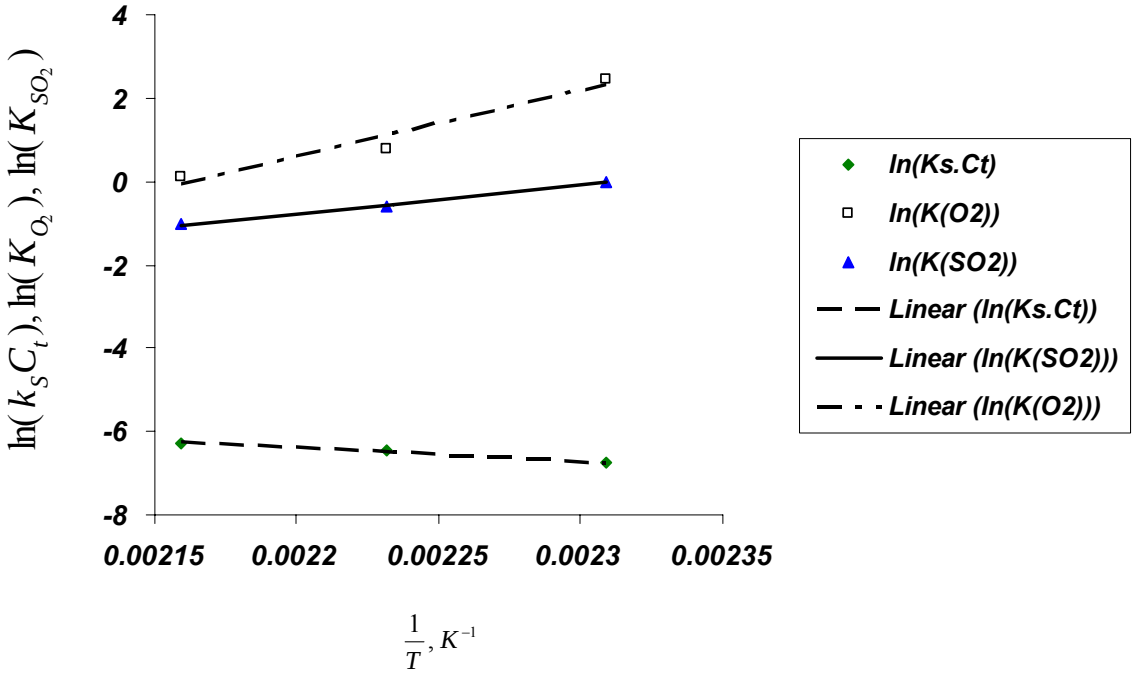

Fig. 6.5: Determination of activation energy, adsorption energy and frequency factors

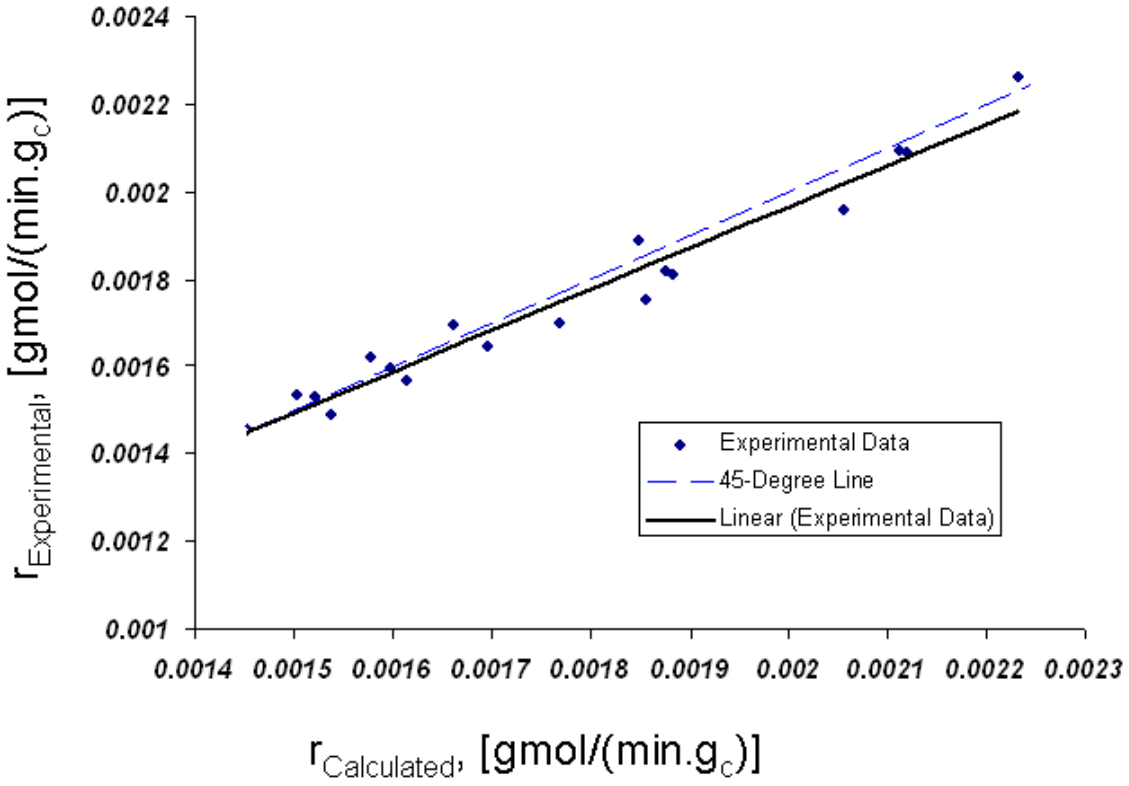

Fig. 6.6: comparison of the calculated and experimental values for reaction rates

6.1.4. Langmuir-Hinshelwood surface reaction model

Assuming the surface reaction (6-8) to be rate controlling for the oxidation of hydrogen sulphide and having sorption and desorption stages at equilibrium, the surface concentration can be written as follows;

From Eq. (6-6): $C_O = K_{O_2}^{0.5}.P_{O_2}^{0.5}.C_v$ (6-36)

From Eq. (6-7): $C_{H_2S} = K_{H_2S}.P_{H_2S}.C_v$ (6-37)

From Eq. (6-9): $C_{H_2O} = K_{H_2O}.P_{H_2O}.C_v$ (6-38)

From Eq. (6-10): $C_S = K_S.P_S.C_v$ (6-39)

From Eq. (6-12): $C_{SO_2} = K_{SO_2}.P_{SO_2}.C_v$ (6-40)

Site balance is as follows;

$$C_t = C_v + C_O + C_{H_2S} + C_{H_2O} + C_S + C_{SO_2} \quad (6\text{-}41)$$

The balance of vacant sites will be;

$$C_v = C_t - C_O - C_{H_2S} - C_{H_2O} - C_S - C_{SO_2} \quad (6\text{-}42)$$

where;

C_i = The surface concentration of sites occupied by species i

C_v= The concentration of vacant sites`

C_t= The total concentration of active sites

The reaction rate can be expressed using Eq. (6-8):

$$r_{H_2S} = k_S.C_{H_2S}.C_O - k'_S.C_{H_2O}.C_S \quad (6\text{-}43)$$

Substitution of (6-36), (6-37), (6-38), and (6-39) in Eq. (6-43), one has;

$$r_{H_2S} = k_S.K_{H_2S}.P_{H_2S}.C_v.K_O^{0.5}.P_{O_2}^{0.5}.C_v - k'_S.K_{H_2O}.P_{H_2O}.C_v.K_S.P_S.C_v \quad (6\text{-}44)$$

$$r_{H_2S} = k_S.K_{H_2S}.K_O^{0.5}.C_v^2(P_{H_2S}.P_{O_2}^{0.5} - \frac{k'_S.K_S.K_{H_2O}}{k_S.K_{H_2S}.K_O^{0.5}}.P_{H_2O}.P_S) \quad (6\text{-}45)$$

Using Equations (6-42), (6-36), (6-37), (6-38), and (6-40), one has;

$$z = \frac{C_t - C_S}{C_v} = 1 + K_O^{0.5}.P_{O_2}^{0.5} + K_{H_2S}.P_{H_2S} + K_{H_2O}.P_{H_2O} + K_{SO_2}.P_{SO_2} \quad (6\text{-}46)$$

If K is assumed as $\frac{k_S.K_{H_2S}.K_O^{0.5}}{k'_S.K_S.K_{H_2O}}$, then, Eq. (6-45) can be written as follows;

$$r_{H_2S} = \frac{k_S.K_{H_2S}.K_O^{0.5}.C_t^2\left(P_{H_2S}.P_O^{0.5} - \frac{1}{K}P_{H_2O}.P_S\right)}{\left(1 + K_O^{0.5}P_O^{0.5} + K_{H_2S}P_{H_2S} + K_{H_2O}P_{H_2O} + K_{SO_2}P_{SO_2}\right)^2}\left(1 - \frac{C_S}{C_t}\right)^2 \quad (6\text{-}47)$$

$\left(1 - \frac{C_S}{C_t}\right)^2$ can be considered as a deactivation term and the ratio of C_S/C_t can be replaced by $\frac{W_S}{W_S^\infty}$ where; W_S=The total amount of sulphur which is produced per unit mass of carbon at time t and W_S^∞ = The amount of sulphur produced when all sites are covered

Eq. (6-47) can be written as:

$$32 * r_{H_2S} = \frac{dW_S}{dt} = 32 * r_0.\left(1 - \frac{W_S}{W_S^\infty}\right)^2 \quad (6\text{-}48)$$

Where: $r_0 = \frac{k_S.K_{H_2S}.K_O^{0.5}.C_t^2}{z^2}\left(P_{H_2S}.P_O^{0.5} - \frac{1}{K}.P_{H_2O}.P_S\right)$ (6-49)

After integration, Eq. (6-48) becomes;

$$\frac{1}{W_S} = \left(\frac{1}{32r_0}\right)\left(\frac{1}{t}\right) + \frac{1}{W_S^\infty} \quad (6\text{-}50)$$

Therefore, using a plot of $\frac{1}{W_S}$ vs. $\frac{1}{t}$ at each temperature (See Fig. 6-7), W_S^{∞} can be calculated. These values are given in Table 6-3.

Therefore, Eq. (6-47) can be written as follows;

$$\left(\frac{P_{H_2S}.P_{O_2}^{0.5}-\frac{1}{K}.P_{H_2O}.P_S}{r_{H_2S}}\right).\left(1-\frac{W_S}{W_S^{\infty}}\right)^2=\frac{(1+K_O^{0.5}P_O^{0.5}+K_{H_2S}P_{H_2S}+K_{H_2O}P_{H_2O}+K_{SO_2}P_{SO_2})^2}{k_S.K_{H_2S}.K_O^{0.5}.C_t^2} \tag{6-51}$$

$$\left(\frac{P_{H_2S}.P_{O_2}^{0.5}-\frac{1}{K}.P_{H_2O}.P_S}{r_{H_2S}}\right)^{0.5}.\left(1-\frac{W_S}{W_S^{\infty}}\right)=A+B.P_{H_2S}+C.P_{H_2O}+D.P_{SO_2}+E.P_{O_2}^{0.5} \tag{6-52}$$

where,

$$A=\frac{1}{\left(k_S.C_t^2.K_{H_2S}.K_O^{0.5}\right)^{0.5}} \tag{6-53}$$

$$B=\left(\frac{K_{H_2S}}{k_S.C_t^2.K_O^{0.5}}\right)^{0.5} \tag{6-54}$$

$$C=\frac{K_{H_2O}}{\left(k_S.C_t^2.K_{H_2S}.K_O^{0.5}\right)^{0.5}} \tag{6-55}$$

$$D=\frac{K_{SO_2}}{\left(k_S.C_t^2.K_{H_2S}.K_O^{0.5}\right)^{0.5}} \tag{6-56}$$

$$E=\left(\frac{K_O^{0.5}}{k_S.C_t^2.K_{H2S}}\right)^{0.5} \tag{6-57}$$

Ghosh and Tollefson (1986) found that the equilibrium constant (K) varied from 8.56 $*10^{23}$ (at 125 ^oC) to 3.79$*10^{19}$ (at 200 ^oC). Also, the value of P_S is initially very small

Table 6.3 : Values of constants in Eq. (6-58) as a function of temperature

Temp. (^oC)	A	B	C	D	E	W_S^{∞} (g_s/g_C)
160	7.526	7.564	0.159	10.721	11.356	0.967
175	9.631	7.448	0.146	10.520	8.910	1.114
190	10.341	7.510	0.143	10.956	7.653	1.162

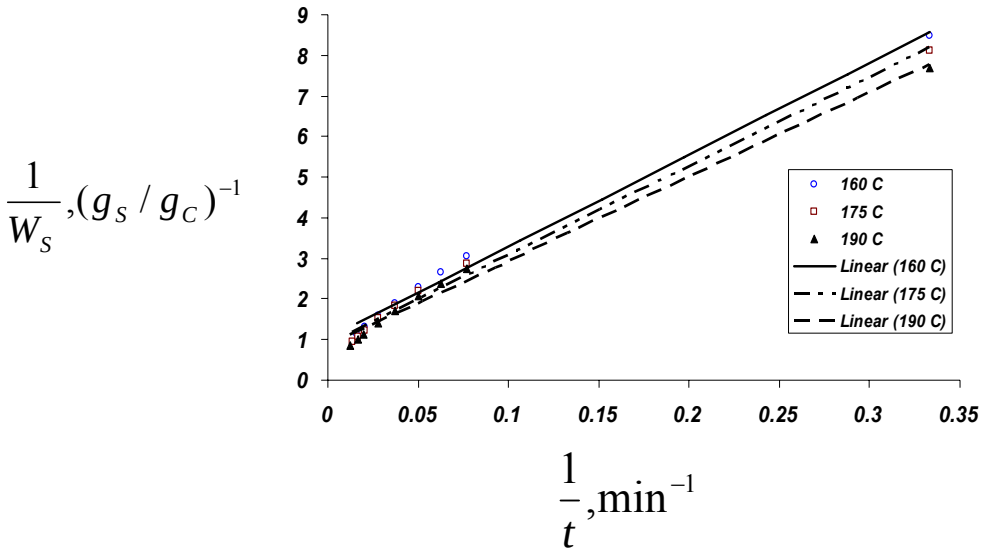

Fig. 6.7: Relationship between reciprocal of time and reciprocal of sulphur deposited on carbon

because practically all sulphur produced is deposited in the pores. Then, the term of $\frac{P_{H_2O}.P_S}{K}$ in Eq. (6-52) can be neglected and this Equation reduces to:

$$\left(\frac{P_{H_2S}.P_{O_2}^{0.5}}{r_{H_2S}}\right)^{0.5}.\left(1-\frac{W_S}{W_S^{\infty}}\right)=A+B.P_{H_2S}+C.P_{H_2O}+D.P_{SO_2}+E.P_{O_2}^{0.5} \qquad (6\text{-}58)$$

To determine E, a series of runs were conducted in which the partial pressure of H_2S was kept approximately constant and partial pressures of H_2O and SO_2 were zero while the partial pressure of oxygen and temperature were varied at three different levels for each of them (See Table 3.1). $\left(\frac{P_{H_2S}P_{O_2}^{0.5}}{r_{H_2S}}\right)^{0.5}\left(1-\frac{W_S}{W_S^{\infty}}\right)$ was plotted against $(P_{O2})^{0.5}$ for three different temperatures (See Fig. 6.8). The slope was E for each temperature. The values of E are presented in Table 6.3.

To determine B , a series of runs were conducted in which the partial pressures of H_2O and SO_2 were kept constant at zero while the partial pressure of H_2S and temperature were varied at three different levels for each of them (See Table 3.2). $\left(\frac{P_{H_2S}P_{O_2}^{0.5}}{r_{H_2S}}\right)^{0.5}\left(1-\frac{W_S}{W_S^{\infty}}\right)-EP_{O_2}^{0.5}$ was plotted against P_{H_2S} for three different temperatures (See Fig. 6.9). The slope was B for each temperature. The values of B are presented in Table 6.3.

To determine C , a series of runs were conducted in which the partial pressures of O_2 and H_2S were kept constant and partial pressure was SO_2 was zero while the partial pressure of H_2O and temperature were varied at three different levels for each of them (See Table 3.3). For this series of experiment, a humidifier was connected to the reactor setup before the reactor and the feed stream was saturated with different amounts of

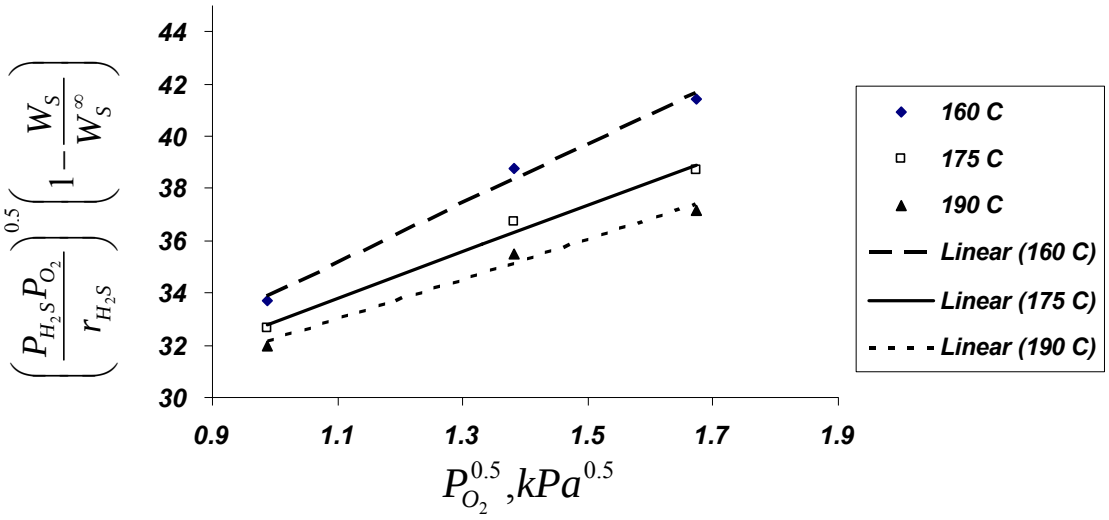

Fig. 6.8: Determination of variable E in Eq. (6-58)

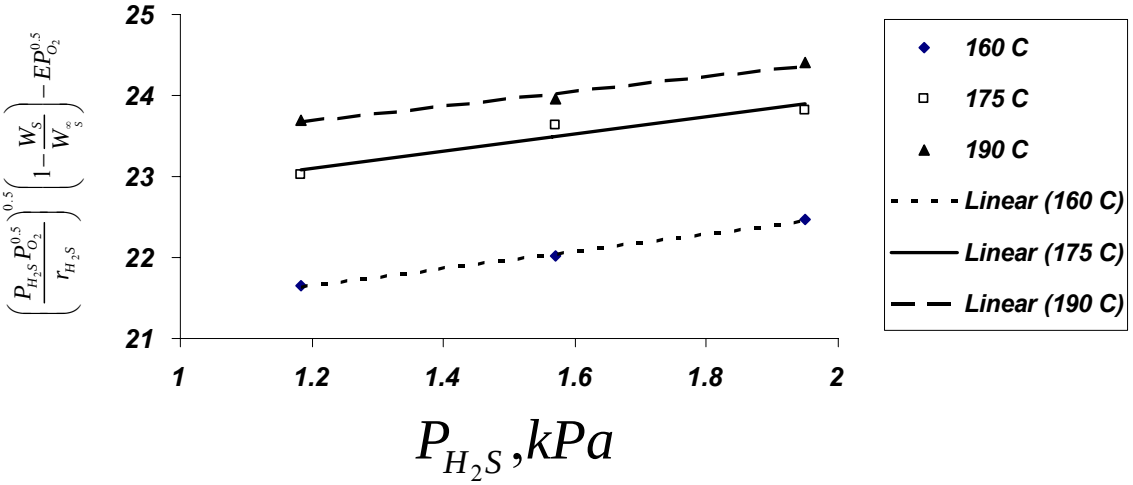

Fig. 6.9: Determination of variable B in Eq. (6-58)

water by varying the humidifier temperature (See Fig. 3.2). The amount of water used for saturation of feed stream was determined by the weight loss of the humidifier.

$\left(\frac{P_{H_2S}P_{O_2}^{0.5}}{r_{H_2S}}\right)^{0.5}\left(1-\frac{W_S}{W_S^{\infty}}\right)-EP_{O_2}^{0.5}-BP_{H_2S}$ was plotted against P_{H_2O} for three different temperatures (See Fig. 6.10). The slope was C for each temperature. The values of C are presented in Table 6.3.

To determine D and A , a series of runs were conducted in which the partial pressures of O_2 and H_2S were kept constant and partial pressure was H_2O was zero while the partial pressure of SO_2 and temperature were varied at three different levels for each of them (See Table 3.4). For this series of the experiment, a 0.5 mol% SO_2 in nitrogen was used.

$\left(\frac{P_{H_2S}P_{O_2}^{0.5}}{r_{H_2S}}\right)^{0.5}\left(1-\frac{W_S}{W_S^{\infty}}\right)-EP_{O_2}^{0.5}-BP_{H_2S}-CP_{H_2O}$ was plotted against P_{SO_2} for three different temperatures (See Fig. 6.11). The slope was D and the intercept was A for each temperature. The values of D and A are given in Table 6.3. Raw results for kinetic study are given in Appendix (H).

Using the calculated values for A, B, C, D, and E, and Equations (6-53)-(6-57), $\ln(K_{O_2}),\ln(K_{H_2S}),\ln(K_{SO_2}),and\ \ln(K_S C_t^2)$ were plotted against the inverse of temperature (See Fig. 6.12). The following equations are resulted from these plots;

$$\ln(K_{H_2S}) = -7.00 + \frac{14.71}{RT} \qquad (6-59)$$

$$\ln(K_{O_2}) = -17.45 + \frac{58.72}{RT} \qquad (6-60)$$

$$\ln(K_{SO_2}) = -5.87 + \frac{16.32}{RT} \qquad (6-61)$$

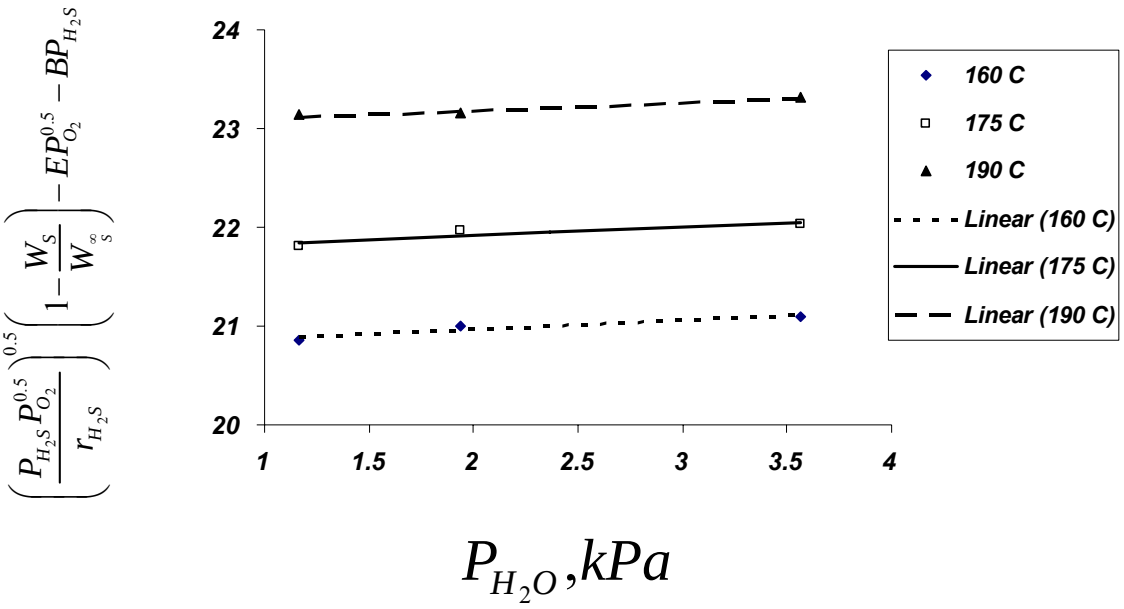

Fig. 6.10: Determination of variable C in Eq. (6-58)

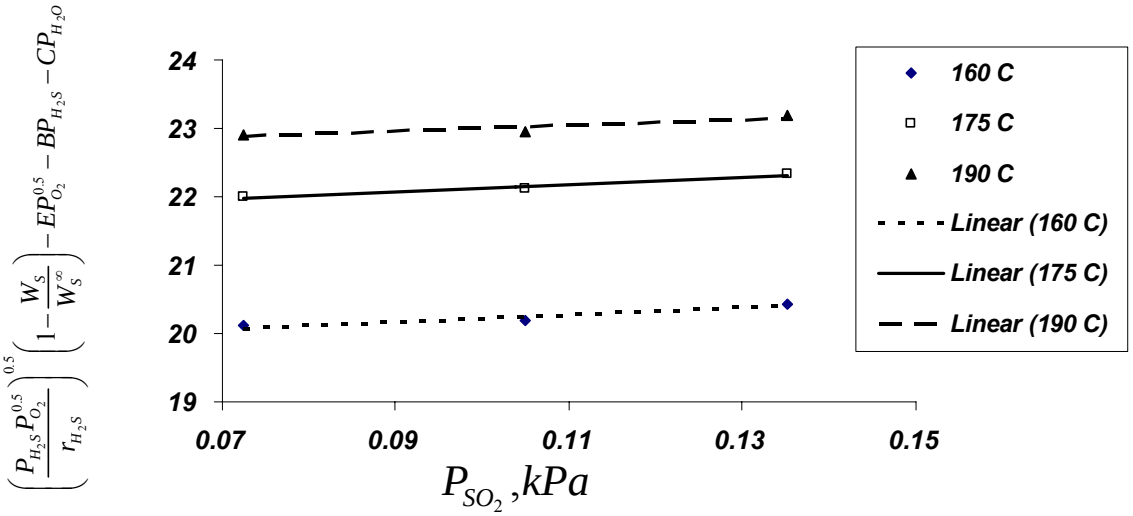

Fig. 6.11: Determination of variables D and A in Eq. (6-58)

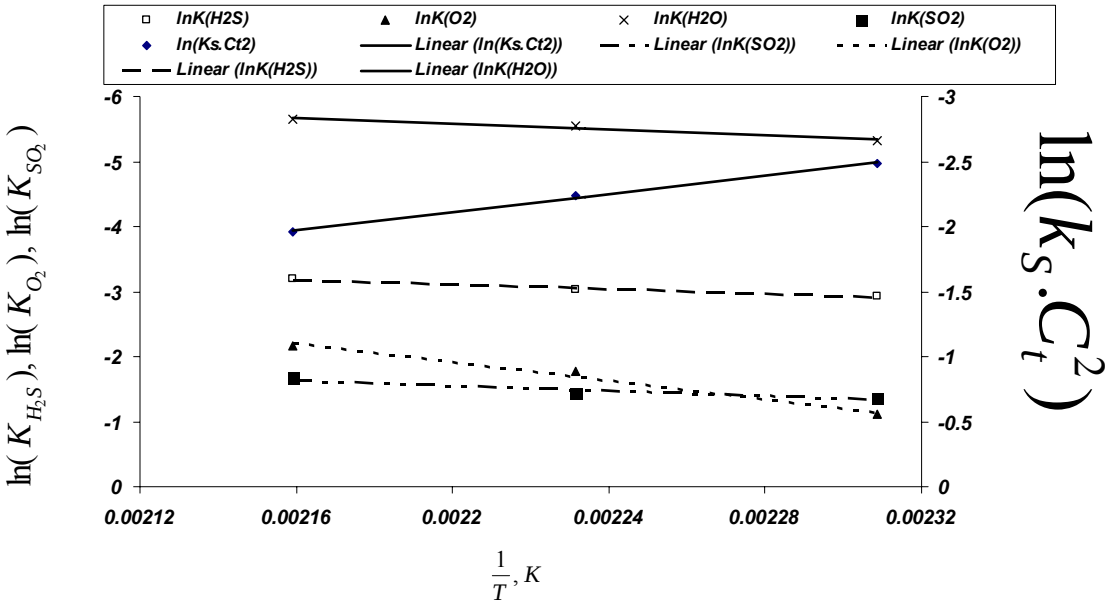

Fig. 6.12: Determination of activation energy, adsorption energy and frequency factors

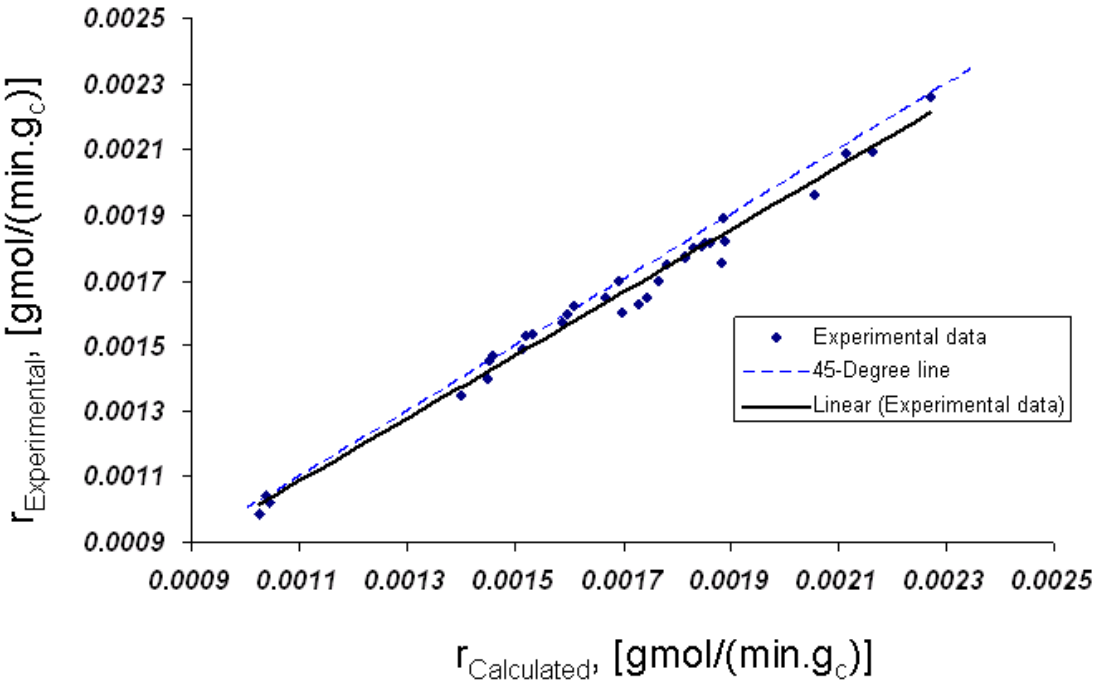

Fig. 6.13: Comparison of the calculated and experimental values for reaction rates

$$\ln(K_{H_2O}) = -10.47 + \frac{18.48}{RT} \qquad (6-62)$$

$$\ln(K_S C_t^2) = 5.65 - \frac{29.32}{RT} \qquad (6-63)$$

Therefore, the activation energy for H_2S oxidation was 29.3 kJ/gmol and heat of adsorption for H_2S, O_2, H_2O, and SO_2 are -14.7, -58.7, -18.5 and -16.3 kJ/gmol, respectively. These values show that adsorption of O_2 on active sites is chemical in nature, but that for H_2S, H_2O and SO_2 can be physical.

The rate of reaction using the above equations can be written as follows;

$$r_{H_2S} = \frac{k_S C_t^2 K_{H_2S} K_{o_2}^{0.5} P_{H_2S} P_{O_2}^{0.5}}{(1 + K_{H_2S} P_{H_2S} + K_{O_2}^{0.5} P_{O_2}^{0.5} + K_{H_2O} P_{H_2O} + K_{SO_2} P_{SO_2})^2} \left(1 - \frac{W_S}{W_S^{\infty}}\right)^2 \qquad (6-64)$$

Fig. 6.13 shows that R^2 for experimental and calculated reaction rates is equal to 98%. R^2 for runs of oxygen-effect, H_2S-effect, water-effect, and SO_2-effect is 95%, 99%, 84%, and 96%, respectively. Summary of reaction orders and activation energies obtained by other researchers are shown in Table 6.4. The value of activation energy calculated in this study agrees with results of other researchers.

These results show that the value of heat of adsorption for oxygen calculated for first mechanism (-131.1 kJ/gmol) was too large in comparison with the values calculated by Otake et al (1971), Ghosh and Tollefson (1986) and Dalai and Tollefson (1998), which were -71.1, -73.8, and -16 kJ/gmol. In addition, R^2 calculated for the runs of SO_2-effect for the first mechanism was lower than that for the second mechanism (77% versus 96%). For the first mechanism, dW/dt versus W graph did not show a linear trend in Fig. 6.2. If the model proposed for the reaction mechanism supports the experimental data, this

Table 6.4: Summary of reaction orders and activation energy for H_2S oxidation over activated carbon obtained by researchers

Researchers	Temperature range (^oC)	Reaction order with respect to H_2S	Reaction order with respect to O_2	Activation energy (kJ/gmol)
[Puri et al, 1971]	120-240	0	0.1	25.6
[Sreeramamurthy and Menon , 1975]	70-100	1.0	0.5	6.7-29.3
[Carioso and Walker, 1975]	100-160	1.0	0	20.1
[Steijns et al, 1976]	170-190	0.24 (Oxidation) 0.60 (Reduction)	0.2 (Oxidation) 0 (Reduction)	37.0 52.0
[Coskun and Tollefson, 1980]	24-188	0.5	0	23.4-48.9
[Klein and Henning, 1984]	100-250	0.8 [H_2S/O_2 >1] 0 [H_2S/O_2 <1]	0.5 [H_2S/O_2 >1] 0 [H_2S/O_2 <1]	28.0 40.0
[Ghosh and Tollefson, 1986]	125-200	0.5	1.0	23.6
[Dalai et al, 1992]	110-240	1.0	1.0	2.6 (T>130 ^oC) 16.9(T<130 ^oC)
[Dalai and Tollefson, 1998]	125-200	1.0	0.5	34.2
[Gardner et al, 2002]	145-175	1.0	0.3	34.4
Current study E-R* mechanism L-H* mechanism	 160-190 160-190	-	-	 26.6 29.3

* E-R: Eley-Rideal, L-H: Langmuir-Hinshelwood

graph must be linear, as we can see in Fig. 6.7 for the second mechanism. These facts show that Langmuir-Hinshelwood mechanism can better support the experimental data.

7.0 Conclusions and recommendations

The most important results of this thesis include investigation on physical (steam) and chemical (KOH) activations of a coal-based precursor (Luscar char) and a biomass-based precursor (biochar), development of two models for the BET surface area and reaction yield of each activation process, optimization of the operating conditions to obtain activated carbons with large surface area and reasonable yield, use of these activated carbons as the base catalysts for direct oxidation of hydrogen sulphide to sulphur, study the effect of porous structure, surface chemistry, and ash content on the performance of activated carbon for catalytic oxidation of hydrogen sulphide to sulphur , study the type of sulphur products in the oxidation reaction, study the effects of impregnating agents and impregnating solvents on the performance of activated carbons for this reaction, and kinetic studies.

7.1. Summary and Conclusions

The main advantage of using activated carbon catalysts for catalytic reactions is the cheap precursors used for the production of catalyst. Coal (lignite coal) and biomass (agricultural wastes and forest residues) are two abundant and low-cost carbon based precursors which are available in Canada. They can be converted to value-added products such as activated carbons with many environmental applications. Both common methods of activation, physical and chemical, were used in this study. Activated carbons' porous structure and product yield are functions of operating conditions. Using a novel approach, the internal surface area and reaction yield for each activation method were correlated to the operating conditions. In addition, these correlations were used to calculate the

optimum operating conditions required for the production of activated carbons with relatively large surface area and high reaction yield. Through this study, the following summary and conclusions were obtained:

a) Production of activated carbons from biochar

1. Two common activation methods were used for production of activated carbons from biochar; physical (steam) activation and chemical (potassium hydroxide) activation. Experiments were designed using the central composite design method.
2. Two models were developed for the BET surface area and reaction yield of process for each activation method.
3. These models showed that activation temperature and mass ratio of steam to bichar were dominant factors in physical activation. Higher activation temperature and/or mass ratio of steam to char increased the BET surface area but decreased the reaction yield for physically activated carbon.
4. Using the models for the BET surface area and reaction yield, the optimum operating conditions for producing physically activated carbon with high BET surface area and large yield was calculated. The results calculated by models were in good agreement with the results for the sample produced at the calculated operating conditions.
5. The models developed for chemically activated carbons showed that activation temperature and mass ratio of KOH to biochar were dominant factors in chemical activation. The BET surface area increased with an increase in mass

ratio up to a maximum and then decreased. This can be due to pore widening and gasification on the external surface of activated carbon at higher mass ratios. The BET surface area increased by an increase in activation temperature and nitrogen flow rate.

6. Reaction yield decreased by an increase in activation temperature. Increasing the nitrogen flow rate at high temperatures decreased the reaction yield, but at low temperatures had the reverse effect.
7. The optimum operating conditions were calculated using the models. The results calculated by models were in good agreement with the results for the sample produced at the calculated operating conditions.
8. The isotherm plots for chemically and physically activated carbons produced from biochar were types I and IV isotherms.

b) Production of activated carbons from luscar char

1. Activated carbons were produced using the physical (steam) activation of luscar char. Two models were developed for the BET surface area and reaction yield of process for each activation method.
2. By increasing the activation temperature, the BET surface area decreased beyond a certain limit. It can be due to collapsing the pore walls or the effect of high ash content of precursor. An increase in mass ratio had the same effect.
3. The optimum operating conditions were calculated using the models. The results calculated by models were in good agreement with the results for the sample produced at the calculated operating conditions.

4. The isotherm plot for physically activated carbon produced from luscar char was type IV isotherm.

c) Hydrogen sulphide oxidation to sulphur using activated carbon catalyst

Activated carbons prepared from coal-based and biomass-based precursors were used as catalyst for the direct oxidation reaction of hydrogen sulphide to sulphur. They showed good potential for this reaction. To improve the performance of steam-activated carbons, acid-treatment followed by thermal desorption was used as the modification method. This modification method improved the performances of steam-activated carbons for H_2S oxidation reaction. This method improved surface characteristics of catalysts and increased the active sites on the carbon surface. Impregnation method was effective for H_2S oxidation reaction and aprotic solvent had a better effect on the penetration of KI in porous structure of activated carbon comparing with protic solvents. XANES was used for study the sulphur species in reaction product. Through this study, the following summary and conclusions were obtained:

1. Originally activated carbons (physically and chemically) showed the activity and selectivity of activated carbons for the oxidation of H_2S to sulphur by relatively suitable break-through time and low production rate for SO_2.
2. To improve the performance of steam-activated carbons for the H_2S oxidation reaction, acid (HNO_3)-treatment/thermal desorption was used as the modification method.

3. Analysis of porous characteristics showed that acid-treatment/thermal desorption method increased micropore, mesopore, and total pore volume by 11 % for BioAC-O-D(750) and 43 % for LusAC-O-D(650). This increase in pore volumes provides larger surface area for active sites and higher space for storing sulphur product resulting in longer break-through time.
4. Improvement in porous structure not only allows a better access to active sites using mesopores, but also increased micropore volume, especially supermicropore volume.
5. The performance of acid-treated samples was not better than the originally steam activated carbons because of the presence of many acidic groups on the carbon surface which was confirmed by Boehm titration and TPD.
6. Thermal desorption of acid-treated samples drastically increased the performance of these activated carbons. This step removed many acidic groups such as carboxylic groups from the carbon surface and increased the ratio of basic to acidic groups on the carbon surface in comparison to the oxidized samples, as shown by TPD and Boehm titration.
7. In this study, ash composition showed no role in the performance of catalysts. High amount of ash content in the activated carbons prepared from luscar char can be one of the reasons for their lower performance as compared to the similar activated carbons prepared from biochar.
8. Sulphur L-edge X-ray near edge structure (XANES) showed that the elemental sulphur was the dominant sulphur species in the product for all activated

carbons used in this study for the oxidation reaction under different operating conditions.

9. Use of impregnating agents for LusAC-O-D(650) improved the performance of catalyst by increasing the break-through time and amount of sulphur captured by unit mass of catalyst, but for most cases it increased the SO_2 production in small extent too.
10. During H_2S oxidation reaction, SO_2 production reached its maximum before the point at which maximum conversion of H_2S ceases to occur and then it decreased.
11. Use of an aprotic solvent such as dimethyl sulfoxide instead of a polar protic solvent such as water, as solvent for catalyst impregnation, increased the performance of LusAC-O-D(650)-K(5%) because of better penetration of impregnating agent in the porous structure of activated carbon.
12. An increase in the reaction pressure up to 700 kPa could increase the performance of catalyst and decreasing the SO_2 production.
13. An increase in the reaction temperature from 160 to 205 ^{o}C showed that the SO_2 production increased at higher temperature.
14. Thermal regeneration of impregnated, modified catalysts prepared from luscar char for 24 hours showed that after two rounds of reaction/regeneration the performance of catalyst remained constant and comparing the fresh catalyst the amount of sulphur captured by unit mass of catalyst decreased by 36%.

15. Kinetic study for temperature range of 160-190 ^{o}C, oxygen to hydrogen sulphide molar ratio of 1-3, and H_2S concentration of 6000-10000 ppm at 200 kPa, for LusAC-O-D(650) was performed and the values of activation energy of the oxidation reaction were 26.6 and 29.3 kJ/gmol for Eley-Rideal and Langmuir-Hinshelwood mechanisms, respectively.

7.2. Recommendations

1) There are some methods for modification of nitrogen functionalities called high-temperature methods. In these treatments, nitrogen tends to appear within the aromatic ring structure which enhances the basicity. These methods were effective for other applications. The effects of the high-temperature treatments on the performance of activated carbon for H_2S oxidation at high temperatures can be investigated.

2) There are two main assumptions about the source of basicity of activated carbons. First one suggests that the basic surface functionalities such as chromene and pyrones are responsible for basicity of activated carbon and the second one introduces the delocalized π-electrons of the graphene layers as the source of basicity. Although, there are some characterization methods to quantify the basicity (such as Boehm titration) but the real interpretation of these results and source of basicity need more investigation. This information can be used to develop the actual mechanism for each application of activated carbon. It helps to tailor and produce suitable activated carbon by activation methods and the required chemical processes.

3) Although ash content (metal impurities) composition showed no effect on this reaction for this study, but the oxide forms of some metal impurities (such as iron, copper, and vanadium) are generally considered as catalysts for H_2S oxidation reaction. A systematic study is needed for understanding the effect of ash content components on the reaction.

8.0 References

Adams L. B., C. R. Hall, R. J. Holmes, R. A. Newton, An examination of how exposure to humid air can result in changes in the adsorption properties of activated carbons, Carbon 26 (1988) 451-459.

Adib F., A. Bagreev, T. J. Bandosz, Effect of pH and surface chemistry on the mechanism of hydrogen sulphide removal by activated carbons, Journal of Colloid interface science 216 (1999) 360-369.

Adib F., A. Bagreev, T. J. Bandosz, Adsorption/oxidation of hydrogen sulphide on nitrogen activated carbons. Langmuir 16 (2000) 1980-1986.

Allen D., D. Shonnard, Green Engineering: Environmentally conscious design of chemical processes, Prentice Hall PTR, USA, 1st ed., 2002, Chapter 1.

Ania C. O., J. B. Parra, J. J. Pis, Influence of oxygen-containing functional groups on active carbon adsorption of selected organic compounds. Fuel Processing Technology 79 (2002) 3: 265-271.

Arenas E., F. Chejne, The effect of the activating agent and temperature on the porosity development of physically activated coal chars, Carbon 42 (2004) 2451-2455.

ATSDR: The Agency for Toxic Substances and Disease Registry (2006) Web site: http://www.atsdr.cdc.gov/toxprofiles/tp114.pdf

Bagreev A., T. J. Bandosz, A role of sodium hydroxide in the process of hydrogen sulphide adsorption/oxidation on caustic-impregnated activated carbon, Industrial and Engineering Chemistry Research, 41 (2002) 672-679.

Bagreev A., J. A. Menendez, I. Dukhno, Y. Tarasenko, T. J. Bandosz, Bituminous coal-based activated carbons modified with nitrogen as adsorbents of hydrogen sulphide, Carbon 42 (2004) 469-476.

Bagreev A., S. Bashkova, T.J. Bandosz, Adsorption of SO_2 on activated carbons: the effect of nitrogen functionality and pore size. Langmuir 18 (2002a) 1257-1264.

Baker F. S., C. E. Miller, A. J. Repik, E. D. Tolles, In: Kirk-Othmer encyclopedia of chemical technology, 27th Volume, John Wiley, New York, 5th ed., 1992, 1015-1037.

Balbuena P. B., K. E. Gubbins, Classification of adsorption behavior: simple fluids in pores of slit-shaped geometery, Fluid phase equilibria 76 (1992) 21-35.

Bandosz T. J., A. bagreev, F. Adib, A. Turk, Unmodified versus caustic-impregnated carbons for control of hydrogen sulphide emissions from sewage treatment plants, Environment Science and Technology 34 (2000) 1069-1074.

Bansal R., J. B. Donnet, H. F. Stoeckli, Active carbon, Marcel Dekker, New York, 1st ed., 1988, Chapters 3 and 4.

Barrett E.P., L. G. Joyner, P.P. Halenda, The Determination of Pore Volume and Area Distributions in Porous Substances. I. Computations from Nitrogen Isotherms, Journal of the American Chemical Society 73 (1951) 373-380.

Bashkova S., F. S. baker, X. Wu, T. R. Armstrong, V. Shwartz, Activated carbon catalyst for selective oxidation of hydrogen sulphide: on the influence of pore structure, surface characteristics, and catalytically-active nitrogen, Carbon 45 (2007) 1354-1363.

Beasley T., R. G. Abry, Managing hydrogen sulphide the natural way, Energy processing Canada, Sep./Oct. (2003).

Boehm H., Some aspects of the surface chemistry of carbon blacks and other carbons, Carbon 32 (1995) 5: 759-769.

Boehm H. P. Surface oxides on carbon and their analysis: a critical assessment, Carbon 40 (2002) 2: 145-149.

Boehm H. P., M. Voll, Basische Oberflächenoxide auf Kohlenstoff—I. Adsorption von säuren, Carbon 8 (1970) 2: 227-280.

Boehm H.P., Chemical identification of surface groups: In: Advances in catalysis, vol. 16 New York: Academic Press, 1966, 179-274.

Brazhhnyl D. V., Y. P. Zaitsev, I. V. Bacherikova, V. A. Zazhigalov, J. Stoch, A. Kowal, Oxidation of H_2S on activated carbon KAU and influence of the surface state, Applied Catalysis B: Environmental 70 (2007) 557-566.

Brunauer, S., P. H. Emmett, E. Teller, Adsorption of gases in multimolecular layers, Journal of the American Chemical Society, 60 (1938) 309-319.

Busca, G., C. Pistarino, Technologies for the abatement of sulphide compounds from gaseous streams: a comparative overview, Journal of loss prevention in the process industries 16 (2003) 5: 363-371.

Byrne, J. F., H. Marsh In Porosity in carbons: Characterization and applications; Patrick, Jr W. (Ed.) Edward Arnold: 1st ed., London, UK, 1995, chapter 1.

Cal M. P., B. W. Strickler, A. A. Lizzio, High temperature hydrogen sulphide adsorption on activated carbon I: Effects of gas composition and metal addition, Carbon 38 (2000) 13: 1757-1765.

Cariaso O. C., Jr P. L. Walker, Oxidation of hydrogen sulfide over microporous carbons, Carbon 13 (1975) 3: 233-239.

Chandra V., Fundamentals of Natural gas, V. Chandra, Penn Well Co., USA, 1st ed., 2006, 36.

Chen W., F. S. Cannon, J. R. Rangel-Mandez, Ammonia-tailoring of GCA to enhance perchlorate removal II: Perchlorate adsorption, Carbon 43 (2005) 3: 581-590.

Chiang H.-L., J.-H. Tsai, C.-L. Tsai, Y.-C. Hsu, Adsorption characteristics of alkaline activated carbon exemplified by water vapor, H_2S, and CH_3SH, Gas. Sep. Sci. Technol. 35 (2000) 903.

Choi J. J., M. Hirai, M. Shoda, Catalytic oxidation of hydrogen sulphide by air over an activated carbon fiber, Applied Catalysis A: General 79 (1991) 241-248.

Chowdhury A. I., E. L. Tollefson. Catalyst modification and process design considerations for the oxidation of low concentrations of H_2S in natural gas, The Canadian Journal of Chemical Engineering 68 (1990) 449-454.

Chun S. W., J. Y. Jang, D. W. Park, H. C. Woo, J. S. Chung, Selective oxidation of H_2S to elemental sulfur over TiO_2/SiO_2 catalysts, Appl. Catal. B 16 (1998) 235-243.

Contescu A., M. Vass, C. Contescu, k. Putyera, J. A. Schwarz, Acid buffering capacity of basic carbons revealed by their continuous pK distribution, Carbon 36 (1998) 3: 247-258.

Corapcioglu M. O., C. P. Huang, The surface acidity and characterization of some commercial activated carbons, Carbon 25 (1987) 4: 569-579.

Craige, B. D., D. S. Anderson, Handbook of corrosion data, ASM International, USA, 2nd ed., 1995, 470-480.

Crammore R. G., E. Stanton, Modern petroleum Technology, Vol. 1 Upstream, , R. A. Dawe (ed.), John Wiley & Sons Ltd., England, 6th ed., 2000, 356-360.

Coskun I., E. L. Tollefson, Oxidation of low concentration of hydrogen sulphide over activated carbon, The Canadian Journal of Chemical Engineering 58 (1980) 72-76.

Dalai, A. K., Majumdar A., Chowdhury A., Tollefson, E. L., The effects of pressure and temperature on the catalytic oxidation of hydrogen sulphide in natural gas and regeneration of the catalyst to recover the sulphur produced, The Canadian Journal of Chemical Engineering 71 (1993) 75-82.

Dalai A. K., A. Majumdar, E. L. Tollefson, Kinetics of hydrogen sulphide oxidation over an activated carbon catlayst in the pressure range of 712-3436 kPa and temperature range of 110-240 ^{0}C, K. J. Smith, E. C. Sanford (ed.), Progress in Catalysis 72 (1992) 367-375.

Dalai, A. K., E. L. Tollefson, Kinetics and reaction mechanism of catalytic oxidation of low concentrations of hydrogen sulphide in natural gas over activated carbon, The Canadian journal of Chemical Engineering, 76 (1998) 902-914.

Dalai A. K., J. Zaman, E. S. Hall, E. L. Tollefson, Preparation of activated carbon from Canadian coals using a fixed-bed reactor and a spouted bed-kiln system, Fuel 75 (1996) 2: 227-237.

Dalrymple D. A., T. W. Trofe; Gas industry assesses new ways to remove small amounts of H_2S, Oil & Gas Journal, May (1994) 54-60.

Dastgheib, S. A., T. Kavanfi, The effect of the physical and chemical characteristics of activated carbons on the adsorption energy and affinity coefficient of Dubinin equation, Journal of Colloid and Interface Science 292 (2005) 312-321.

Dastgheib S. A., T. Karanfil, Adsorption of oxygen heat-treated granular and fibrous activated carbons, Journal of Colloid and Interface Science 274 (2004) 1-8.

Derbyshire F., M. Jagtoyen, M. Thwaites. In: Jr. W. Patric (ed.), Porosity in carbons: characterizations and applications, Edward Arnold, UK, 1st ed., 1995, 227-253.

Donnet J. B., The chemical reactivity of carbons, Carbon, 6 (1968) 2: 161-176.

Driel J. In: A. Capelle, F. de Vooys (ed.), Activated carbon-A fascinating material, The Netherlands: Norit, Amersfoort, 1983, 40-57.

Dubinin M. M., V. A. Astahakov, Adv. Chem. Soc. (1971) 102: 69 [In: Lowell et al, 2004]

Dynamotive energy systems corporation, http://www.dynamotive.com/assets/articles/2007/Task_34_Booklet.pdf, 1997

El-Hendawy A. A., S. E. Samra, B. S. Girgis, Adsorption characteristics of activated carbons obtained from corncobs, Colloids and Surfaces A: Physicochemical and Engineering Aspects 180 (2001) 209-221.

Epstein B. D., E. Dalle-Molle, J. A. Mattson, Electrochemical investigations of surface functional groups on isotropic pyrolytic carbon, Carbon 9 (1971) 5: 609-615.

Everett D. H., J. C. Powl, Journal of Chemical Society, Faraday Trans. I 72 (1976) 619 [Webb and Orr, 1997].

Fabish, T. J., D. E., Schleifer, Surface chemistry and the carbon black work function, Carbon 22 (1984) 1: 19-38.

Fan M., W. Marshall, D. Daugaard, R. C. Brown, Steam activation of chars produced from oat hulls and corn stover, Bioresource Technology 93 (2004) 1: 103-107.

Fanning P.E., M. A. Vannice, A DRIFTS study of the formation of surface groups on carbon by oxidation. Carbon 31 (1993) 5: 721-730.

Figueiredo J. L., M. F. R. Pereira, M. M. A. Freitas, J. J. M. Orfao, Modification of the surface chemistry of activated carbons, Carbon 37 (1999) 9: 1379-1389.

Fogler H. S., Elements of chemical reaction engineering, Prentice Hall PTR, USA, 3rd ed., 1999, 581-809.

Frössling N., Gerlands Beitr. Geophys. 52 (1938) 170, In: [Fogler, 1999, p702].

Gamson, B. W., R. H. Elkins, Sulphur from hydrogen sulphide, Chemical Engineering progress, 94 (1953) 4: 203-215.

Gardner T. H., D. A. Berry, K. D. Lyons, S. K. Beer, A. D. Freed, Fuel processor integrated H_2S catalytic partial oxidation technology for sulphur removal in fuel cell power plants, Fuel 81 (2002) 2157-2166.

Garten V. A., D. E. Weiss, A new interpretation of acidic and basic structures in carbons II. The Chromene-Carbonium ion couple in carbon, Australian Journal of Chemistry 10 (1957a) 309-328.

Gary J. H., G. E. Handwerk. Petroleum Refining: Technology and economics, Marcel Dekker Inc., USA, 4th ed., 2001: 261-287.

Ghosh T. K., E. L. Tollefson, Kinetics and reaction mechanism of hydrogen sulphide oxidation over activated carbon in the temperature range of 125-200 ^{o}C, The Canadian Journal of Chemical Engineering 64 (1986) 969-976.

Gonzales J. C., A. Sepulveda-Escribano, M. Molina-Sabio, F. Rodriguez-Reinoso, Production, properties and applications of activated carbon. In: Characterization of porous solids. Vol. IV, McEnaney (ed.), The royal society of chemistry, Cambridge,1st ed., 1997, 9-16.

Greenwood M. N., A. Earnshaw, Chemistry of the Elements. Pergamon Press, Oxford, 1986, In: [Moreno-castilla, 1998].

Gregg S. J., K. S. W. Sing, Adsorption, surface area and porosity, 1st ed., London, Academic press, 1982: 49.

Grove D. M., In: porous carbon solids, R. L. Bond (ed.), 1958, London, Academic press, 155, [B. McEnany, T. J. Mays, In Porosity in carbons: Characterization and applications; Patrick, Jr W. (ed.) Edward Arnold, London, UK, 1st ed., 1995, chapter 4].

Gua J., Y. Luo, A. C. Lua, R. Chi, Y. Chen, X. Bao, S. Xiang, Adsorption of hydrogen sulphide (H_2S) by activated carbons derived from oil-palm shell, Carbon 45 (2007) 2: 330-336.

Hayden R. A., Method for reactivating nitrogen-treated carbon catalysts. US patent 5,466,645 (1995).

Heguy D. L., G. J. Nagel, Consider optimizes iron-redox processes to remove sulphur, Hydrocarbon processing, 82 (2003) 1: 53-57.

Hewitt G. F., J. R. Morgen, Progress in applied materials research (1964) 5 : 167 [B. McEnany, T. J. Mays, In Porosity in carbons: Characterization and applications; Patrick, Jr W. (ed.) Edward Arnold, London, UK, 1st ed., 1995, chapter 4].

Hewitt G. F., Chemistry and physics of carbon (1965) 1 : 73, In: [B. McEnany, T. J. Mays, In Porosity in carbons: Characterization and applications; Patrick, Jr W. (ed.) Edward Arnold, London, UK, 1st ed., 1995, chapter 4].

Higashiyama K., Action of nickel catalyst during steam gasification of bituminous and brown coals, Fuel 64 (1985) 1157-1162.

Highman C., M. Van der Burgt, Gasification, 1st ed., Elsevier Science, USA, 2003, Chapter 3

Hutchins R.A., Chemical Engineering 87 (1980) 101-110, In: [Marsh and Rodriguez Reinoso, 2006].

Ishizaki C., I. Marti, Surface oxide structures on a commercial activated carbon, Carbon 19 (1981) 409-412.

Iwasawa Y., S. Ogasawara, Catalytic oxidation of hydrogen sulphide on polynaphthoquinone, Journal of Catalysis 46 (1977) 132-142.

Kadlec, O., In: Rodriguez-Reinoso F, Rouquerol, Sing K.S.W.and Unger K.K. (ed.) Charcterization of porous solids-II, 1991, Amesterdam: Elsevier, 759.

Kensell W., D. Leppin, "Review of the H_2S direct oxidation processes" , 7th GRI sulphur recovery conference, 1995

Kohl A. L., R. Nielsen, Gas purification, Gulf professional publication Co., 5th edition, Huston, 1997 [Wu et al, 2005].

Kyotani, T., Control of pore structure in carbon, Carbon 38 (2000) 269-286.

Lahaye J., G. Nanse, A. Bagreev and V. Strelko, Porous structure and surface chemistry of nitrogen containing carbon from polymers, Carbon 37 (1999) 4: 585-590.

Laine J., A. Calafat, Factors affecting the preparation of activated carbons from coconut shell catalyzed by potassium, Carbon 29 (1991)7: 949-953.

Langmuir I., Journal of American Chemical Society, 38 (1916) 2221, In: [Rouquerol, 1999, 97].

Lastoskie C. M., K. E. Gubins, N. Quirke, Pore size heterogeneity and the carbon slit pore: a density functional theory model, Langmuir 9 (1993) 2693-2702.

Lastoskie C., K. E. Gubbins, N. Quirke, Journal of Physical Chemistry 97 (1993a) 4786, In: [Lowell et al, 2004].

Lazic Z. R., Design of experiments in chemical engineering, Wiley-VCH Verlag GmbH, Weinheim, 1st ed., 2004, Chapter 2.

Leboda R., J. Skubiszewka-Zieba , W. Grzegorczyk , Effect of calcium catalyst loading procedure on the porous structure of active carbon from plum stones modified in the steam gasification process Carbon 36 (1998) 417-425.

Leon Y., C. A. Leon, L. R. Radovic, Interfacial chemistry and electrochemistry of carbon surfaces. In: P. A. Thrower (editor) Chemistry and physics of carbon, Vol. 24, Marcel Dekker, NewYork, 1st ed., 1994, 213-310.

Leon Y., C. A. Leon, J. M. Solar, V. Calemma, L. R. Radovic, Evidence for the protonation of basal plane sites on carbon, Carbon 30 (1992) 5: 797-811.

Li K. T., C. S. Yen, N. S. Shyu, Mixed-metal oxide catalysts containing iron for selective oxidation of hydrogen sulfide to sulfur, Applied Catalysis A 156 (1997) 117-130.

Lillo-Rodenas M. A., D. Cazorla-Amoros, A. Linares-Solano, Understanding chemical reactions between carbons and NaOH and KOH: An insight into the chemical activation mechanism, Carbon 41 (2003) 267-275.

Lillo-Ródenas M. A., D. Lozano-Castelló, D. Cazorla-Amorós, A. Linares-Solano, Preparation of activated carbons from Spanish anthracite: II. Activation by NaOH, Carbon 39 (2001) 751-759.

Linares-Solano A., I. Martin-Gullon, C. Salinas-Martinez de lecea, B. Serrano-Talaverra, Activated carbons from Bituminous coal : Effect of mineral matter content, Fuel 79 (2000) 6: 635-643.

Lizama H. M., B. M. Sankey. Conversion of hydrogen sulphide by acidophilic bacteria, Applied Microbial Biotechnical 40 (1993) 438-441.

Lizzio A. A., J. A. DeBarr, Effect of surface area and chemisorbed oxygen on the SO_2 adsorption capacity of activated char, Fuel 75 (1996) 1515-1522.

Lowell S., J. E. Shields, M. A. Thommes, M. Thommes, Characterization of porous solids and powders: Surface area, pore size and density, Kluwer Academic Publishers, Netherlands, 1st ed., 2004, 100-148.

Lozano-Castello D., M.A. Lillo-Rodenas, D. Cazorla-Amoros, A. Linares-Solano, Preparation of activated carbons from Spanish anthracite I. Activation by KOH, Carbon 39 (2001) 5: 741-749.

Lua A. C., T Yang, Effect of activation temperature on the textural and chemical properties of potassium hydroxide activated carbon prepared from pistachio-nut shell, J of Colloid and Interface Science 274 (2004) 594-601.

Lynch J., Physico-chemical analysis of industrial catalysts: a practical guide to characterization; Editions Technip; 2003, Paris, France, chapter 1.

Mahajan O.P., C. Moreno-Castilla, J.R. Walker, Surface-treated Activated Carbon For Removal Of Phenol From Water, Separation and Science Technology 15 (1980) 1733-1752.

Mangun C. L., J. A. DeBarr, J. Economy, Adsorption of SO_2 on ammonium-treated activated carbon fibers, Carbon 39 (2001) 11: 1689-1696.

Marchon B., J. Carrazza, H. Heinemann, G. A. Somorjai, TPD and XPS studies of O_2, CO_2, and H_2O adsorption on clean polycrystalline graphite, Carbon 26 (1988) 4: 507-514.

Marsh H., A tribute to Philip L. Walker, Carbon 29 (1991) 6: 703-704.

Marsh H., F. Rodriguez-Reinoso, Activated carbon, UK, Elsevier, 1st ed., 2006, chapter 6.

Mattson J. S., H. B. Mark, Activated carbon, New York, Marcel Dekker, 1971,1st ed. In: [Rodriguez-reinoso, 1998].

Matviya T. M., R. A. Hayden, Catalytic carbon; US patent 5,356,849 (1994).

McEnaney B., in: Handbook of porous solids; Schuth, F.; Sing, K. S. W.; Weitkamp, J.; , Vol 3, Wiley-VCH Verlag GmbH, Weinheim, Germany,1st ed., 2002, Chapter 4.

McEnaney B., T. J. Mays, In Porosity in carbons: Characterization and applications; Patrick, W. J. (ed.), Halsted Press: London, UK, 1st ed., 1995, Chapter 4.

McEnaney, B. In Carbon materials for advanced technologies; Burchell , T. D.Elsevier science Ltd: Oxford, UK, 1999 [B. McEnany, T. J. Mays, In Porosity in carbons: Characterization and applications; Patrick, Jr W. (ed.) Edward Arnold, London, UK, 1st ed., 1995, chapter 4].

McEnany, B., Adsorption and structure in microporous carbons, Carbon 26 (1988) 267-274.

Meeyoo V., D. L. Trimm, Adsorption-reaction processes for the removal of hydrogen sulphide from gas streams, Journal of Chemical Technology and Biotechnology 68 (1997) 411-416.

Menendez J. A., J. Phillips, B. Xia, L. R. Radovic, On the modification and characterization of chemical surface properties of activated carbon: In the search of carbon with stable basic properties, Langmuir 12 (1996) 4404-4410.

Menendez J. A. ; R. L. Radovic ; B. Xia, J. Phillips, Low-temperature generation of basic carbon surfaces by hydrogen spillover, Journal of Physical Chemistry 100 (1996a) 17243.

Menendez J. A., D. Suarez, E. Fuente, M. A. Montes-Moran, Contribution of pyrone-type structures to carbon basicity : Theoretical evaluation of the pK_a of model compounds, Carbon 37 (1999) 1002-1006.

Mikhail R. Sh., S. Brunauer, E. E. Bodor, Investigation of a complete pore structure analysis: I. Analysis of micropores, Journal of colloid and interface science 26 (1968) 45-53.

Mikhalovsky S. V., Y. P. Zaitsev, Catalytic properties of activated carbons: I. Gas-phase oxidation of hydrogen sulphide, Carbon 35 (1997) 9: 1367-1374.

Miller B. G., Coal energy systems, Elsevier Inc., USA, 1st ed., 2005, chapter 1.

Mochida I., Y. Korai, M. Shirahama, S. Kawano, T. Hada, Y. Seo, M. Yoshikawa, A. Yasutake. Removal of SO_x and NO_x over activated carbon fibers. Carbon 2000, 38: 227-239.

Mokhatab S., W. A. Poe, J. G. Speight, Handbook of natural gas transmission and processing, , Elsevier Inc., UK, 1st ed, 2006, Chapter 7.

Molina-Sabio M., M. A. Munecas, F. Rodriguez-Reinoso, Characterization of porous solids II, Elsevier, Holland, 1st ed., 1991.

Monendez J. A., D. Suarez, E. Fuente, M. A. Montes-Moran, Correspondence, Carbon 37 (1999) 6: 1002-1006.

Montes-Moran M. A., J. A. Menendez, E. Fuente, D. Suarez, Contribution of the Basal Planes to Carbon Basicity: An Ab Initio Study of the H3O+-π Interaction in Cluster Models, J. phys chem. B 102 (1998) 29: 5595-5601.

Moreno-Castilla F., F. Carrasco-Marin, F.J. Maldonado-Hodar, J. Rivera-Utrilla, Effects of non-oxidant acid treatments on the surface properties of an activated carbon with very low ash content, Carbon 36 (1998) 1-2: 145-151.

Morgan, P. Carbon fibers and their composites CRC press: Boca raton, FL, USA, 2005, 1st ed.

Montes-Moran M. A., D. Suarez, J. A. Menendez, E. Fuente, On the nature of basic sites on carbon surfaces : An overview, Carbon 42 (2004) 1219-1225.

Montgomery D. C., Design and analysis of experiments, John Wiley & Sons, USA, 4th ed., 1997, Chapter 13.

Muhlen H., K. H. Van Heek, In Porosity in carbons: Characterization and applications; Patrick, W. J. (ed.), Halsted Press: London, UK, 1st ed, 1995, Chapter 5.

Munoz-Guillene M. J., M. J. Illian-Gomez, J. M. Martinez, A. Linares-Solano, A. Salinas-Martinez de lecea, Activated carbons from Spanish coals. I. Two-stage carbon dioxide activation, Energy and Fuels 6 (1992) 9-15.

Natural Resources Canada (NRCan) "Estimated Production, Consumption and Surplus Mill Wood Residues in Canada, 2004: A National Report" Canadian Forest Service, Economics and Industry Branch, and Forest Products Association of Canada, Prepared by BW McCloy & Associates Inc and Climate Change Solutions, November 2005.

Natural Resources Canada (NRCan), Annual Report 2008 (http://canadaforests.nrcan.gc.ca/rpt#QuickFacts)

Olivier J. P., Modeling physical adsorption on porous and nonporous solids using density functional theory, Journal of porous materials 3 (1995) 9-17.

Otake Y., R. G. Jenkins, Characterization of oxygen-containing surface complexes created on a microporous carbon by air and nitric acid treatment, Carbon 31 (1993) 1: 109-121.

Otowa T., Y. Nojima, T. Miyazaki, Development of KOH activated high surface area carbon and its application to drinking water purification, Carbon 35 (1997) 9: 1315-1319.

Otowa T., R. Tanibata, M. Itoh, Production and adsorption characteristics of MAXSORB: High-surface-area active carbon Gas separation and purification 7 (1993) 241-245.

Papirer E., E. Guyon, Contribution to the study of the surface groups on carbons-I: Acidimetric methods and formation of derivatives, Carbon 16 (1978) 127-131.

Park D. W., B. K. Park, K. D. Park, H. C. Woo, Vanadium-antimony mixed oxide catalysts for the selective oxidation of H_2S containing excess water and ammonia, Applied Catalysis A 223 (2002) 215-224.

Pels J. R., F. Kapteijn, J. A. Moulijn, Q. Zhu, K. M. Thomas, Evolution of nitrogen functionalities in the carbonaceous materials during pyrolysis. Carbon 33 (1995) 11: 1641-1653.

Perez-Cadenas A. F., F. J. Maldonado-Hodar, C. Moreno-Castilla, On the nature of surface acid sites of chlorinated activated carbons, Carbon 41 (2003) 3: 473-478.

Phillips J., Creating basic carbon surfaces, Energeia 7 (1996) 5: 1-4.

Pradhan B. K., N. K. Sandle, Effect of different oxidizing agent treatments on the surface properties of activated carbons, Carbon 37 (1999) 8: 1323-1332.

Przepiorski J., S. Yoshida, A. Oya, Structure of K_2CO_3-loaded activated carbon fiber and its deodorization ability against H_2S gas, Carbon 37 (1999) 12: 1881-1890.

Puri, B. R., In: Walker Jr P. J. (editor), Chemistry and physics of carbon, vol. 6, New York, Marcel Dekker, 1970, 191-282.

Puri, B. R., B. Kumar; K. C. Kalra, Studies in catalytic reactions of carbon: Part IV-Oxidation of hydrogen sulphide, Ind. J. Chem. 9 (1971) 970-972.

Radovic L. R., Rodriguez-Reinoso F., In: Chemistry and physics of carbon; Thrower, P. A.; Vol 25; Marcel Decker: New York, NY, USA, 1997, In: [Marsh and Rodriguez-Reinoso, 2006].

Rivin D., Proc. 5th conference on carbon, University Park, PA Vol. 2, New York, Pergamon Press, 1963: 199.

Robau-Sanchez A., A. Aguilar-Elguezabal, J. Aguilar-Pliego, Chemical activation of Quercus agrifolia char using KOH: Evidence of cyanide presence, Microporous and mesoporous materials 85 (2005) 331-339.

Rodriguez-Reinoso F., The role of carbon materials in heterogeneous catalysis
Carbon 36 (1998) 3: 159-175.

Rodriguez-Reinoso F., in: Handbook of porous solids; Schuth, F.; Sing, K. S. W.; Weitkamp, J.; , Vol 3, Wiley-VCH Verlag GmbH, Weinheim, Germany, 2002, Chapter 4.

Rodriguez-Reinoso F., In: Fundamental issues in control of carbon gasification reactivity, J. Lahaye, P. Ehrburger (Eds.), Martinus Nijhoff Publisher, Dordrecht, Nitherland, 1990, 533-571.

Rodriguez-Reinoso F., In: Marsh, H., Heintz E. A., Rodriguea-reinoso F. (editors), Introduction to carbon technologies, Spain, Secretariado de publicaciones, 1997: 35-101.

Rodriguez-Reinoso F., M. Molina-Sabio. Textural and chemical characterization of microporous carbons, Advances in colloid and interface science 76-77 (1998) 271-294.

Rodriguez-Reinoso F., C. Salinas-Martinez de Lecea, A. Sepulveda-Escribano, J. D. Lopez-Gonzalez, Effect of support porosity in the preparation and catalytic activity for CO hydrogenation of carbon-supported Fe catalysts. Catal. Today, 1990, 287-298.

Rodriguez-Reinoso F., in: ed. F. Schuth, K. S. W. Sing and J. Weitkamp, Handbook of porous solids, Vol. 3, 1st ed., Wiley-VCH Verlag GmbH, Weinheim, 2002, Chapter 4.

Rojey A., in: ed. C. Jaffret, M. Marshall, Natural gas: Production, processing, transport, TECHNIP, France, 1997, 293.

Rouquerol F., J. Rouquerol, K. Sing, Adsorption by powders and porous solids: priciples, methodology and applications Academic press: San Diego, USA, 1st ed., 1999, Chapter 8.

Saito A., H. C. Foley, Argon porosimetry of selected molecular sieves: experiments and examination of the adapted Horvath-Kawazoe model, Microporous Material 3 (1995) 531.

Saskatchewan Government, "Challenges of Assessing Organic Crop Residue Values" www.se.gov.sk.ca 2004.

Satterfield C. N., Heterogeneous catalysis in industrial practice, USA, 2nd ed., 1991: 471-539.

Schlögl R., In: Handbook of porous solids, Schuth F., K. S. W. Sing, J. Weitkamp (editors), Vol. 3, Wiley-VCH Verlag GmbH, Weinheim, Germany, 2002, Chapter 4.

Seaton N. A., J. P. R. B. Walton, N. Quirke, A new analysis method for the determination of the pore size distribution of porous carbons from nitrogen adsorption measurements, Carbon 27 (1989) 6: 853-861.

Shen W., J. Zheng , Z. Qin , J. Wang , Y. Liu , The effect of temperature on the mesopore development in commercial activated carbon by steam activation in the presence of

yttrium and cerium oxides, Colloids and surfaces A: Physiochem. Eng. Aspects 229 (2003) 55-61.

Sing K. S. W., in: Jr W. Patrick (Ed.), Porosity in carbons: Characterization and Applications, 1st ed., Halsted Press, London, 1995; Chapter 2 .

Sing, K. S. W. In: "Porosity in carbons: Characterization and Applications", Jr. W. Patrick (editor), 1st ed., London, Halsted Press, 1995: 49-67.

Sing K. S. W., D. H. Verett, R. A. W. Haul, L. Moscou, R. A. Pierotti, J. Roquerol, T. Siemieniewska, Pure appl chem. 57 (1985) 603, In: [Rodriguez-Reinoso, 1997].

Sreerammurthy R., P. G. Menon, Oxidation of H_2S on active carbon catalyst, Journal of Catalysis 37 (1975) 287-296.

Steijns M., F. Derks, A. Verloop, P. Mars, The mechanism of the catalytic oxidation of hydrogen sulphide, Journal of Catalysis 42 (1976) 87-95.

Steijns, M., P. Mars, The role of sulphur trapped in micropores in the catalytic partial oxidartion of hydrogen sulphide with oxygen, Journal of Catalysis 35 (1974) 11-17.

Steijns M., P. Mars, Catalytic Oxidation of Hydrogen Sulfide. Influence of Pore Structure and Chemical Composition of Various Porous Substances, Industrial and Engineering Chemistry Product Research Development 16 (1977) 35-41.

Stoeckli H. F., Microporous carbons and their characterization: The present state of the art, Carbon 28 (1990) 1: 1-6.

Stohr J. NEXAFS spectroscopy, Springer series in surface science, Vol. 25, Berlin: Springer, 1st ed., 1992, 114-161.

Stohr, B., H. P. Boehm, R. Schlogl, Enhancement of the catalytic activity of activated carbons in oxidation reactions by the thermal treatment with ammonia or hydrogen cyanide and observation of a superoxide species as a possible intermediate, Carbon 29 6: (1991) 707-720.

Studebaker M. L., Rubber Age (1955) 77: 69 [In: Kinoshita K., Carbon: Electrochemical and physiochemical properties, John Wiley & Sons Inc., 1st ed., USA , 1988].

Sublette K. L., Aerobic oxidation of hydrogen sulphide by Thiobacillus denitrificans, Biotechnology and bioengineering, 29 (1987) 690-696.

Swaddle T. W., Inorganic chemistry: an industrial and environmental perspective, New York, USA: Academic press,1st ed., 1997, 191-204.

Teng H., T. Yeh , L. Hsu , Preparation of activated carbon from bituminous coal with phosphoric acid activation, Carbon 36(1998) 9: 1387-1395.

Teng H., L. Y. Hsu, High-Porosity Carbons Prepared from Bituminous Coal with Potassium Hydroxide Activation, Industrial and Engineering Chemistry Research 38 (1999) 2947-2953.

Tennant M. F., D. W. Mazyck, Steam-pyrolysis activation of wood char for superior odorant removal, Carbon 41 (2003) 12: 2195-2202.

Thomas C. L., Catalytic processes and proven catalysts, Academic Press, New York, 1st ed., 184.

Tremblay G., F. J. Vastola, P. L. Walker Jr., Thermal desorption analysis of oxygen surface complexes on carbon, Carbon, 16 (1978) 1: 35-39.

Trim D. L., Catalysis, Vol. 4, The Royal Society of Chemistry, London, U. K.,1st ed., 1981, 210.

Turk A., E. Sakalis, O. Rago, H. Karamitsos, Activated carbon systems for removal of light gases, Ann. NY Acad. Sci. 661 (1991) 221.

Uzio D., Physical-chemical analysis of industrial catalysts: A practical guide to characterization, Lynch J. (ed.), Paris, Editions Technip, (2001) Chapter 1.

Voll M.and H. M. Boehm, Basische Oberflächenoxide auf Kohlenstoff—IV. Chemische Reaktionen zur Identifizierung der Oberflächengruppen, Carbon 9 (1971) 4: 481-488.

Walker Jr P. L., A. Almagro, Activation of pre-chlorinated anthracite in carbon dioxide and steam, Carbon 33 (1995) 2: 239-241.

Wang R., Investigation on a new liquid redox method for H_2S removal and sulfur recovery with heteropoly compound, Separation and purification Tech. 31 (2003) 1: 111-121.

Webb P. A., C. Orr, Analytical methods in fine particle technology, USA, Micromeritics Instrument Corp., 2nd ed., 1997, 53 – 155.

Wieckowska J., Catalytic and adsorptive desulphurization of gases, Catalysis Today 24 (1995) 405-465.

Williams P. T., A. R. Reed, High grade activated carbon matting derived from the chemical activation and pyrolysis of natural fibre textile waste, Journal of Analytical and Applied Pyrolysis 71 (2004) 2: 971-986.

Wu X., V. Schwartz, S. H. Overbury, T. R. Armstrong, Desulphurization of gaseous fuels using activated carbons catalysts for the selective oxidation of hydrogen sulphide, Energy & Fuels 19 (2005) 1774-1782.

Wu X., A. K. Kercher, V. Schwartz, S. H. Overbury, T. R. Armstrong, Activated carbons for selective catalytic oxidation of hydrogen sulphide to sulphur, Carbon 43 (2005) 5: 1084-1114.

Yan J., J. Yang, Z. Liu, SH radical: The key intermediate in sulphur transformation during thermal processing of coal, Environmental science and technology 39 (2005) 5043-5051.

Yang, A., E. L. Tollefson, A. K. Dalai, Oxidation of low concentrations of hydrogen sulphide: Process optimization and kinetic studies, The Canadian Journal of Chemical Engineering, 76 (1998) 76-86.

Zhuang Q-L, T. Kyotany, A. Tomita, The change of TPD pattern of O_2-gasified carbon upon air exposure, Carbon 32 (1994) 539-540.

Zhuang Q-L, T. Kyotany, A. Tomita, Ext. Abstracts Carbon ’94, Granada, Spain, 1994b, 466.

Zhuang Q-L, T. Kyotany, A. Tomita, DRIFT and TK/TPD Analyses of Surface Oxygen Complexes Formed during Carbon Gasification, Energy and Fuels 8 (1994a) 714-718.

Zielke U., K. J. Huttinger, w. P. Hoffman, Surface-oxidized carbon fibers: I. Surface structure and chemistry, Carbon 34 (1996) 8: 983-998.

Appendix (A): Calibration curves for mass flow meters, temperature controllers, and gas chromatographs

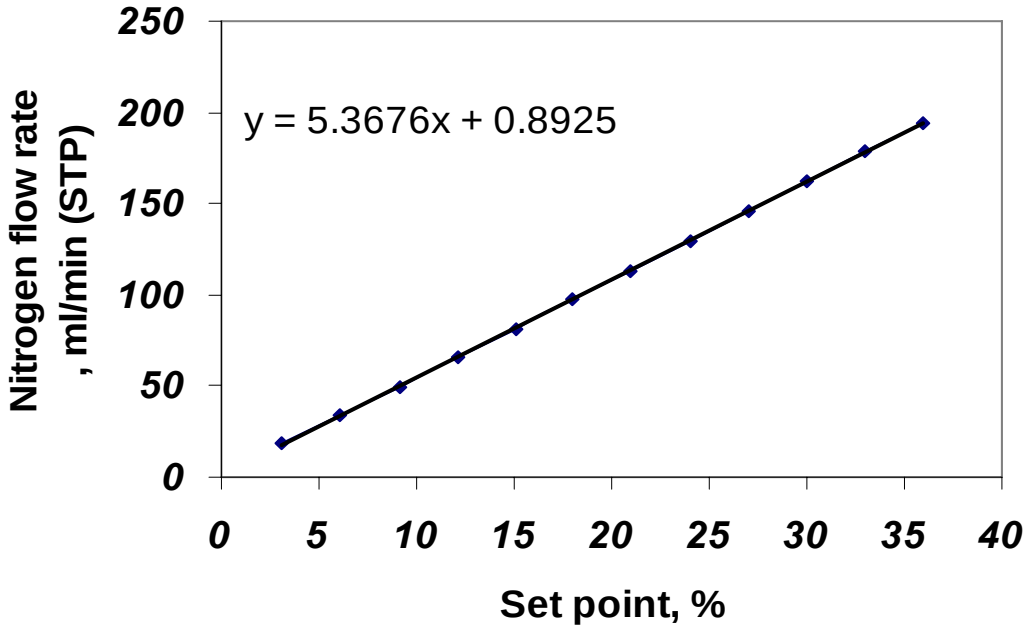

Fig. A.1: Mass flow meter calibration of nitrogen flow rate for physical activation of luscar char (for nitrogen flow rate range of 20-200 ml/min)

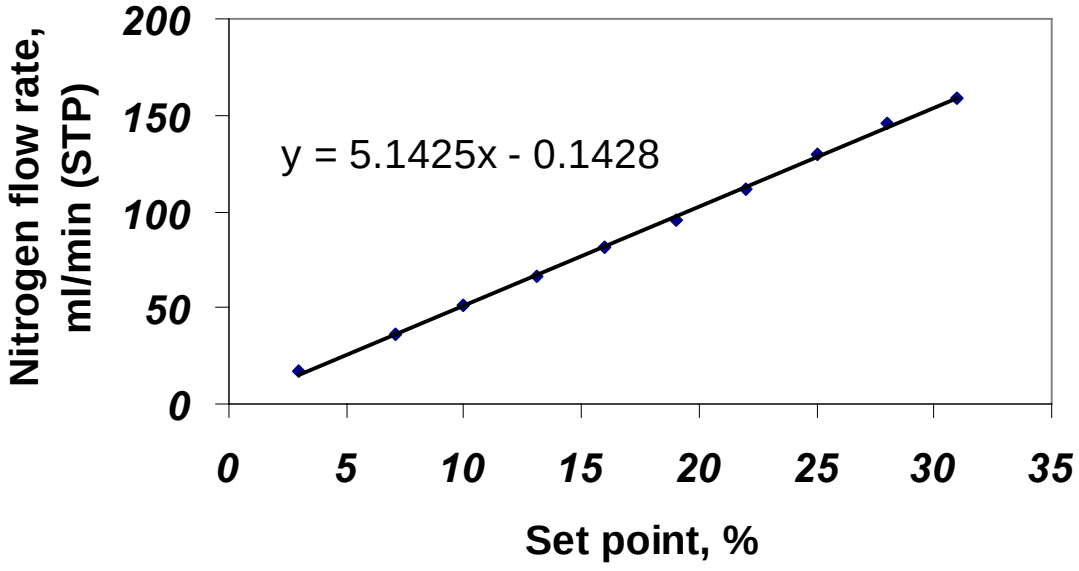

Fig. A.2: Mass flow meter calibration of nitrogen flow rate for physical and chemical activation processes of biochar (for nitrogen flow rate range of 20-170 ml/min)

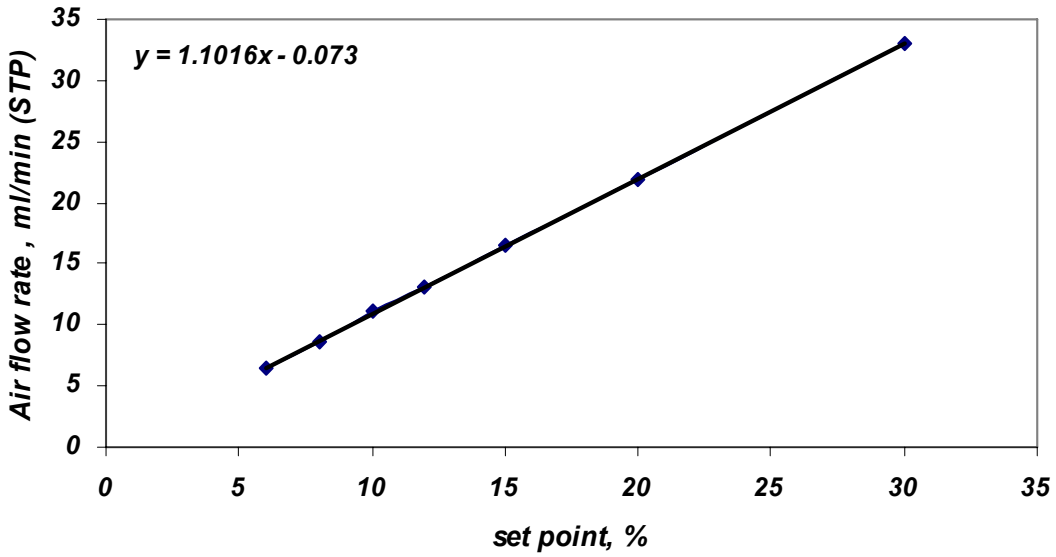

Fig. A.3: Calibration curve of air flow rate for hydrogen sulphide oxidation reaction of activated carbons produced from luscar char (for air flow rate range of 5-32 ml/min)

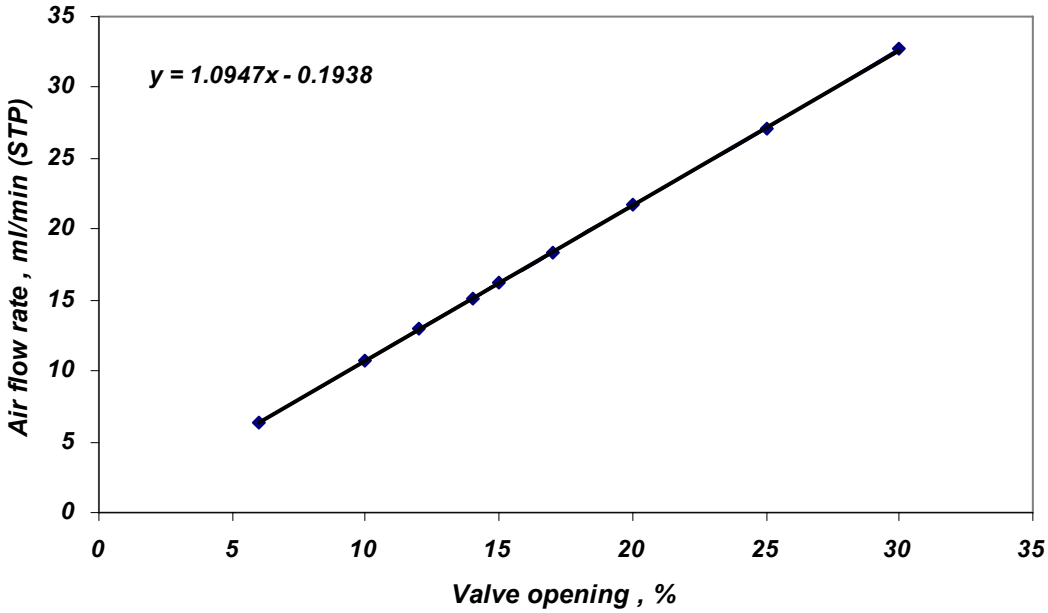

Fig. A.4: Calibration curve of air flow rate for hydrogen sulphide oxidation reaction of activated carbons produced from biochar (for air flow rate range of 5-34 ml/min)

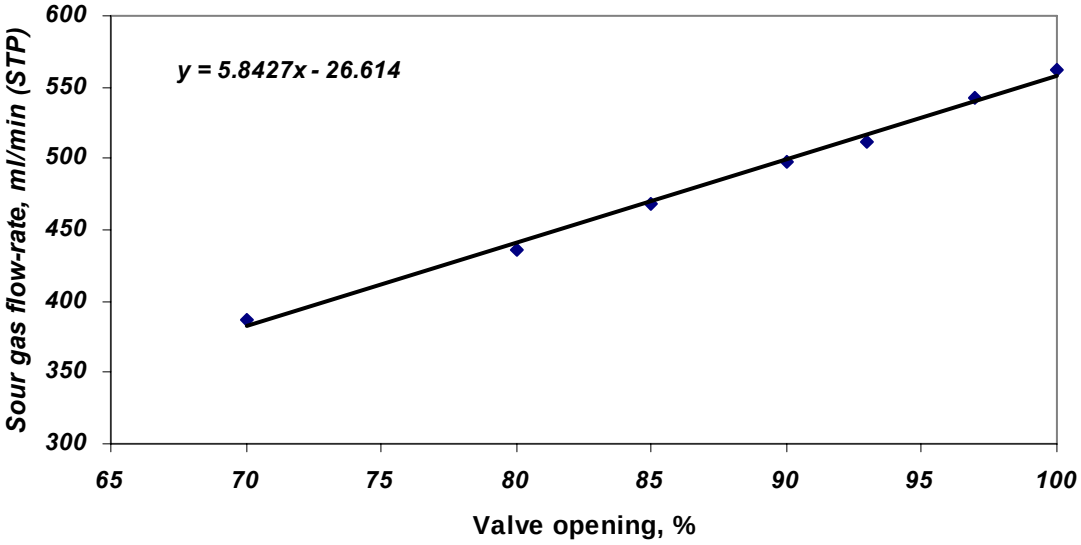

Fig. A.5: Calibration curve of sour gas (H_2S: 1 mol %) flow rate for hydrogen sulphide oxidation reaction of activated carbons produced from luscar char (for sour gas flow rate range of 370-560 ml/min)

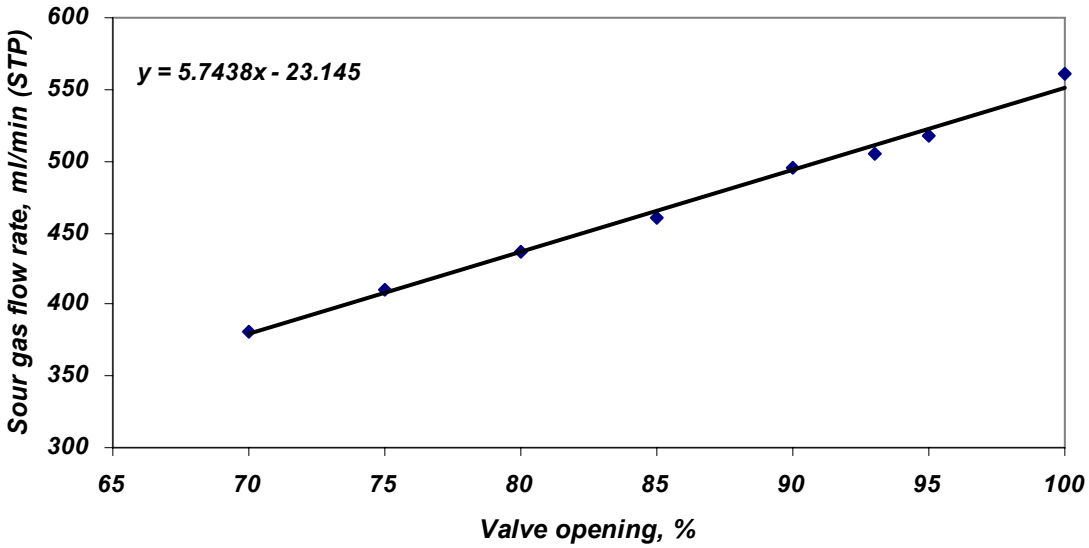

Fig. A.6: Calibration curve of sour gas (H_2S: 1 mol %) flow rate for hydrogen sulphide oxidation reaction of activated carbons produced from biochar (for sour gas flow rate range of 370-550 ml/min)

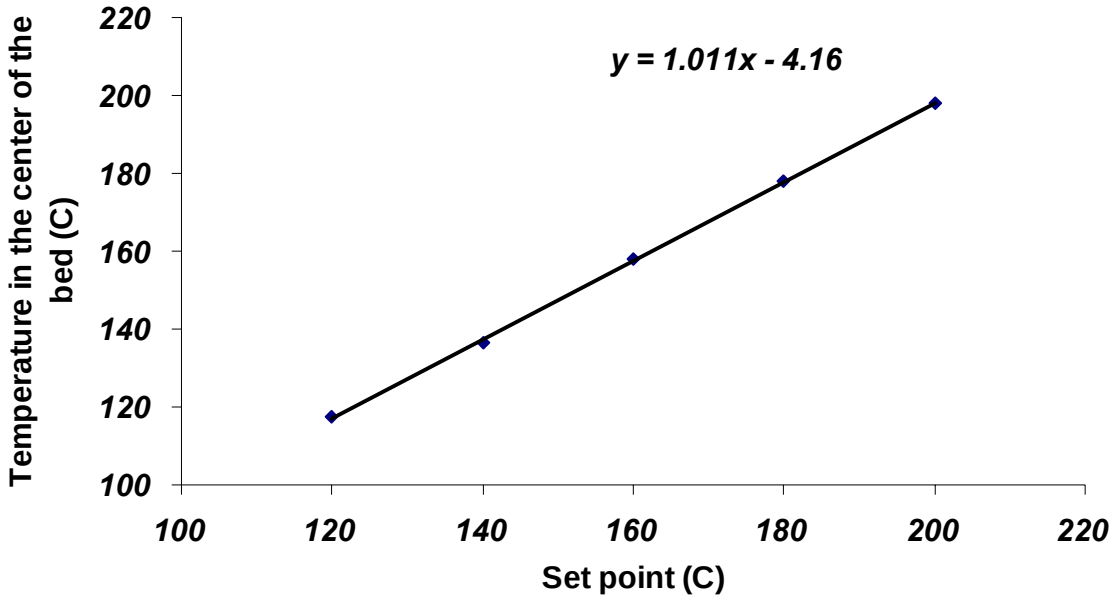

Fig. A.7: Calibration curve of temperature at the center of catalyst bed for hydrogen sulphide oxidation reaction using activated carbons prepared from luscar char (for temperature range of 115-200 ^{o}C)

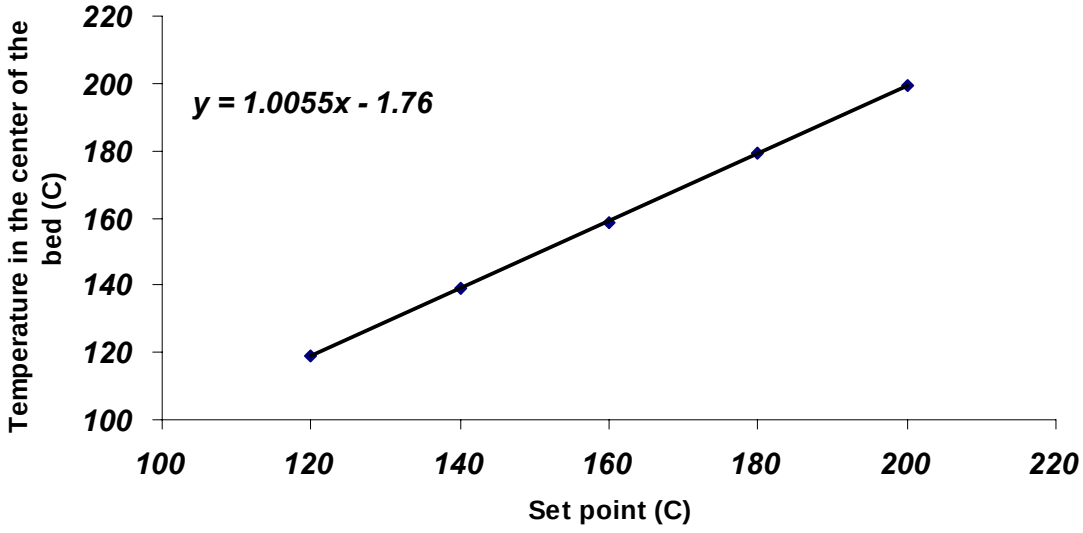

Fig. A.8: Calibration curve of temperature at the center of catalyst bed for hydrogen sulphide oxidation reaction using activated carbons prepared from biochar (for temperature range of 120-200 ^{o}C)

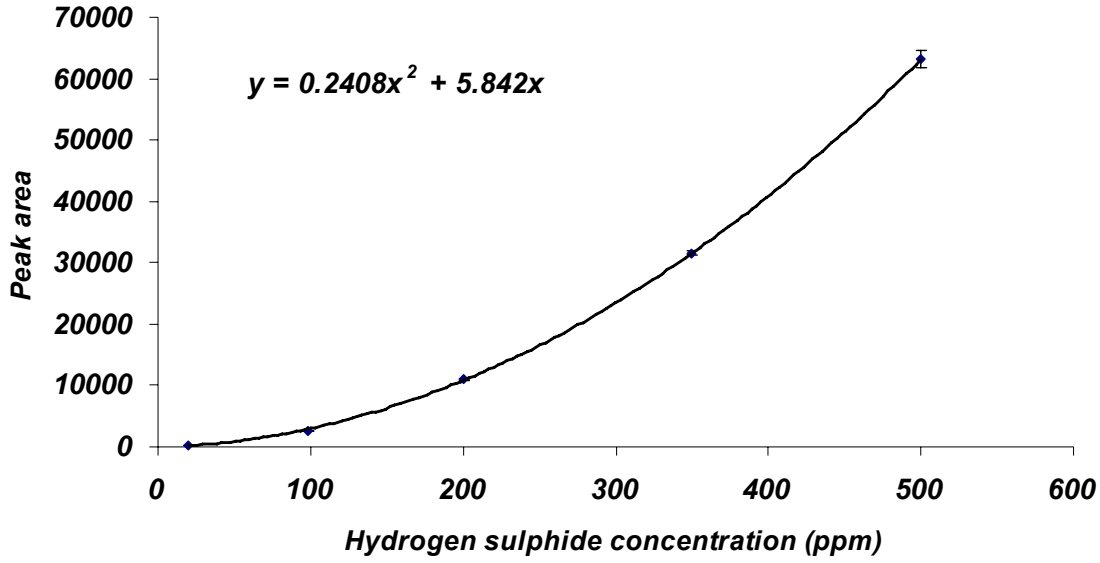

Fig. A.9: Calibration curve for hydrogen sulphide (H_2S) with concentration range of 0-500 ppm

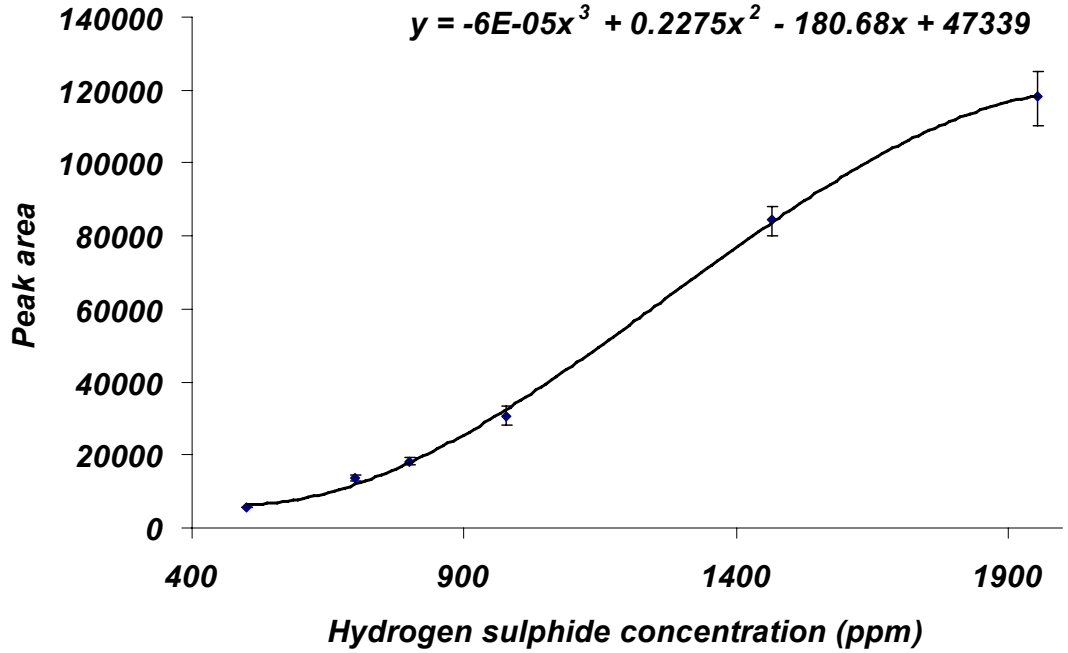

Fig. A.10: Calibration curve for hydrogen sulphide (H_2S) with concentration range of 500-1954 ppm

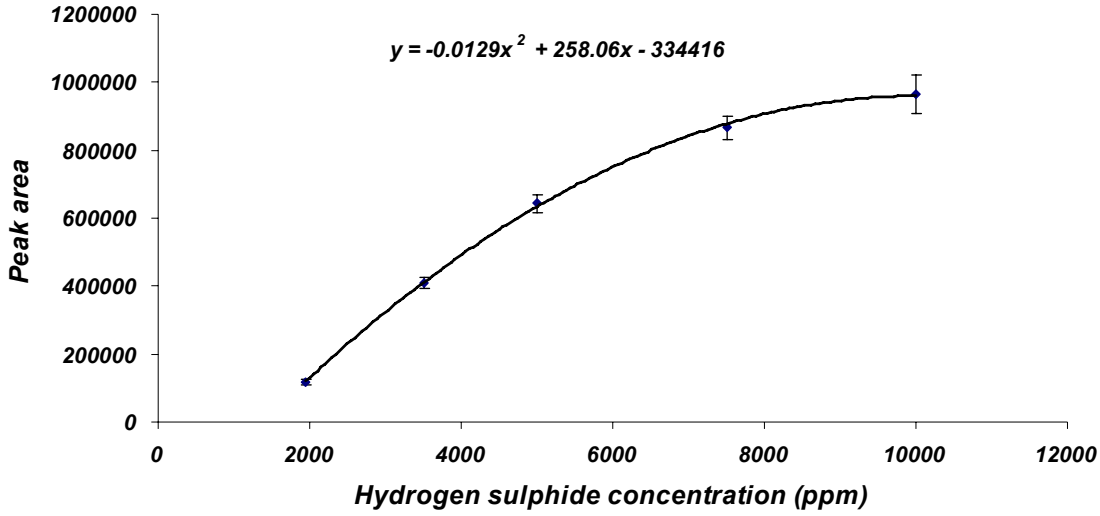

Fig. A.11: Calibration curve for hydrogen sulphide (H_2S) with concentration range of 1954-10000 ppm

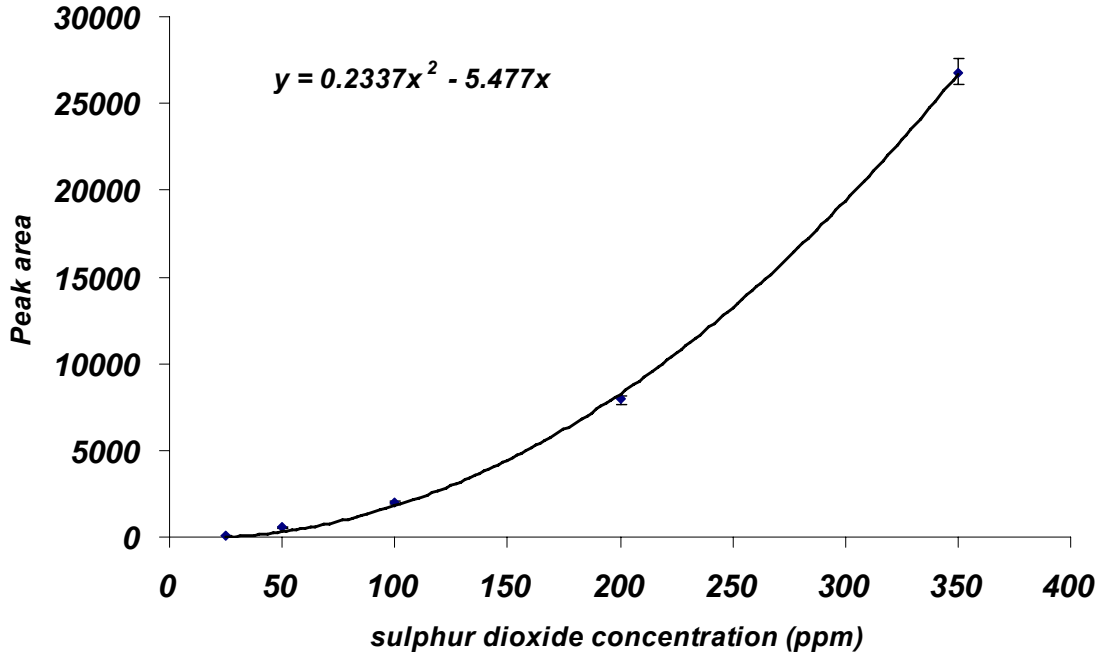

Fig. A.12: Calibration curve for slphur dioxide (SO_2) with concentration range of 0-350 ppm

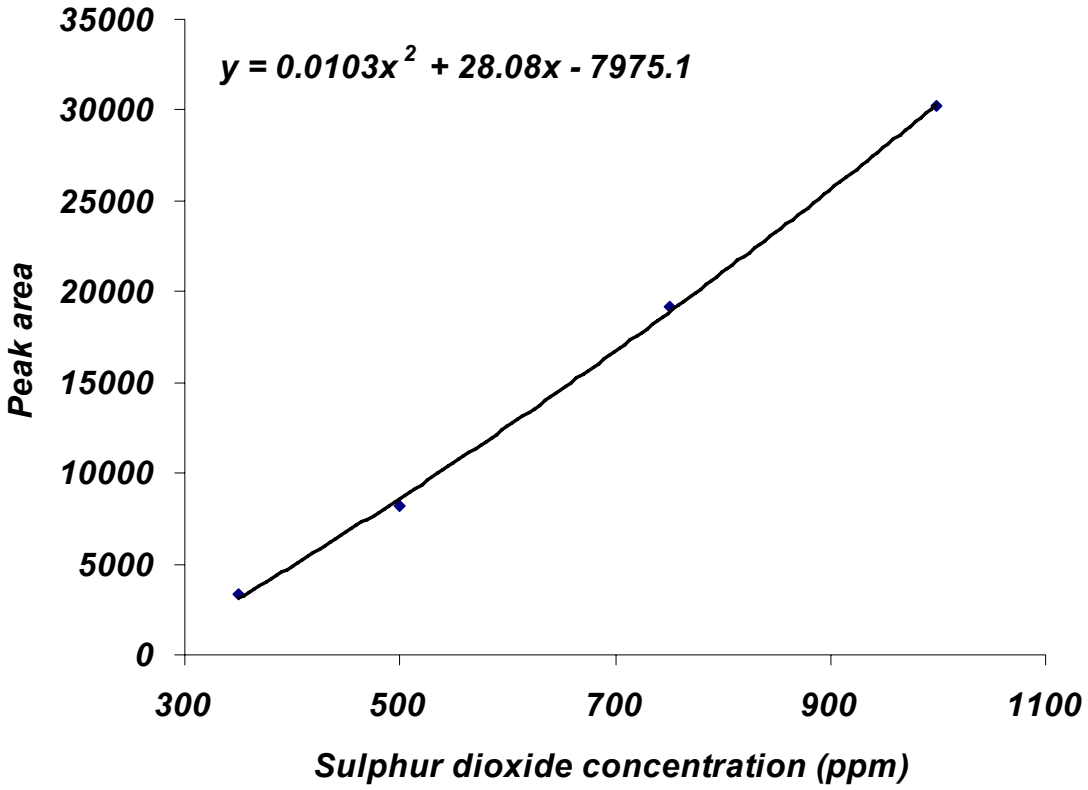

Fig. A.13: Calibration curve for slphur dioxide (SO_2) with concentration range of 350-999 ppm

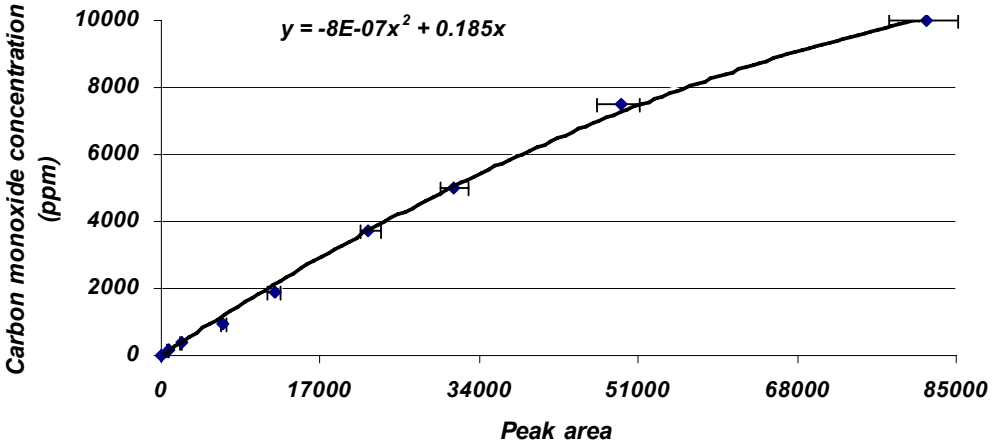

Fig. A.14: Calibration curve for carbon monoxide (CO) with concentration range of 0-1000 ppm

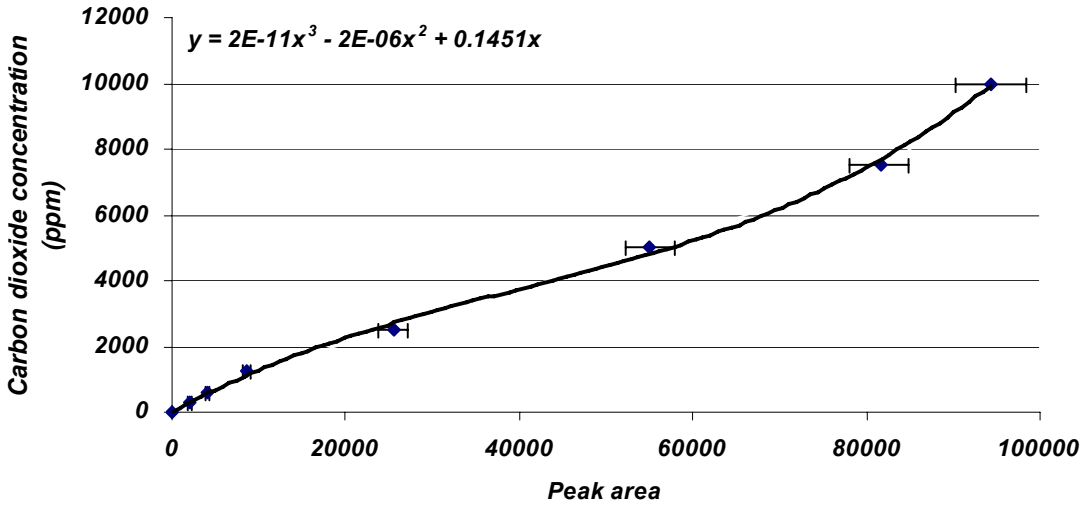

Fig. A.15: Calibration curve for carbon dioxide (CO_2) with concentration range of 0-12000 ppm

Appendix (B): Determination of BET surface area

The BET (Brunauer, Emmett, and Teller) equation was used to measure the internal surface area of activated carbon samples. It utilizes physical adsorption of nitrogen to obtain information on the surface area and porous structure of solid materials. The sample first was degassed to remove water and other volatile compounds on the carbon surface. Then, the sample was exposed to nitrogen gas at a series of different pressures at -196 ^{o}C. Using the adsorption data the BET surface area can be determined by the BET equation:

$$\frac{P}{V(P_0 - P)} = \frac{1}{V_m C} + \frac{C-1}{V_m C}\frac{P}{P_0} \qquad \text{(B1)}$$

The straight line $P/V(P_o-P)$ as a function of P/P_o can be used to obtain gradient (α) and ordinate at the origin (β) of the straight line, where:

$$\alpha = \frac{C-1}{V_m C} \qquad (B2)$$

$$\beta = \frac{1}{V_m C} \qquad (B3)$$

Then, V_m and C can be calculated as follows:

$$V_m = \frac{1}{\alpha + \beta} \qquad (B4)$$

$$C = \frac{\alpha}{\beta} + 1 \qquad (B5)$$

The surface area is determined by the following equation:

$$S_{BET} = \frac{N_A A_M V_m 10^{-20}}{m_s V_M} \quad \text{(B6)}$$

where;

S_{BET} is the BET surface area (m^2/g)

N_A is Avogadro's number ($6.023 * 10^{23}$ molecules/mole)

A_M is the area occupied by an adsorbate molecule (16.2 $Å^2$ for nitrogen)

V_m The quantity of gas adsorbed for monolayer coverage of surface (cm^3), it is calculated using Eq. (B4)

m_s is the mass of the solid analyzed (g)

V_M is the molar volume of gas (22,414 cm^3/mol)

For nitrogen as adsorptive gas, Eq. (B6) becomes:

$$S_{BET} = \frac{4.35\, V_m}{m_S} \quad \text{(B7)}$$

Appendix (C): Error analysis For ICP and Boehm titration analyses

ICP analysis:

Table C.1: Error analysis for ICP analysis results

Element	1st measurement (ppm)	2nd measurement (ppm)	Avg. value (ppm)	Error (Absolute)	Error (%)
Mg	165	164	164.5	± 0.5	0.30
Al	632	633	632.5	± 0.5	0.08
Mn	19	20	19.5	± 0.5	2.56
Fe	186	188	187	± 1	0.53
Zn	16	15	15.5	± 0.5	3.22
Zr	1	1	1	0	0.00

Sample: BioAC-O-D(750)

Boehm titration method:

Table C.2: Error analysis for Boehm titration method

Sample Number	1st measurement (ml)	2nd measurement (ml)	Avg. value (ml)	Error (Absolute)	Error (%)
1	4.4	4.5	4.45	± 0.05	1.12
2	4.4	4.4	4.40	± 0.00	0.00
3	2.2	2.3	2.25	± 0.05	2.22

Sample 1: BioAC-O-D(750) mixed with NaOH

Sample 2: BioAC-Chem mixed with HCl

Sample 3: BioAC-O mixed with $NaHCO_3$

Appendix (D): Particle size distribution of precursors and activated carbons prepared at optimum operating conditions

Table D.1: Particle size distribution of Luscar char and LusAC

Particle size range (μm)	Luscar char (vol % of particles)	LusAC (vol % of particles)
< 850	0.0	11.4
850-1180	21.0	26.6
1180-1700	45.0	35.2
1700-1999	20.9	14.6
1999-2380	13.1	12.2

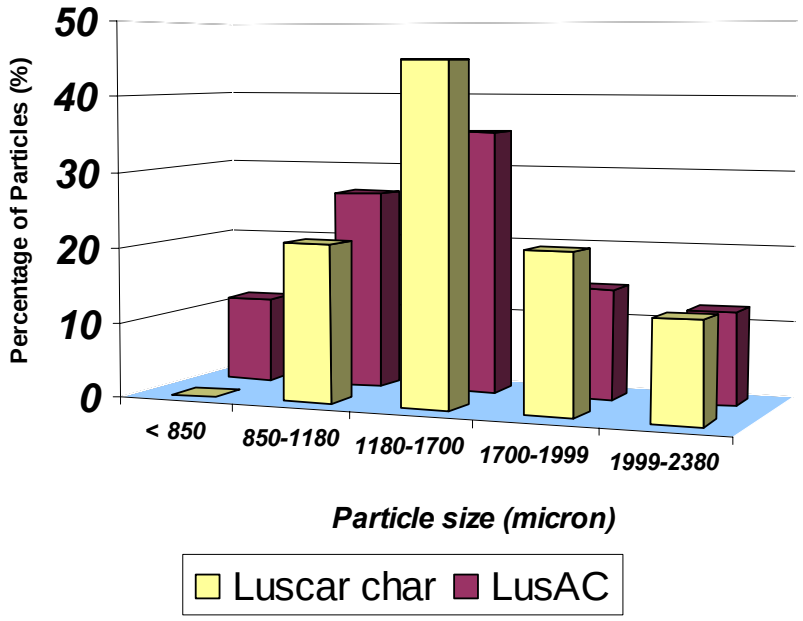

Fig. D.1: Particle size distribution of luscar char and LusAC

Table D.2: Particle size distribution of Biochar, BioAC, BioAC-Chem

Particle size range (μm)	Biochar (vol % of particles)	BioAC (vol % of particles)	BioAC-Chem (vol % of particles)
<150	0.0	2.9	8.4
150-250	27.7	29.4	28.1
250-354	24.5	23.9	22.9
354-600	47.8	43.8	40.5

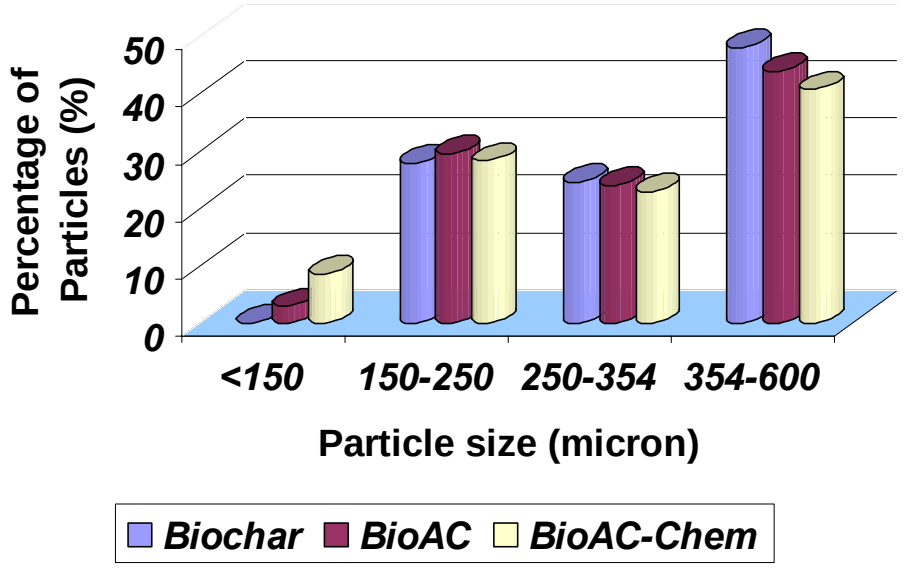

Fig. D.2: Particle size distribution of biochar, BioAC, and BioAC-Chem

Appendix (E): Data for H_2S conversion and SO_2 production in the oxidation reaction and reproducibility of data

Reproducibility of H_2S oxidation run for LusAC-O-D(650)-K(5%) (impregnated using DMSO as impregnating solvent) catalyst at reaction temperature and pressure of 175 ^oC and 700 kPa, respectively, and oxygen concentration of 1.05 times of stoichiometry

Run #1:

Reaction time	***H_2S outlet Concentration (ppm)***	***SO_2 outlet Concentration (ppm)***
0	0	0
41	0	0
44	0	20
47	0	32
50	0	43
53	0	59
56	0	58
59	0	30
62	0	68
65	0	73
68	0	69
71	0	75
74	0	85
77	0	68
80	0	94
83	0	92
86	0	90
89	0	80
92	0	75
95	0	72
98	0	50
101	9	54
105	15	47
108	26	47
111	40	44
114	60	39
117	86	32
120	116	23
123	166	20
126	232	18
129	315	15
132	418	0

135	534	0
138	678	0
141	858	0
144	1051	0
147	1266	0
150	1509	0
153	1751	0
155	2000	0

Run #2:

Reaction time	***H_2S outlet Concentration (ppm)***	***SO_2 outlet Concentration (ppm)***
0	0	0
34	0	0
37	0	5
40	0	27
43	0	36
46	0	30
49	0	41
52	0	44
55	0	53
58	0	57
61	0	61
64	0	79
67	0	71
70	0	84
73	0	86
76	0	90
79	0	87
82	0	94
85	0	102
88	0	75
91	0	81
94	0	84
97	0	75
102	0	50
105	0	38
108	11	43
111	18	32
114	27	24
117	42	28
120	67	28
123	93	20
126	135	16
129	207	19

132	270	0
135	365	0
138	486	14
141	612	13
144	807	14
147	969	6
150	1126	0
153	1402	5
156	1610	0
159	1850	0
161	2000	0

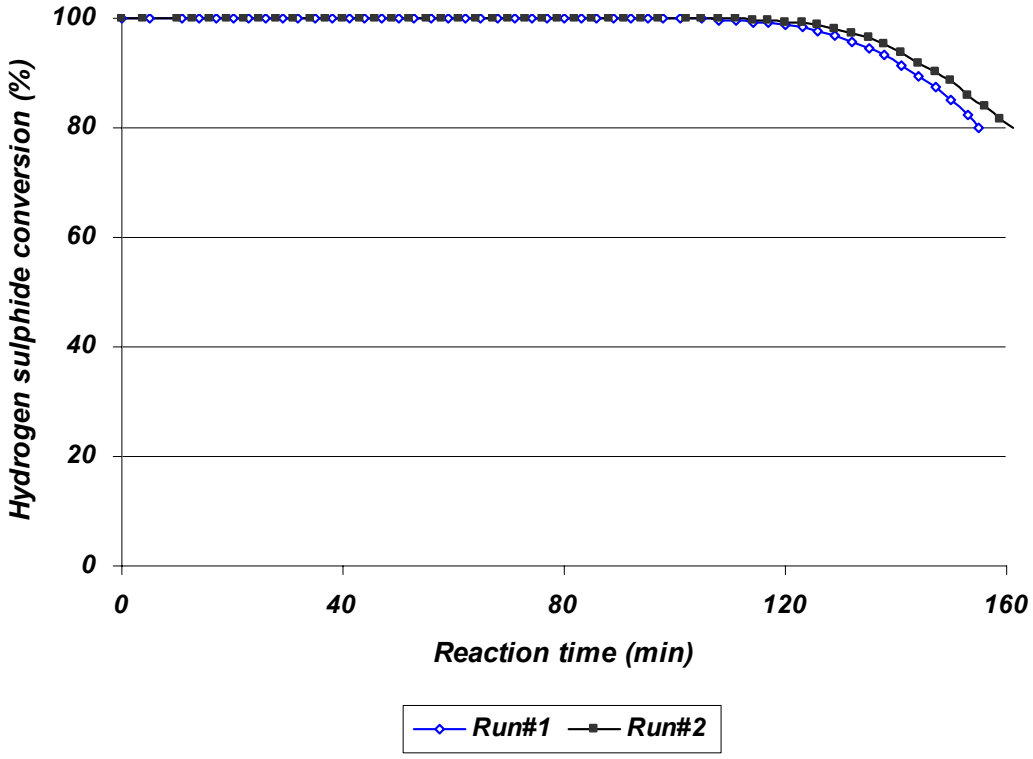

Fig. E.1:H_2S conversion vs. reaction time for LusAC-O-D(650)-K(5%) catalyst impregnated using DMSO as impregnating solvent at reaction temperature and pressure of 175 ^{o}C and 700 kPa, respectively, and oxygen concentration of 1.05 times of stoichiometry

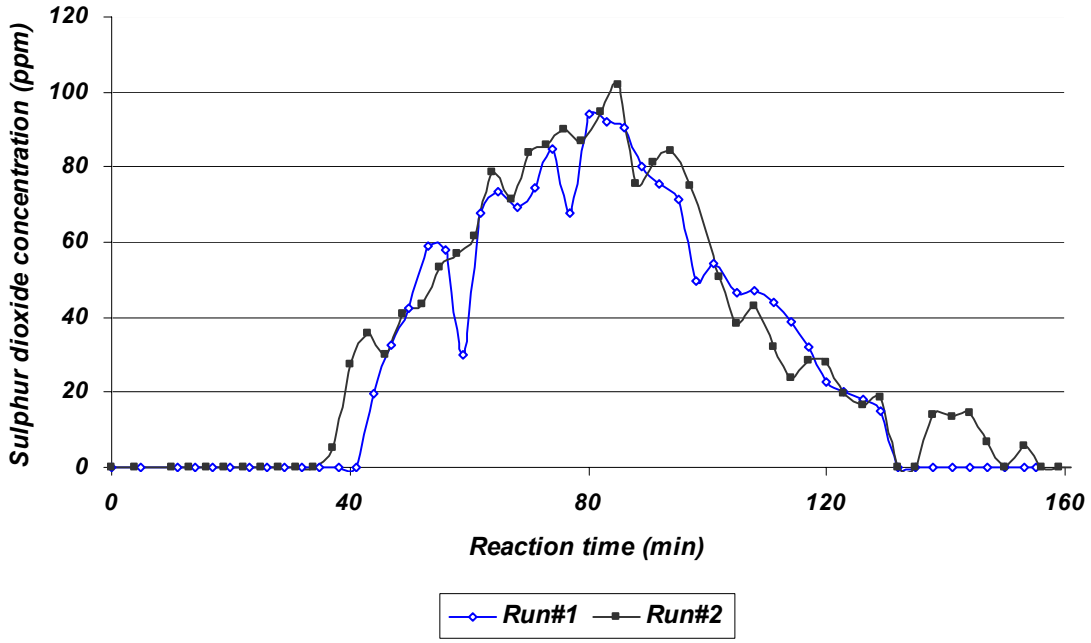

Fig.E.2:SO_2 concentration vs. reaction time for LusAC-O-D(650)-K(5%) catalyst impregnated using DMSO as impregnating solvent at reaction temperature and pressure of 175 ^{o}C and 700 kPa, respectively, and oxygen concentration of 1.05 times of stoichiometry

Table E.1: Results of runs repeated for LusAC-O-D(650)-K(5%) impregnated using DMSO as impregnating solvent

	Break-through time (min)	g_s/g_c	Avg. SO_2 production (as % of H_2S fed)
Run #1	155	0.995	0.307
Run #2	161	1.032	0.328
Difference (%)	3.87	3.72	6.84

Appendix (F): Sample calculation of mass transfer coefficient and boundary layer thickness using Frössling correlation

For particle size in the range of 1000-2380 μm, the average particle size (d_p) is 0.169 cm. The free stream velocity of fluid (u) can be calculated as follows;

$$u = \frac{Q}{S_r} = \frac{512.5 \frac{ml}{\min} * \frac{1m^3}{10^6 ml} * \frac{1\min}{60s}}{\pi \frac{(12.7*10^{-3})^2}{4} m^2} = 0.0674 \frac{m}{s} \quad \text{(F1)}$$

Density calculation: Methane compressibility factor (Z) at 0 ^{0}C and 100 kPa can be calculated by Table 3-172 of Perry's Handbook (5th ed.). From this table, Z value for methane at 0 ^{o}C and atmospheric pressure (Z_1) is 0.9974 and that (Z_2) for 175 ^{0}C and 200 kPa is 0.9997 .

The density (ρ_1) of the methane gas including 1 mol % of H_2S at 0^{o}C and 100 kPa can be calculated as follows using Table 3-30 of Perry's Handbook (5th ed.);

ρ_{gas} = (99*0.0448+1*0.0961)/100=0.0453 lb/ft^3

The density of the mixture can be calculated as follows;

$$\frac{\rho_1}{\rho_2} = \left(\frac{p_1}{p_2}\right)\left(\frac{Z_2}{Z_1}\right)\left(\frac{T_{a2}}{T_{a1}}\right) \quad (F2)$$

$$\frac{0.0453}{\rho_2} = \left(\frac{1}{2}\right)\left(\frac{0.9997}{0.9974}\right)\left(\frac{448.15}{273.15}\right) \quad (F3)$$

Therefore, ρ_2 = 0.0551 lb/ft^3

ρ_2 is the density of the gas mixture at 175 ^{0}C and 200 kPa.

Calculation of dynamic viscosity:

The dynamic viscosity of nitrogen at 448.15 K (175 ^{0}C) and 100 kPa were calculated using Table 3-309 of Perry's Handbook (5th ed.). It is equal to 0.156 * 10^{-4} Pa.s .

$$\mathrm{Re} = \frac{\rho u d_p}{\mu} = \frac{\left(0.0551\frac{lb}{ft^3} * \frac{16.018\frac{kg}{m^3}}{1\frac{lb}{ft^3}}\right) * \left(0.0674\frac{m}{s}\right) * (0.00169m)}{0.156 * 10^{-4} Pa.s} = 6.44 \qquad \text{(F4)}$$

$$Sc = \frac{\mu}{\rho D_e} = \frac{0.156 * 10^{-4} Pa.s}{\left(0.0551\frac{lb}{ft^3} * \frac{16.018\frac{kg}{m^3}}{1\frac{lb}{ft^3}}\right) * \left(0.0216 * 10^{-4}\frac{m^2}{s}\right)} = 8.183 \qquad \text{(F5)}$$

D_e is calculated in Appendix (G).

$$Sh = 2 + 0.6(\mathrm{Re})^{\frac{1}{2}}(Sc)^{\frac{1}{3}} = 2 + 0.6(6.44)^{\frac{1}{2}}(8.183)^{\frac{1}{3}} = 5.068 \qquad \text{(F6)}$$

$$Sh = \frac{k_c.d_p}{D_e} \quad , \quad 5.068 = \frac{k_c(0.00169m)}{0.0216 * 10^{-4}\frac{m^2}{s}} \qquad \text{(F7)}$$

Therefore, $k_c = 0.00648$ m/s .

$$k_c = \frac{D_e}{\delta} \quad , \quad 0.00648\frac{m}{s} = \frac{0.0216 * 10^{-4}\frac{m^2}{s}}{\delta} \qquad \text{(F8)}$$

Therefore, $\delta = 3.3 * 10^{-4}$ m .

Appendix (G): Sample calculation of Weisz-Prater parameter (C_{WP})

Calculation of effective diffusivity: Eq. (G1) is based on the modern kinetic theory and the Lennard-Jones expression for intermolecular forces [Hirschfelder et al, 1954] and can be used for calculation of effective diffusivity of binary gas mixtures [Satterfield, 1970]:

$$D_{AB} = \frac{0.001858 * T_a^{\frac{3}{2}} * [(M_1 + M_2)/M_1 M_2]^{\frac{1}{2}}}{p * \sigma_{12}^2 * \Omega_D} \quad \text{(G1)}$$

where,

D_{AB} : effective diffusivity for a binary gas mixtures, T_a : temperature (K), M_i : Molecular weight of species i, p : pressure (atm), Ω_D : collision integral (a function of kT_a/ε_{12})

σ and ε : the force constants in the Lennard-Jones potential function, k : the Boltzmann constant

D_{AB} for oxidation of hydrogen sulphide at 175 ^oC as reaction temperature and pressure of 2 atm can be calculated as follows:

T = 175+273.14=448.14 K, M_1=34, M_2=32, P=2 atm

$$\sigma = \frac{(\sigma_1 + \sigma_2)}{2} = \frac{(3.623 + 3.467)}{2} = 3.545 \ \overset{0}{\text{A}} \quad \text{(G2)}$$

(Values of σ_1 and σ_2 were obtained from Table 1.3 of [Satterfield, 1970]), then,

$$\frac{\varepsilon_{12}}{kT_a} = (\frac{\varepsilon_1}{k})^{0.5} * (\frac{\varepsilon_2}{k})^{0.5} * (\frac{1}{T_a}) = (301.1)^{0.5} * (106.7)^{0.5} * (\frac{1}{448.14}) = 0.4 \quad \text{(G3)}$$

(Values of ε_1/k and ε_2/k were obtained from [Satterfield, 1991]),

$$\frac{kT_a}{\varepsilon_{12}} = \frac{1}{0.4} = 2.5 \quad \text{(G4)}$$

$\Omega_D = 0.9996$ [Satterfield, 1970]. Therefore, D_{12} can be calculated as follows:

$$D_{AB} = \frac{0.001858*(448.14)^{1.5}*((\frac{1}{34})+(\frac{1}{32}))^{0.5}}{2*(3.545)^2*0.9996} = 0.1728\frac{cm^2}{s} \quad \text{(G5)}$$

If D_{AB} was calculated for H_2S – Air, It would be equal to 0.17734cm^2/s and therefore there is not a large difference (< 4.6%) between D_{12} calculated for H_2S-Oxygen mixture and that for H_2S-Air mixture.

$$D_e = D_{AB}*\frac{\theta}{\tau} = 0.1728*\frac{0.5}{4} = 0.0216\frac{cm^2}{s} \quad \text{(G6)}$$

Where θ is porosity of catalyst and τ is tortuosity factor.

In the absence of other information a value of θ=0.5 and a value of τ = 4 are recommended for estimation purposes [Satterfield, 1991].

$$R = \frac{0.150+0.208}{2} = 0.0895\ mm = 0.00895\ cm \quad \text{(G7)}$$

$$C_{AS} = \frac{500*\left(\frac{101.325}{8314*298.15}\right)*0.01}{500} = 4.09*10^{-7}\ \frac{gmol}{cm^3} \quad \text{(G8)}$$

$$\rho_C = 0.433\ \frac{g}{cm^3} \quad \text{(G9)}$$

For particle size in the range of 150-208 μm , $-r_{A(obs.)}$ is as follows:

$$(-r_{H_2S(obs.)}) = 0.001812\ \frac{gmol}{\min.g_C} \quad \text{(G10)}$$

The C_{WP} can be calculated using Eq. (6.11) as follows:

$$C_{WP} = \frac{0.001812*0.433*(0.00895)^2}{0.0216*60*4.09*10^{-7}} = 0.119 \quad \text{(G11)}$$

There is another method for calculation of effective diffusivity (D_e) [Fogler, 1999] using Eq. (G12);

$$D_e = \frac{D_{AB}\phi_p\sigma}{\tau} \qquad \text{(G12)}$$

Where, $\tau = tortuosity = \dfrac{actual\ distance\ a\ molecule\ travels\ between\ two\ points}{shortest\ distance\ between\ those\ two\ points}$

$$\phi_p = pellet\ porosity = \frac{volume\ of\ void\ space}{total\ volume\ (voids\ and\ solids)}$$

$\gamma = constriction\ factor$

The constriction factor accounts for the variation in the cross-sectional area that is normal to diffusion. Typical values of the constriction factor, the tortuosity, and the pellet porosity are, respectively, σ=0.8, τ=3.0, and ϕ_p=0.40. Therefore, the effective diffusivity can be calculated as follows;

D_e=0.1728*(0.4*0.8)/3=0.01843 cm^2/s

C_{WP} calculated using this value of D_e, by Eq. (6.11), is 0.139 which is less than one.

Appendix (H): Data for the kinetic study

Table H.1: Raw results for the oxygen concentration effect

H_2S flow rate = 500 ml/min (STP), H_2O flow rate = 0, SO_2 flow rate = 0 ml/min

Pressure = 200 kPa, and Catalyst weight = 0.07 g

Run	***T(^{o}C)***	***O_2/H_2S ratio (* stoichiometric)***	***Reaction rate*10^3 gmol/(min*g_c)***
1.1	160	1	1.699
1.2	160	2	1.755
1.3	160	3	1.820
1.4	175	1	1.812
1.5	175	2	1.958
1.6	175	3	2.087
1.7	190	1	1.887
1.8	190	2	2.093
1.9	190	3	2.260

Table H.2: Raw results for the Hydrogen sulphide concentration effect

H_2S flow rate = 500 ml/min (STP), H_2O flow rate = 0, SO_2 flow rate = 0 ml/min

Pressure = 200 kPa, and Catalyst weight = 0.07 g

Run	***T(^oC)***	***H_2S pressure (kPa)***	***Reaction rate*10^3 gmol/(min*g_c)***
2.1	160	1.183	0.986
2.2	160	1.570	1.351
2.3	160	1.950	1.699
2.4	175	1.183	1.020
2.5	175	1.570	1.399
2.6	175	1.950	1.812
2.7	190	1.183	1.040
2.8	190	1.570	1.472
2.9	190	1.950	1.887

Table H.3: Raw results for the water concentration effect

H_2S flow rate = 500 ml/min (STP), O_2/ H_2S = 1*st., SO_2 flow rate = 0 ml/min

Pressure = 200 kPa, and Catalyst weight = 0.07 g

Run	***T(^oC)***	***H_2O flow rate (% of feed flow rate)***	***Reaction rate*10^3 gmol/(min*g_c)***
3.1	160	0.6	1.645
3.2	160	1.0	1.625
3.3	160	1.8	1.601
3.4	175	0.6	1.798
3.5	175	1.0	1.773
3.6	175	1.8	1.750
3.7	190	0.6	1.814
3.8	190	1.0	1.804
3.9	190	1.8	1.769

Table H.4: Raw results for the sulphur dioxide concentration effect

H_2S flow rate = 500 ml/min (STP), O_2/ H_2S = 1*st., H_2O flow rate = 0 ml/min

Pressure = 200 kPa, and Catalyst weight = 0.07 g

Run	***T(^oC)***	***SO_2 flow rate (ml/min)***	***Reaction rate*10^3 gmol/(min*g_c)***
4.1	160	40	1.599
4.2	160	60	1.533
4.3	160	80	1.456
4.4	175	40	1.645
4.5	175	60	1.570
4.6	175	80	1.490
4.7	190	40	1.697
4.8	190	60	1.624
4.9	190	80	1.537

Appendix (I): Sample calculation of hydrogen sulphide oxidation reaction rate

The oxidation reaction rate can be calculated by the expression given below showing the gmoles of hydrogen sulphide converted per minute per gram of catalyst.

$$-r_{H_2S}{}' = Q\left(\frac{P}{RT_a}\right)_{Std}\left(\frac{a}{100}\right)\left(\frac{\xi}{100}\right)\left(\frac{1}{W}\right) \quad \text{(I1)}$$

Where, Q: feed gas flow rate (ml/min), P: total pressure (kPa), R: gas constant, 8314 kPa.ml/(gmol.K), T_a: temperature (K), a: H_2S mole percentage in the feed gas, ξ: percentage conversion, and W: catalyst mass (g)

For H_2S inlet and outlet concentration of 10000 and 6036 ppm, respectively, oxidation reaction rate for a catalyst mass equal to 0.07 g can be calculated as follows;

$$-r_{H_2S}{}' = 500.0\left(\frac{101.325}{8314*298.15}\right)\left(\frac{1}{100}\right)\left(\frac{10000-6036}{10000}\right)\left(\frac{1}{0.070}\right) = 1.157*10^{-3}\,\frac{gmol}{\min.g_{Cat}} \quad \text{(I2)}$$

Appendix (J): Sample results for density fuctional theory

Sample results for LusAC-O-D(650)

Full Report Set

ASAP 2020 V3.01 H Unit 1 Serial #: 694

Sample: 000-025LusAC-O-D(650)
Operator: RA
Submitter: RA
File: C:\2020\000-025.SMP

Started: 4/14/2008 4:08:45PM	Analysis Adsorptive: N2
Completed: 4/16/2008 6:17:16PM	Analysis Bath Temp.: 76.913 K
Sample Mass: 0.1984 g	Warm Free Space: 27.8847 cm³ Measured
Cold Free Space: 88.4636 cm³	Equilibration Interval: 45 s
Low Pressure Dose: 3.000 cm³/g STP	Automatic Degas: Yes

Summary Report

Surface Area

Single point surface area at p/p° = 0.205837866: 720.7281 m²/g

BET Surface Area: 735.7092 m²/g

t-Plot Micropore Area: 402.4015 m²/g

t-Plot External Surface Area: 333.3078 m²/g

Pore Volume

t-Plot micropore volume: 0.175076 cm³/g

Isotherm Tabular Report

Relative Pressure (p/p°)	Absolute Pressure (mmHg)	Quantity Adsorbed (cm^3/g STP)	Elapsed Time (h:min)	Saturation Pressure (mmHg)
			00:52	713.338867
0.000001566	0.001117	3.0525	01:51	
0.000000589	0.000420	6.1081	02:39	
0.000000373	0.000266	9.1635	03:29	
0.000000294	0.000210	12.2191	04:23	
0.000000269	0.000192	15.2746	05:22	
0.000000288	0.000205	18.3302	06:30	
0.000000311	0.000222	21.3859	07:46	
0.000000361	0.000258	24.4416	09:10	
0.000000430	0.000307	27.4971	10:29	
0.000000529	0.000378	30.5530	11:43	
0.000000652	0.000467	33.6089	13:25	
0.000000838	0.000600	36.6646	14:56	
0.000001057	0.000756	39.7203	16:32	
0.000001346	0.000964	42.7488	18:04	
0.000001713	0.001227	45.7781	19:41	
0.000002192	0.001571	48.8094	20:58	
0.000002786	0.001997	51.8377	22:25	
0.000003529	0.002530	54.8902	23:59	
0.000004488	0.003219	57.9414	25:25	
0.000005692	0.004084	60.9913	26:48	
0.000007184	0.005156	64.0395	28:05	
0.000009057	0.006502	67.0851	29:21	
0.000011371	0.008165	70.1280	30:36	
0.000014524	0.010431	73.1840	31:12	
0.000018292	0.013139	76.2397	31:47	
0.000022979	0.016508	79.2949	32:21	
0.000028885	0.020753	82.3494	32:51	
0.000036335	0.026108	85.4035	33:21	
0.000045816	0.032924	88.4567	33:47	
0.000057880	0.041597	91.5089	34:12	
0.000073305	0.052687	94.5596	34:35	
0.000093057	0.066889	97.6081	34:58	
0.000118348	0.085075	100.6543	35:18	
0.000150523	0.108213	103.6974	35:40	
0.000191586	0.137744	106.7366	36:01	
0.000244012	0.175450	109.7708	36:21	

0.000310635	0.223371	112.7984	36:42	
0.000394983	0.284044	115.8178	37:01	
0.000501843	0.360917	118.8262	37:21	
0.000637147	0.458254	121.8214	37:38	
0.000807096	0.580529	124.7997	37:58	
0.001021300	0.734654	127.7563	38:17	
0.001288209	0.926722	130.6866	38:38	
0.001621795	1.166779	133.5829	38:56	
0.002034353	1.463701	136.4398	39:17	
0.002544975	1.831213	139.2457	39:35	
0.003168292	2.279850	141.9920	39:51	
0.003940551	2.835755	144.7339	40:10	
0.004864859	3.501152	147.3901	40:28	
0.005952022	4.283865	149.9448	40:47	
			40:56	719.756775
0.007139176	5.141837	152.3088	41:06	
0.008461999	6.099360	154.5114	41:18	
0.010030426	7.238387	156.7742	41:36	
0.012063672	8.711922	159.1958	41:47	
0.013931370	10.075154	161.1211	42:09	
0.017033979	12.331007	163.8211	42:24	
0.019430539	14.086050	166.3313	42:46	
0.024636473	17.872839	169.5578	42:57	
			42:59	725.556885
0.028317320	20.543501	171.3016	43:10	
0.030799889	22.342243	172.4157	43:20	
0.038974755	28.269382	175.8782	43:30	
0.044460774	32.244881	177.8463	43:41	
0.048101280	34.881542	179.0336	43:51	
0.053095488	38.499222	180.5995	44:01	
0.057707570	41.839108	181.9137	44:11	
0.060355290	43.754250	182.6402	44:21	
0.062295746	45.156788	183.1304	44:30	
0.075013726	54.369606	186.3454	44:41	
0.107314111	77.771164	193.1204	44:53	
0.142994617	103.615158	199.4275	45:06	
			45:08	724.593872
0.163047247	118.122009	202.4790	45:19	
0.205837866	149.093353	208.4749	45:31	
0.255057552	184.711472	214.4962	45:42	
0.339304655	245.671112	224.4070	45:55	
0.440659099	318.994080	235.8548	46:07	
0.539480170	390.442322	247.5866	46:21	
0.639465261	462.700378	261.4084	46:35	
0.730342500	528.311218	276.8344	46:52	
0.802029849	580.008179	291.7239	47:09	

			47:11	723.151855
0.862769353	623.863037	306.4795	47:29	
0.882421188	638.033203	311.5148	47:43	
0.900527663	651.084290	316.3426	47:57	
0.922826372	667.161560	322.2066	48:12	
0.940220663	679.694275	326.9543	48:26	
0.950848037	687.343079	329.7762	48:37	
0.960508618	694.289185	332.3587	48:49	
0.970494666	701.469788	335.2438	49:01	
0.980375636	708.573669	338.5639	49:13	
			49:15	722.750854
0.985658550	712.385559	340.8562	49:26	
0.990196807	715.665588	343.2862	49:37	

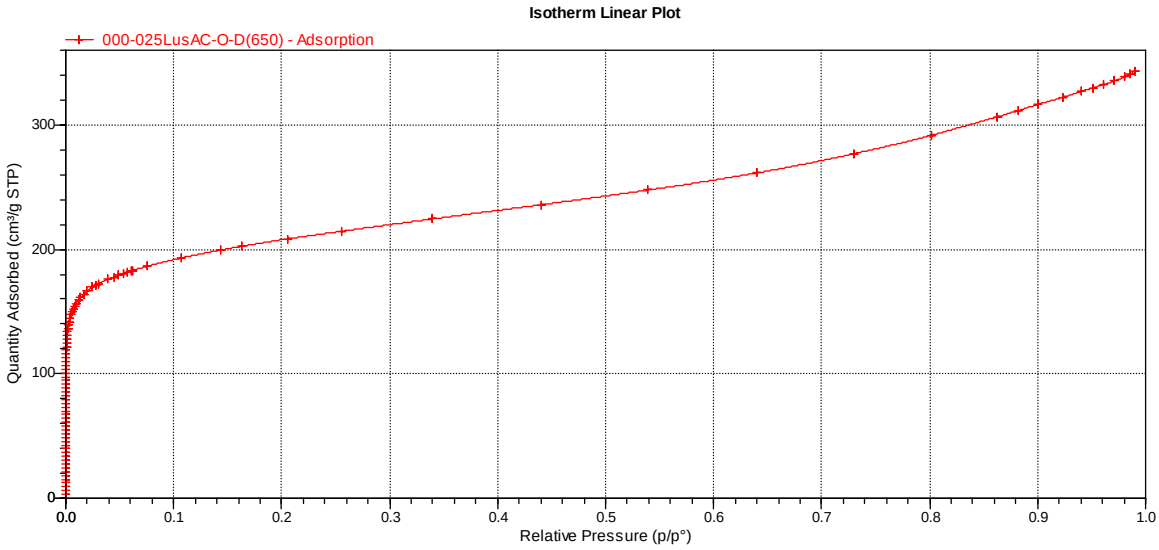

Porosity Distribution by Original Density Functional Theory
Model: N2 @ 77K on Carbon, Slit Pores
Method: Non-negative Regularization; No Smoothing

Volume in Pores < 4.65 Å : 0.00000 cm^3/g
Total Volume in Pores <= 1366.77 Å : 0.43259 cm^3/g
Area in Pores > 1366.77 Å : 15.711 m^2/g
Total Area in Pores >= 4.65 Å : 754.291 m^2/g

Pore Size Table

Pore Width (Å)	Cumulative Volume (cm^3/g)	*Incremental Volume (cm^3/g)*	Cumulative Area (m^2/g)	*Incremental Area (m^2/g)*
4.65	0.00000	0.00000	0.000	0.000
5.00	0.11338	0.11338	453.154	453.154
5.36	0.11338	0.00000	453.154	0.000
5.90	0.11338	0.00000	453.154	0.000
6.43	0.11338	0.00000	453.154	0.000
6.79	0.12442	0.01104	485.670	32.516
7.33	0.13622	0.01180	517.885	32.215
8.04	0.15029	0.01407	552.888	35.003
8.58	0.15029	0.00000	552.888	0.000
9.29	0.15029	0.00000	552.888	0.000
10.01	0.15029	0.00000	552.888	0.000
10.90	0.15029	0.00000	552.888	0.000
11.79	0.17211	0.02181	589.876	36.988
12.69	0.18550	0.01339	610.981	21.106
13.58	0.19429	0.00880	623.935	12.953
14.83	0.20612	0.01183	639.883	15.948
15.91	0.21272	0.00660	648.184	8.302
17.16	0.21709	0.00436	653.271	5.086
18.59	0.22065	0.00357	657.111	3.840
20.02	0.22380	0.00314	660.251	3.140
21.62	0.22804	0.00425	664.180	3.928
23.41	0.23364	0.00559	668.958	4.778
25.20	0.24038	0.00674	674.310	5.352
27.34	0.24850	0.00812	680.248	5.938
29.49	0.25561	0.00711	685.070	4.822
31.81	0.26282	0.00721	689.601	4.531
34.31	0.27087	0.00806	694.299	4.697

36.99	0.27738	0.00651	697.817	3.518
40.03	0.28445	0.00707	701.350	3.532
43.25	0.29215	0.00770	704.909	3.559
46.64	0.30017	0.00803	708.350	3.441
50.40	0.30887	0.00869	711.800	3.450
54.33	0.31773	0.00886	715.063	3.263
58.80	0.32646	0.00873	718.033	2.969
63.44	0.33536	0.00890	720.837	2.805
68.45	0.34434	0.00898	723.462	2.625
73.99	0.35144	0.00710	725.381	1.919
79.88	0.35847	0.00703	727.140	1.759
86.32	0.36716	0.00869	729.154	2.014
93.11	0.37568	0.00852	730.985	1.830
100.61	0.38197	0.00629	732.236	1.251
108.66	0.38773	0.00576	733.296	1.060
117.23	0.39303	0.00529	734.199	0.903
126.53	0.39791	0.00488	734.971	0.772
136.71	0.40241	0.00451	735.630	0.659
147.61	0.40665	0.00424	736.204	0.574
159.41	0.41049	0.00384	736.686	0.482
172.10	0.41382	0.00333	737.073	0.387
185.86	0.41670	0.00287	737.382	0.309
200.69	0.41921	0.00252	737.633	0.251
216.60	0.42150	0.00229	737.844	0.212
233.93	0.42357	0.00207	738.021	0.177
252.52	0.42534	0.00177	738.161	0.140
272.71	0.42684	0.00150	738.271	0.110
294.51	0.42781	0.00097	738.337	0.066
317.92	0.42862	0.00081	738.388	0.051
343.30	0.42950	0.00088	738.439	0.051
370.64	0.43019	0.00069	738.477	0.037
400.31	0.43084	0.00065	738.509	0.032
432.30	0.43129	0.00046	738.530	0.021
466.79	0.43168	0.00039	738.547	0.017
503.96	0.43210	0.00042	738.563	0.017
544.17	0.43238	0.00028	738.574	0.010
587.60	0.43253	0.00014	738.579	0.005
634.42	0.43259	0.00006	738.580	0.002
684.99	0.43259	0.00000	738.580	0.000
739.68	0.43259	0.00000	738.580	0.000
798.65	0.43259	0.00000	738.580	0.000
862.45	0.43259	0.00000	738.580	0.000
931.26	0.43259	0.00000	738.580	0.000
1005.60	0.43259	0.00000	738.580	0.000
1085.66	0.43259	0.00000	738.580	0.000
1172.33	0.43259	0.00000	738.580	0.000

1265.80	0.43259	0.00000	738.580	0.000
1366.77	0.43259	0.00000	738.580	0.000

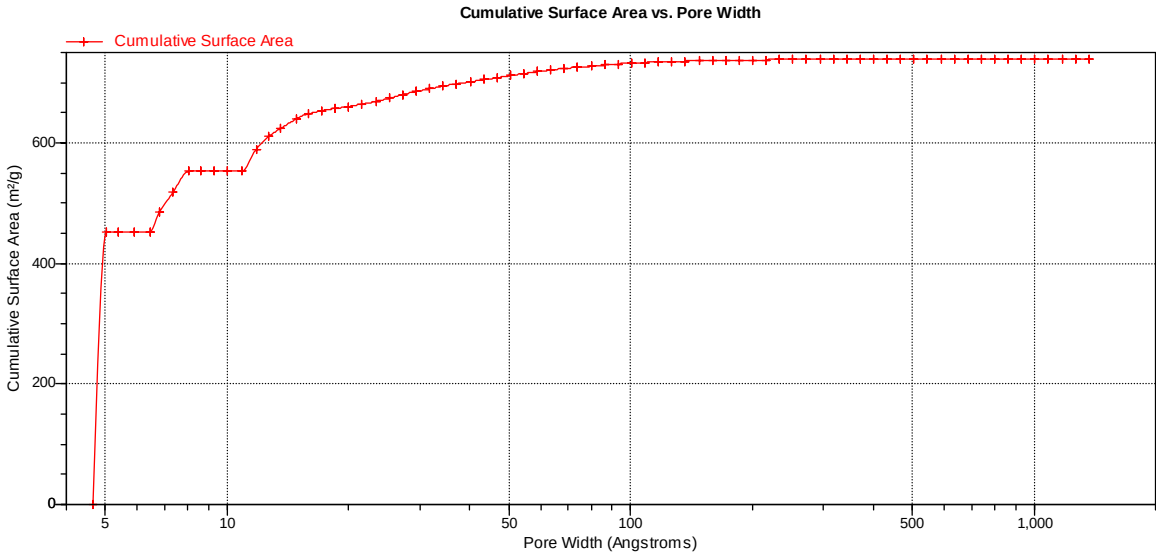

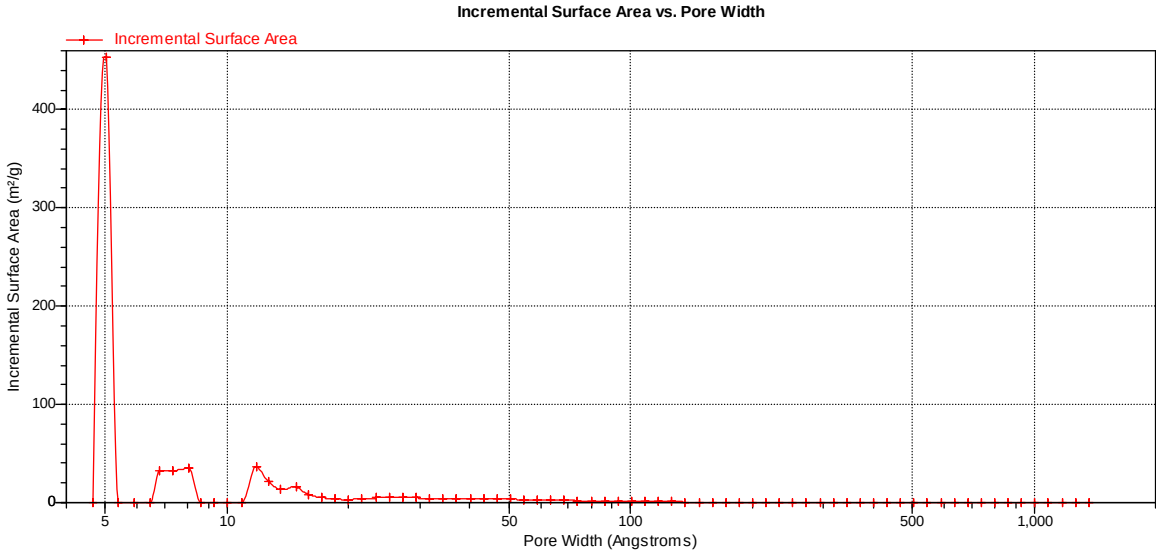

Cumulative Pore Volume vs. Pore Width

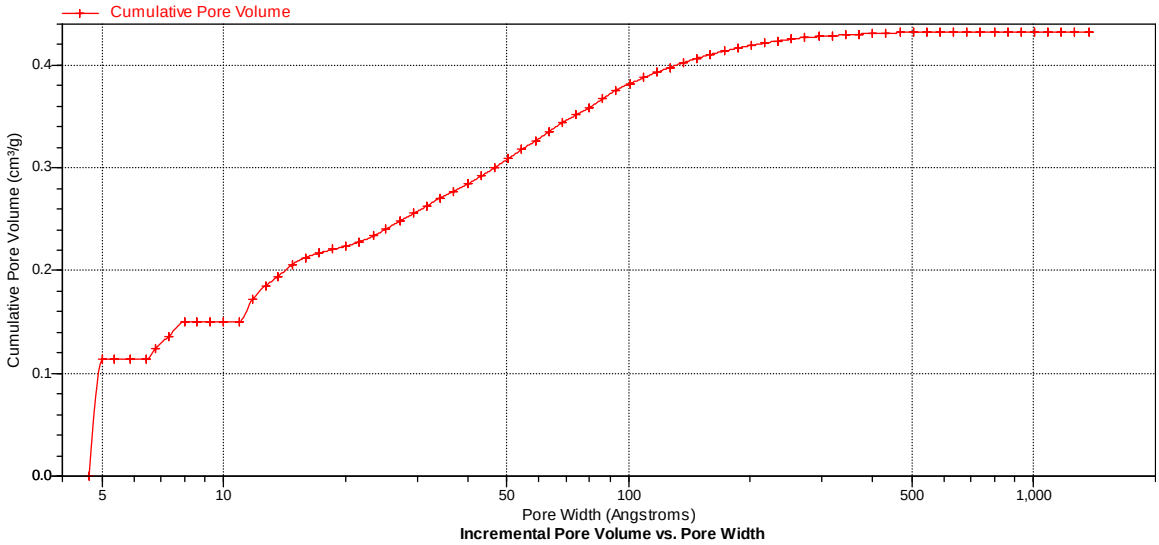

Incremental Pore Volume vs. Pore Width

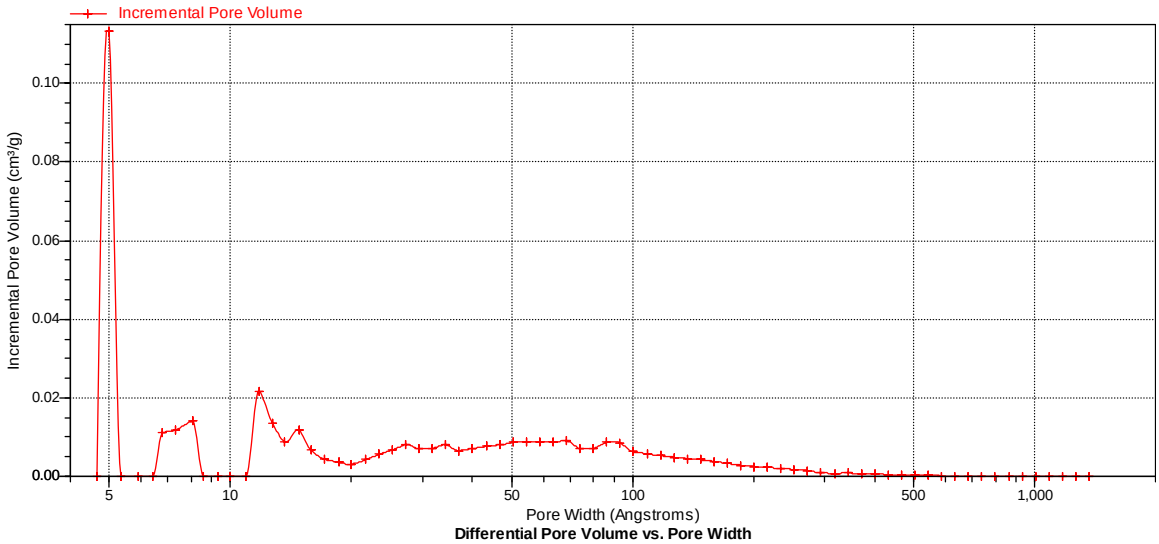

Differential Pore Volume vs. Pore Width